EXPERIMENTAL DETERMINATION OF VOLUTE EFFECTS ON THE STABILITY OF LOW SPECIFIC SPEED CENTRIFUGAL PUMPS

by

Scott B. Sandler

B.S. Mechanical Engineering
Worcester Polytechnic Institute, 1990

SUBMITTED TO THE DEPARTMENT OF AERONAUTICS AND ASTRONAUTICS
IN PARTIAL FULFILLMENT OF THE REQUIREMENTS FOR
THE DEGREE OF

MASTER OF SCIENCE

at the

MASSACHUSETTS INSTITUTE OF TECHNOLOGY
June 1992

Signature of Author _____
Department of Aeronautics and Astronautics
May 8, 1992

Certified by _____
Dr. Jack L. Kerrebrock
R.C. MacLaurin Professor of Aeronautics and Astronautics
Thesis Supervisor

Approved by _____
Professor Harold Y. Wachman
Chairman, Department Graduate Committee

EXPERIMENTAL DETERMINATION OF VOLUTE EFFECTS ON THE STABILITY OF LOW SPECIFIC SPEED CENTRIFUGAL PUMPS

by

Scott B. Sandler

Submitted to the Department of Aeronautics and Astronautics on May 8, 1992
in partial fulfillment of the requirements for the degree of
Master of Science

ABSTRACT

The work discussed in this thesis represents a third phase in a multi-phase program addressing pump instabilities. This report describes detailed experimental pressure and laser velocity measurements, a pump redesign for improved stability and a stability evaluation of the new design.

A component investigation of the original pump was conducted to determine how the volute, impeller, tongue and diffuser influence the shape of the overall pump performance characteristic. The results showed that the tongue region became quite unstable as the mass flow was reduced. Since the tongue is part of the volute, an extensive velocity mapping in the volute just upstream of the tongue was carried out.

The laser velocimetry study demonstrated the highly three dimensional and complex nature of the volute flow. The flow structure is highly vortical and strongly influenced by the impeller radial discharge jet. The discharge jet sets up two lobes of secondary circulation. One lobe occurs in the half of the volute facing the inlet and the other in the half facing the impeller backplane. As shut-off is approached, the latter lobe increases in strength and is recirculated in the volute passage.

The majority of the losses in the pump are derived from the mixing of the fluid exiting the impeller with the fluid in the volute. The LDV measurements confirm that the mixing losses vary with flow coefficient and increase at off design mass flows. To achieve absolute stability, the peak pressure rise must be reduced to the level of the shut-off head. The volute was redesigned to diffuse the flow in the initial stages of the scroll. This diffusion has the effect of increasing the mixing losses near the peak pressure rise thus reducing the head. However, at high mass flows there is an increase in head due to a reduction in the mixing losses. The final result produced a pump characteristic which is relatively flat over the entire range of flow rates. The head rise at the best efficiency point was not significantly compromised. A stability test of the modified pump produced the expected improvement in the stable operating range of the pump.

Thesis Supervisor: Professor J. L. Kerrebrock

Title: R.C. MacLaurin Professor of Aeronautics and Astronautics

TABLE OF CONTENTS

Abstract	II
Table of Contents	III
Acknowledgements	VI
Dedication	VII
List of Symbols	VIII
List of Figures	XI
Chapter 1 - Introduction	1
1.1 Problem Statement	1
1.2 Background	2
1.3 Goals and Objectives	6
1.4 Research Plan	7
1.5 Organization of Research Report	8
Chapter 2 - The M.I.T. Centrifugal Pump Facility	10
2.1 Centrifugal Pump Facility Overview	10
2.2 Pump Components	10
2.3 Instrumentation	12
2.3.1 Global Performance Measurements	12
2.3.2 Scanivalve Pressure Measuring System	13
2.3.3 Laser Doppler Velocimeter System	14
2.4 Data Acquisition and Processing	15
2.4.1 Computer Hardware	15
2.4.2 Computer Software	16
2.5 Facility Preparation	17
Chapter 3 - Steady-State Evaluation of Original Volute	18
3.1 Experimental Procedures	18
3.2 Steady-State Pump Parameters	19
3.3 Static Pressure Rise Through the Pump	20
3.4 Radial Pressure Gradients in the Volute	21
3.4.1 Volute Throat	22
3.4.2 Upstream of the Throat	22
3.5 Tongue Pressure Differential	23

3.6 Component Pressure and Slope Contributions 23
3.6.1 Diffuser 24
3.6.2 Tongue Region 25
3.6.3 Impeller 26
3.6.4 Volute 26
3.7 Summary of Component Pressure Analysis 26
3.8 LDV Experimental Procedures 27
3.9 Volute Velocity Profiles 29
3.9.1 Volute Throat 29
3.9.2 Surveys Upstream of the Tongue 31
3.10 Losses in Hydraulic Machinery 32
3.10.1 Slip Factor 32
3.10.2 Volute Mixing Losses 33
3.11 Summary of Velocity Surveys 33

Chapter 4 - Volute Modification 35
4.1 Motivation for Volute Re-design 35
4.2 Summary of Computational Study 35
4.3 Impact of Volute Modifications on Head Rise 36
4.3.1 Increased Impeller Backpressure 36
4.3.2 Volute Mixing Losses 36
4.3.3 Shut-off Head and Peak Pressure Rise 37

Chapter 5 - Pump Performance with Modified Volute and Stability Evaluation 38
5.1 Experimental Procedures 38
5.2 Modified Pump Parameters 39
5.3 Overall Pump Performance Characteristic 40
5.4 Static Pressure Rise Through the Pump 41
5.5 Volute Throat Pressure Gradient 42
5.6 Tongue Pressure Differential 42
5.7 Component Pressure and Slope Contributions 43
5.7.1 Diffuser 43
5.7.2 Tongue Region 43
5.8 Unsteady Operation with Modified Volute 44
5.8.1 Dynamic System Parameters 44

5.8.2 The Stability Boundary 44
5.9 Summary of Modified Volute Performance 45

Chapter 6 - Conclusions 46
6.1 Summary of Experimental Results 46
6.2 Recommendations 47

Bibliography and References 48
Figures 50
Appendices 139
A Laser Velocimetry Theory 139
B Scanivalve Pressure Sampling Code 141
B.1 PRESCAN5 Instructions 141
B.2 PRESCAN5 Source Code 146
C. Slip Factor Calculations 156

ACKNOWLEDGEMENTS

As the culmination of this research and thesis approaches rapidly, I look back over the course of my two years in the Gas Turbine Lab and realize that this work is not my accomplishment alone, but is the product of the efforts of many people. Everyone who participated in this work should be proud of their contributions and I am very grateful for your support. I would like to thank several individuals for their significant contributions.

Thanks to Prof. Jack Kerrebrock, my advisor, for for all his encouragement, praise and insight. Prof. Kerrebrock has made my stay at MIT an enjoyable learning experience. I would also like to thank Professors Greitzer, Marble and Johnston and Dr. Gerry Guenette for taking an interest in my progress. When you see that others are interested in your work it not only makes you feel good about what you are doing but encourages you to work harder. A special thanks to my fellow pump "expert", Furio and best wishes for future success. Thanks to Sundstrand Corporation, their financial support is gratefully acknowledged.

I would like to thank all my friends in the GTL for their support, conversation and most of all good humor. Thanks to the GTL technical staff, Victor Dubrowski, Jim Nash and James Letendre for their hard work in preparing the test facility and their assistance with all the general lab problems. A special thanks to Holly, Diana, Robin and Jean for the help with paperwork, purchasing and funding.

I would also like to thank two people who are no longer affiliated with the GTL, but were instrumental in this work. Thanks to Dr. Belgacem Jaroux for his efforts as project advisor and Dr. Andrew Wo for his long distance support.

Thanks to Howard Brenner and Jeff and Beverly Wain for the use of their Macintosh computers.

Finally, I would like to thank my family for all their love, encouragement and understanding during the past years. This is really their moment in the spotlight. I love you all. My friends, Charlene, Andy, John, Ken, Bryan, Dave, Martin and Dilip are one in a million. Thanks for keeping me smiling.

DEDICATION

I would like to dedicate this work to the loving memory
of my Grandmother, Goldie Sandler.

LIST OF SYMBOLS

$A(\theta)$	Volute Cross-Sectional Area
A_0	Volute Throat Area
A_c	Area of Compressor Flow Through
a	Speed of Sound
a	Particle Diameter (μm)
B	B Parameter - $U_{tip} / 2\,\omega_{unst}\,L_p$
b_2	Discharge Width of Impeller
$C_{\theta 2}$	Absolute Tangential Velocity Exiting Impeller
C_p	Pressure Rise Coefficient
c_f	Skin Friction Coefficient
D_2	Discharge Diameter of Impeller
f	Moody Friction Factor
g	Gravitational Constant
h	Height Coordinate in Volute
H	Head (ft.)
k	Constant
L	Linear Distance From Tap V0 to Discharge Tap
L_p	Inertial Length Scale of Pump
L_c	Length of Compressor Duct (effective)
$\dot{m}$	Mass Flow Rate
n	Rotational Speed (rev/sec)
N_s	Specific Speed
N_s'	Non-Dimensional Specific Speed
P	Pressure
Q	Volume Flowrate Through Pump (Q_{imp} - $Q_{leakage}$)
Q_{imp}	Volume Flowrate Through Impeller
$Q_{leakage}$	Leakage Volumetric Flowrate
R_h	Hydraulic Radius
$\underline{r}$	Radial Position from Center of Impeller
$\bar{r}$	Radius to Centroid of Volute Area
Re	Reynolds Number
s	Streamwise Coordinate in Volute
S	Volute Surface Area
T	Torque

u	Volute Tangential Velocity
U_{tip}	Impeller Tip Speed
U_{in}	Velocity at Diffuser Inlet
v	Volute Radial Velocity
V_0	Velocity of Particle in Probe Volume
V	Component of V_0 Perpendicular to the Bisector of the Beams
V_2	Volume of Air in Small Plenum
w_2	Impeller Discharge Velocity in Rotating Reference Frame
w	Local Width of Volute
z	Number of Blades
β_2	Blade Discharge Angle
Δh_f	Head Loss Due to Friction in Volute
h_{mixing}	Head Loss Due to Mixing of Impeller Jet with Volute Flow
h_{loss}	Head Loss Due Friction in Turbulent Pipe Flow
ΔP	Pressure Rise/Drop
η	Efficiency - $Q_{imp}\,\Delta P / \Omega T$
ϕ	Flow Coefficient - $\dot{m}/\rho\pi D_2 b_2 U_{tip}$
ψ	Head Coefficient - $\Delta P/2\rho U^2_{tip}$
σ	Slip Factor - $C_{\theta\,2,\,actual} / C_{\theta\,2,\,theoretical}$
θ	Angular Position from Tongue
θ	Incidence Angle Between Laser Beams
ρ	Density of Water (Standard Conditions)
υ	Kinematic Viscosity
ω_{unst}	Frequency of Unsteadiness in Pump (Hz)
ω_{red}	Reduced Frequency - ω_{unst} / Ω
Ω	Frequency of Impeller Rotation (rad/sec)

Subscripts

2	Impeller Outlet Conditions
st	Static Property
t	Total Property
cr	Transition to Instability
θ	Tangential Direction
act	Actual
th	Theoretical
imp	Impeller

Operators

$\partial()/\partial()$	Partial Derivative
Δ	Difference

Abbreviations

BEP	Best Efficiency Point
LDV	Laser Doppler Velocimetry
RPM	Revolutions per Minute
GPM	Gallons per Minute
FFT	Fast-Fourier Transform
DVM	Digital Voltmeter
SNR	Signal-to-Noise Ratio
HPU	High Pressure Unit
SDIU	Scanivalve Digital Interface Unit
GPIB	General Purpose Interface Bus
ROA	Receiving Optics Assembly
RMS	Root Mean Square

LIST OF FIGURES

1.1	Relationship Between Pump Geometry, Efficiency and Specific Speed
1.2	Comparison of Rotating Stall and Surge Head-Capacity Curves
1.3	Instability Criteria
1.4	Relationship Between Specific Speed and Characteristic Shape
1.5	Instability Map, ϕ_{cr} Versus B Parameter
2.1	Schematic of Test Facility
2.2	Properties of Plexiglass
2.3	Pump Inlet Geometry
2.4	Original and Modified Volute Comparison
2.5	Plenum Construction
2.6	Motor Assembly
2.7	Impeller Shaft Assembly
2.8	Pump Loop Water Transfer System
2.9	Global Instrumentation Map
2.10	Schematic of Scanivalve System
2.11	LDV Hardware
3.1	Pressure Tap Locations for Original Volute
3.2	Static Pressure Rise Along Pump Centerline (23% Speed)
3.3	Static Pressure Rise Along Pump Centerline (50% Speed)
3.4	Qualitative movement of the tongue separation streamline
3.5	Radial Pressure Variation at Volute Throat
3.6	Radial Pressure Variation - 10 Degrees Upstream of Throat
3.7	Radial Pressure Variation - 20 Degrees Upstream of Throat
3.8	Radial Pressure Variation - 30 Degrees Upstream of Throat
3.9	Pressure Differential Across the Tongue Tip
3.10	Component Pressure Contributions - 23% Design Speed
3.11	Component Pressure Contributions - 50% Design Speed
3.12	Slope Of Component Characteristics - 23% Design Speed
3.13	Slope Of Component Characteristics - 50% Design Speed
3.14	Diffuser Pressure Rise Coefficient versus Flow Coefficient
3.15	Tongue Wall Pressure Rise
3.16	Volute Sidewall Pressure Rise
3.17	Influence of Impeller Geometry on Stability

3.18 LDV Grid Locations
3.19 LDV Coordinate System
3.20 LDV Optics Arrangement
3.21 Streamwise Velocity Profile at Tongue Tip (ϕ = 0.102)
3.22 Streamwise Velocity Profile at Tongue Tip (ϕ = 0.042)
3.23 Cross-Steam Velocity Profile at Tongue Tip (ϕ = 0.102)
3.24 Cross-Steam Velocity Profile at Tongue Tip (ϕ = 0.042)
3.25 Radial Velocity Profile (θ = 5° and ϕ = 0.102)
3.26 Radial Velocity Profile (θ = 15° and ϕ = 0.099)
3.27 Radial Velocity Profile (θ = 30° and ϕ = 0.099)
3.28 Radial Velocity Profile (θ = 5° and ϕ = 0.05)
3.29 Radial Velocity Profile (θ = 15° and ϕ = 0.05)
3.30 Radial Velocity Profile (θ = 30° and ϕ = 0.05)
3.31 Tangential Velocity Profile (θ = 5° and ϕ =0.102)
3.32 Tangential Velocity Profile (θ = 15° and ϕ = 0.099)
3.33 Tangential Velocity Profile (θ = 30° and ϕ = 0.099)
3.34 Tangential Velocity Profile (θ = 5° and ϕ = 0.05)
3.35 Tangential Velocity Profile (θ = 15° and ϕ = 0.05)
3.36 Tangential Velocity Profile (θ = 30° and ϕ = 0.05)
3.37 Tangential Velocity Approaching the Tongue - (h=.25 and ϕ = 0.099)
3.38 Tangential Velocity Approaching the Tongue - (h=.5 and ϕ = 0.099)
3.39 Tangential Velocity Approaching the Tongue - (h=.75 and ϕ = 0.099)
3.40 Tangential Velocity Approaching the Tongue - (h=.25 and ϕ = 0.05)
3.41 Tangential Velocity Approaching the Tongue - (h=.5 and ϕ = 0.05)
3.42 Tangential Velocity Approaching the Tongue - (h=.75 and ϕ = 0.05)
3.43 Outlet Velocity Diagram
3.44 Trends in Slip Factor with Head Rise (50% Speedline)
3.45 Trends in Slip Factor with Head Rise (80% Speedline)
3.46 Trends in Slip Factor with Head Rise (100% Speedline)
3.47 Losses in Tangential Velocity with Reduced Flow (θ =5°)

4.1	Comparison of Volute Width
4.2	Blueprint of Modified Volute
5.1	Modified Volute Pressure Taps
5.2	Reynolds Number Effects on Performance Characteristic
5.3	Pump Characteristic - 23% Speedline, Modified Volute
5.4	Pump Characteristic - 50% Speedline, Modified Volute
5.5	Comparison of Original and Modified Volute Performance at 23% of Design Speed
5.6	Comparison of Original and Modified Volute Performance at 50% of Design Speed
5.7	Detail of Unstable Segment of Characteristic at 23% Speed
5.8	Detail of Unstable Segment of Characteristic at 50% Speed
5.9	Static Pressure Rise Along Pump Centerline (23% Speed)
5.10	Static Pressure Rise Along Pump Centerline (50% Speed)
5.11	Volute Throat Pressure Variations at 23% Speedline
5.12	Comparison of Tongue Tip Pressure Differential for the Original and Modified Volute Scroll (23% Speed)
5.13	Component Pressure Contributions - 23% Design Speed
5.14	Component Pressure Contributions - 50% Design Speed
5.15	Slope Of Component Characteristics - 23% Design Speed
5.16	Slope Of Component Characteristics - 50% Design Speed
5.17	Tongue Wall Pressure Rise
5.18	Predicted Pump Stability Map
5.19	Reduced Frequency vs. Air Volume in Plenum
5.20	Oscillation Frequency vs. Air Volume in Plenum
5.21	Experimental Pump Stability Map
5.22	Comparison of Volute, Tongue and Diffuser Performance for the Original and Modified Volutes
A.1	Fringe Pattern Diagram
A.2	Probe Volume Diagram

CHAPTER 1
INTRODUCTION

1.1 Problem Statement

Current trends in fuel systems for gas turbines and in hydraulic systems for rocket propulsion are towards higher pressure ratios and lower flow rates. This range of operation is met by low specific speed centrifugal pumps, which are capable of delivering a high power density while maintaining a conveniently small size (typical impeller diameters are about 3 centimeters). Specific speed is a characteristic number used to categorize pumps according the head rise and volume flow at their best efficiency points. The performance of geometrically similar machines, i.e., machines belonging to one family, is governed by similarity laws and may be represented for the entire family by non-dimensional characteristics. There are two forms of specific speed used in practice, a dimensional and non-dimensional form.

In non-dimensional form:

$$N_s' = \frac{n\, Q^{1/2}}{g\, H^{3/4}} \tag{1.1}$$

and in dimensional form:

$$N_s = \frac{(RPM)\, Q^{1/2}}{H^{3/4}} \tag{1.2}$$

In Equation (1.1), n is in rev/sec and the other quantities are expressed in a consistent manner. For Equation (1.2), Q is in gal/min and H is in feet. It turns out that specific speed is directly related to the most efficient pump design as shown in Figure 1.1. A low specific speed means a low Q and high H, hence a centrifugal pump, and a large specific speed implies an axial pump.

Much of the operating range of these pumps in an aircraft engine fuel system corresponds to flow conditions below 10% of the nominal design flow. These flight regimes include level cruising flight and approach for landing. In some applications low flow rates are accomplished through a bypass. However, the high power

densities of low specific speed centrifugal fuel pumps can cause fluid overheat in a bypass configuration. Therefore, direct throttling is required over the entire range of operating mass flow rates.

The major drawback of low specific speed pumps is that they become unstable at low flow rates, usually well below their best efficiency point (BEP). These instabilities occur in the operating regimes mentioned previously. Development tests showed these oscillations begin at flow rates below 40% of the design point and may reach amplitudes near 50% of the design pressure rise. Prolonged operation in this regime can be catastrophic for the fuel pump and the systems connected to it. These system instabilities (i.e. surge) result in a reduced operating mass flow range for low specific speed centrifugal pumps. To meet the demands of modern fuel systems, it is necessary to understand the nature of the fluid flow near the instability inception point and how this flow influences the shape of the head-capacity curve especially near shut-off. The results of this research will hopefully lead to improved designs for centrifugal pumps with a broader stable flow range.

1.2 Background

The nature of surge flow was first characterized in radial compressors in the 1950's by Emmons, Pearson and Grant [9]. In their paper, large scale instabilities called surge were differentiated from the localized flow fluctuations known as rotating stall. Figure 1.2 pictorially demonstrates the difference between surge and rotating stall on a pump characteristic. When a system experiences rotating stall it will continue to operate in an essentially steady state, averaged over the entire flow area, but the operating values of the head and capacity will be much reduced. During surge, the system exhibits large oscillations in head and capacity and will not return to a steady operating point on the pump characteristic.

Later studies of global dynamic flow phenomena were quite successful. The most notable was that by Greitzer [14], who determined a suitable parameter for estimating the possibility of surge. This parameter, called the B parameter, is the ratio of compliance to inertia in the pumping system. The compliant elements of the system can store energy through compression of a gas. The compliance in a real pumping system is a function of the compressibility of the working fluid and the deformation of the piping network resulting from pressure perturbations. The inertial elements are mostly the geometry of the piping sections. The B parameter in

a gas compression system can be expressed in terms of the geometric and physical system parameters as follows:

$$B = \frac{U_{tip}}{2\,a}\sqrt{\frac{V_c}{L_c A_c}} \tag{1.3}$$

A value of the B parameter below some critical value means the system will experience only static instabilities. If the B parameter is above the critical value, the system will experience dynamic instabilities or surge.

While the magnitude of the B parameter determines if surge can occur, a positively sloped pump characteristic is a requisite for dynamic instabilities. Figure 1.3 shows the physical mechanism for instability as developed by Greitzer [14]. On the positively sloped portion of the characteristic, the mass flow and pressure perturbations are in phase and the product of the two, the mechanical energy, is always positive. Due to an excess of energy, above that of steady state operation, perturbations will always grow in amplitude. On the negatively sloped portion of the characteristic there is a net energy dissipation so even with a high B parameter all perturbations are damped out. To summarize, surge can occur only when the mechanical energy input from the pump is greater than the energy required during steady flow. This situation can only occur when the characteristic has a positive slope. In light of this discussion of system instability theory Figure 1.4 shows clearly that low specific speed pumps are inherently unstable due to shape of their performance characteristics having a positive slope near shut-off.

The theories and models for dynamic system instabilities were developed for gas compression systems where the working fluid is compliant. However, the experimental facility where this research was conducted uses water as the working fluid and the compliance takes the form of variable volume air bags submerged within plenums. In the test facility, the B parameter scales as:

$$B \propto \frac{U_{tip}\sqrt{V_2}}{2\,L_p} \tag{1.4}$$

and is determined experimentally from the oscillations in pressure:

$$B = \frac{U_{tip}}{2\,\omega_{unst}\,L_p} \tag{1.5}$$

An alternative definition of the B parameter for a pumping system is given by Reference [30]. The B parameter for a pump is defined as the ratio of the time to fill the additional volume resulting from compressibility to the flowthrough time of the pump.

There were two major concerns during the development of the test facility: Could the results from the experiments on a pumping system be analyzed using the theory developed for gas compressors and would the lumped parameter model be valid for an experiment effort? The work by Goulet [13] and Bons [4] gives clear evidence that the theory as applied to gas compression systems holds even for an incompressible fluid such as water. In fact, the MIT facility proves the applicability of the lumped parameter model presented by Greitzer [14] to an actual pumping system by showing that the compliance can be lumped into a single parameter, such as the air in the plenums of the test facility, and its distribution in the system is irrelevant.

While many research studies have focused on the modeling of unsteady behavior of compression systems, there has been minimal effort in determining the internal flow character of pumping systems when operating near the instability inception point. As shut-off is approached, the flow field becomes highly three dimensional and dominated by viscous forces. The complex nature of the flow in typical pumps is not conducive to flow visualization studies without the use of expensive, non-intrusive laser velocimetry equipment and large scale pump models. Many researchers thought of the volute merely as a "collector" and not contributing much to the pump performance. Consequently, during the past three decades emphasis has been placed on measuring and modeling flow in the impellers and the other components of the pump have been neglected. In more recent years the use of low specific speed pumps has increased widely and attention has been focused on improving their range of performance. Worster, in a paper on volute and impeller interactions [29], commented that "pump behavior near zero delivery is the greatest problem facing the pump designer today."

In a paper published in 1936, R.C. Binder and R.T. Knapp [3] characterized some basic volute flow phenomena through pressure and velocity measurements. Binder and Knapp used a single suction Worthington centrifugal pump which had a geometry similar to the MIT turbopump facility. The Worthington pump had a specific speed of 1720 and measurements were made at low, normal and high flow coefficients. This research noted the strong influence of the leakage flow and how it acted as an energy pump to minimize losses. Binder and Knapp also found wide

variations in radial velocity between normal capacity and low flow conditions. These variations were especially evident near the tongue region where an outward radial velocity at normal flow becomes a radially inward flow at low capacity. Also discussed by Binder and Knapp was the angle of the relative exit velocity from the impeller. The slip factor, which is the ratio of the actual impeller tangential discharge velocity to the theoretical impeller tangential discharge velocity, remained constant around the volute for each flow rate except at off design conditions in the region of the tongue.

A similar study by Bowerman and Acosta in 1956 [5] demonstrated the effect of the volute on the impeller performance. This study showed that there was only a small range of flow rates where the volute and impeller were matched and that the volute influenced the performance by effecting the impeller operation rather than through the addition of losses. Bowerman and Acosta theorized that each volute shape caused a different loss distribution within the impeller.

In 1963, Worster [29] published a detailed study on the effects of volutes on centrifugal pump performance. In low specific speed pumps, Worster showed that the losses due to skin friction are very important. The head loss due to skin friction can be estimated by:

$$\frac{\Delta h_f}{H} = c_f \frac{u^2}{2gH} \frac{S}{A_0} \tag{1.6}$$

Comparing two pumps of different specific speeds shows that the friction losses in a pump with N_s= 550 are 22 times larger than for a pump with N_s= 3500. Thus minimizing the ratio of volute surface area to volute throat (discharge) area and the velocity in the volute will reduce the friction losses. Worster also found that volutes having a logarithmic spiral and an Archimedean perform similarly. This similarity suggested that the ideal volute shape might be somewhere in between these two curves. Commenting on Worster's paper, Dr. B.S. Massey noted that for a volute of trapezoidal cross-section the equation for the outer surface of the volute should take the form

$$\theta = k_2 r + k_3 \ln \frac{2r}{D_2} + k_4 \tag{1.7}$$

where k_2, k_3 and k_4 are constants. The shape that this equation represents is an intermediate curve between an Archimedean and logarithmic spiral. Worster does not give any methods for accurately predicting the head rise and characteristic shape near shut-off.

A more recent study by Frost and Nilsen [12] developed a method of predicting the shut-off head of centrifugal pumps and fans. This work stated that the shut-off head was relatively insensitive to the number of vanes, the blade discharge angle and the impeller width. The results of Frost and Nilsen's computations showed that increasing the radial extent of the volute with a fixed impeller geometry and angular velocity will increase the shut-off head leading to greater stability. This approach agrees with Worster's formula for the friction losses which showed the loss due to friction scales as the square of the volute velocity.

1.3 Goals and Objectives

The ultimate goal of this research is to improve the stability range of low specific speed centrifugal pumps. In order to accomplish this task the nature of the flow near the instability inception point must be determined. The prominent features of the flow as the slope of the head-capacity curve becomes positive should give some insight into the fluid mechanical sources of the instability. Second, the influence of these flow phenomenon on the shape of the pump characteristic near shut-off must be evaluated. Finally, the unstable pump component can be isolated and redesigned leading to greater stability. The research work was broken down into the following series of conquerable objectives:

1.) Determine the contributions of each pump component to the overall pump characteristic in terms of pressure rise.

2.) Evaluate the influence of each component on the slope of the pump characteristic.

3.) Identify the component with the largest contribution to the positive slope of the steady state characteristic.

4.) Understand the interactions of the internal flows within the unstable component as the pump is throttled.

5.) Qualitatively determine the relationship between the flow structure and the shape of the pump characteristic.

At this point in the research, the experimental results were used to validate and improve a volute/impeller interaction code. The model was then used to predict the effects of geometrical modifications to the impeller and volute. A detailed parametric study was conducted to determine the optimum shape of the volute scroll. This study formed the basis for modifying the pump to improve its stability characteristics. The results of the computational research are presented in Reference [6]. In conjunction with the computational effort, there was an additional objective to the experimental research:

6.) Provide experimental data to verify and improve the computational model.

In summary, the goals of the research conducted were to understand the nature of the fluid flow mechanisms responsible for surge, determine how these flow phenomena effect the shape of the pump characteristic at low flow conditions and to redesign the pump to improve its range of stable operation.

1.4 Research Plan

The first step in determining the nature of flow instabilities near shut-off was to understand the effects of each individual component of the pump. The individual contributions were broken down into component head rise and component slope. The components studied for this thesis were the impeller, volute, tongue and diffuser. The performance of each of these components effects every other component. It was therefore necessary to define the characteristic of each component separately in order to quantify their individual contributions. The definition of the "tongue region" is actually a measure of the combined interactions of the diffuser, volute, tongue and impeller, for in this region these components all interact simultaneously. Since a positively sloped pump characteristic is a requisite for surge, the contributions of each component to the characteristic slope were quantified and the component(s) responsible for instability were identified. The

measurement of the steady-state component characteristics for the original pump geometry was accomplished using water manometers.

The component identified for its global contribution to the positive sloped characteristic was the focus of a detailed velocity mapping. Using laser velocimetry techniques the velocities were measured at three flow coefficients. Two flow coefficients were on the negative sloped portion of the pump characteristic, one at high capacity and the other close to the maximum point of the characteristic. The third flow coefficient was on the positive sloped portion of the head-capacity curve. This choice of mapping variables facilitates a comparison of the nature of the flow as the instability inception point is approached. The data was examined for trends and variations with angular position in the volute and flow coefficient. The overall character of the flow was compared to References [5,3,12,29] to validate the results and interpretations were made to determine the mechanism of surge.

The computer model was then run, by Ciacci [6], with the same pump parameters and geometry. A comparison was made to verify that the predicted and measured data agree. Once the validity of the model had been established, a parametric study was conducted to determine an optimum pump geometry. The goal of the parametric study was to find a geometry which would have a negative slope over much of the throttling range. From this new characteristic, a second computer model was used to calculate the pump stability map. This map shows the flow coefficient where surge will begin for a given B parameter. A sample stability map is given in Figure 1.5. It is important to notice that there is a lower limit to the B parameter. A system B parameter lower than this limiting value means the pump will remain dynamically stable regardless of the slope of the pumping characteristic.

The optimum geometry determined by the computer model was then used to construct a new volute scroll. A second set of tests were run to check the performance predictions of the model. The steady state pressure contributions were determined. A comparison to those of the original geometry was made to see how the volute modification effected the pump components and performance curve. The stability map of the modified pump was determined to see if any real improvements were made to the range of stability.

1.5 Organization of Research Report

The following section outlines the organization of the findings and the presentation of the research conducted in the remainder of this research report.

Chapter 2 gives a brief overview of the MIT centrifugal pump experimental facility. The construction of the individual pump components and technical specifications are discussed as well as the layout of the facility. The instrumentation used to determine the global pump parameters and the pressure and velocity measurements is presented. Finally, the computer hardware and software, both the commercially available and the custom written, used in the data acquisition system are discussed.

Chapter 3 presents the results of the steady state pressure contributions of the various pump components with the original volute. The experimental procedure and setup is discussed. The component contributions to the head rise and characteristic shape are evaluated and the influence of these components on the shape of the pump characteristic is determined. Localized pressure features are discussed concentrating on the pressure variations in the tongue region. The laser setup and the experimental procedures are presented. The LDV measurements are presented and the nature of the flow structure in the volute is discussed. The relationships between the velocity measurement and the pressure measurement are presented. Finally, the losses in the pump system due to the mixing and slip are discussed

The re-design of the volute is covered in Chapter 4. This section gives a brief description of the parametric study done using the volute/impeller interaction code which was performed by Ciacci [6]. The basics of the fluid mechanics of the solution is presented.

Chapter 5 discusses the steady state characteristic of the modified pump and compares this to the original geometry. The overall pressure rise and efficiency of the two pumps are discussed and the magnitude of improvement is presented. The stability map is compared with the computer predictions and the experimental results from the original pump geometry. The agreement with the model and the realized improvements are discussed.

Chapter 6 provides a summary of the research conducted presenting the major highlights and accomplishments. Recommendations are presented for future work in the area of centrifugal pump stability.

CHAPTER 2
THE M.I.T. CENTRIFUGAL PUMP FACILITY

2.1 Centrifugal Pump Facility Overview

As shown in Figure 2.1 the experimental centrifugal pump facility spans two floors of the MIT Gas Turbine Laboratory. The pump's test section is located on the second level and has a vertical inlet and horizontal discharge. The discharge piping is 8" PVC which empties into a small plenum located on the first level. The small plenum contains variable volume innertubes which comprise the system compliance. The ducting exiting the small plenum is split into a main and bypass channel. Each channel has a separate throttle for controlling the flowrate of the pump. These two channels merge before connecting to the larger inlet plenum. The inlet plenum is also equipped with variable volume air containers and the B parameter of the system is regulated by varying the air volume in both containers. The exit pipe from the inlet plenum is 12" PVC and leads vertically upward to the pump inlet. The entire facility is constructed in a modular fashion to allow for geometrical modification of individual pump components.

2.2 Pump Components

The test section consists of five components, the volute, impeller, diffuser, transition insert and inlet. Each component is constructed from Plexiglass stock. Plexiglass was chosen over Lucite and Lexan because it has a higher Young's Modulus and flexural strength as well as a smaller thermal expansion coefficient. For optical transmittance, Plexiglass is superior to Lexan and comparable to Lucite. The properties of Plexiglass are given in Figure 2.2.

The impeller is a single suction, shrouded variety. It has an outer diameter of 61cm (24 in.) and an inlet diameter of 20 cm (8 in.). The impeller consists of four full blades and four splitter blades with a backswept discharge. The discharge angle, β_2 , is approximately 34 degrees and the discharge height, b_2 , is 0.59".

The inlet tube serves as a wear ring for the sleeve seal as shown in Figure 2.3. The inlet pipe has a contraction with a half angle of 16 degrees.

The volute is a single vaneless scroll with a rectangular cross section. The original volute geometry has a circumferential profile comprised of four circular arcs. The modified volute is comprised of two parabolic arcs. Both volutes have the same throat area, recirculation area and tongue geometry. The main difference between the two shapes is that the modified volute has a rapid expansion downstream from the tongue followed by a slowly increasing cross section. This geometry provides a greater radial extent to the volute over a larger angular portion of the scroll. Figure 2.4 shows a comparison sketch of the two volute shapes.

After the volute exit is a transition insert where the cross section changes from rectangular to circular. The pipe diffuser is conical and the Plexiglass fabrication provides for easy viewing of flow distortions. It has a half angle of 4 degrees and an area ratio of 1.7:1. The diffuser discharges into 8" PVC ducting.

The plenums are constructed from 5/8" thick 5083 aluminum plate. The small plenum is designed to hold 3 innertubes and has a maximum internal air volume of 500 liters. The large plenum has a maximum internal air volume of 1000 liters. Figure 2.5 shows the construction and layout of the plenums. The inlet plenum volume is large enough to uncouple any perturbations from recirculating within the pump.

The motor used to power the pump is a 15 hp, 4 pole A/C drive. An adjustable frequency A/C drive controller is used to vary the wheel speed over the desired range from 0 to 450 RPM. Noise and vibrations are reduced by mounting the motor on the ceiling above the pump and running it in a direct drive configuration. This arrangement eliminates possible vibrations caused by a belt transmission. The motor set-up is depicted in Figure 2.6. Two couplings, a fixed sleeve and a flexible coupling are used to transmit torque. The impeller shaft is hollow to allow for rotating frame pressure measurement via a slip ring assembly as shown in Figure 2.7. Three ports on the bearing housing below the lip seal allow the measurement of the back plate leakage flow. This flow is collected in a manifold and reinjected into the inlet pipe. The leakage flow was shown to be significant near shut-off during development test of the original High Pressure Unit.

The throttling of the pump is accomplished through one 8" butterfly servovalve and a 1" ball valve also servo actuated. Both valves have positioning systems that enable a prescribed voltage to be input with automatic position hunting that ensures better repeatability.

The transfer system shown in Figure 2.8 is designed to contain the entire pump water volume for storage during modification and down time. The system consists of five valves, a pump and a storage tank.

2.3 Instrumentation

The instrumentation discussed here includes both that for the global pump performance measurements and that for detailed local component evaluation. For measuring the global pump performance, there are two flowmeters. One flowmeter is used for evaluating the flow in the discharge pipe and the second is to measure the backplate leakage flow. There is also a torque meter and a RPM meter. For the localized pressure and velocity measurements a Laser Doppler Velocimetry (LDV) System is employed as well as water manometers and a Scanivalve system. Figure 2.9 sketches the location of the instrumentation used for this research.

2.3.1 Global Performance Measurements

The volume flow rate of the pump is measured using a Yokogawa ADMAG Series AM220 8" magnetic flow meter. This meter was placed in the discharge duct approximately 2 meters downstream from the diffuser outlet. The ADMAG internal electrodes are sampled at 75 Hz and the measured electric field has a magnitude which is proportional to the water volumetric flowrate. The response time can adequately resolve the low frequency flow oscillations of 0.4 Hz which are characteristic of the test loop. The accuracy is stated by the manufacturer to be 0.5% of the flowrate between 150 and 1500 GPM. Below 150 GPM the accuracy is $\pm$0.75%. The magnetic flow meter is well suited for measurements in unsteady flows for it is only weakly dependent on the velocity profile. It is also capable of measuring reverse flows and its variable current output is easily interfaced to the data acquisition system.

The back plate leakage flow is measured by an Omega FP5300 1 1/4" turbine flow meter. The meter is located after the collection manifold. The signal from the turbine flow meter is processed using an Omega FPM704A Digital Indicator. In the research presented by Reference [4] it was shown that the leakage flow only varies by 10%. Given the difficulty of sampling the turbine flowmeter at high frequencies, the output is manually keyed into the computer as a time averaged value. The total

flowrate through the impeller is the sum of the back plate leakage and the discharge duct flow.

The shaft torque is measured by means of a Lebow 1604 Torque Sensor. The signal is processed through a Lebow 7540 Strain Gage Indicator and fed into the data acquisition system. The impeller rotational frequency is measured using a Lebow 1604 Rotary Transformer and the same strain gage indicator. The output is calibrated using a standard stroboscope.

2.3.2 Scanivalve Pressure Measuring System

The measurements made on the original volute geometry were acquired using a standard 4 ft. water manometer board. This board was pressurized on the "atmospheric" side to allow for a greater range of impeller speed settings. This method allows measurements to be made at speeds up to 50% of the design speed.

Subsequently, a model DSS-48C7/MK4 Double Scanivalve System was purchased for water scanning applications. The model DSS is capable of multiplexing differential pairs of static and slowly varying pressures. This system is able to scan 48 differential pairs of analog pressures or 96 individual pressures (two modules of 48) at rates up to 8 ports/second. The Scanivalve modules are precision, rotary pneumatic selectors with extremely low internal volume. The Scanivalve modules and channel encoder are synchronized to a stepper motor drive and to each other by a common shaft and timing belt. The channel encoder provides an absolute digital address for each input position. The individual Scanivalve modules are model CX123, which are capable of being connected to customer furnished transducers. Figure 2.10 gives an exploded view of the Scanivalve cabinet.

The transducers selected for the Scanivalve system are Validyne model P305 differential pressure transducers. These transducers provide DC input and output with a wet-wet capability. The transducers accept an 11-32 VDC input signal, and output a 5 VDC signal which is proportional in magnitude to the measured pressure differential. The accuracy of these transducers is stated by the manufacturer to be $\pm$0.25% full scale, including linearity, hysteresis and repeatability. They can be overpressured up to 200% full scale with less than a 0.5% zero shift. Both zero and span adjustments are provided under the cover.

The analog to digital conversions and host computer control are accomplished with a Scanivalve Digital Interface Unit (SDIU). The SDIU allows the host computer to communicate via either RS-232 or IEEE-488. Local control and display of data

are possible through the front panel. The SDIU is designed to accept optional A/D cards. With the A/D card, the SDIU automatically acquires data and corrects each analog transducer output signal for zero offset and span. The SDIU retains data in two types of memory, thus minimizing the time the host computer is dedicated to the Scanivalve. The host computer may acquire data at any time in one of several formats. This data can then be sent to the host computer while the Scanivalve continues to acquire data uninterrupted. The SDIU can hold up to 6 A/D cards, thus servicing a total of 12 scanning modules.

2.2.3 Laser Doppler Velocimeter System

For detailed localized velocity surveys, a Laser Doppler Velocimeter is used. This system uses a Lexel Model 95 Argon-Ion Laser. Argon ion lasers produce the highest visible power levels and have up to ten lasing wavelengths in the blue and green spectrum. The most prominent wavelengths are the 514.5 nm green line, which is 43% of the power, and the 488.0 nm blue line, which is 20% of the output power. Two colors are used to resolve velocities in two spatial directions. The laser output is 4 watts maximum and it is cooled by supplying a minimum of 2.0 gpm of water at 20 psi. The power output is regulated with a Lexel power supply though either the current or light control knob. The light control knob provides greater power stabilization by splitting off a portion of the output beam and measuring the power in a photocell.

The signal processing is performed by a TSI model 1990C Counter-type Signal Processor. This processor provides accurate measurements on short bursts of data such as the Doppler signal used in laser velocimetry. The 1990C measures the time taken for a given number of cycles in a Doppler burst using a high resolution clock ($\pm$1 ns). The processor has both a high and low pass filter with a total of 24 settings. The 1990C has a resolution of 0.25% at 40 MHz and 1.25% at 200 MHz.

The probe volume movement is controlled by a Model 9400 Mirror Mount Traverse System. This system allows for movement in three linear directions. The Model 9430 Position Controller is a microprocessor controlled stepper motor drive. This controller is interfaced to the host computer through a RS-232 interface and is software driven. The LDV Traverse System has the following specifications:

Axial	Travel	Precision

x	600 mm	0.01 mm
y	600 mm	0.01 mm
z	600 mm	0.01 mm

A Model 1980 Frequency Shifter is used to increase the range of the LDV system. The optics module contains an acousto-optics cell (Bragg Cell) to shift the light beam frequency a fixed 40 MHz. The cell is driven by a 40 MHz, 2 watt signal provided by a power amplifier located in the electronics module. The electronic module also contains downmix circuitry. A frequency shift of 40 MHz is often too large, and downmixing allows the decreasing of the effective frequency shift of the photodetector output to values from 2 kHz to 10 MHz.

A model 9160 photomultiplier system is used to amplify the signal before being conditioned are processed. The specifications for the photomultiplier are:

Tube Type	RCA 4526
Quantum Efficiency	632.8 nm, 13%
	500 nm, 22%
Cathode Sensitivity	300 microamperes/lumen
Overall Sensitivity	40,000 V/lumen
Aperature Diameter	2 mm
Bandwidth	200 MHz

A sketch of a typical LDV system set up in backscatter mode is given in Figure 2.11.

2.4 Data Acquisition and Processing

2.4.1 Computer Hardware

The data acquisition system is composed of two personal computers, an IBM PC-AT and an Apple Macintosh SE. The IBM computer is used for instrument control and data acquisition and the Macintosh is primarily used for data analysis and presentation. The PC is equipped with several expansion boards. The analog voltage signals from the flowmeter, torque meter and shaft encoder are processed to digital signals using a Data Acquisition DT2801 board. This I/O board has an A/D throughput of 13.5 kHz and 16 single ended or 8 differential channel inputs. The DT2801 board comes with PCLAB software which provides callable routines for

several programming languages. For control of the Scanivalve system, an Omega MBC-488 General Purpose Interface Bus (GPIB) board is used. This board allows for instrument communication with up to 15 devices. Control is accomplished by opening the GPIB as both an input and output file, and writing and reading to this file through a programming language. The LDV system uses a model 1998K Interface module provided by TSI Inc. to transfer data from the counter to the IBM PC.

The data acquired on the PC is then transferred to the Macintosh through a DaynaFile Drive. The DaynaFile can read both PC and Apple formatted diskettes. Final data analysis is done on the Macintosh using Kaliedagraph software.

2.4.2 Computer Software

The instrument control and data analysis of the LDV surveys are processed through the TSI Data Analysis Software. The software allows control of the counter systems. Since the software is written in BASIC, it is easily modified to match individual needs. A traverse controller option was added to the main menu of the program MENU.BAS, to allow fast, accurate movement of the probe volume throughout the entire grid network. The data output is customized to allow the velocity data to be graphed using the Kaliedagraph software on the Apple Macintosh computer.

The Scanivalve control and data acquisition is monitored through a computer code, PRESCAN5, written in BASIC for IBM PC compatibles. This code uses the file read/write functions of the GPIB to acquire the data from the SDIU. The program allows the user to perform two separate data acquisition options. First, there is an option for taking steady state component data. This option scans all pressure taps and calculates a time averaged performance characteristic for each. The second option allows the user to scan only the discharge pressure at a prescribed frequency (up to 8 Hz) for a specified time period. The code then determines both the time averaged and time resolved measurements along with the frequency of the system unsteadiness. The source code and a discussion of the PRESCAN5 program is presented in Appendix B.

The data reduction for the water manometer measurements is performed with a code PH2O written by Dr. Andrew Wo, a post-doctoral researcher working on the centrifugal pump stability research. The user inputs the manometer readings and the code performs the data reduction and presents the results in non-dimensional form.

2.5 Facility Preparation

The procedure followed for preparing the centrifugal pump facility for measurements is relatively simple. The pump throttle is opened fully. This setting corresponds to a readout of 3.05 volts on the DVM. The pump is turned on and brought up to a high enough speed to establish a leakage flow, roughly 50% of the design speed. Air trapped in the clearance space above the impeller can be bled off as the pump is being brought up to speed by opening the valve in leakage flow line. Once the leakage flow has been established, the pump is brought to the desired speedline. The RPM readout is not zeroed and a reading of 247 corresponds to an actual speed of 50% design (210 RPM).

The measurements can now be taken for the first throttle setting. The throttle is closed in small increments down to 0.5 volts. This covers the entire range of flow coefficients. The throttle must be fully opened again before any new measurements are made. This is to release trapped air in the impeller which builds up during low flow conditions. It is a suggested that the pump be run for two hours before making measurements to let all the dissolved gases come out of solution naturally.

When the pump is being emptied or filled it is important to open the red valve at the top of the discharge stack to allow air to enter and/or escape. When filling the pump valves 1,4 and 5 are opened and the rest are closed. When draining the pump into the tank valves 1,4 and 6 are opened. If the entire system is to be emptied into the sewer, valves 1, 2, 4 and 6 are opened.

CHAPTER 3
STEADY-STATE EVALUATION OF ORIGINAL VOLUTE

3.1 Experimental Procedures

The head rise contributions of the various pump components were evaluated using water manometers. The manometers were a suitable choice of measuring instruments for steady state applications and in fact provided an added visual element which electronic pressure measurement devices did not. The first step towards understanding the flow mechanisms which govern the shape of the head-capacity curve was to characterize what happens to the pressure of the fluid as it traverses the pump from inlet to discharge. The highly three dimensional nature of the flow and the high degree of component interaction makes quantifying the extent to which each component contributes to stability difficult. The components that were evaluated include the impeller, volute, tongue and diffuser as well as the overall pump performance characteristic.

The pressure tap numbering designations for the original volute geometry are given in Figure 3.1, which is a top view of the pump test section. There are 12 taps located along the centerline of the volute channel. In the section of the volute just upstream of the cutwater is a high concentration of taps which were used to determine the radial pressure variations in the tongue region. The taps closest to the impeller were designated as "B" and the taps near the outer wall were denoted by the letter "D". The tongue itself has four taps and the outside volute wall opposite the tongue contains eight taps. These taps should give evidence of flow separation along the walls in the tongue region if it should occur. Continuing down the centerline of the pump, there are 4 additional taps in the transition region, where the geometry of the scroll changes from rectangular to circular. Finally, there are 6 pressure taps along the midline of the diffuser. Not shown in this figure are eight pressure taps located circumferentially around the inlet pipe, the pump inlet tap which is located approximately 1 meter below the floor line and the pump discharge tap which is located about 1.5 meters downstream of the diffuser exit.

Each pressure tap has a non-dimensionalized head rise defined by the static pressure difference between that tap and the pump inlet pressure. The component characteristics are defined by the pressure rise from inlet to outlet of a given component and are based on the tap numbering system just described. The somewhat arbitrary definitions of the component characteristics are:

1.) Impeller	V1 - Inlet
2.) Volute	V7 - V1
3.) Tongue	TR1 - V7
4.) Diffuser	Exit - TR1
5.) Overall	Exit - Inlet

The pump was run at both 23% and 50% of the design speed of 420 RPM. The use of water manometers limited the range of the design speeds that pressure measurements could be made to 50% and below. Above 50% of the design speed, the pressure rise would be to large for the 4 feet tall manometers to handle. The open end of the manometers had to be pressurized to allow for measurements at 50% design speed. Operation of the pump at 23% of the design speed is desirable since the Reynolds number is matched with the prototype pump. In determining the non-dimensional pump characteristic, there are some variations with impeller speed caused by Reynolds Number effects. The Re effects are discussed further in Chapter 6.

3.2 Steady-State Pump Parameters

The following table lists the values of the major pump parameters at BEP for the two speeds evaluated.

	50% Speed	23% Speed
N_s	601	628
Q (GPM)	221.33	108.48
Torque (in-lb)	165.68	36.92
η	0.88	0.86
ψ	1.228	1.1926
ϕ	0.075	0.078
Ω (RPM)	203	96.6
Re	9.6E4	4.57E4
U_{tip} (m/s)	6.47	3.08
ΔP_{total} (psi)	3.73	0.82

The definitions of these terms are given in the section entitled List of Symbols. There are some differences between these values and those of the previous work presented in [4,13]. The major reason is the impeller discharge height, which was scaled incorrectly in Reference [4]. Since then, a new impeller has been constructed with the proper impeller discharge height. There are however still discrepancies between the data on the developmental pump and the MIT model. These inconsistencies are attributed to the difference in surface roughness between the two pumps.

3.3 Static Pressure Rise Through the Pump

The centrifugal pump used in this research was designed for a constant pressure in the volute. Volute design is accomplished by prescribing an area distribution so that the volute area increases in proportion to the increase in mass flow such that,

$$A(\theta) = \frac{Q\theta\bar{r}}{2\pi u r} \tag{3.1}$$

Designing a pump using this theory has drastic ramifications on the flow at off design conditions. Since the flow in the volute matches the geometry only at the design flow rate, there are large losses due to hydraulic effects during off design operation. These off design effects are seen in Figures 3.2 and 3.3, which show the static pressure rise around the volute at 23% and 50% of the design impeller speed. The pressure rise is plotted against a non-dimensionalized linear distance around the centerline of the pump. On these figures are data curves for four flow coefficients. A flow coefficient of $\phi = 0.103$ is close to the design point. The other three flow coefficients correspond respectively to flows with the throttle wide open, and on the negatively and positively sloped portion of the characteristic close to the peak pressure rise.

With the throttle wide open a sudden pressure drop occurs in the region before the tongue ($0.52 < X/L < 0.7$). At lower flow rates there is a sudden rise in pressure in this same region. This phenomenon might be explained by the movement of the tongue separation streamline. At high flow rates, the separation streamline forms a nozzle type contraction causing the flow to accelerate prior to the transition

insert, thus the drop in pressure. At lower flow rates, the separation streamline moves out into the volute creating a diffuser type geometry thereby decelerating the flow and increasing the pressure. Figure 3.4 shows the movement of the separation streamline qualitatively as the throttle is closed. The flow pattern around the tongue is similar to that seen at the leading edge of an airfoil. At high flow, the angle of attack is large and a separated region is seen on the suction surface. At low flow rates, the angle of attack is small and/or negative and a potential for separation on the pressure side exists. This variable flow pattern around the tongue effects the environment the diffuser operates in and is a potential cause of diffuser performance degradation. The performance characteristic of the tongue and diffuser will be discussed later in this chapter.

The shape of the pressure rise curves given in Figures 3.2 and 3.3 show an interesting feature in the volute (V1 to V7) section. At high flow rates, this curve is "parabolic" and concave upward. However, at low mass flow, the shape of the curve seems to be a "periodic" function with a minimum occurring at tap V5 (x/L = 0.35) and a peak at V2 (x/L = 0.106). The V2 tap is 60.4 degrees downstream of the tongue and the V5 tap is 195.4 degrees downstream from the tongue. This circumferential pressure variation in the volute could be a result of the mismatch between the area distribution and the mass flow at off design conditions. It is interesting to note that the time is takes for a fluid particle moving with the mean volute flow to travel from the tongue tip to the volute throat is on the order of 2 impeller revolutions at all flow rates. Thus each time a particle experiences a maximum in pressure, the impeller is in the same angular position. It is clear that the pressure perturbations at the tongue are propagated both upstream and downstream where they show up as an oscillating pressure rise in the volute. The flow exiting the impeller is reduced in the neighborhood of the tongue, therefore, there must be a corresponding increase in the flow rate at other portions of the volute. Because the pressure is non uniform around the volute circumference, the losses will also vary with angular location.

3.4 Radial Pressure Gradients in the Volute

In modeling the pump behavior, a simplified mathematical approach is adopted. The volute/impeller computer code assumes that the radial variations of pressure and velocity in the volute are small. Even though the error in such an assumption is small $\Delta\psi/\psi$ = 5% [4], this assumption is a contradiction of the

conservation of angular momentum. Physically these second order effects are important and should be included in the model if it is to be used as an accurate predictor of the pump performance characteristic. The radial pressure taps in the tongue region of the volute provide some insight into the magnitude of these pressure gradients.

3.4.1 Volute Throat

At high flow rates, Figure 3.5 shows that the pressure decreases across the width of the volute throat from the tongue to the periphery. The impeller jet exiting into the center of the volute channel is being diffused by the mixing process and the static pressure gradient is transmitted through the boundary layer. As the throttle is closed, this pressure gradient becomes smaller until at the design flow coefficient there is no radial pressure gradient. A further reduction in mass flow showed the opposite pressure gradient. The fluid is passing over the tongue suction surface smoothly. The pressure is now increasing across the volute. The flow tends to be re-circulated in the volute rather than exiting through the diffuser. Re-circulation causes the overall head to be reduced and as the throttle is closed, the magnitude of the reduction increases due to the increasing inlet pressure. The magnitude of the radial pressure difference at the throat varies between $0\% < \psi_{BEP} < 4.2\%$.

These variations in the throat radial pressure gradient suggest some degree of flow separation in the transition/diffuser combination. With the throttle open, the results of hydrogen bubble measurements presented in [4] showed that there was a region of intermittent backflow or separation along the tongue outside wall. Near shut-off, the region of backflow and/or separation moved to the outside wall of the volute, thus "forcing" the flow back towards the tongue. The large region of separated flow at low flow rates is evident in Figure 3.5 where the radial pressure gradient disappears near shut-off, indicating a flow stagnation region.

3.4.2 Upstream of the Throat

The static pressure rise around the pump which was discussed in Chapter 3 indicated that there were some unusual pressure variations in the circumferential direction at off design flow rates just upstream of the tongue. Figures 3.6 through 3.8 show the radial pressure differences at 10, 20, and 30 degrees upstream of the tongue. In Figure 3.6, the pressure increases in the radial direction for the entire

range of flow coefficients. The clearance space beneath the impeller and shroud allows flow to leak back into the inlet pipe through a rotating seal. This shroud leakage most likely influences the pressure gradients around the volute scroll. In Figures 3.7 and 3.8 the pressure difference is constant with flow coefficient. At 30 degrees upstream of the tongue the pressure gradient is much larger than at 10 degrees. Just upstream of the tongue at the 10° station, the magnitude of the radial pressure difference varies from 0% of the BEP head rise when the throttle is wide open to 3.36% of ψ_{BEP} near the peak pressure rise. In comparison, at 30° upstream of the tongue, this variation is a maximum at high flow (roughly 6.9% of ψ_{BEP}) and a minimum near shut-off.

With the throttle open, the radial pressure difference decreases as the flow approaches the tongue. However, at low flow rates, the radial pressure increases in magnitude as the flow nears the tongue. This behavior shows the difference in flow patterns on the stable and unstable segments of the performance characteristic and suggests a highly vortical flow in the volute.

3.5 Tongue Pressure Differential

An interesting feature of the tongue region is the pressure difference across the tip of the tongue. Figure 3.9 is a comparison of the pressure taps located on either side of the tongue for the pump running at 23% of the design speed. Tap V0 is located on the impeller side of the tongue and tap V11B is located on the diffuser side (see Figure 3.1). At high flow rates the pressure on the impeller side of the tongue is higher. As the throttle is closed, the pressure on this side is reduced until at a flow coefficient of 0.117 the pressures on either side of the tongue are equal. This flow coefficient must correspond to the design point. At lower flow rates the diffuser side pressure is much higher.

The shape of the V0 pressure characteristic gives an idea as to how the impeller is performing. When the pump is throttled back, the pressure rise at this location decreases. The impeller is probably pumping more fluid than the volute can handle and the flow is accelerating through the passage. Near shut-off, the fluid in the volute and moves in a solid body rotation. Hence the leveling off of the pressure rise as the flow rate is decreased.

3.6 Component Pressure and Slope Contributions

The contributions of each pump component and the overall pump performance characteristic are plotted in Figure 3.10 for 23% design speed. Figure 3.11 shows the same data for 50% of the design speed. A fifth order polynomial curve fit to the experimental data is shown as the lines. Such a curve fit is justified by two different studies [15,20] and the prior research performed at the MIT centrifugal pump facility. These studies show that there are significant random "presurge" oscillations that occur just prior to the instability inception point. Thus, local features of the steady-state performance characteristic are effectively "smoothed out" by the wandering pump operating point. The higher order curve fit will pick up these localized perturbations in the characteristic and will give a more accurate curve slope. The slopes of each component characteristic, derived from the curve fits, are plotted as functions of the flow coefficient in Figures 3.12 and 3.13 for the two speedlines considered. At 23% speed, $\partial\psi/\partial\phi = 0$ occurs at $\phi = 0.55$ and at 50% speed, $\partial\psi/\partial\phi = 0$ occurs at $\phi = 0.58$. The critical flow coefficient for instability occurs at flow rates less then the peak pressure rise flow rate. This is due to the averaging effect of the limit cycle behavior.

3.6.1 Diffuser

The shape of the diffuser characteristic shows that the pressure rise in the diffuser becomes negligible near shut-off. This shape can be easily understood by realizing that the maximum pressure rise in the diffuser is given by,

$$\Delta P_{st,\,diffuser} = \frac{1}{2} C_p \rho U_{in}^2 \tag{3.2}$$

where U_{in} is the velocity of the fluid entering the diffuser. The pressure rise coefficient can be evaluated in terms of the experimental data by solving Equation (3.2) for C_p and substituting in the definition of the non-dimensional pressure rise coefficient:

$$C_p = (\psi_{DF6} - \psi_{TR1}) \frac{U_{tip}^2}{U_{in}^2} \tag{3.3}$$

Figure 3.14 shows the experimentally determined pressure coefficient plotted as a function of the flow coefficient. The pressure rise coefficient is a constant function

equaling 0.55. Since the best a diffuser can do is recover approximately 70% of the dynamic head at its entrance, there is some possibility for improvement of the diffuser in terms of the head rise.

From the standpoint of increasing stability, refinement of the diffuser would be fruitless. Figures 3.12 and 3.13 both show that while the diffuser always has a positive sloped characteristic, the magnitude of the slope decreases with flow coefficient such that $\partial\psi/\partial\phi$ of the diffuser approaches zero near shut-off.

3.6.2 Tongue Region

The shape of the tongue region performance characteristic can be understood in terms of the arguments presented in Section 3.3. The pressure drop in this region at high flow rates is caused by the location of the tongue separation streamline producing an acceleration of the flow just past the tongue. As the throttle is closed, the separation streamline moves out into the volute channel until at the BEP, the streamlines are matched to the scroll geometry. Further throttling causes a restriction in the flow passage ahead of the tongue. The separation streamline is now in the middle of the volute channel and directs a considerable portion of the flow in a re-circulating pattern through the volute. As the amount of re-circulating flow increases a corresponding drop in the pressure occurs.

Confirmation of the separation streamline movement is seen from the pressure data on the walls of the volute just downstream of the tongue. Figure 3.15 shows the pressure rise along the tongue wall. The locations of the "TN" pressure taps are given in Figure 3.1. When the throttle is fully opened, the pressure increases along the wall of the tongue. This indicates a strong diffusion. At a flow coefficient less than the design point, the pressure drops along the tongue wall. This indicates an acceleration of the flow.

The opposite trends are seen along the periphery of the volute. These taps are labeled "TS" in Figure 3.1. At high flow rates, the static pressure drops as the flow traverses the volute sidewall, thus indicating an accelerating flow field. Once the throttle is closed past the design point, the pressure increases along the volute sidewall as a result of flow diffusion. The pressure variations along the volute sidewall are given in Figure 3.16.

In Figures 3.12 and 3.13 the slope of the tongue characteristic is seen to contribute to instability at low flow rates. It seems fairly clear that this peripheral non uniformity of the flow is one source of the positive slope of the tongue region

characteristic at low flows. The geometry of the volute also influences the shape of this characteristic. In the tongue region, the volute scroll stops curving continuously in width. This geometry sets up a "diffuser" section in the region upstream of the tongue where the passage area increases more rapidly than in the rest of the volute.

3.6.3 Impeller

The impeller contributes the largest percentage to the overall pressure rise of the pump. This is in agreement with Reference [12], which gives results showing that the impeller contributes about 80% of the overall head rise. The impeller characteristic is flatter than the overall pump characteristic. Figures 3.12 and 3.13 both show that the impeller is rather benign in terms of its contribution to instability in so far as the characteristic is flat. However, Figure 3.17 from Reference [24] shows that the current impeller geometry is not a stable configuration. With the current blade discharge angle of 34° and 8 blades, the ratio of the shut-off head to the peak head rise is about 0.98. Since the peak head rise is larger that the shut-off head, that portion of the pump characteristic will have a positive slope and be unstable. Increasing the sweep back of the blades ($\beta < 34°$) will improve the stability. Further re-design of the impeller does not seem warranted from the standpoint of the component breakdown.

3.6.4 Volute

Only a percentage of the dynamic head in the volute is recovered, thus the positive sloped characteristic with the throttle opened. However, near shut-off, the volute contribution to the pressure rise begins to increase and the characteristic has a negative slope. This increase in head rise near shut-off may be attributed to the increased re-circulating flow in the volute which gives an additional dynamic head.

3.7 Summary of Component Pressure Analysis

The results of the component pressure evaluations demonstrate that the volute, especially the tongue region has the greatest effect on the stability at low mass flows, except for the diffuser. The radial pressure gradients in the tongue region vary greatly with flow rate and there are significant differences between

pump operation on the stable and unstable portions of the characteristic. At low flow rates, the fluid exiting the impeller tends to re-circulate in the volute causing the pressure rise in the volute to decrease rapidly. The re-circulation leads to a shift of the tongue separation streamline and thus the fluid losses in the tongue region are large at off design conditions. The result of the pressure analysis led to a more detailed survey of the flow field in the tongue region using Laser Velocimetry techniques.

3.8 LDV Experimental Procedures

Laser Velocimeter measurements were taken in the volute at locations from 0° to 30° upstream of the tongue and at locations between 65° and 80° downstream of the tongue in 5° increments. The locations of the LDV grids are sketched in Figure 3.18. The measurements were concentrated in the tongue region based on the pressure analysis, which provided evidence that this portion of the volute contributed to a positively sloped characteristic at low flow rates. To determine how the flow field changed with the slope of the characteristic, the velocity was measured at three flow coefficients. The first flow coefficient corresponded to a high mass flow rate. The other two were on either side of the pump characteristic's peak peak pressure rise.

The angular position of the measuring plane was determined from location markers on the volute stiffening ring. These markings gave a position accuracy to within $\theta \pm 0.02$ radians. The LDV coordinate system was not aligned with the (r,s,h) flow coordinates. An appropriate coordinate transformation was done through the basic geometrical considerations shown in Figure 3.19. The angle of rotation for the coordinate transformation must then be entered into the computer program, CURRENT.BAS, before data can be acquired. Each angular position had an associated LDV grid which was 3 X 7 (upstream locations only), for a total of 21 data points. Figure 3.19 depicts the layout for a typical LDV measurement grid. The three points in the height direction were evenly spaced with the middle point corresponding to the impeller discharge plane height. The seven points were evenly spaced across the width of each grid. The pump was run at 23% of design speed which corresponds to a blade passing frequency of 12.9 Hz. Initiation of data acquisition was synchronized to the shaft encoder. This phase locking procedure was triggered on a once per revolution basis. The parallel port on slot 7 of the PC was used for this signal. Pin 4 was connected to positive (between +3 and +6 volts), and pin 25 was grounded. A

WAIT command was added to the computer code, SAMPLE.BAS, to pause execution until the signal was received.

The following table list the important LDV parameters:

Number of Samples	2048
Number of Cycles	8
Sampling Frequency	156.25 Hz
Comparison	7%
Focal Lens Length	450 mm
Lens Half Angle	4.94 deg.
Number of Fringes	23
Fringe Spacing	2.7 μm
Probe Volume Diameter	0.07 mm
Probe Volume Length	0.81 mm
Flow Sensitivity	3.0 m/s per MHz

Briefly, the LDV optics perform the following functions. The beam exits the argon-ion laser and passes through a beam collimator. The collimator regulates the beam divergence (the increasing of the beam's diameter). If the minimum beam diameter (beam waist) does not occur at the measurement location the fringes will not be parallel and invalid readings will result. The beam then enters the color separator assembly. Next, a beam attenuator separates the polarity of the light. Light with horizontal polarity is passes through, while light with vertical polarity is filtered. The beam now passes through a dispersion prism. The prism separates the light into its color components by passing the light through at the Brewster angle. The blue beam at 488 nm and the green beam at 514 nm are used to set up the LDV system. There are four mirrors which are used to direct the blue and green beams to the optical axis. Once the beams are aligned with the optical axis, they are split using a beamsplitter module. The blue beam is split horizontally and the green beam vertically. A single beam of each color component passes through the frequency shifter (Bragg Cell). Beam steering modules are used for fine adjustments to the beam location. The receiving optics assembly (ROA) collects the scattered light and focuses it on the photodetector. Since the system operates in backscatter mode, the scattered light from a particle must travel back the same path as the laser light to reach the ROA. A field stop system is used to reduced the effects of background flare, extraneous light sources and laser light reflections on the LDV signal. Next, a beam

stop is used to block extra beams from being transmitted any further down the optics path. Beam spacers are used to reduce the beam spacing from 22mm to 9mm. Finally, a beam expander is used to enlarge the beam diameter. The model used increases the diameter by a factor of 3.75. This increase results in a theoretical decrease of the measurement volume length by a factor of 14. Beam expansion also decreases then measurement volume diameter by a factor of 3.75 and improves the signal-to-noise ratio (SNR) by a factor of 50 (Reference [25]). Detailed explanations of each optics module as well as alignment instructions can be found in the TSI System 9100-7 Laser Doppler Velocimeter Instruction Manual. A diagram of teh laser optics assembly is given in Figure 3.20

Before measurements are made, the signal output should be viewed on an oscilloscope. The Doppler bursts should be well defined and any pedestal component of the signal can be filtered out using the high and low pass filters on the signal conditioner. The data rate, measured in kHz, can be read for each channel from the counter. A good rule of thumb is that the data rate should be about 5 times the sampling frequency. This rule assures that a valid data point will always be available when a measurement is made. If the data rate is low, check the optics alignment before adding particle seeding. For these experiments, the city water was filtered to particle sizes less than 5 μm, then titanium dioxide was used to seed the flow.

The accuracy of the LDV system was determined by measuring the impeller tip speed with the laser. The LDV measurements were compared to those obtained from the RPM meter. The calibration of the RPM meter is ±4 RPM at design speed of 420 RPM. The LDV consistently measured the impeller tip speed to within ±0.6% of the RPM readout.

3.9 Volute Velocity Profiles

3.9.1 Volute Throat

The LDV mapping was concentrated in the volute region just upstream of the tongue to resolve the flow features responsible for the sudden pressure rise just ahead of the tongue. The component pressure contributionas also show that the tongue region exhibits a strong instability at low flow. Since this plane is not radially outward from the impeller, but is perpendicular to the midline of the diffuser, a somewhat non-conventional coordinate system was adopted for these measurements.

The measurements for this plane were performed at 50% of the design speed. The data is presented in non-dimensional form which is independent of speedline. Both the radial and tangential velocity components are non-dimensionalized by the impeller tip speed. The distance across the channel is plotted as a percentage of the channel width. The tip of the tongue is arbitrarily set as 0% of the channel width and the outside volute wall is 100% of the channel width. The channel height, which is constant for the entire volute (h = 2.468 in.), is plotted as a percentage also. The volute floor (bottom) is considered 0% and the top surface is considered 100% of the height. The complete flow coordinate system is thus given by a radial, tangential (or streamwise) and height direction denoted by (r,s,h) respectively.

In Figures 3.21 and 3.22 the streamwise component of the velocity (parallel to the diffuser midline) is plotted versus the distance across the channel at the angular position of the volute throat. Thus, r/w = 0 is the tip of the tongue and r/w = 1 is the periphery of the volute. Figure 3.21 which is at a high mass flow (ϕ = 0.102), show a nearly uniform velocity profile across the entire section. The center height location has a slightly larger velocity than the top and bottom height locations. This give the typical parabolic type profile in the h,s plane. The average velocity in the channel at high flow is about 55% of the impeller tip speed. In Figure 3.22, which is for a flow coefficient of the positively sloped portion of the characteristic (ϕ = 0.042), the average channel velocity decreases to about 26% of the impeller tip speed. The reduced flow on the outside wall at r/w = 1 indicates a stagnation region at low flow conditions.

The radial component of the velocity at the same plane shows that there is a tendency for the recirculating flow to increase as the throttle is closed. In Figure 3.23, which shows the radial velocity at a high flow rate (ϕ = 0.102), the profiles show a circulatory secondary flow pattern. The fluid exits the impeller along the centerline of the volute height (h=.5), travels to the outside wall of the volute where it reverses direction an flows back toward the impeller along the bottom of the channel (h=.25). In the upper half of the volute channel, this circulation is not seen. The fluid mechanics of the flow in the upper half of the channel is strongly driven by the pumping action of the flow within the impeller clearance space.

At lower flow coefficients the direction of the flow is inward toward the tongue across the entire channel width and over the full height. Figure 3.24 shows the radial velocity profile in the (s,r) coordinate system at a flow coefficient of ϕ = 0.042. The blockage resulting from the diffusion in the tongue region of the volute diverts the flow inward, hence the velocities are negative.

3.9.2 Surveys Upstream of the Tongue

Similar surveys at locations upstream of the tongue indicate strong secondary flow in the volute, which is probably driven by the radial jet exiting the impeller. Figures 3.25 through 3.30 show the radial velocity profiles at high and low flow coefficients for angles of 5, 15 and 30 degrees upstream of the tongue plotted against the non-dimensionalized radius. The radius of the measurement location in non-dimensionalized by the radius of the impeller. Thus, r/R = 1 is at the impeller outlet and r/R > 1 is across the volute width.

At high flow (Figures 3.25 to 3.27), the secondary circulation can be seen from the radially inward flow near the top of the channel (h=0.75), while the centerline and bottom exhibit outward flow. As the flow proceeds from 30 degrees (Figure 3.27) toward the tongue (Figure 3.23), the inward velocity on the upper plane is reduced until at 5 and 0 degrees, the flow is outward over almost the entire portion of the channel.

At a low flow coefficient (Figures 3.28 to 3.30), on the unstable portion of the pump characteristic, the reverse pattern is seen. As the flow proceeds from 30 degrees (Figure 3.30) toward the tongue, the radially inward flow on planes h=0.25 and h= 0.75 increases in magnitude. This indicates a much stronger streamwise vortical motion as the flow approaches the tongue. At the station just before the tongue tip (5 degrees), a strong circulation can be seen close to the impeller exit. This circulation is shown in Figure 3.28 and suggests a tendency for the flow to re-circulate in the volute channel.

The tangential velocity components are shown for high and low flows at angles of 5, 15 and 30 degrees upstream of the tongue in Figures 3.31 through 3.36. Since the tangential velocity is nearly independent of height, these figures suggest a fully developed, well mixed turbulent velocity profile. The mixing due to the secondary flow is strong enough so that tangential momentum is approximately conserved. Figures 3.34 to 3.36 show that for low flow coefficients the velocity decreases near the periphery of the volute as the flow approaches the tongue. This is due to the blockage that was previously discussed. At high flow, the 5 degree station shows an acceleration of the flow on the periphery, which is promoted by blockage on the tongue side of the volute.

The variations in the volute pressure rise discussed in Chapter 3 are clearly seen in the velocity profiles. When the throttle is open, the velocity profile remains

fairly constant as the flow approaches the tongue. This is seen in Figures 3.37 to 3.39, which show the tangential velocity contours for volute locations from 30° to 5° upstream of the tongue for h=0.25, h=0.5 and h=0.75. These figures also depict the influence of the tongue on the velocity profiles. The contours for $\theta = 5°$ show that the velocity is nearly uniform across the entire channel due to the retarding effects of the tongue on the flow. Closer to the peak of the performance characteristic, at a flow coefficient of $\phi = 0.05$, the strong diffusion is evident from the reduction in tangential velocity as the flow nears the tongue as shown in Figures 3.40 to 3.42. The influence of the tongue on the flow is not as pronounced at the low flow coefficients as it was at high flows.

3.10 Losses in Hydraulic Machinery

3.10.1 Slip Factor

The pressure variations across the blades of the impeller not only give rise to the blade circulation associated with lift, but the non-uniform velocity distribution is responsible for the mean direction of the flow leaving the impeller deviating from the actual blade discharge angle. This deviation causes a reduction in the impeller discharge tangential velocity from $C_{\theta\,2,\,theoretical}$ to $C_{\theta\,2,\,actual}$. The slip factor, σ, is defined by:

$$\sigma = \frac{C_{\theta 2,\,actual}}{C_{\theta 2,\,theoretical}} \tag{3.4}$$

where the real velocity triangle is shown by the dotted lines in Figure 3.43, while the solid lines show the ideal case.

Several studies [22,27] have demonstrated that the slip factor is a function of the flow coefficient and angular location around the volute. This variation of slip reduces the head rise in the pump from its ideal value by a factor of $\sigma(\phi, \theta)$. The slip factor is determined experimentally from the LDV measurements (Appendix C). The experimental data show the trends in the variation of slip factor with both the flow rate and volute position (or pressure rise). The slip factor and pressure rise is plotted against volute angular position. The pressure rise is scaled down by a factor of 1/2, since only the qualitative variations are compared to the slip factor. Figures 3.44 to 3.46 show the the variation of σ at flow coefficients of $\phi = 0.05$, $\phi = 0.6$ and

ϕ = 0.99. These figures show that as the pressure increases the slip factor decreases. However, from the lack of experimental data the exact functional relationship cannot be determined. The other trend that is evident in this data is that the slip factor increases with flow rate.

3.10.2 Volute Mixing Losses

The overall shape of the performance characteristic is strongly influenced by the losses incurred due to the mixing of the fluid in the volute with the jet exiting from the impeller. The mixing losses can be estimated from Figure 3.47 which shows the the tangential velocity contours for the three flow coefficients measured. At the high flow rate the impeller discharge velocity is 1.7 m/s. The fluid in the volute is moving with a velocity of 1.57 m/s. The overall loss in potential dynamic head is 10.3%. For low mass flow rates, the impeller discharge velocity remains approximately the same except for the variation with slip factor, hence the impeller discharge velocity is 1.62 m/s. The volute mean velocity is 1.17 m/s. Thus the loss in the potential dynamic head is 27.6% . The losses at high ϕ are 2.67 times less than the losses at low ϕ. The minimum loss occurs at the design flow coefficient.

Although no measurements of the volute velocities were made at flow rates above the design point, the computer model predicts that the volute velocity will be greater than the impeller discharge velocity and the associated mixing losses will be larger than at the design point. The losses due to mixing can be estimated by modeling the processes as two co-flowing streams in a variable area duct.

$$h_{mixing} \propto (C_{\theta 2} - u)^2 \qquad (3.5)$$

Since $\partial P_{t\infty} / \partial P < 0$, raising the level of static pressure at which the mixing occurs will increase the loss in dynamic head. Thus, the mixing losses are not uniform around the volute. The overall effect of the mixing losses is to decrease the head rise at of design flow rates. This reduction contributes to the positive sloped characteristic at low flows and the decrease in head above the design point.

3.11 Summary of Velocity Surveys

The LDV data in the tongue region indicates that the volute flow is strongly influenced by the impeller exit jet. Similar to the pressures measurements, the velocity profiles indicate flow stagnation in the tongue region at low flow rates. There are also two strong lobes of circulation in the volute. The circulation in the upper half of the volute channel seems to be most effected by throttling. At high flow, the circulation decreases in magnitude as the flow approaches the tongue. Conversely, at low flow, the vortical motion increases in strength as the flow nears the tongue. The LDV measurements clearly show a change in the nature of the flow pattern as the pump operating point moves from a stable position toward instability. An increase in the re-circulating flow in the volute near the peak pressure rise is a precursor to potential instability.

The velocity surveys also demonstrate that computationally a constant value of the slip factor does not model the fluid mechanics of the real system sufficiently. The slip factor varies with both flow rate and head rise. The mixing loss mechanism is also shown to play an important role in determining the shape of the pump performance characteristic. The mixing loss increase proportionally to the square of the velocity differential between the two mixing streams. At the design point, where the velocity difference is small, the mixing losses are minimal. However, at off design conditions, the velocity difference increases rapidly.

CHAPTER 4
VOLUTE MODIFICATION

4.1 Motivation for Volute Re-design

The pump re-design was accomplished by conducting a parametric study with the volute/impeller interaction code. The complete details of this computational research are presented in Reference [6]. The direction of the study was guided by the results of the component pressure and tongue region velocity experiments. The component pressure evaluation lead to the conclusion that the tongue region pressure rise characteristic is the most significant contributor to a positive sloped performance curve at low flows. During off design operation, the mismatch of the flow and the volute geometry cause strong losses in the tongue region. The velocity measurements show that the losses due to the mixing between the tangential impeller discharge velocity and the mean flow in the volute are large at off design flow rates. Off design flow in the tongue region is strongly influenced by the secondary circulation in the volute. At low flow rates, the circulation increases in magnitude contributing to a loss of head in the tongue region and a decrease in diffuser performance. There is also a tendency for the fluid in the volute to be re-circulated at flows below the BEP.

4.2 Summary of Computational Study

The computational study examined several volute shapes and evaluated their effects on stability. The results of this study suggested a correlation between the volute cross-sectional area and the velocity mismatch between the impeller exit velocity and the mean flow in the volute. The proposed area re-distribution is intended to obtain a better matching of the velocities over a broader range of flow rates. The computational model inferred that the early expansion would be effective in reducing the speed of the flow in the volute, especially as low flow rates, when most of the fluid is being re-circulated. A second computational study shows that the benefits of the volute expansion

diminish if the expansion is not completed in the first 40° of the volute, especially if the area ratio between the old and the new volutes is small.

The final area distribution was a compromise between the predictions and the practical geometric constraints of the experimental facility. The tongue geometry remains constant so the effects of the volute expansion are isolated. A comparison of the volute width is shown in Figure 4.1. The original volute width increases linearly from the tongue tip to about 340° around the scroll. At this point the geometry of the volute changes due to the transition region connection. The effects of this sudden rise were discussed in Chapter 3. The area for the modified volute increases parabolicly to 340° where the same expansion is seen. A blueprint of the modified volute is given in Figure 4.2

4.3 Impact of Volute Modifications on Head Rise

The goal of the volute modification is to improve the pump stability without sacrificing the head rise at the best efficiency point. The expansion of the volute in the region just downstream of the tongue effects the overall characteristic in three ways in order to accomplish this goal.

4.3.1 Increased Impeller Backpressure

The pressure in the volute passage provides the working environment for the impeller. Diffusing the flow in the initial stages of the volute scroll causes the pressure level in the volute to increase. The high backpressure at the impeller exit reduces the the velocity through the impeller passages. The impact of this change can easily be seen from the Euler equation for head. If we neglect the inlet angular momentum, the theoretical head rise is:

$$H = \frac{U_{tip}^2}{g} - \frac{U_{tip} \cot \beta_2}{\pi D_2 b_2 g} Q_{imp} \qquad (4.1)$$

The increased pressure in the volute causes a reduction in the volumetric flowrate through the impeller. By decreasing the flowrate, the head rise is increased. This effect is more significant at high flows than at low.

4.3.2 Volute Mixing Losses

The competing result of the volute modification is the redistribution of the volute mixing losses over the range of throttle settings. As the computer model showed, the mean velocity on the volute is larger than the impeller discharge tangential velocity at flow rate above the BEP. Below, the BEP the opposite is true. Increasing the volute area diffuses the flow more initially, thus reducing the magnitude of the mean volute velocity of the entire range of flow rates.

In the modified volute, the losses above the BEP will be less than in the original volute since the difference between the two velocities has been reduced. At low flow rates, the losses increase due to the larger velocity differential. The overall consequence of the volute expansion on mixing is to increase the head rise at high flow rate and decrease the head rise at low flows, thus flattening the performance characteristic. Combining the effects of mixing loss with the increased head rise due to the raised level of impeller backpressure is to maintain the level of head at BEP, give additional head above BEP and reduce the head below the BEP.

4.4 Shut-Off Head and Peak Pressure Rise

Another major factor in the shape of the pump characteristic is the value of the shut-off head. The theoretical head rise given by Equation (4.1) shows that the head at shut-off should by equal to $\psi = 1.0$. However, due to circulation between the blades and the effects of prerotation in the inlet duct, this value is not a good estimate of the real head at shut-off. Reference [24] states that the shut-off head is typically given by, $\psi = 1.17$, but does give a physical explanation. The implications of the shut-off head on stability are quite important. If the shut-off head is less than the peak head rise, the pump must have a positive slope over some portion of the characteristic. This implies that the largest head rise from a centrifugal pump is $\psi \approx 1.17$ if the pump is to remain dynamically stable to shut-off.

CHAPTER 5
PUMP PERFORMANCE WITH MODIFIED VOLUTE AND STABILITY EVALUATION

5.1 Experimental Procedures

The component pressure evaluation for the modified volute was obtained using the Scanivalve pressure scanning system. Additional pressure taps were added on the volute scroll for the geometrically modified pump. These additional pressure tap stations and their numbering designations are given in Figure 5.1. The original numbering system of Chapter 3 was maintained for the original set of pressure taps. Ten new taps were added to the top surface of the volute around the impeller periphery. These were used to measure the pressure variations and circumferential non-uniformity around the backplate clearance gap. A "TP" designation was used to denote the backplate pressure taps. Radial taps were also added at several locations around the volute to better resolve the radial pressure variation around the entire volute scroll. The additional taps on the volute periphery were denoted by an "E" and the new taps at the impeller discharge were marked "A".

The steady state pump characteristic was determined from 20 throttle settings covering a range of flow coefficients from 0.14 to 0.09. The pressure ports were scanned at a rate of 8 ports/second. A total of 8 scans were taken and averaged to obtain the steady-state measurement.

The unsteady experiments were run under the same conditions as given in Reference [4]. The air volume in the large (inlet) plenum was kept constant at 300 liters. The overall loop was not pressurized and the hydrostatic head was kept constant. The air filling procedure used was a volumetric displacement technique. The pump was filled and the water level was noted on the discharge stack water level tube. Next, the pump was run for 1 to 2 hours to allow dissolved gasses in the water to come out of solution. A desired volume of water was emptied from the loop through a water meter at the base of the small (discharge) plenum. A compressed air line at 50 psig was then used to bring the water back to the same level on the discharge stack. The volume of water removed should be the same as the volume of air put into

the system. The pump was then brought up to speed and beginning near the peak pressure rise, data was collected at progressively smaller throttle settings. Measurements of pump pressure rise, volume flow rate, torque, shaft RPM and leakage flow were taken. The instability transition point, ϕ_{cr} , was indicate by the formation of a constant peak-to-peak amplitude oscillation greater then 3% of the BEP pressure rise. This 3% cutoff value is determined by the background noise level of the pump running at low flow rates and is the same value used in the original stability test on the pump.

The time-resolved measurements were acquired at a frequency of 8 Hz, which is about 20 times greater then the expected surge frequency. The data was continuously taken until the throttle was in the shut-off position. The surge cycles are referenced by the average value of the flow rate over one oscillation cycle. The B parameter is a function of the experimentally derived frequency of oscillation, ω_{unst} , and is determined from a Fast Fourier Transformation of the transient data.

The experiment was run at 80% of the pump's design speed. Since the frequency of oscillation varies inversely as the square root of the volume it is possible to obtain the same value of the B parameter by varying the impeller tip speed (i.e. the percentage of design speed) and the air in the small plenum. Thus, the instability should be independent of speedline and only one speedline was measured.

In order facilitate comparison the performance of the MIT pump with the prototype unit, the frequency of oscillation is non-dimesionialized by the shaft rotation frequency. This non-dimensional value is called the reduced frequency and is calculated as a percentage of the shaft frequency.

5.2 Modified Pump Parameters

The following table lists the values of the major pump parameters at BEP for the modified volute at 23% and 50% of design speed. For reference, these value on the original volute scroll were presented in Chapter 3.

	50% Speed	23% Speed
N_s	704	670
Q (GPM)	275.57	116.20
Torque (in-lb)	193.77	40.1
η	0.856	0.852

ψ	1.1554	1.1319
ϕ	0.09	0.0869
Ω (RPM)	203	96.6
Re	9.6E4	4.57E4
U_{tip} (m/s)	6.47	3.08
ΔP_{total} (psi)	3.51	0.78

The modified volute has a 6% drop in the BEP head rise. At 50% of the design speed, the BEP flow coefficient increased by 16.6% and at 23% of the design speed there was a 10% increase. Figure 5.2 shows the steady state pump performance characteristics at several speedlines for the modified volute. A decrease in the pump performance is seen with decreasing Reynolds Number. The effect of Re is explained through the losses due to friction. The head loss due to friction for a fully developed turbulent flow in a non-circular duct can be expressed as:

$$h_{loss} = f \frac{L}{4R_h} \frac{C^2}{2g} \qquad (5.1)$$

where the friction factor, f, is a function of both Reynolds Number and relative roughness. A Moody Diagram shows that a decrease in Re will cause a larger head loss for a hydraulically smooth pump than for a rough.

5.3 Overall Pump Performance Characteristic

The qualitative change in the characteristic shape the volute/impeller interaction code predicts, occurs in the experimental facility. The modified volute has a much flatter characteristic and should exhibit an increase in the stable operating range. The performance characteristic of the pump with the modified volute and the efficiency curves are given in Figures 5.3 and 5.4 for 23% and 50% of design speed. In both cases the volute modification leads to a slight loss in BEP head rise, however the BEP flow rate and the pump efficiency were not compromised significantly. The efficiency curves are very flat near their peak and this leads to some degree of uncertainty in estimating the best efficiency point. In this work, the BEP is defined as the centerpoint of the flat portion of the efficiency curve.

A comparison of the pumping characteristics for the original and modified volute geometry shows the flattening effect of the volute expansion. At high flow rates, above the BEP, the pump actually has an increase in head rise. Figures 5.5 and 5.6 show the comparison of the performance characteristics. In Figures 5.7 and 5.8, which show the detail of the unstable characteristic segment, the decrease in positive slope is evident. The peak pressure rise occurs at roughly the same flow coefficient for each volute. In both the original and modified volutes, the shallowness of the characteristic eliminates the possibility of static instability.

5.4 Static Pressure Rise Through the Pump

The modification to the volute scroll changes the pressure distribution around the volute at all flow conditions. In Figures 5.9 (23% Speedline) and 5.10 (50% Speedline), the static pressure rise around the pump is plotted for three flow rates. These flow rates represent a wide open throttle, the BEP and a low flow. The overall pressure level in the modified volute is higher than in the original casing. This elevated pressure is due to the sudden expansion of the flow in the region downstream of the tongue. The taps located between $0 < X/L < 0.7$ show the head rise from the tongue to the volute throat. At the open throttle and BEP flow coefficients, the pressure is continuously rising in the volute. At the low flow rate, the pressure is oscillating around the volute passage. The sudden jump in pressure in the region ahead of the tongue is not as pronounced with the modified volute. This reflects the additional head rise in the volute and possible better matching of the flow at off design operation.

The volute performs much of the diffusion in the modified configuration. This is beneficial for the overall performance since there is less chance of flow breakdown in the volute than in the diffuser. In the volute, the impeller jet is constantly adding angular momentum to the flow and this helps keep the boundary layers attached in the adverse pressure gradient.

The same trends in the tongue region from the original geometry are also evident in the modified volute. At high flow rates there is a strong acceleration of the flow in the tongue region and a corresponding pressure drop. However, at lower flows (below BEP), the sudden pressure rise in the tongue region which was seen in the original volute is not present in the modified scroll. The pressure rise around the volute is very close to being linear. This suggests that

the modified tongue performance characteristic is not as unstable as in the original pump.

5.5 Volute Throat Pressure Gradient

The pressure gradient across the volute throat shows the same overall trends for both volute shapes. In Figure 5.11, which gives the head rise for the volute throat pressure taps, the modified volute has a larger magnitude in the gradient at high and low flows. Again, at high flow, the pressure decreases across the volute width from the tongue tip to the volute periphery. Near shut-off the pressure gradient is in the opposite direction, with the pressure increasing across the throat. The most significant difference between the original and modified volutes occurs near shut-off. In the original geometry, the pressure is constant across the volute at very low flows, $\phi < 0.03$, suggesting a region of separated flow. The modified volute scroll does not exhibit this behavior even at flows less than $\phi = 0.02$. This gradient suggests that a separation region is not present and the fluid is continuing to move through the volute throat. The continued flow through the throat is a result of the increase in pressure in the expanded segment of the volute. Under these conditions, the incremental difference in the head rise as the throttle is closed becomes reduced, thus producing a stabilized tongue region characteristic.

5.6 Tongue Pressure Differential

The pressure rise at the tongue (tap V0) has a markedly different nature with the modified volute scroll. In the case of the original volute (Section 3.5), the tongue pressure rise decreases with a decreasing flow coefficient (positively sloped characteristic). This behavior is due to the acceleration of the flow to accommodate the increase mass of fluid passing through the re-circulation area of the volute. The modified volute tongue pressure rise, shown in Figure 5.12, depicts an increase in head rise (negatively sloped) with reductions in the mass flow. In the original volute, the pressure differential across the tongue tip increased as the pump was throttled back. With the modified volute, this pressure differential is much smaller over the same throttling range. Thus the tendency for the flow to re-circulate is reduced.

It is interesting to note the flow coefficient where the pressures on either side of the tongue are equal. At this condition, the flow passes the tongue with minimum shock losses. In the original volute, this flow rate is the so called design point. With the original configuration, the pressure across the tongue reaches an equilibrium at a flow rate of $\phi = 0.117$. The modified volute scroll has its "design point" as the same flow rate, $\phi = 0.117$.

5.7 Component Pressure and Slope Contributions

The contribution of each component and the overall pump performance curves are plotted in Figures 5.13 (23% Speedline) and 5.14 (50% Speedline).

5.7.1 Diffuser

The diffuser performance characteristic is similar in shape for the two volute geometries. There is no contribution from the diffuser to stability. Its slope of positive over the entire throttling range. Removal of the conical diffuser and replacing it by a dump diffuser would increase the pump stability in terms of the slope of the performance characteristic. If the pump performance characteristic is defined in terms of the pressure rise from the pump inlet to the volute throat (tap V11), the characteristic would have a negative slope from shut-off to a wide open throttle. This characteristic can be seen in Figure 5.11, however, the head rise of the diffuser at high flows would be lost. A better solution would be to remove the diffuser and expand the flow within the volute such that the volute throat area would equal the diffuser exit area. Computationally, this method has much more potential to increase the pump stability with little loss in head rise [6].

5.7.2 Tongue Region

The major improvements to the pump stability can be seen in the tongue region characteristic. Both Figures 5.15 and 5.16 show that the slope of the tongue region is negative until a flow coefficient of $\phi \approx 0.0225$. For the original volute, this figure is $\phi \approx 0.054$. This corresponds to a 22% improvement in the throttling range with the tongue region remaining dynamically stable.

The head rise along the tongue wall is significantly different for the modified volute. In Figure 5.17, the pressure of the fluid continues to rise as the flow passes the tongue from tap TN1 to TN4 even at very low flow rates. In the original volute, the pressure dropped along the tongue wall at low flows due to the location of the tongue separation streamline. The pressure data for the modified volute shows that the separation streamline does not move out into the volute as far as it does in the original scroll.

5.8 Unsteady Operation of the Modified Volute

The focus of this section is to demonstrate the real improvement of the modified volute geometry in terms of an increase in the stable operating range of the pump. The experimental results show that the computational models are able to predict the qualitative effects of geometrical modification to the pump. The results from the computational stability analysis are shown in Figure 5.18. The two experimental pump performance characteristics (original and modified volute) are used as inputs to the code which predicts an increase in the stable operating range of the pump.

5.8.1 Dynamic System Parameters

The reduced frequency of surge is plotted in Figure 5.19 versus the air content is the small plenum. The modified pump exhibits the same behavior as the original as seen by the square root relation between the reduced frequency and the air volume in the discharge plenum. The shift of the curve to the right is indicative of an increase in the threshold value of the B parameter. The actual frequency of oscillation for the pump is shown in Figure 5.20 plotted against the discharge plenum air volume. Again, there is a square root dependence.

5.8.2 The Stability Boundary

The operating point at which the system becomes unstable is referenced by the average flow coefficient over the surge cycle and is denoted by ϕ_{cr} . Figure 5.21 shows a comparison of the stability map for the pump with both the original and modified volute shape. The modified volute is clearly more stable than the original. The threshold value of the B parameter was not determined for the original volute

scroll but Reference [4] clearly shows this value to be much larger than 0.3. The threshold value for the modified volute is approximately B = 0.29. There is a region where a definite improvement in stability occurs depending on the threshold value of the B parameter.

5.9 Summary of Modified Volute Performance

Figure 5.22 outlines the major changes brought about by the volute expansion. The major impact is on the tongue region characteristic. In the original volute the tongue region contributed to instability at a flow coefficient as high as 0.054. The volute expansion through increasing the mixing losses at low flow rates effectively reduced the head rise in the tongue region thus producing a flatter characteristic.

The results also prove that the diffuser is a very destabilizing component. Removal of the conical diffuser and increasing the volute throat area to accomplish all the diffusion in the volute scroll will further improve the pump stability without much reduction in head. The diffusion is better accomplished in the volute where the boundary layers are constantly energized from the impeller exit jet. The risk of flow separation is small and the volute characteristic is quite stable especially at low flow rates.

CHAPTER 6
CONCLUSIONS

6.1 Summary of Experimental Results

Although it is often claimed that volute casings are very efficient, this is a misleading statement since the losses due to mixing and friction that occur in the casing can only reduce the pump output and never add to it. Thus it is important to minimize and distribute these losses over the entire operating range of mass flow rates for improved stability over a wider throttling range.

The experimental component pressure data points to the tongue region of the volute scroll as an unstable element at low flows. The pressure analysis shows that there is a tendency for the flow to re-circulate within the volute at flows below the best efficiency point. This re-circulating pattern is influenced by the mismatch of the flow with the scroll geometry at off design flow coefficients. As the throttle is closed, the tongue separation streamline moves out into the volute. This causes more flow to be directed back into the volute passage. When the re-circulating flow increases, the fluid must accelerate past the tongue tip in order to accommodate the increased mass. This causes the pressure to rise on the impeller side of the tongue and produced a spiral effect on the volume of recirculating flow. When the recirculation increases, the incremental change in head rise when throttling diminishes and the characteristic becomes positively sloped.

The LDV measurements show that there is a significant increase in the losses due to mixing at low flows. The flow in the tongue region of the pump is highly vortical and is strongly influenced by the impeller exit jet entering the volute. There are two lobes of secondary circulation presents. These vortices are of unequal strength. The vortex in the upper half of the channel seems to be more dominant. At high flows, the strength of this vortex decreases as the flow approaches the tongue. However, at low flow rate, the vortex increases in strength. This circulation adds to the mixing losses at low flows and could influence the shape of the performance characteristic.

The overall performance characteristic shape is strongly influenced by the losses in the system at off design flow conditions. These losses are generally a minimum at the BEP and increase as the square of the flow rate. The approach to the volute casing re-design is to modify the pump geometry in such a way that the BEP head rise would remain constant, but the head rise at lower flows would decrease. This is accomplished by reducing the velocity in the volute. By reducing the velocity, the mixing losses at flows above BEP are reduced and additional head is obtained. At low flows, the mixing losses are increased producing a flatter pump characteristic.

The stability tests on the modified volute show an improvement in the stable operating range of the pump. The pressure data and stability data not only show the real improvement in the pump performance, but are instrumental in improving the predictive capabilities of the computational models. The positive results of the experimental effort validated the ability of the computer models to be used as design tools at least in a qualitative manner.

6.2 Recommendations

While the results of this research have led to some improvement in the stable operating range of the pump, further improvements may be made by the removal of the conical diffuser which is unstable over the entire throttling range. Preliminary computational results show large improvements by removing the diffuser and expanding the flow entirely within the volute without much loss of head over the full range of throttle settings. These results should be verified experimentally.

It is also recommended that the further efforts be placed on experimentally determining the variation of the slip factor circumferentially around the entire volute and determining the complete functional relationship, $\sigma = \sigma(\phi,\psi)$.

Finally, it is recommended the impeller geometry be further studied to improve stability. Published data on impeller design shows that the combination of blade discharge angle and the number of blades for the current impeller will not produced a stable pump characteristic. The stability can be improved by reducing the number of blades or by increasing the sweep angle of the blades.

REFERENCES AND BIBLIOGRAPHY

[1] Adler, D. and Levy, Y., "A laser-Doppler Investigation of the Flow Inside a Backswept, Closed, Centrifugal Impeller.", Journal of Mechanical Engineering Science (IMechE), Vol 21. No. 1, 1979, pp. 1-6.

[2] Bendat, Julius S. and Piersol, Allan G., Random Data Analysis and Measurement Procedures. New York: John Wiley and Sons, 1986.

[3] Binder, R.C. and Knapp, R.T. "Experimental Determinations of the Flow Characteristics in the Volute of Centrifugal Pumps". Transactions of the ASME Vol.58, 1936, pp. 649-661.

[4] Bons, Jeffrey P., "Instabilities and Unsteady Flows in Centrifugal Pumps". Master's Thesis, Massachusetts Institute of Technology, 1990.

[5] Bowerman, R.D. and Acosta, A.J. "Effect of Volute on Performance of a Centrifugal-Pump Impeller". Transactions of the ASME Vol. 79 No. 5, 1957, pp. 1057-1069.

[6] Ciacci, Furio. "Theoretical Investigation of Volute Effects on Low Flow Dynamic Stability in a Centrifugal Pump." Master's Thesis, Massachusetts Institute of Technology, 1992.

[7] Dally, James W. et al., Instrumentation for Engineering Measurements. New York: John Wiley and Sons, 1984.

[8] Douglas, J.F. et al., Fluid Mechanics. London: Pitman Publishing Limited, 1985.

[9] Emmons, H.W., Pearson, C.E. and Grant, H.P., "Compressor Surge and Stall Propagation", Transactions of the ASME, Vol. 77, 1955, pp. 455-469.

[10] Fagan, John R. and Fleeter, Sanford. "LDV Measurement of a Mixed-Flow Impeller at Design and Near Stall." , ASME Paper 91-GT-310, 1991.

[11] Fowler, H.S., "Some Measurements of the Flow Pattern in a Centrifugal Compressor Impeller.", ASME paper #65-WA/GTP-7, 1965.

[12] Frost, T. H. and Nilsen, E., "Shut-off Head of Centrifugal Pumps and Fans." Proceedings of the Institute of Mechanical Engineers. Part A: Journal of Power and Energy, Vol. 205, 1991, pp. 217-223.

[13] Goulet, N.R., "An Experimental Facility for the Study of Unsteady Flow in Turbopumps". Master's Thesis, Massachusetts Institute of Technology, 1989.

[14] Greitzer, E.M., "The Stability of Pumping Systems. The 1980 Freeman Scholar Lecture". ASME Journal of Fluids Engineering, Vol. 103, June 1980.

[15] Gysling, D.L., "Dynamic Control of Centrifugal Compressor Surge Using Tailored Structure." Master's Thesis, MIT Department of Aeronautics and Astronautics, August 1989.

[16] Holman, J.P., Experimental Methods for Engineers. New York: McGraw-Hill Book Company, 1989.

[17] Inversen, H.W , Rolling, R.E. and Carlson, J.J. "Volute Pressure Distribution, Radial Force on the Impeller and Volute Mixing Losses of a Radial Flow Centrifugal Pump". ASME Journal of Engineering for Power, April 1960, pp. 136-144.

[18] Karassik, Igor J. et. al., Pump Handbook. New York: McGraw Hill Book Company, 1986.

[19] Miner, S.M. et al. "Laser Velocimeter Measurements in a Centrifugal Flow Pump." ASME Journal of Turbomachinery, Vol. III July 1989.

[20] Pinsley, J.E., "Active Control of Centrifugal Compressor Surge." Master's Thesis, MIT Department of Aeronautics and Astronautics, October, 1988.

[21] Press, William H. et al., Numerical Recipes: The Art of Scientific Computing [Fortran Version]. Cambridge: Cambridge University Press, 1989.

[22] Sakai, Toshimichi, et al. "On the Slip Factor of Centrifugal and Mixed-Flow Impellers." ASME Report No. 67-WA/GT-10, 1967.

[23] Stenning, A.H. "Rotating Stall and Surge", ASME Journal of Fluids Engineering, Vol. 102, 1980, pp. 14-21.

[24] Stepanoff, A.J., Centrifugal and Axial Flow Pumps. New York: John Wiley & Sons, 1957.

[25] "System 9100-7 Laser Velocimeter Instruction Manual", TSI Incorporated, 1987.

[26] White, F.M. Fluid Mechanics. New York: McGraw Gill Book Company, 1986.

[27] Whitfield, A. "Slip Factor of a Centrifugal Compressor and its Variation with Flow Rate." Proceedings of the Institution of Mech. Eng. Vol 188 No.34, 1974.

[28] Wilson, David G., The Design of High Efficiency Turbomachinery and Gas Turbines. Cambridge: The MIT Press, 1984.

[29] Worster, R.C. "The Flow in Volutes and its Effects on Centrifugal Pump Performance". Proceedings of the Inst. of Mech. Eng. Vol. 177 No.31, 1963, pp. 843-875.

[30] Personal Communication with J. Kerrebrock.

[31] Personal Communication with M. Graf.

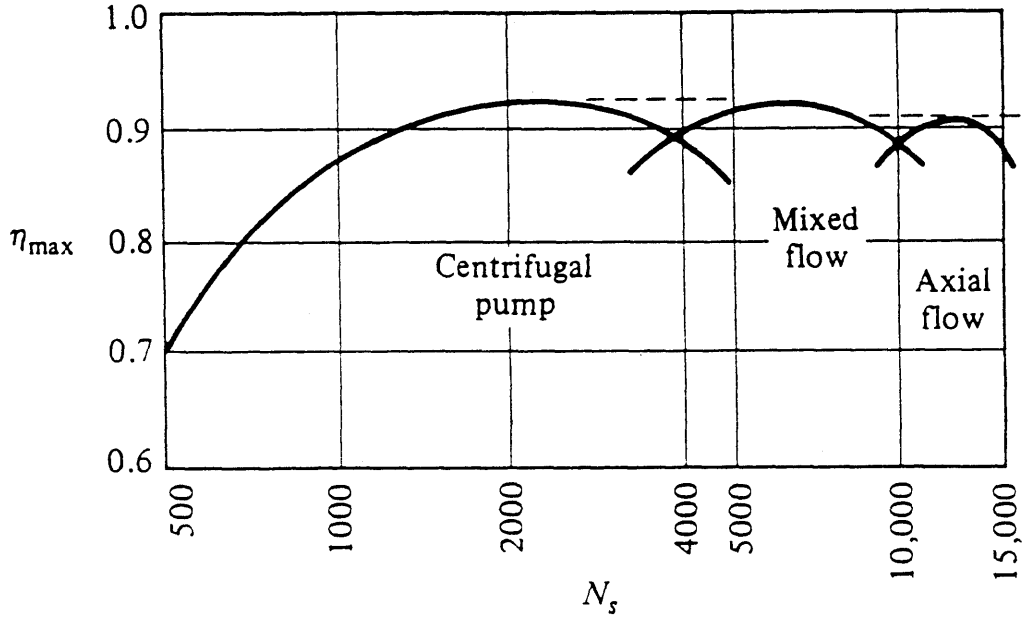

(*a*)

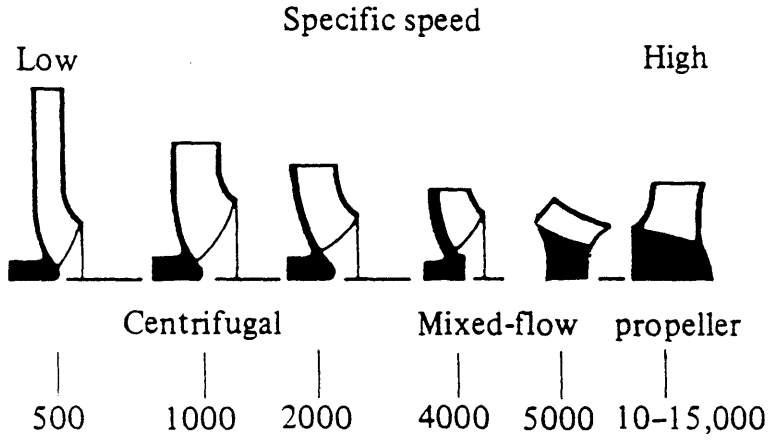

(*b*)

Figure 1.1
from Reference [26]

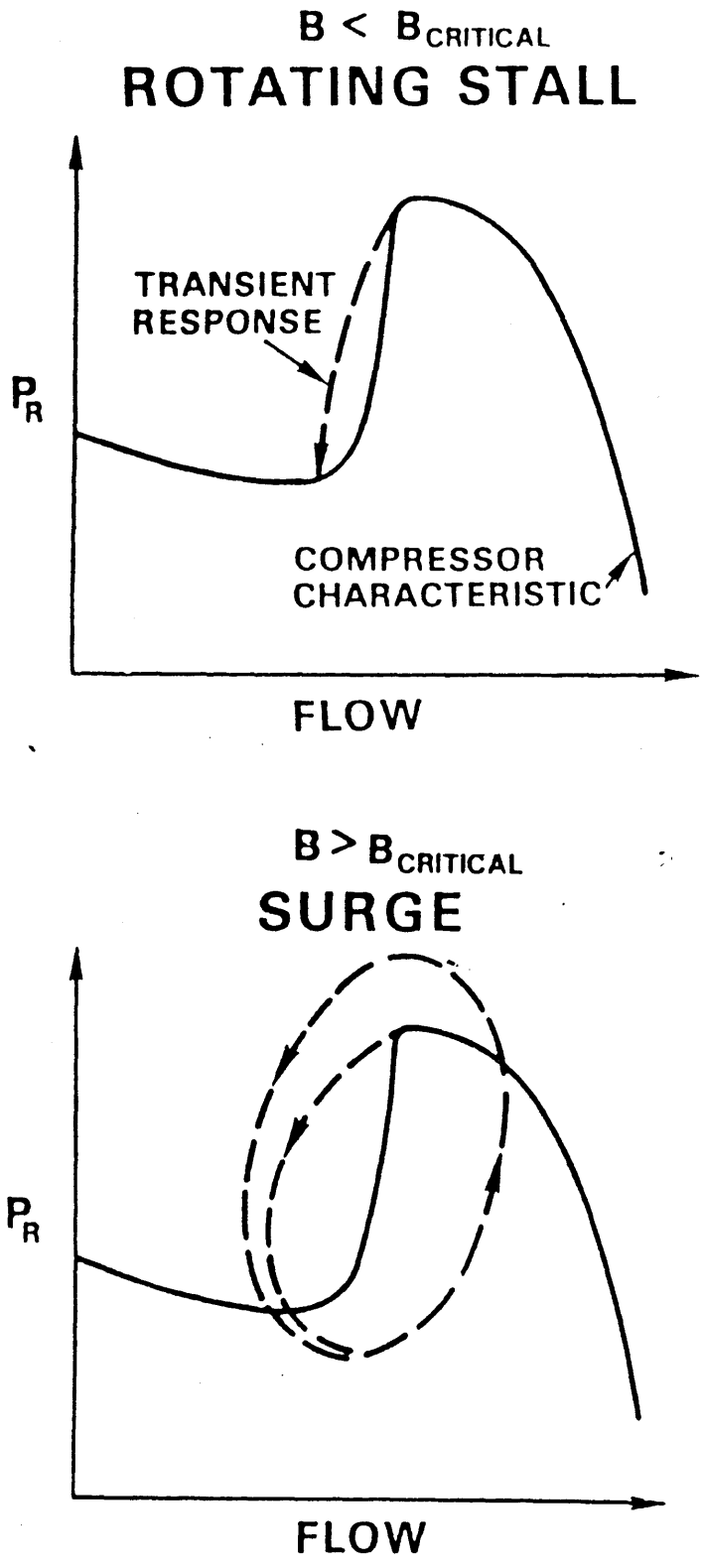

Figure 1.2
from Reference [14]

DYNAMIC INSTABILITY

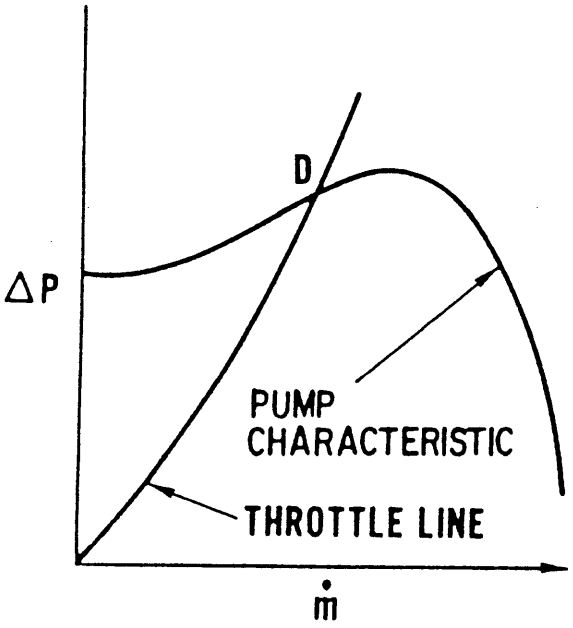

EVEN IF STATICALLY STABLE SYSTEM CAN BE DYNAMICALLY UNSTABLE (POINT D)

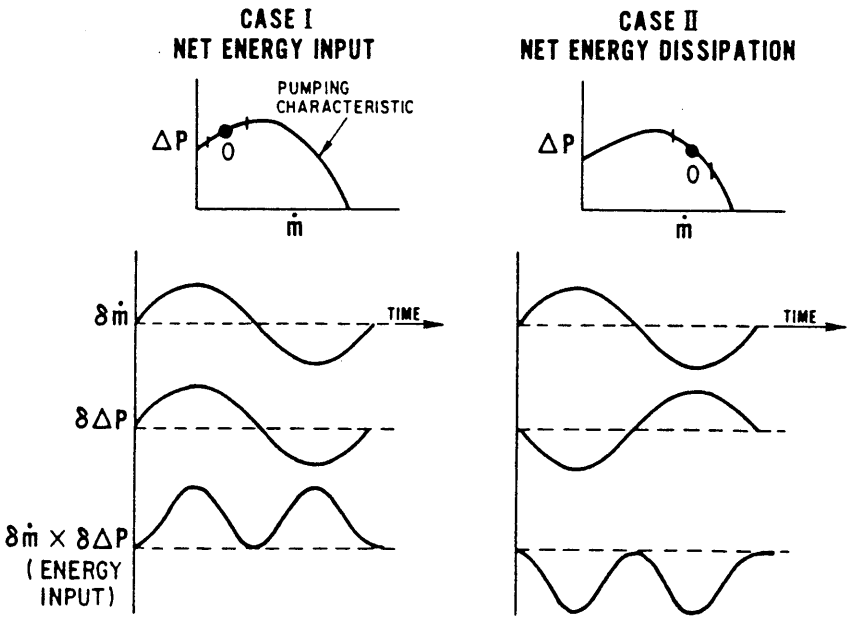

Figure 1.3
from Reference [14]

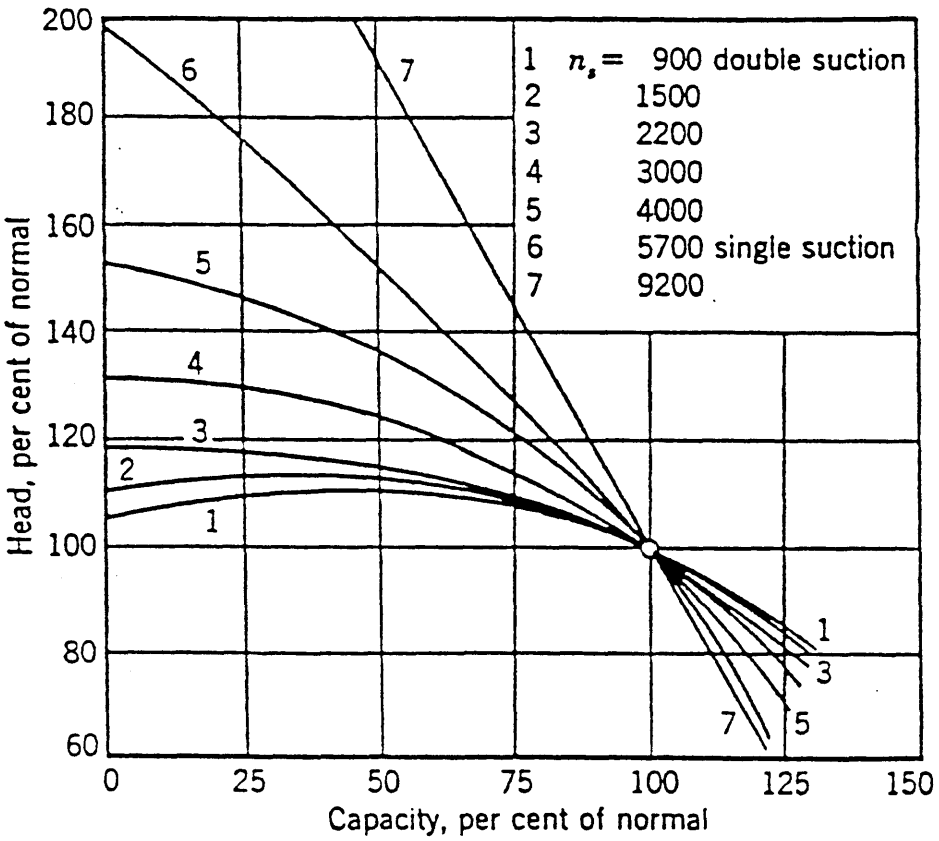

Figure 1.4
from Reference [13]

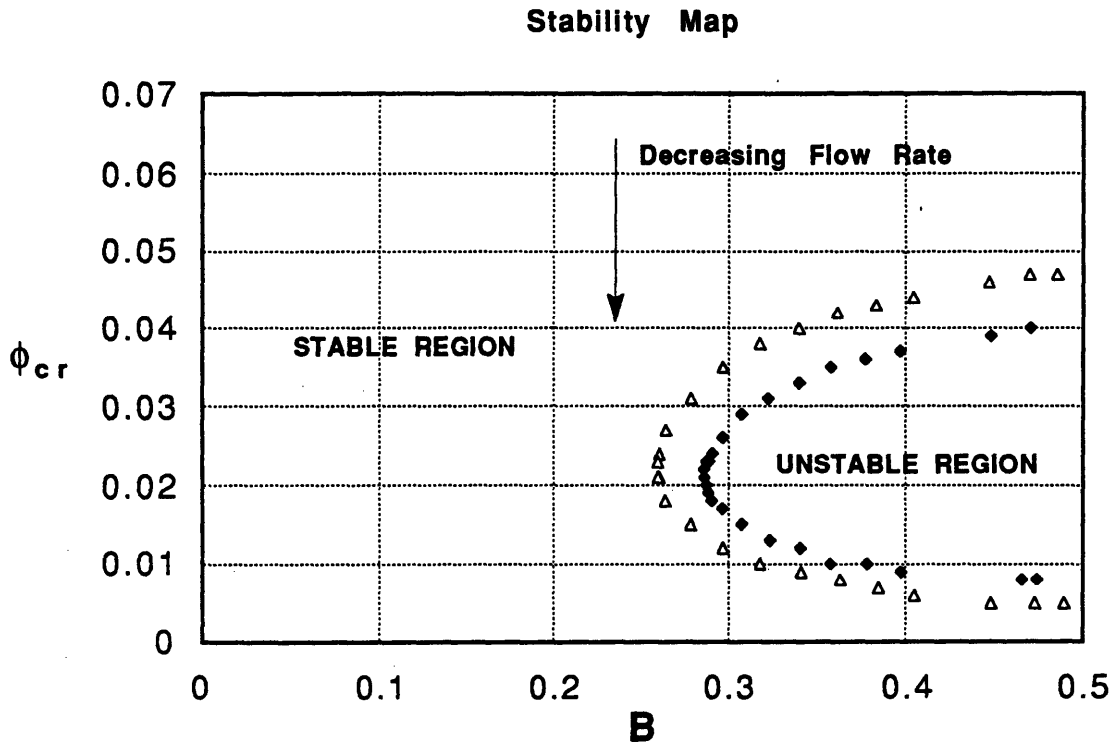

Figure 1.5
from Reference [6]

Schematic of Test Facility

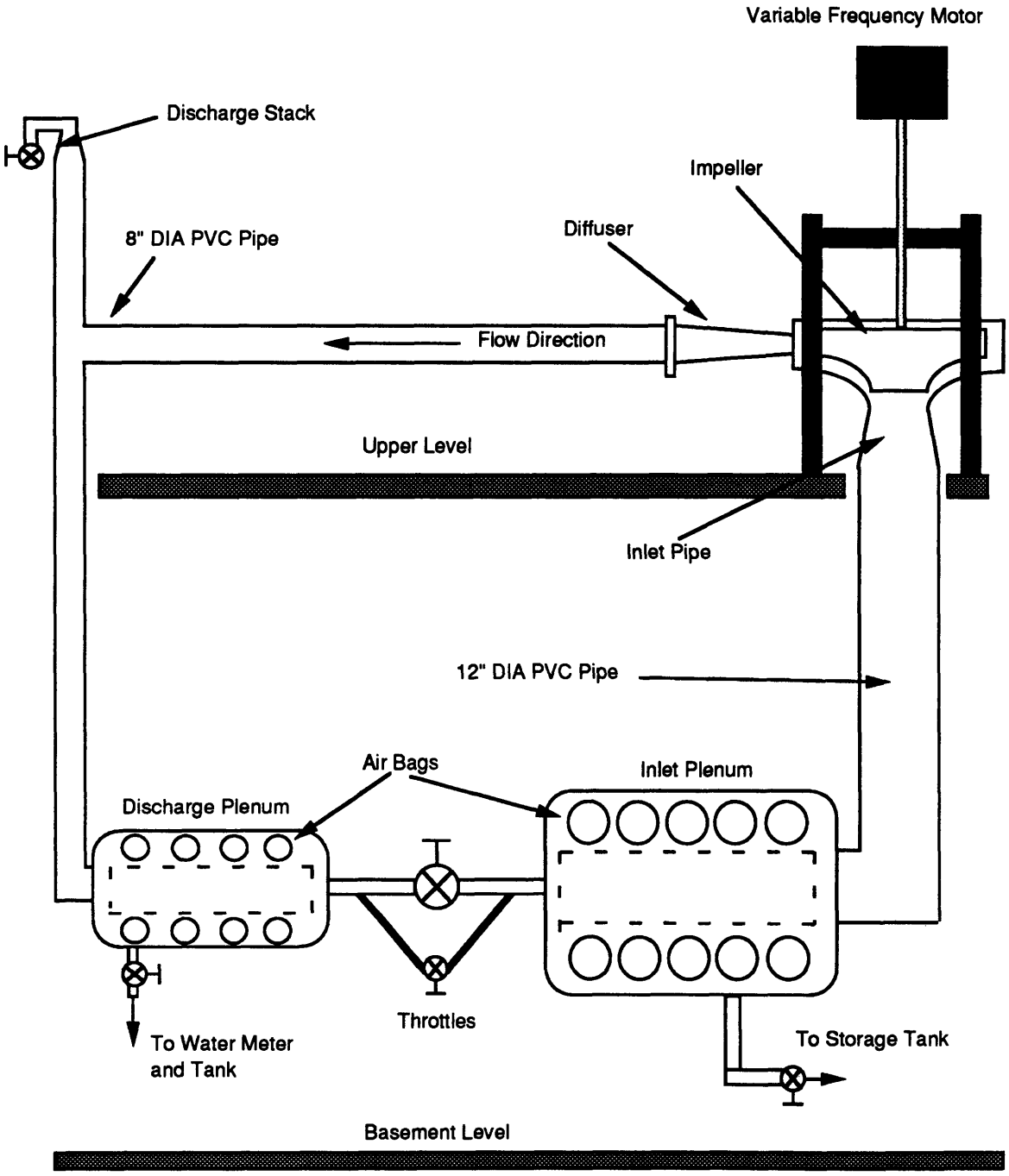

Figure 2.1

Properties of Plexiglass™

Ref. Index	1.5
Transmittance	92%
Young's Modulus	3100 MPa
Tensile Strength	72 MPa
Comp. Modulus	3100 MPa
Comp. Strength	124 MPa
Flexural Modulus	3100 MPa
Flexural Strength	110 MPa
Rockwell Hardness	M 102
Thermal Expansion	5x10E-5 m/m/°C

Figure 2.2
from Reference [13]

PUMP INLET GEOMETRY

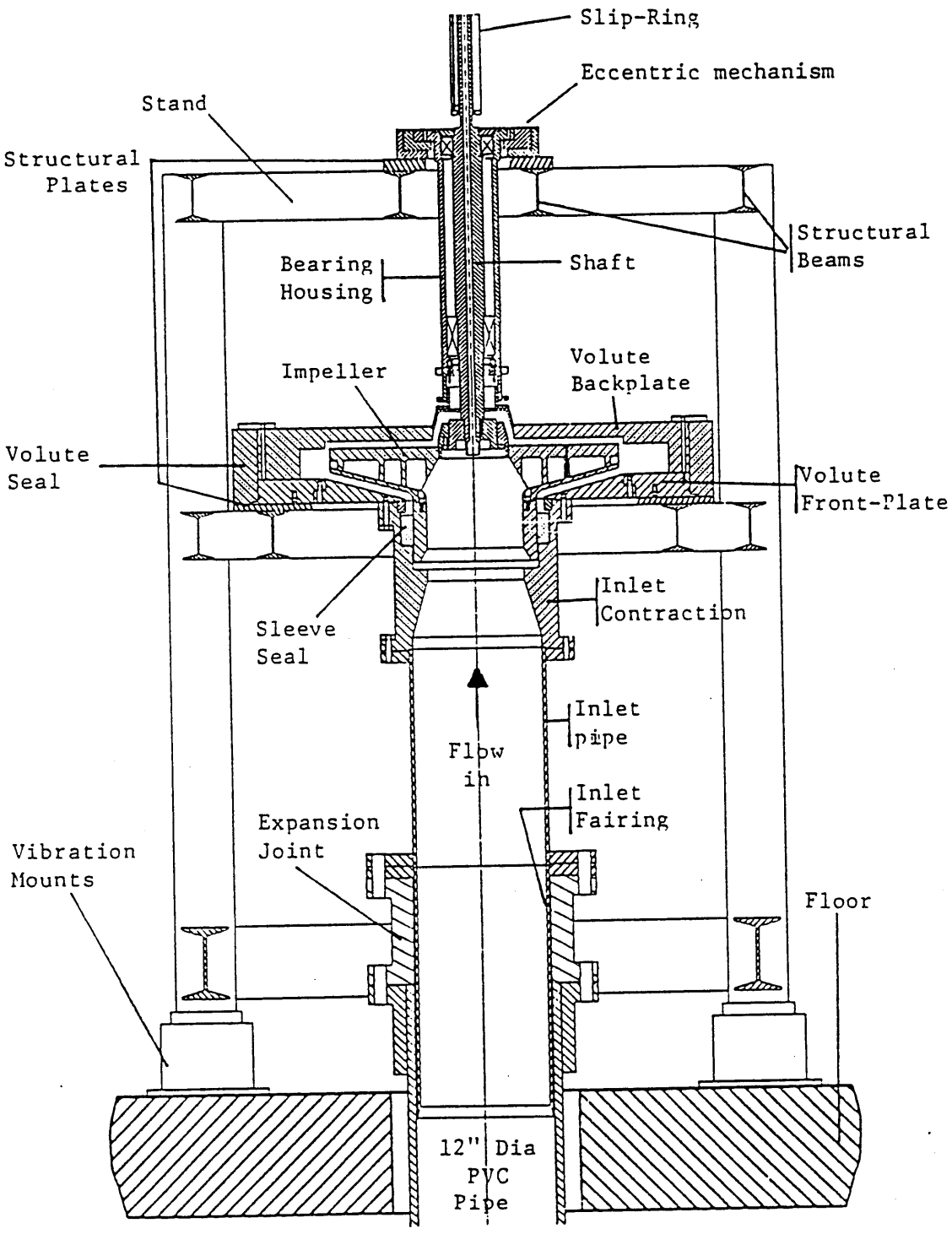

Figure 2.3
from Reference [4]

Comparison Sketch of Original and Modified Volutes

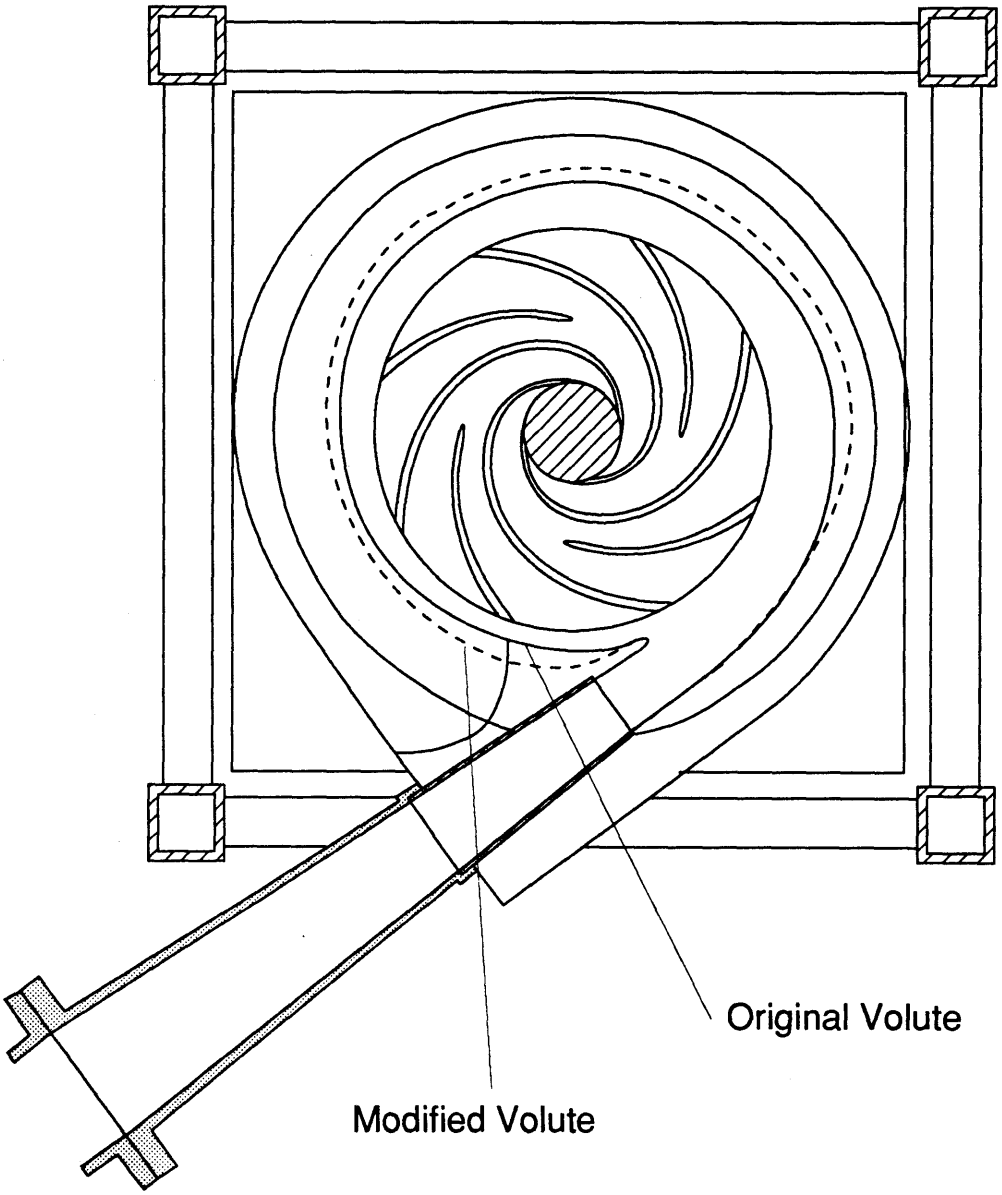

Figure 2.4

PLENUM CONSTRUCTION

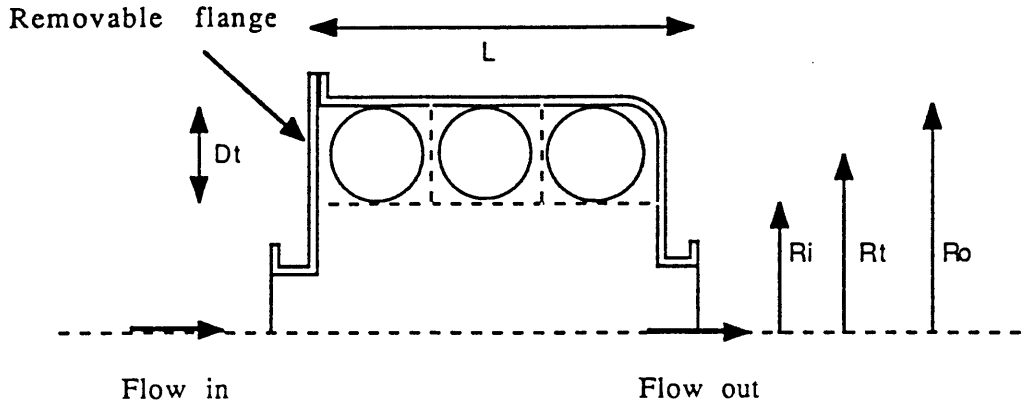

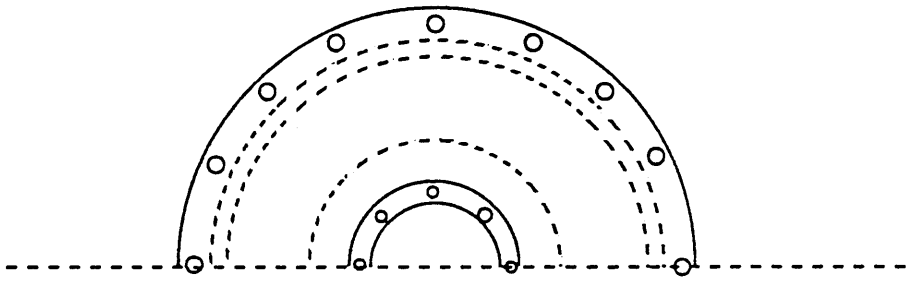

DIMENSION	LARGE PLENUM	SMALL PLENUM
Length (L)	50"	40"
Plenum radius (R_o)	28"	20"
Perforated aluminum radius (R_i)	9.5"	7.5"

(all dimensions in inches)

Figure 2.5
from Reference [4]

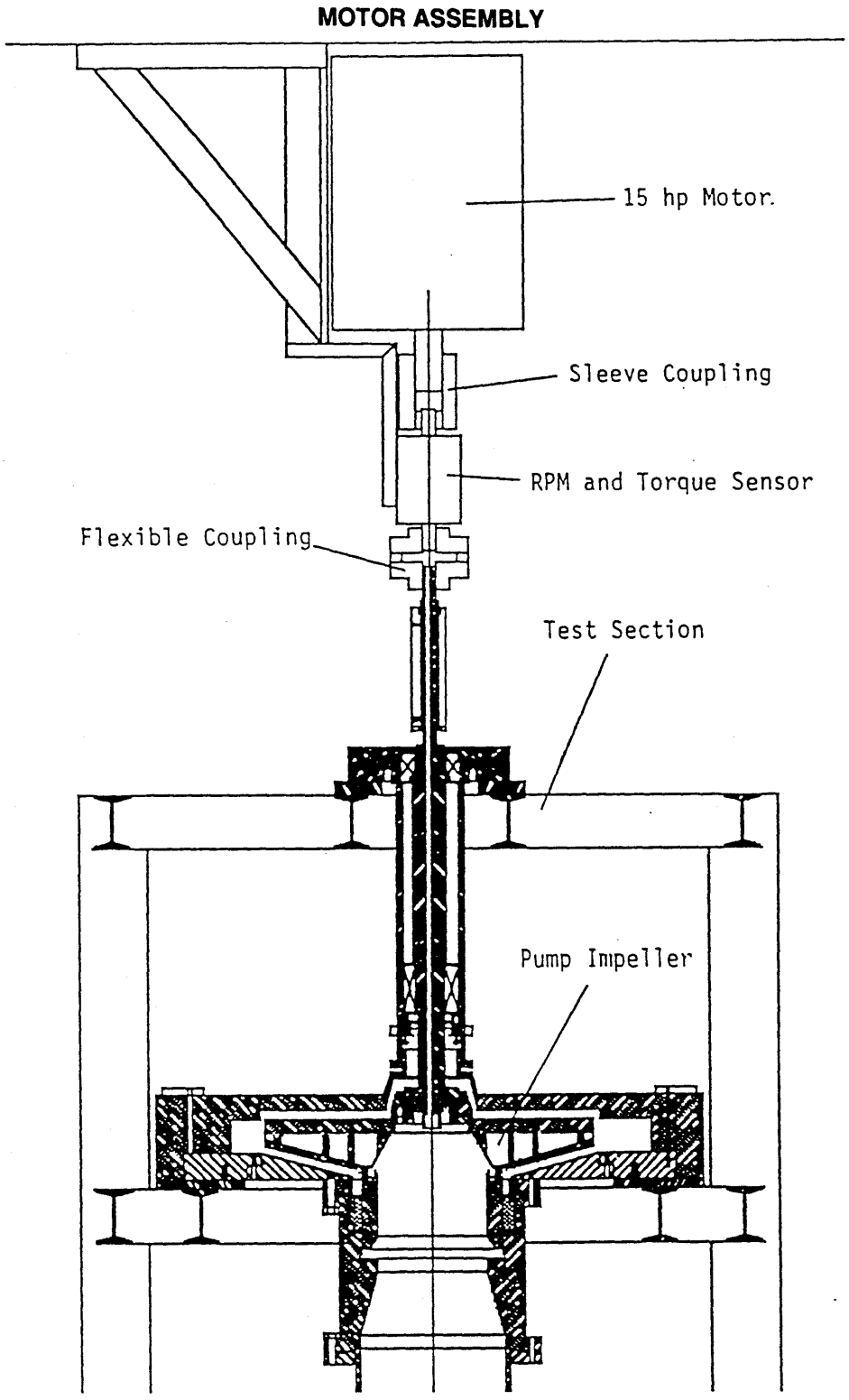

Figure 2.6
from Reference [4]

IMPELLER SHAFT ASSEMBLY

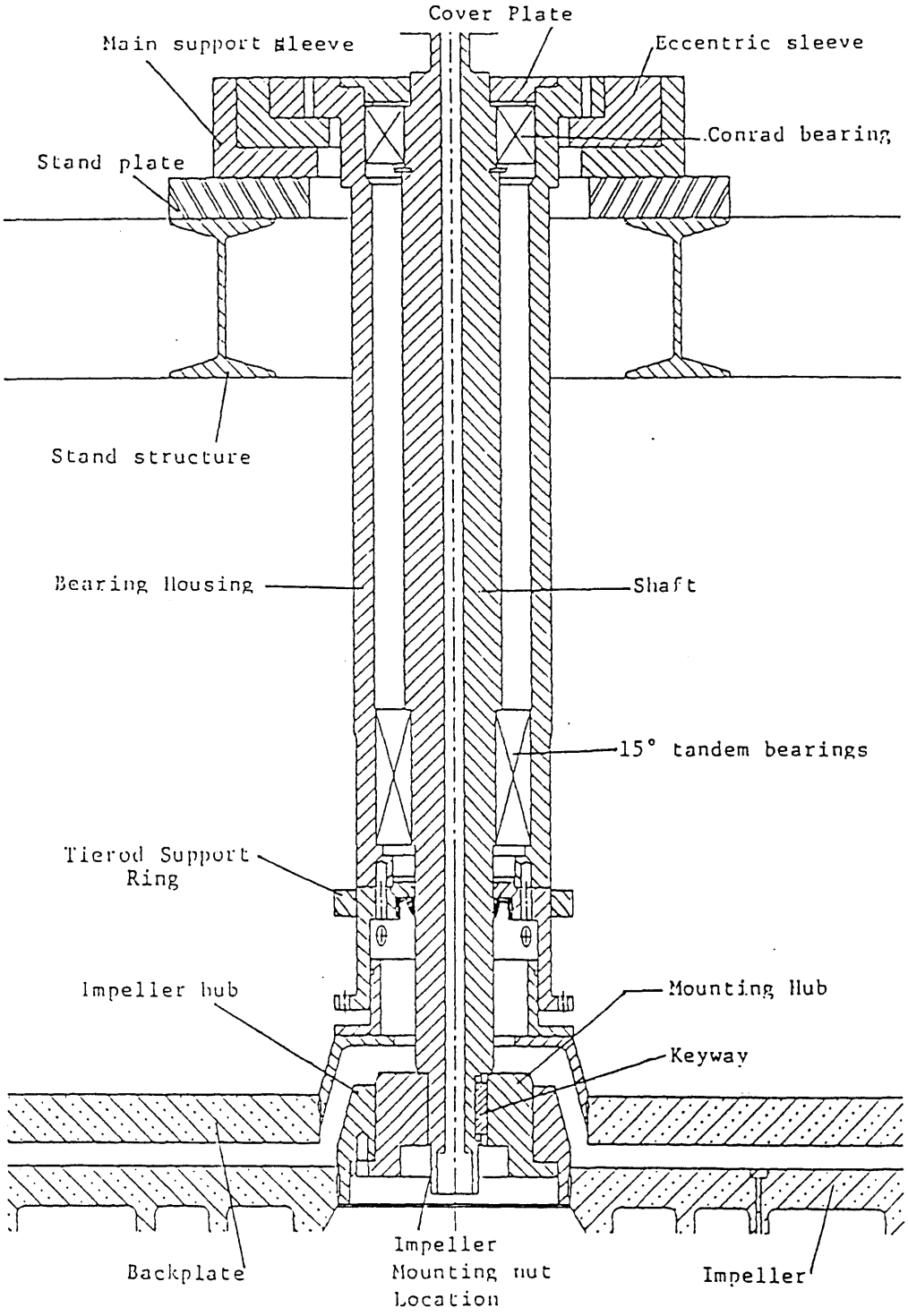

Figure 2.7
from Reference [4]

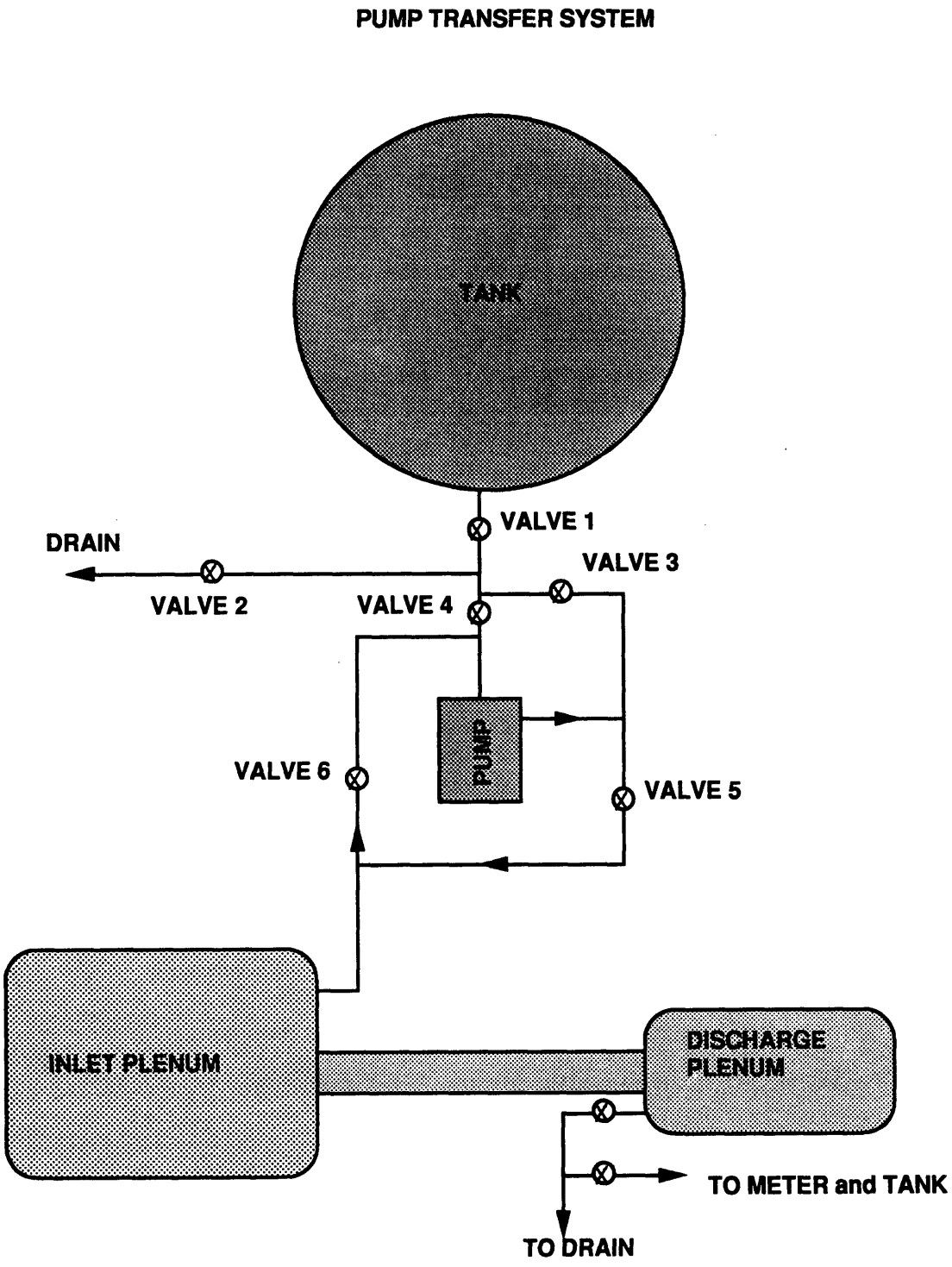
PUMP TRANSFER SYSTEM
TANK
VALVE 1
DRAIN
VALVE 3
VALVE 2
VALVE 4
PUMP
VALVE 6
VALVE 5
INLET PLENUM
DISCHARGE PLENUM
TO METER and TANK
TO DRAIN

Figure 2.8

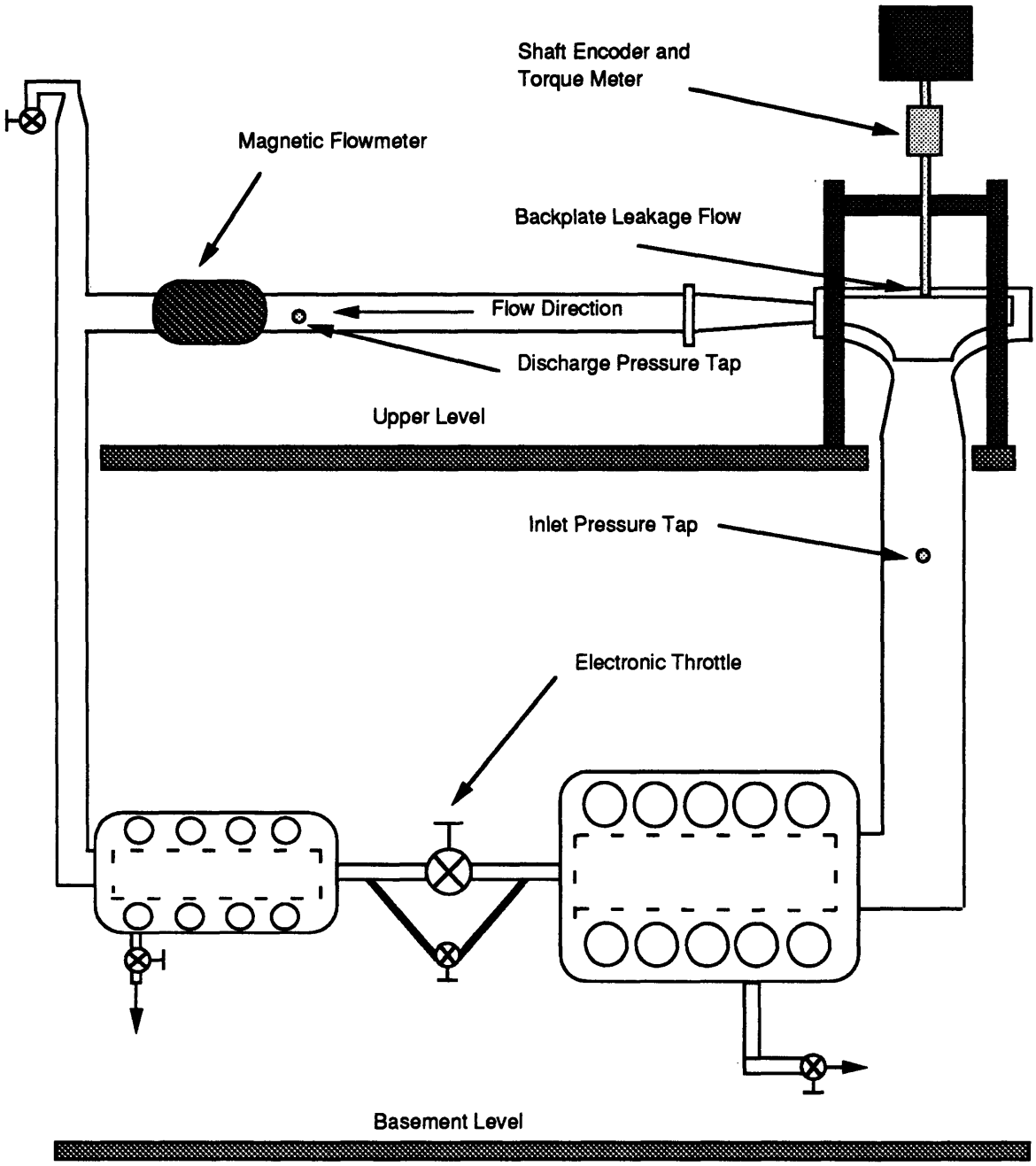
Shaft Encoder and
Torque Meter
Magnetic Flowmeter
Backplate Leakage Flow
Flow Direction
Discharge Pressure Tap
Upper Level
Inlet Pressure Tap
Electronic Throttle
Basement Level

Figure 2.9

SCHEMATIC OF SCANIVALVE SYSTEM

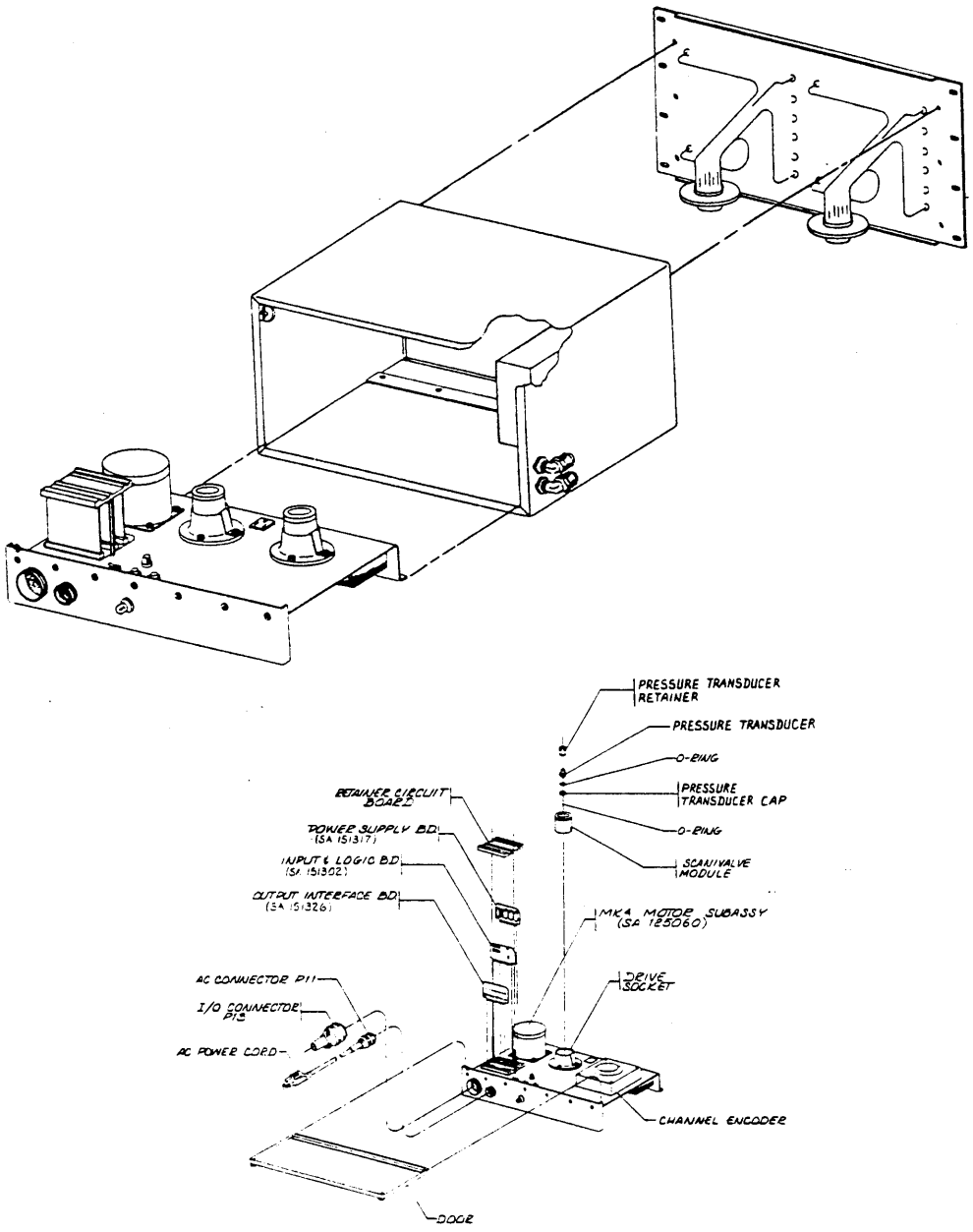

Figure 2.10
from Scanivalve Instruction Manual

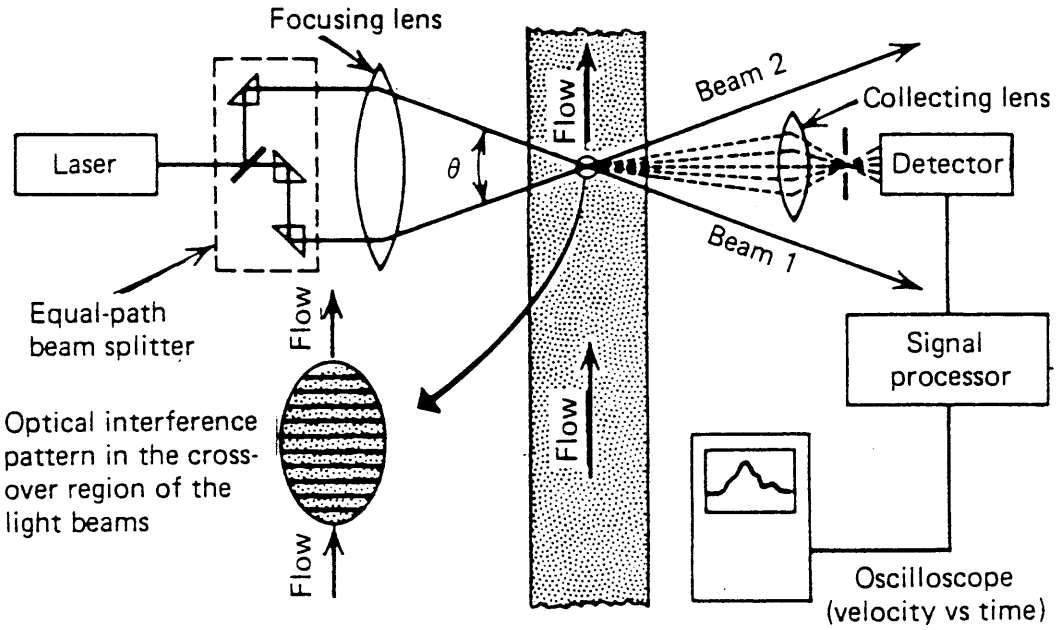

Figure 2.11
from Reference [7]

Original Volute Pressure Tap Locations

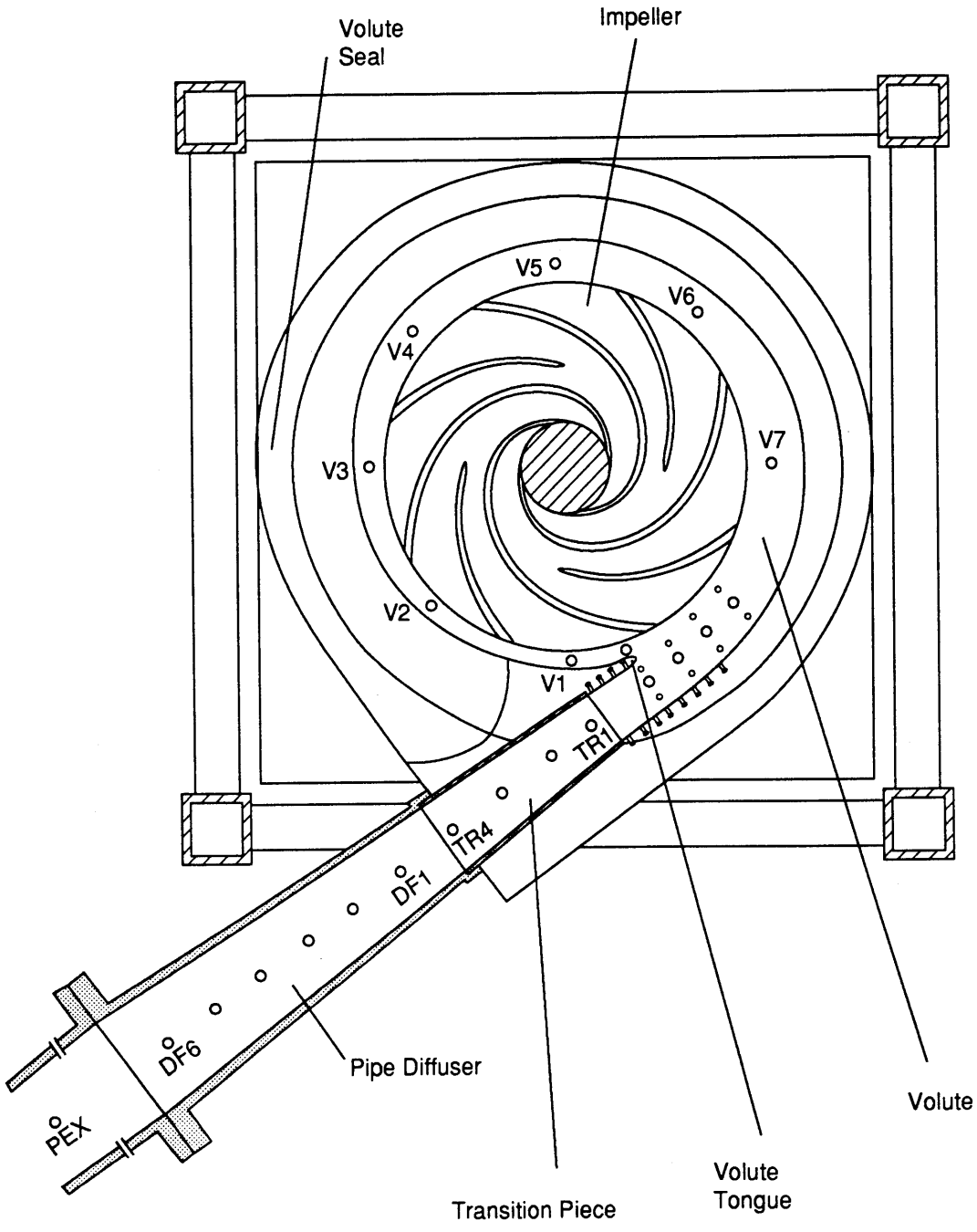

Figure 3.1

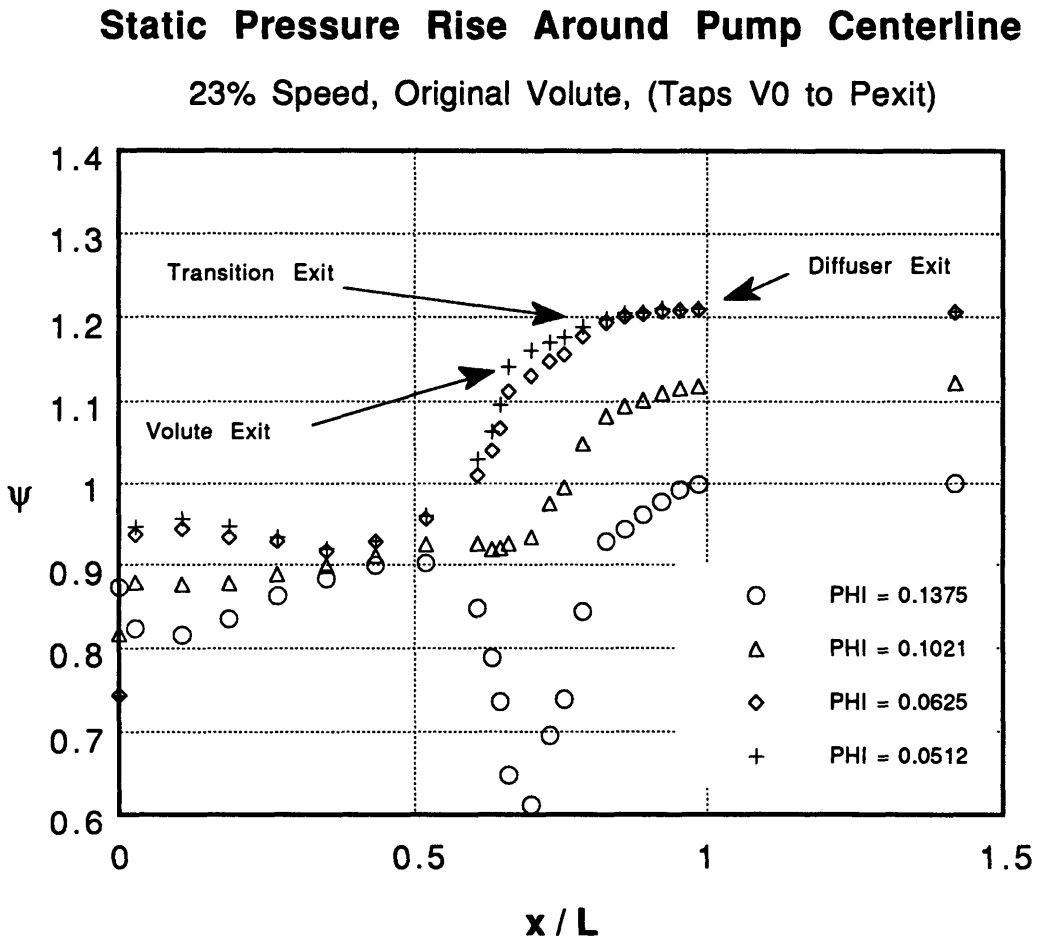
Static Pressure Rise Around Pump Centerline
23% Speed, Original Volute, (Taps V0 to Pexit)
1.4
1.3
1.2
1.1
1
0.9
0.8
0.7
0.6
ψ
0
0.5
1
1.5
x / L
Transition Exit
Diffuser Exit
Volute Exit
PHI = 0.1375
PHI = 0.1021
PHI = 0.0625
PHI = 0.0512

Figure 3.2

Static Pressure Rise Around Pump Centerline

50% Speed, Original Volute, (Taps V0 to Pexit)

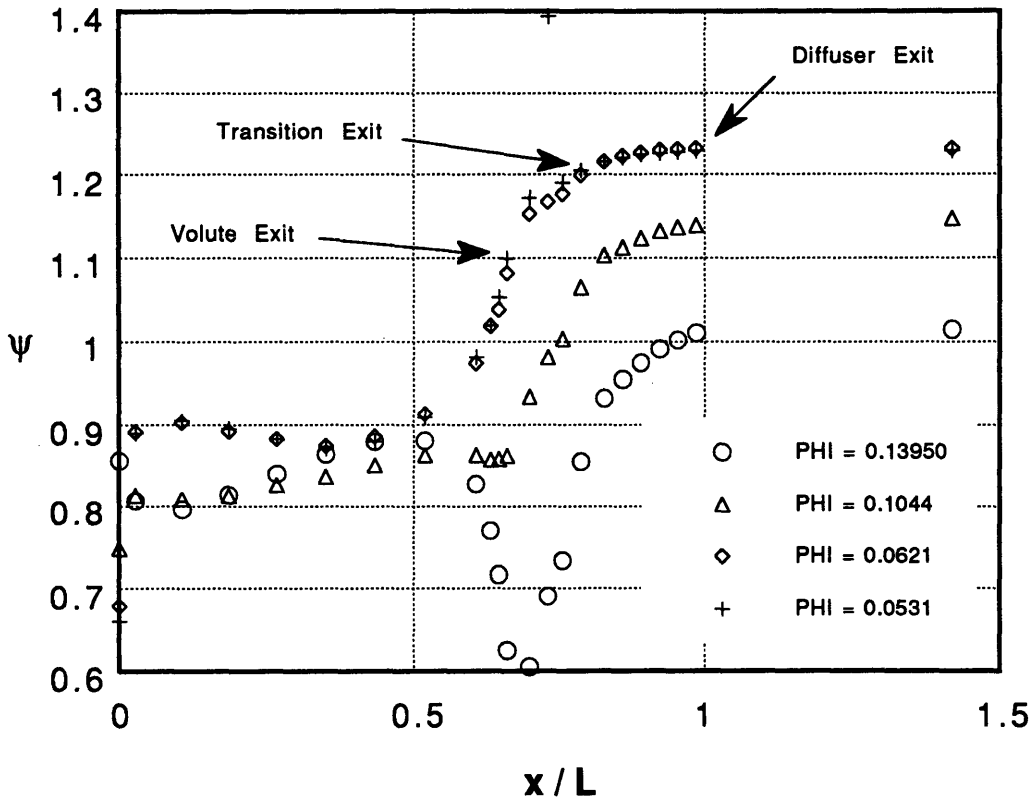

Figure 3.3

MOVEMENT OF TONGUE SEPARATION STREAMLINE

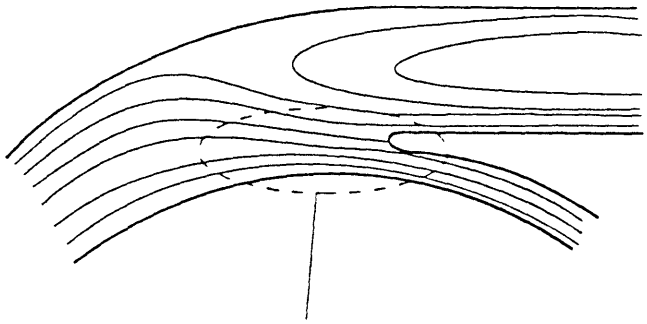

Low flow coefficient

($\Phi \approx 0.01$)

Streamline contraction
Losses are minimal: Small ξ'

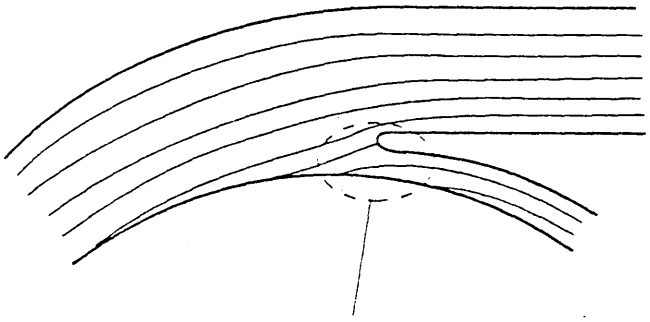

Intermediate flow coefficient

($\Phi \approx 0.08$)

Slight diffusion
Moderate losses: Intermediate ξ'

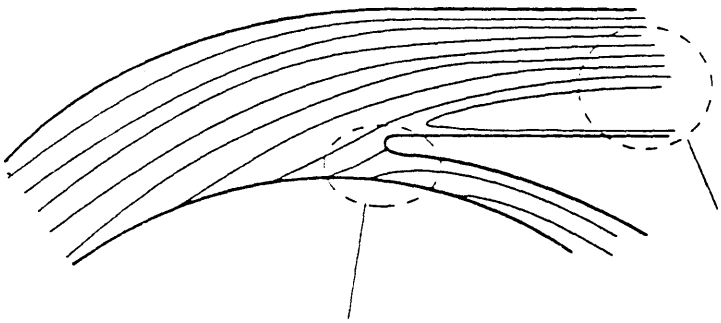

High flow coefficient

($\Phi \approx 0.12$)

Strong diffuser inlet distortion

Strong diffusion
High losses: High ξ'

Figure 3.4
from Reference [13]

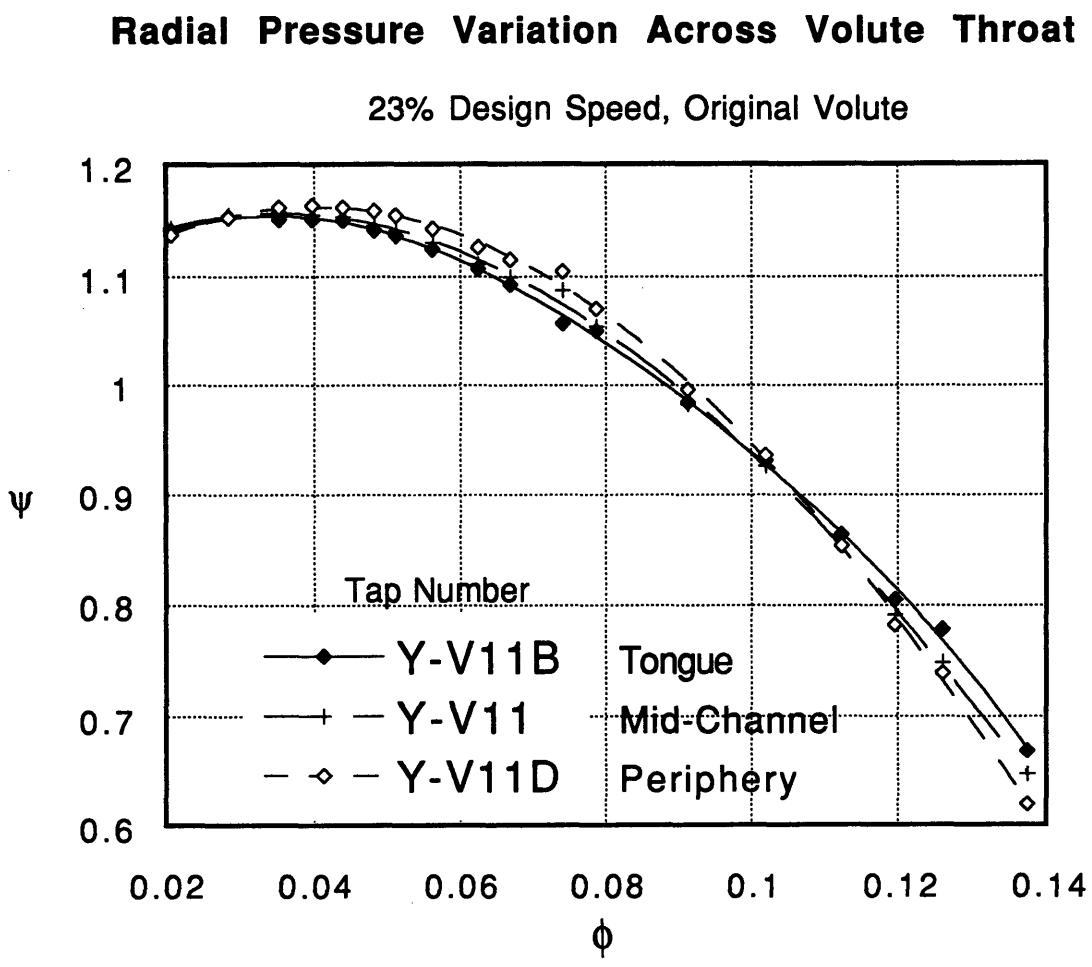
Radial Pressure Variation Across Volute Throat
23% Design Speed, Original Volute
1.2
1.1
1
0.9
0.8
0.7
0.6
ψ
Tap Number
Y-V11B
Tongue
Y-V11
Mid-Channel
Y-V11D
Periphery
0.02
0.04
0.06
0.08
0.1
0.12
0.14
ϕ

Figure 3.5

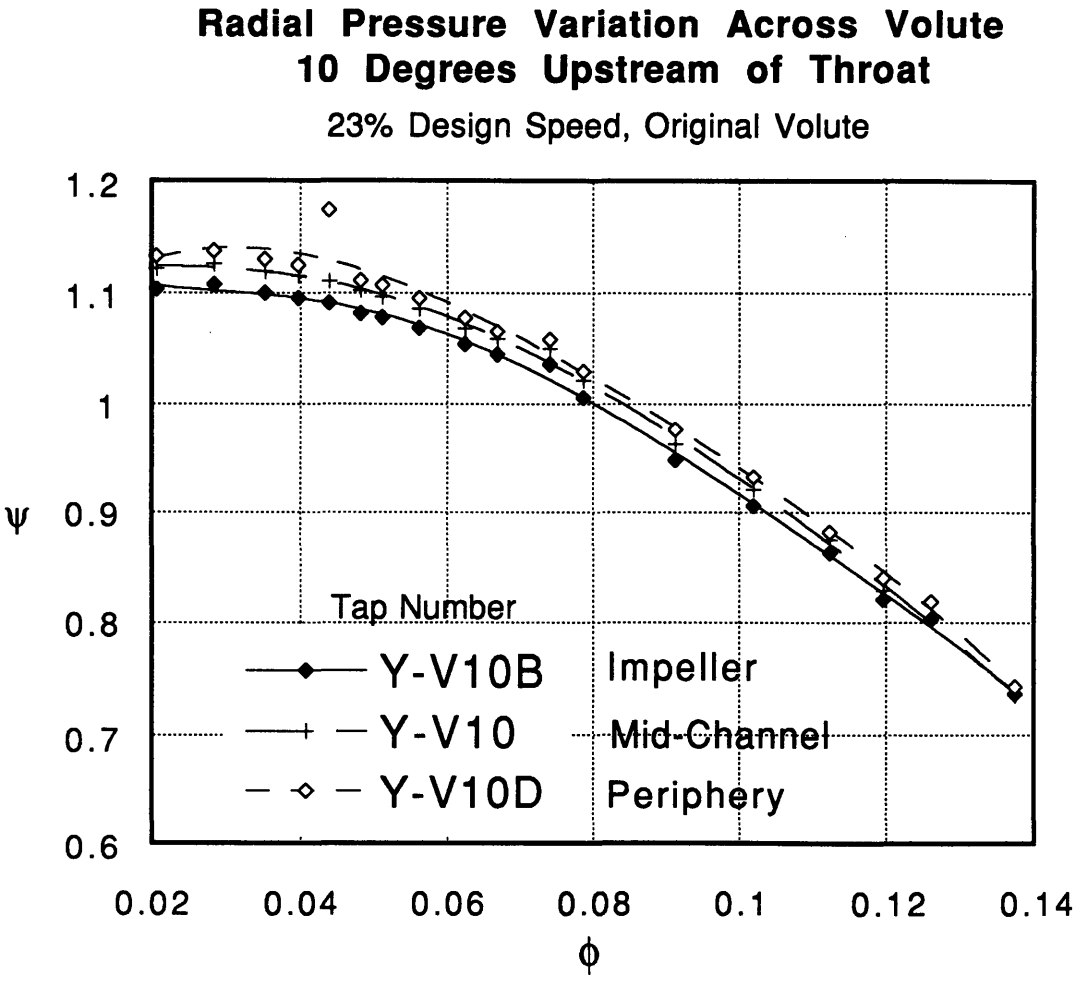
Radial Pressure Variation Across Volute
10 Degrees Upstream of Throat
23% Design Speed, Original Volute
1.2
1.1
1
ψ 0.9
0.8
0.7
0.6
Tap Number
Y-V10B Impeller
Y-V10 Mid-Channel
Y-V10D Periphery
0.02
0.04
0.06
0.08
0.1
0.12
0.14
ϕ

Figure 3.6

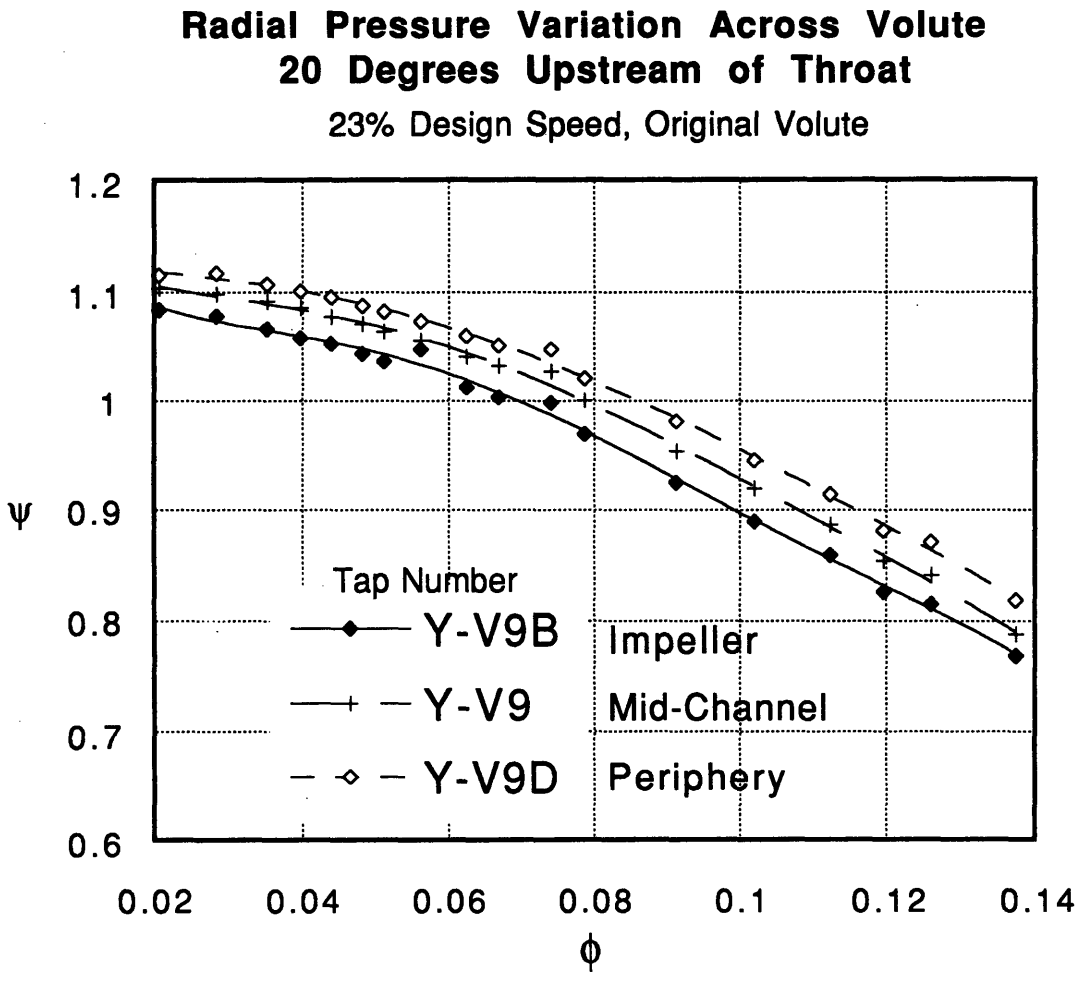
Radial Pressure Variation Across Volute
20 Degrees Upstream of Throat
23% Design Speed, Original Volute
1.2
1.1
1
0.9
0.8
0.7
0.6
ψ
Tap Number
Y-V9B Impeller
Y-V9 Mid-Channel
Y-V9D Periphery
0.02
0.04
0.06
0.08
0.1
0.12
0.14
ϕ

Figure 3.7

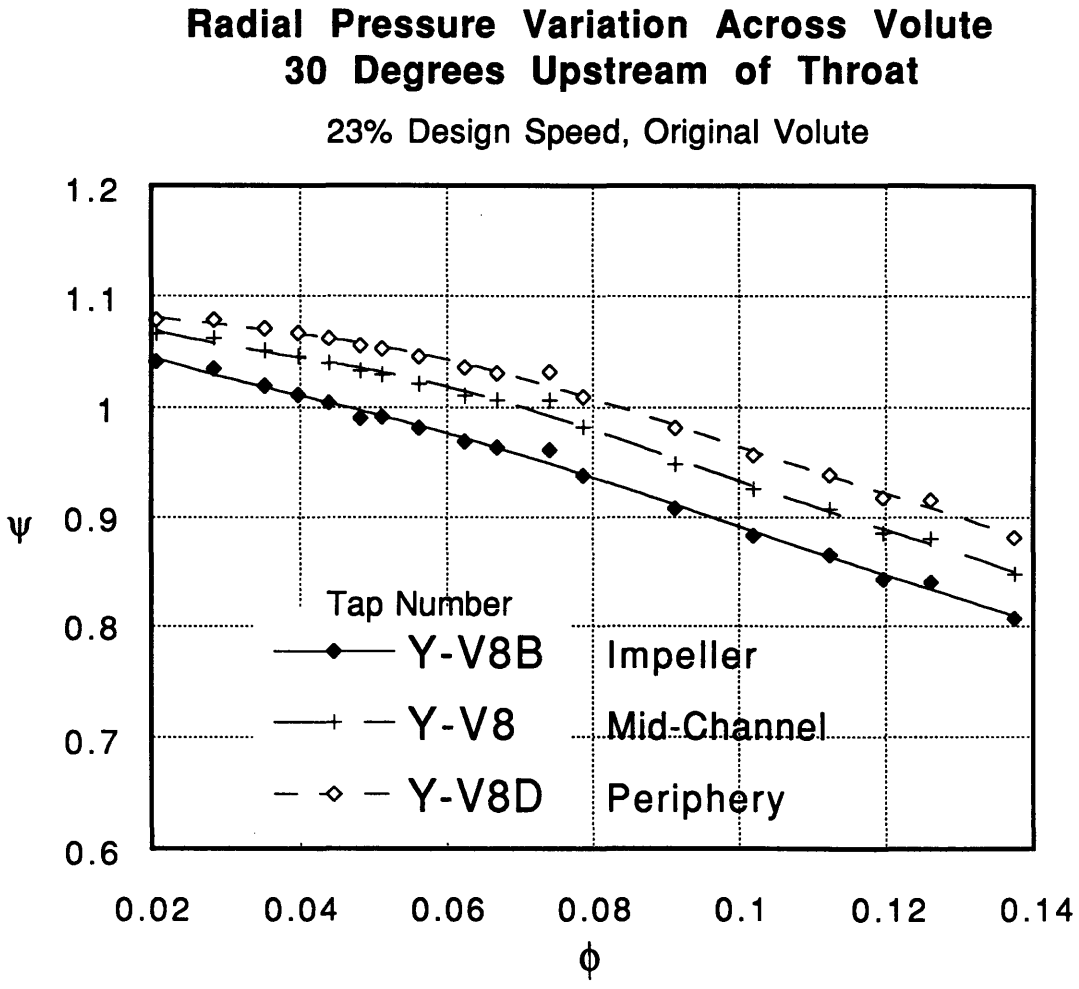
Radial Pressure Variation Across Volute
30 Degrees Upstream of Throat
23% Design Speed, Original Volute
1.2
1.1
1
0.9
0.8
0.7
0.6
ψ
0.02
0.04
0.06
0.08
0.1
0.12
0.14
ϕ
Tap Number
Y-V8B Impeller
Y-V8 Mid-Channel
Y-V8D Periphery

Figure 3.8

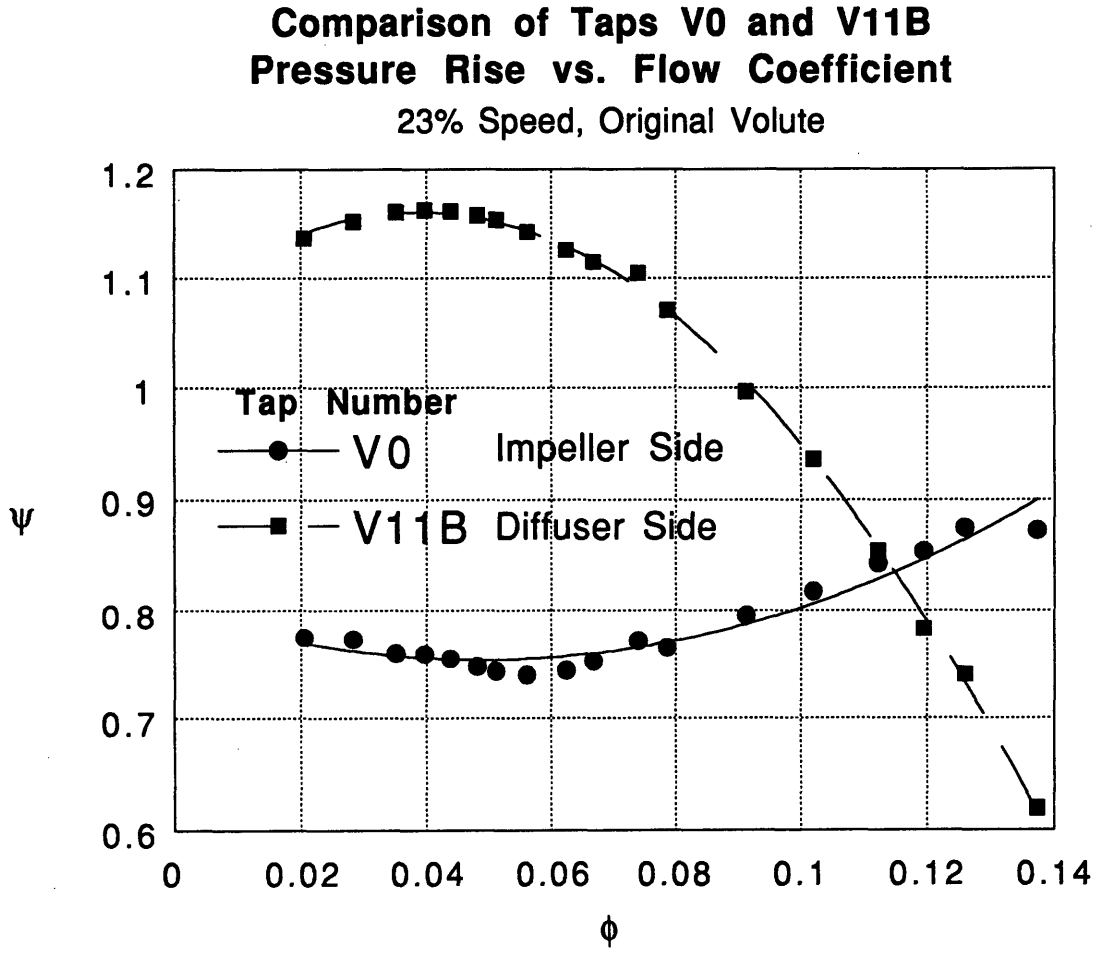
Comparison of Taps V0 and V11B
Pressure Rise vs. Flow Coefficient
23% Speed, Original Volute
1.2
1.1
1
0.9
0.8
0.7
0.6
ψ
Tap Number
V0 Impeller Side
V11B Diffuser Side
0
0.02
0.04
0.06
0.08
0.1
0.12
0.14
ϕ

Figure 3.9

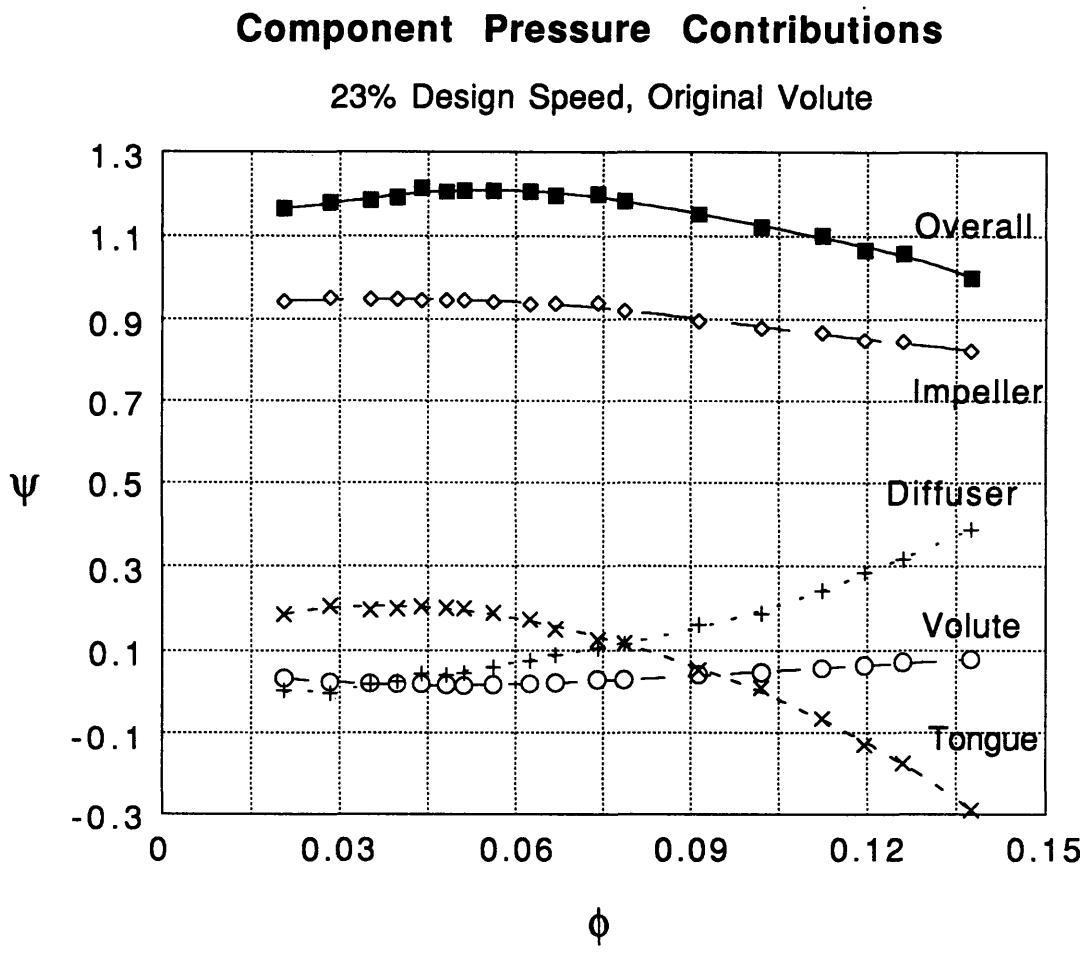
Component Pressure Contributions
23% Design Speed, Original Volute
1.3
1.1
0.9
0.7
0.5
0.3
0.1
-0.1
-0.3
ψ
0
0.03
0.06
0.09
0.12
0.15
ϕ
Overall
Impeller
Diffuser
Volute
Tongue

Figure 3.10

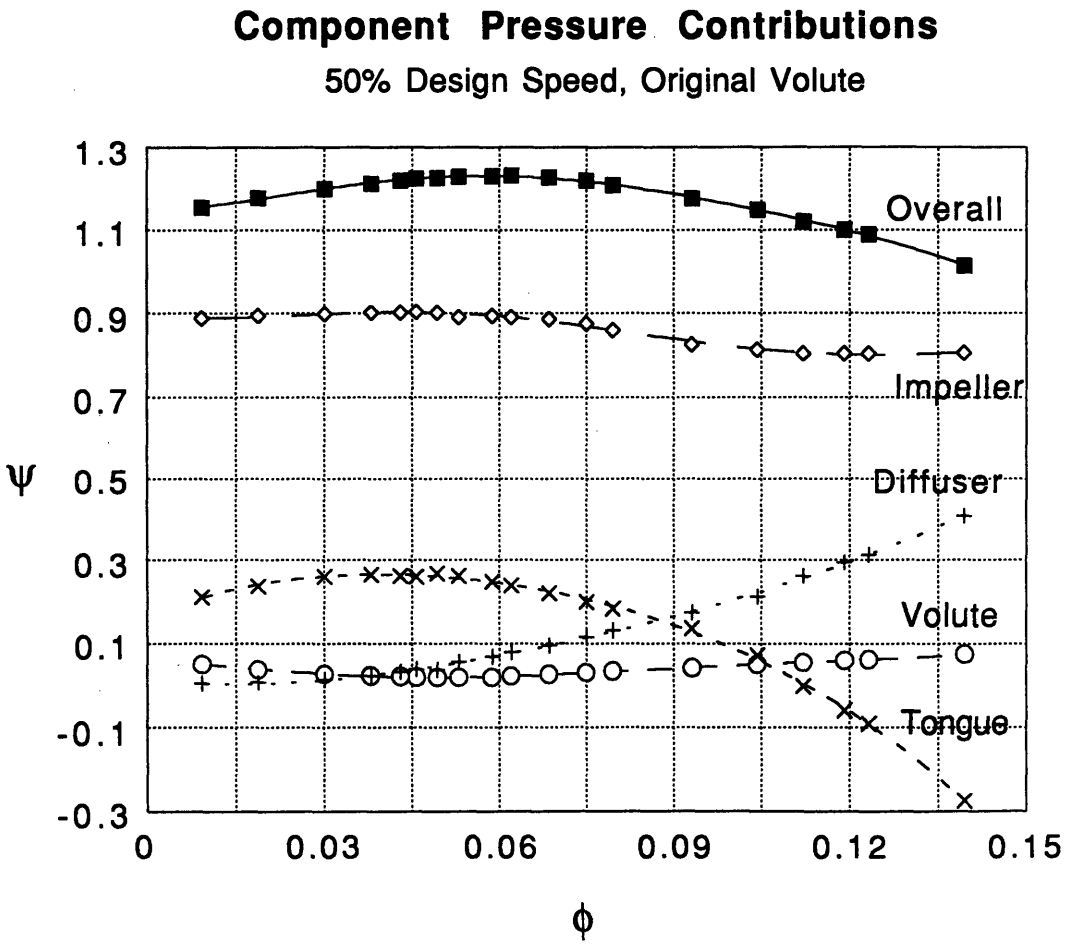
Component Pressure Contributions
50% Design Speed, Original Volute
1.3
1.1
0.9
0.7
0.5
0.3
0.1
-0.1
-0.3
ψ
0
0.03
0.06
0.09
0.12
0.15
ϕ
Overall
Impeller
Diffuser
Volute
Tongue

Figure 3.11

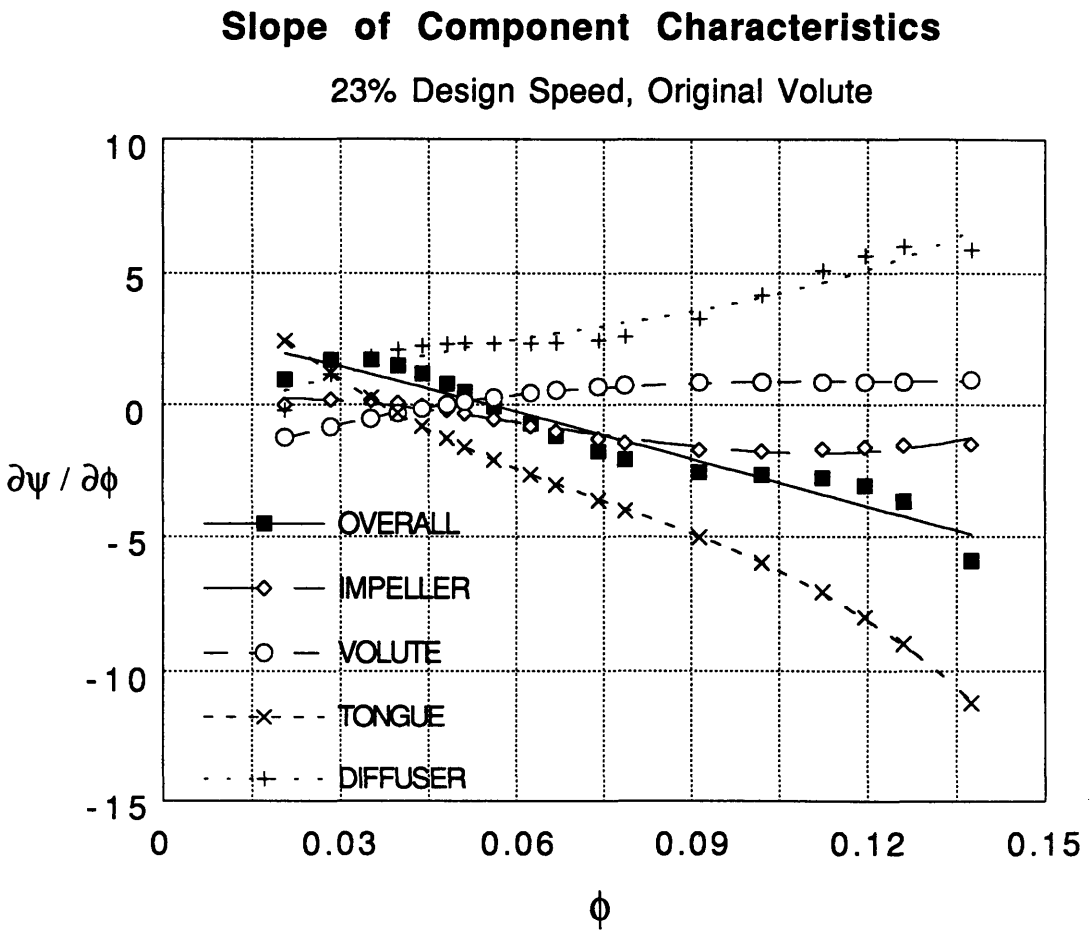
Slope of Component Characteristics
23% Design Speed, Original Volute
10
5
0
-5
-10
-15
∂ψ / ∂ϕ
OVERALL
IMPELLER
VOLUTE
TONGUE
DIFFUSER
0
0.03
0.06
0.09
0.12
0.15
ϕ

Figure 3.12

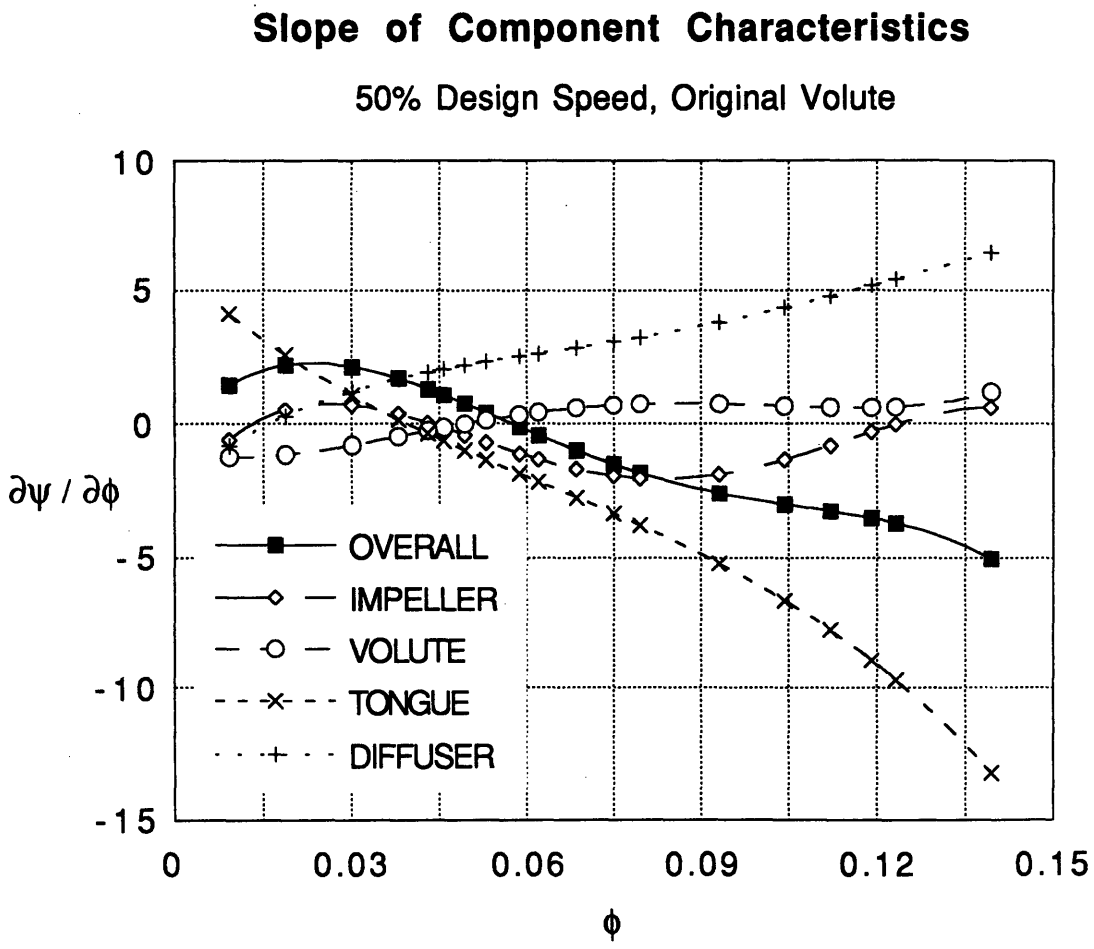
Slope of Component Characteristics
50% Design Speed, Original Volute
10
5
0
-5
-10
-15
∂ψ / ∂ϕ
0
0.03
0.06
0.09
0.12
0.15
ϕ
OVERALL
IMPELLER
VOLUTE
TONGUE
DIFFUSER

Figure 3.13

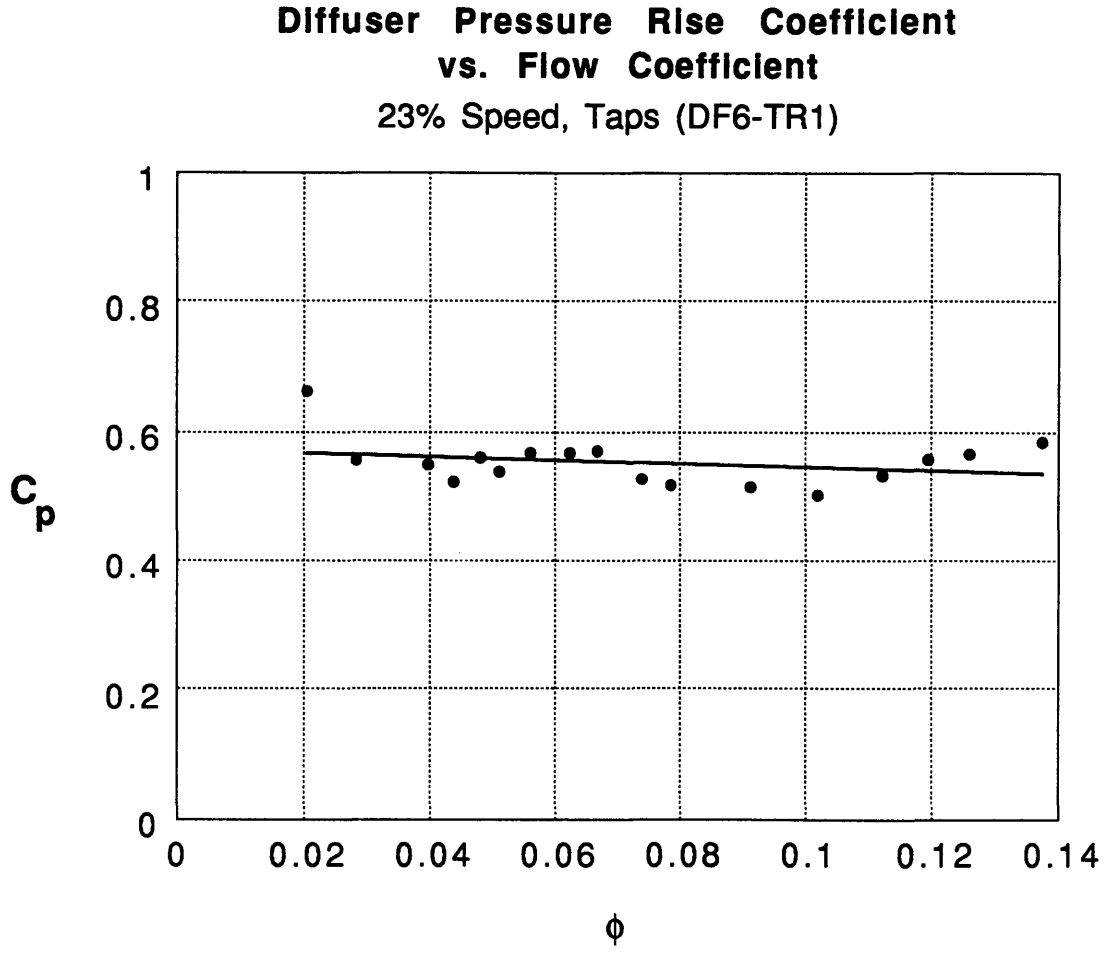
Diffuser Pressure Rise Coefficient
vs. Flow Coefficient
23% Speed, Taps (DF6-TR1)
1
0.8
0.6
0.4
0.2
0
C_p
0
0.02
0.04
0.06
0.08
0.1
0.12
0.14
ϕ

Figure 3.14

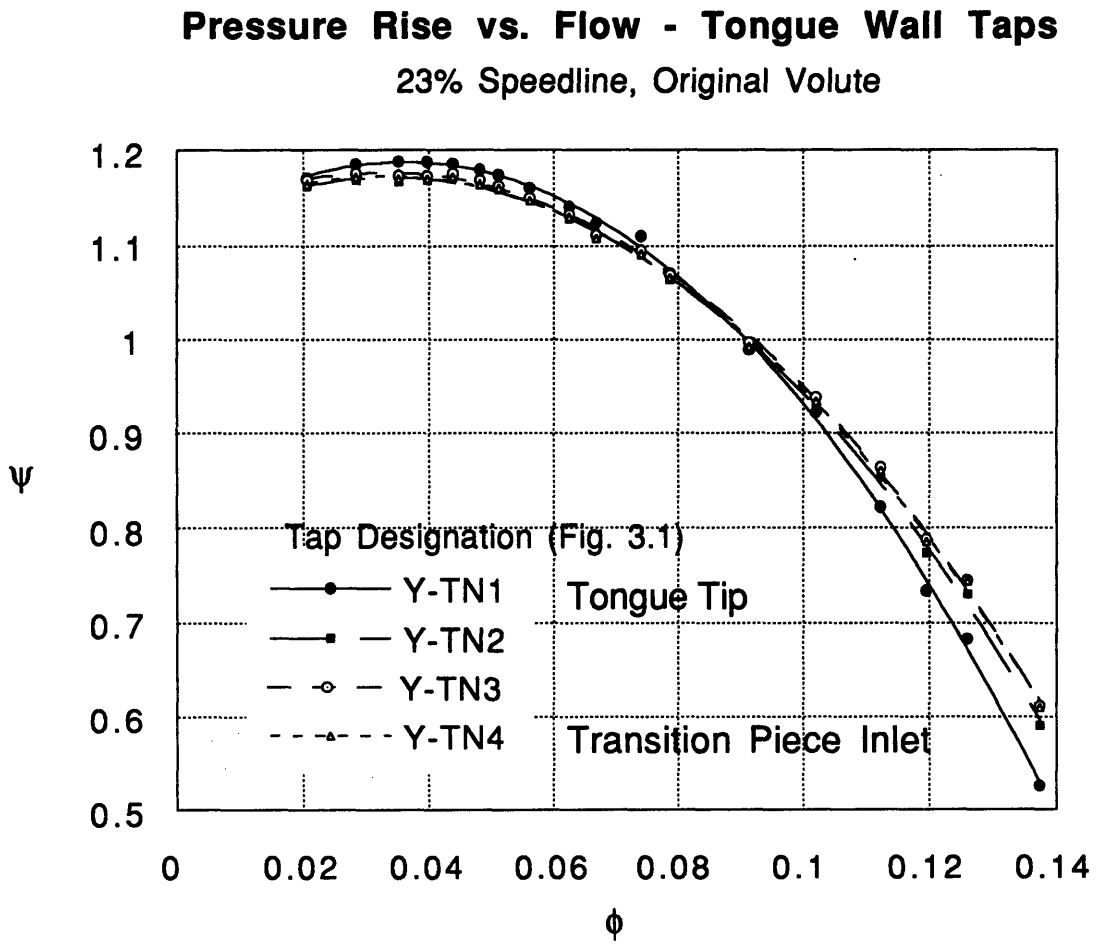
Pressure Rise vs. Flow - Tongue Wall Taps
23% Speedline, Original Volute
1.2
1.1
1
0.9
0.8
0.7
0.6
0.5
ψ
0
0.02
0.04
0.06
0.08
0.1
0.12
0.14
ϕ
Tap Designation (Fig. 3.1)
Y-TN1
Tongue Tip
Y-TN2
Y-TN3
Y-TN4
Transition Piece Inlet

Figure 3.15

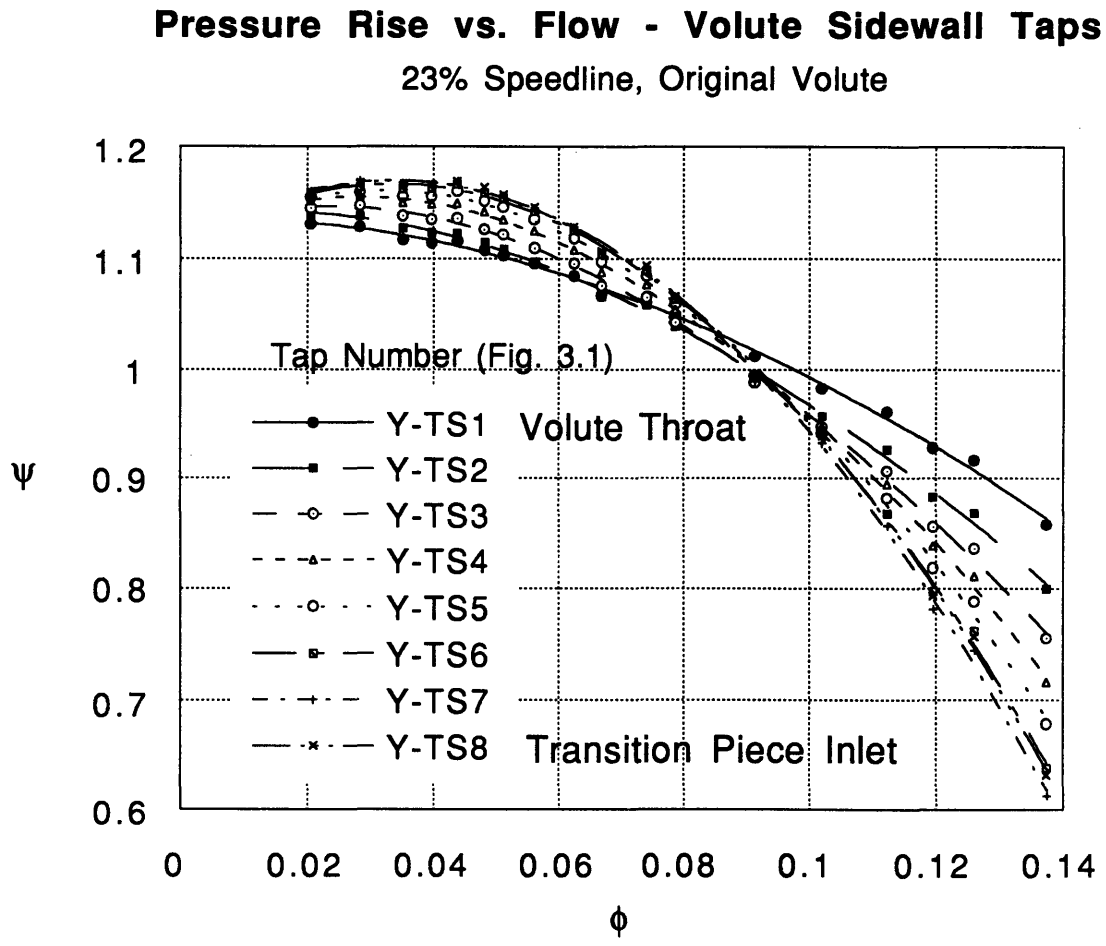
Pressure Rise vs. Flow - Volute Sidewall Taps
23% Speedline, Original Volute
1.2
1.1
1
0.9
0.8
0.7
0.6
ψ
0
0.02
0.04
0.06
0.08
0.1
0.12
0.14
ϕ
Tap Number (Fig. 3.1)
Y-TS1 Volute Throat
Y-TS2
Y-TS3
Y-TS4
Y-TS5
Y-TS6
Y-TS7
Y-TS8 Transition Piece Inlet

Figure 3.16

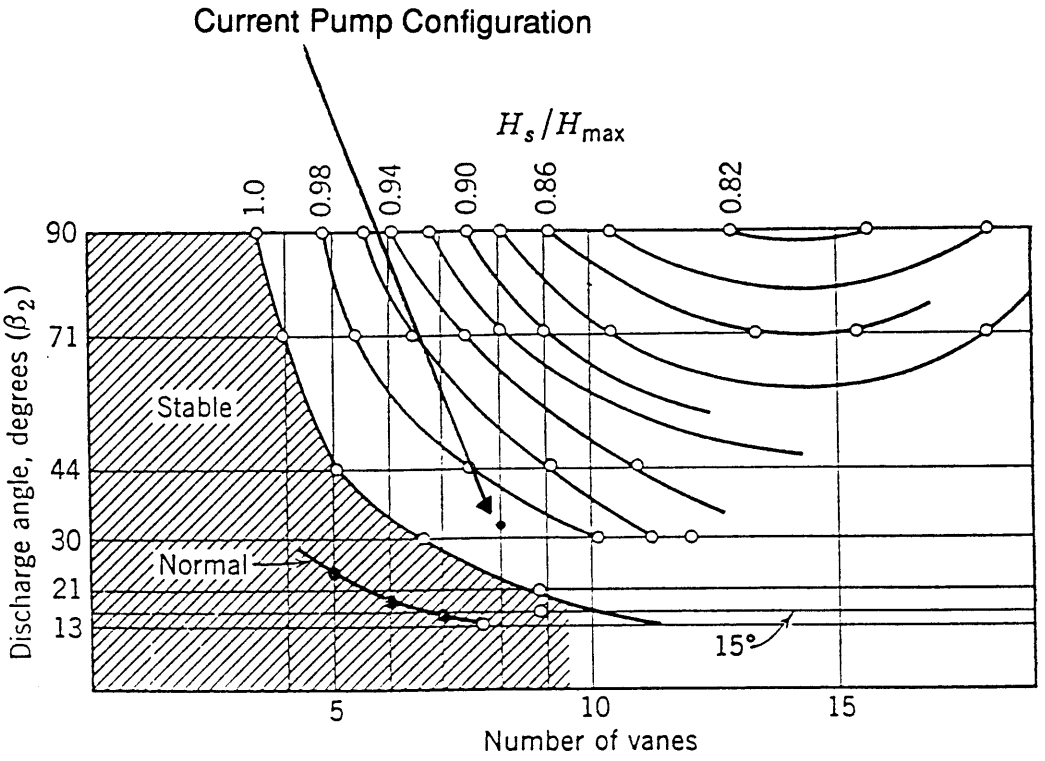

Figure 3.17
from Reference [24]

Volute Locations of LDV Grids

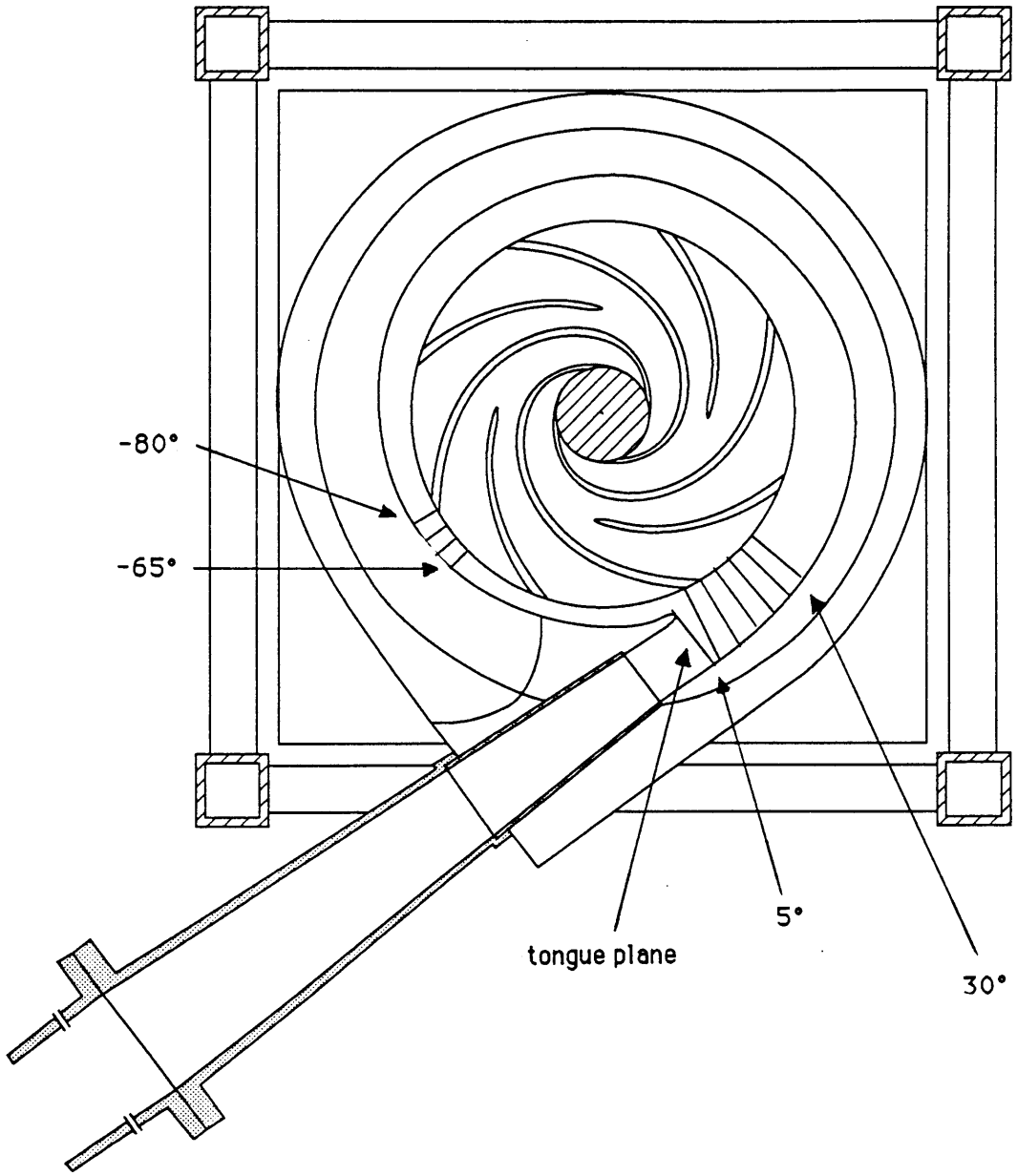

Figure 3.18

LDV Coordinate System

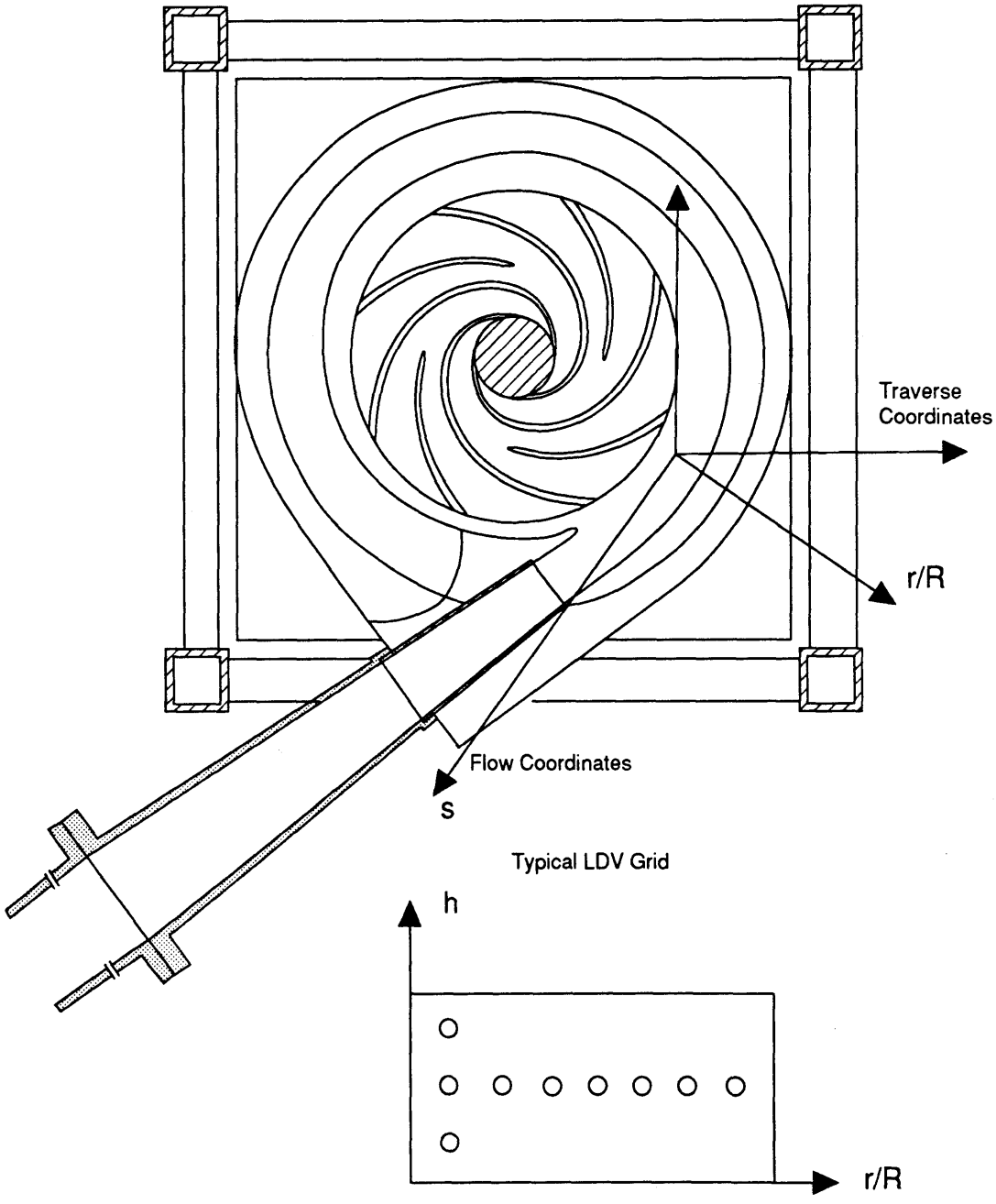

Figure 3.19

Laser Velocimeter Optics Arrangement

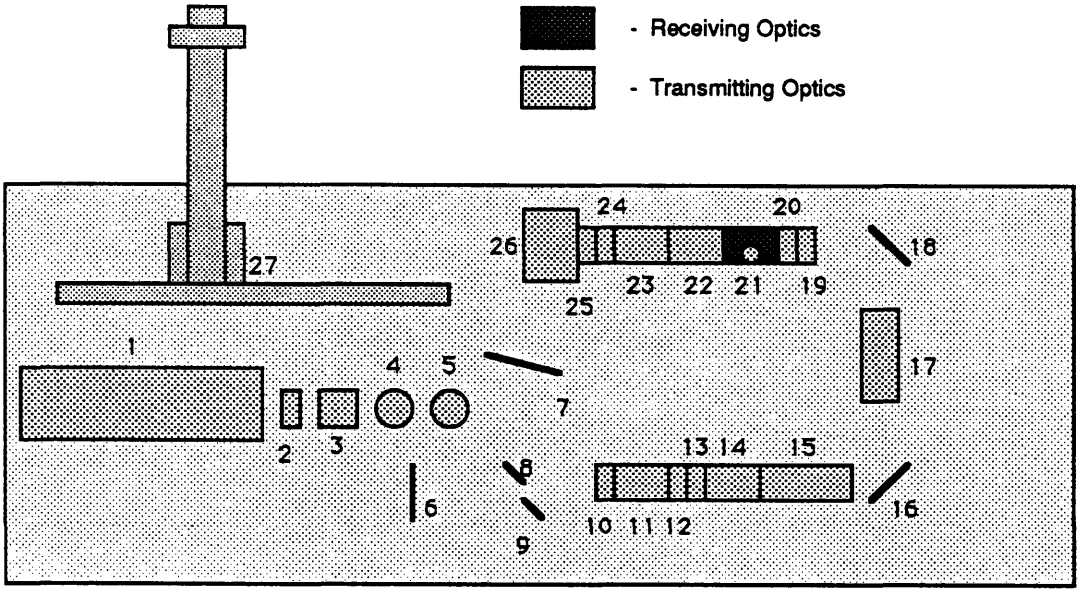

List of Components:
1. Lexal Laser
2. Polarization Rotator
3. Beam Collimator
4. Attenuator
5. Dispersion Prism
6. Mirror
7. Mirror
8. Mirror
9. Mirror
10. Blue Beam Polarization Rotator
11. Beam Splitter
12. Beam Displacer
13. Green Beam Polarization Rotator
14. Beamsplitter
15. Bragg Cell
16. Mirror
17. Bragg Cell
18. Mirror
19. Beam Steering Module
20. Beam Steering Module
21. Receiving Optics Assembly
22. Field Stop
23. Beam Stop
24. Beam Spacer (22mm to 9mm)
25. Beam Spacer
26. Beam Expander
27. XYZ Traverse

Figure 3.20

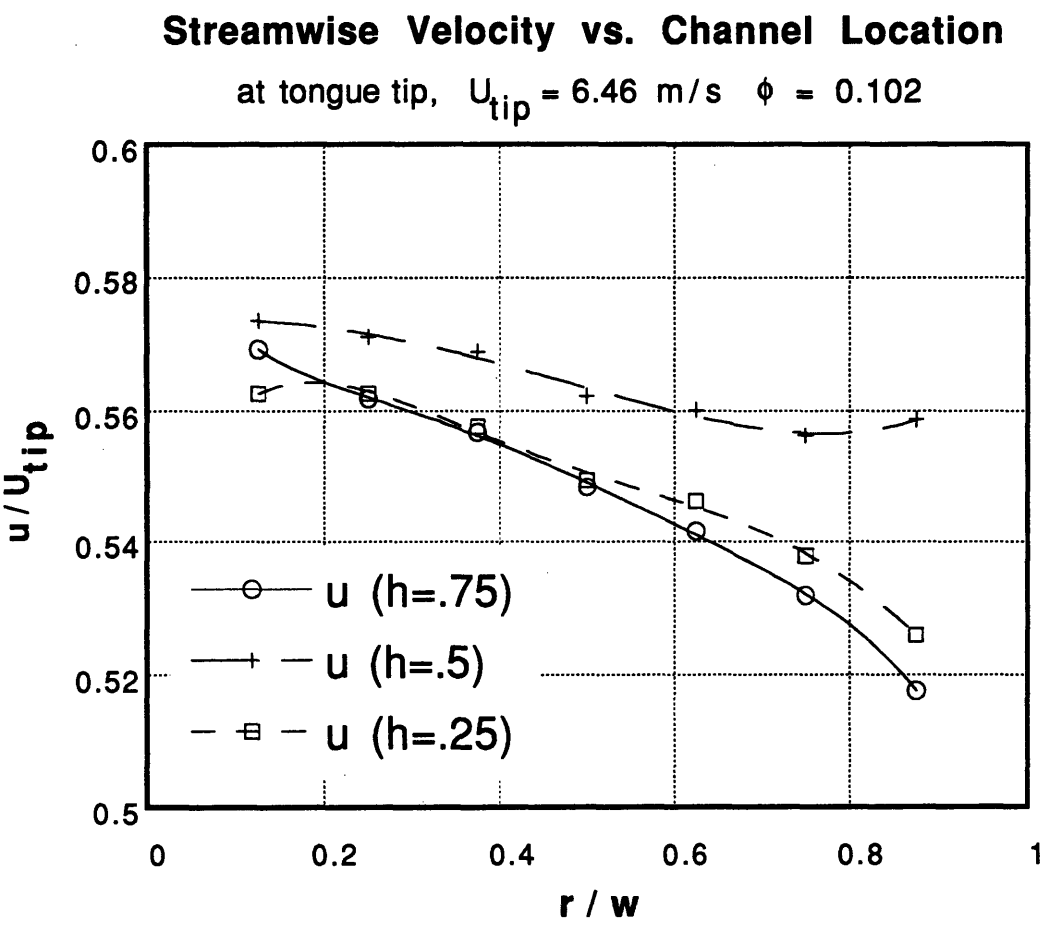
Streamwise Velocity vs. Channel Location
at tongue tip, U_{tip} = 6.46 m/s ϕ = 0.102
u / U_{tip}
0.6
0.58
0.56
0.54
0.52
0.5
0
0.2
0.4
0.6
0.8
1
r / w
u (h=.75)
u (h=.5)
u (h=.25)

Figure 3.21

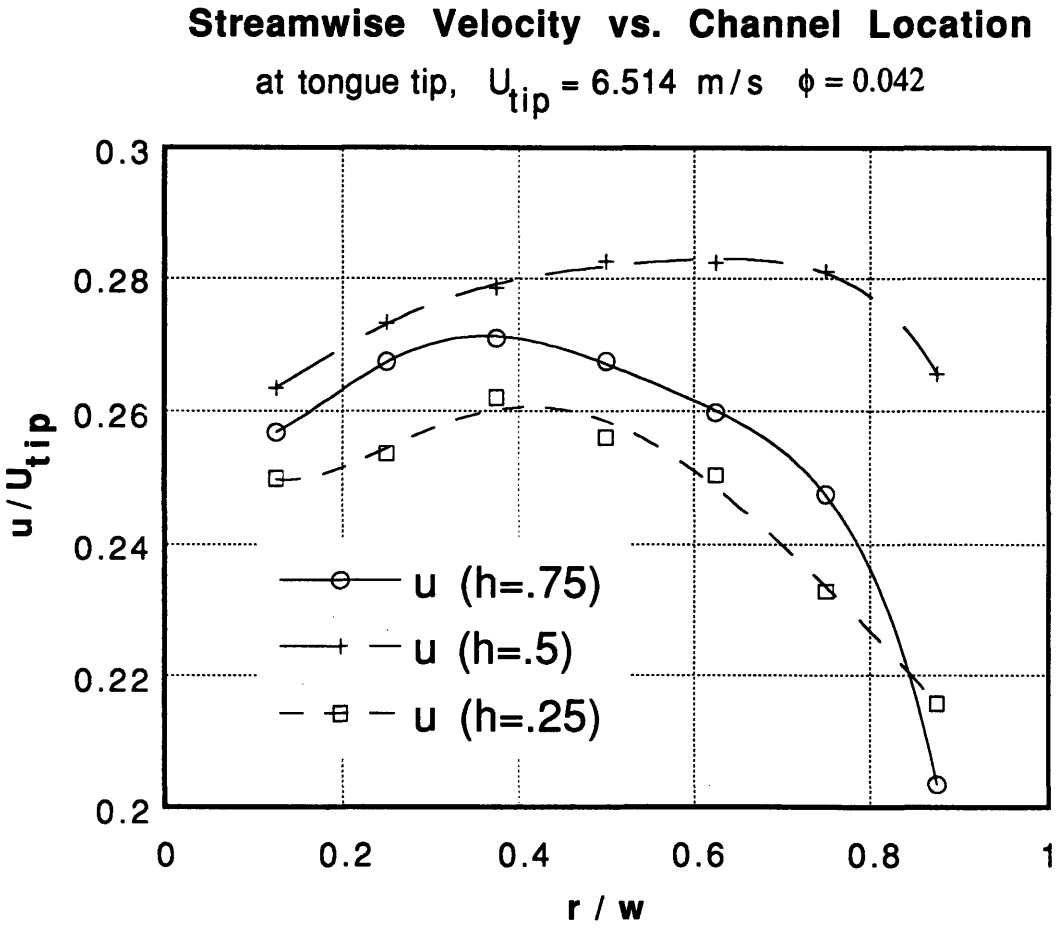
Streamwise Velocity vs. Channel Location
at tongue tip, U_{tip} = 6.514 m/s ϕ = 0.042
0.3
0.28
0.26
0.24
0.22
0.2
u / U tip
0
0.2
0.4
0.6
0.8
1
r / w
u (h=.75)
u (h=.5)
u (h=.25)

Figure 3.22

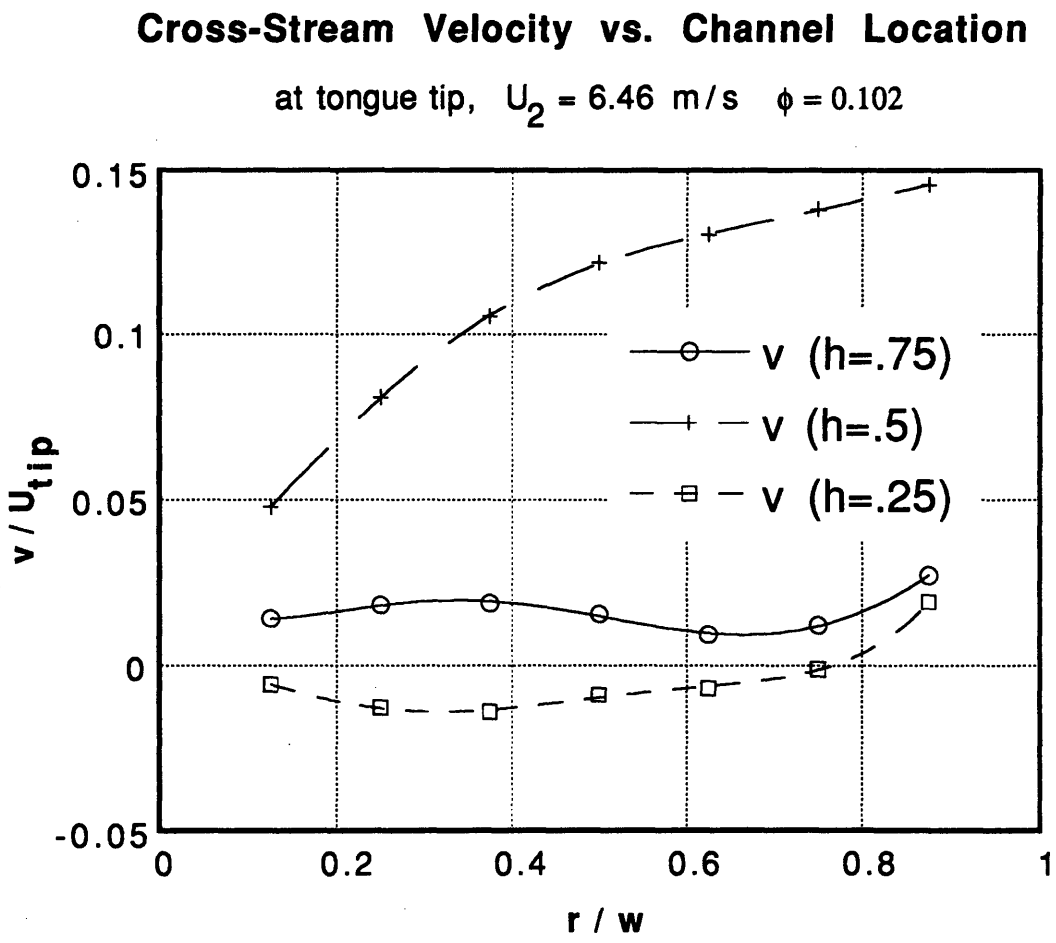
Cross-Stream Velocity vs. Channel Location
at tongue tip, U_2 = 6.46 m/s ϕ = 0.102
0.15
0.1
0.05
0
-0.05
v / U_{tip}
0
0.2
0.4
0.6
0.8
1
r / w
v (h=.75)
v (h=.5)
v (h=.25)

Figure 3.23

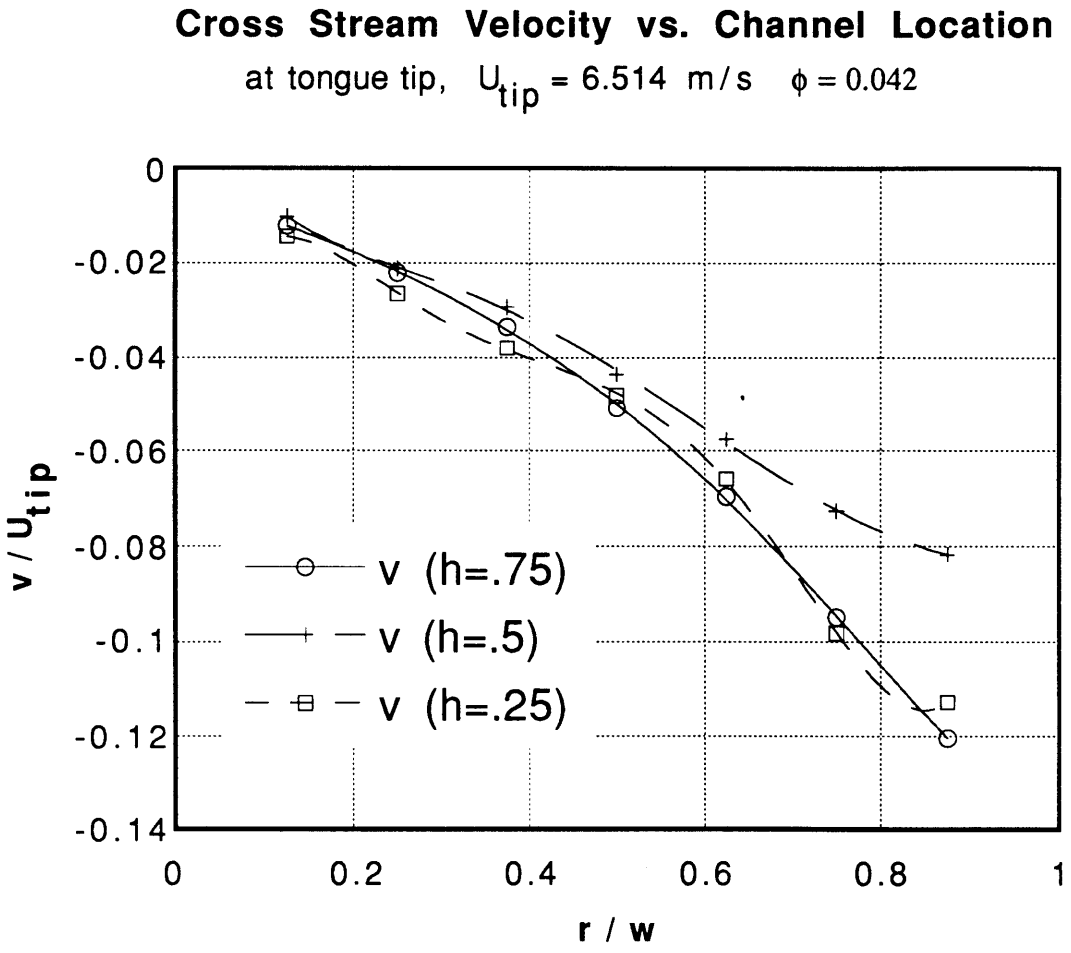
Cross Stream Velocity vs. Channel Location
at tongue tip, U_{tip} = 6.514 m/s ϕ = 0.042
v / U_{tip}
0
-0.02
-0.04
-0.06
-0.08
-0.1
-0.12
-0.14
0
0.2
0.4
0.6
0.8
1
r / w
v (h=.75)
v (h=.5)
v (h=.25)

Figure 3.24

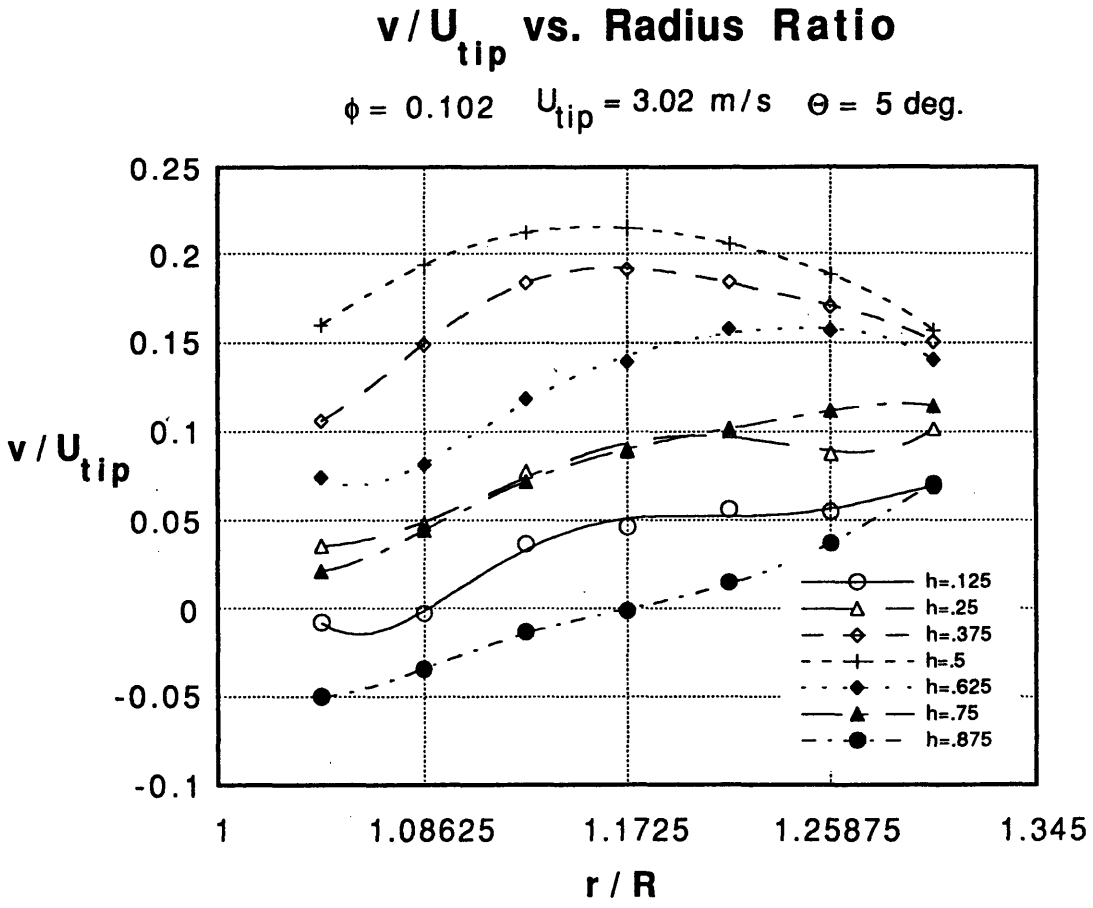
v / U tip vs. Radius Ratio
ϕ = 0.102 U tip = 3.02 m/s Θ = 5 deg.
0.25
0.2
0.15
0.1
0.05
0
-0.05
-0.1
v / U tip
1
1.08625
1.1725
1.25875
1.345
r / R
h=.125
h=.25
h=.375
h=.5
h=.625
h=.75
h=.875

Figure 3.25

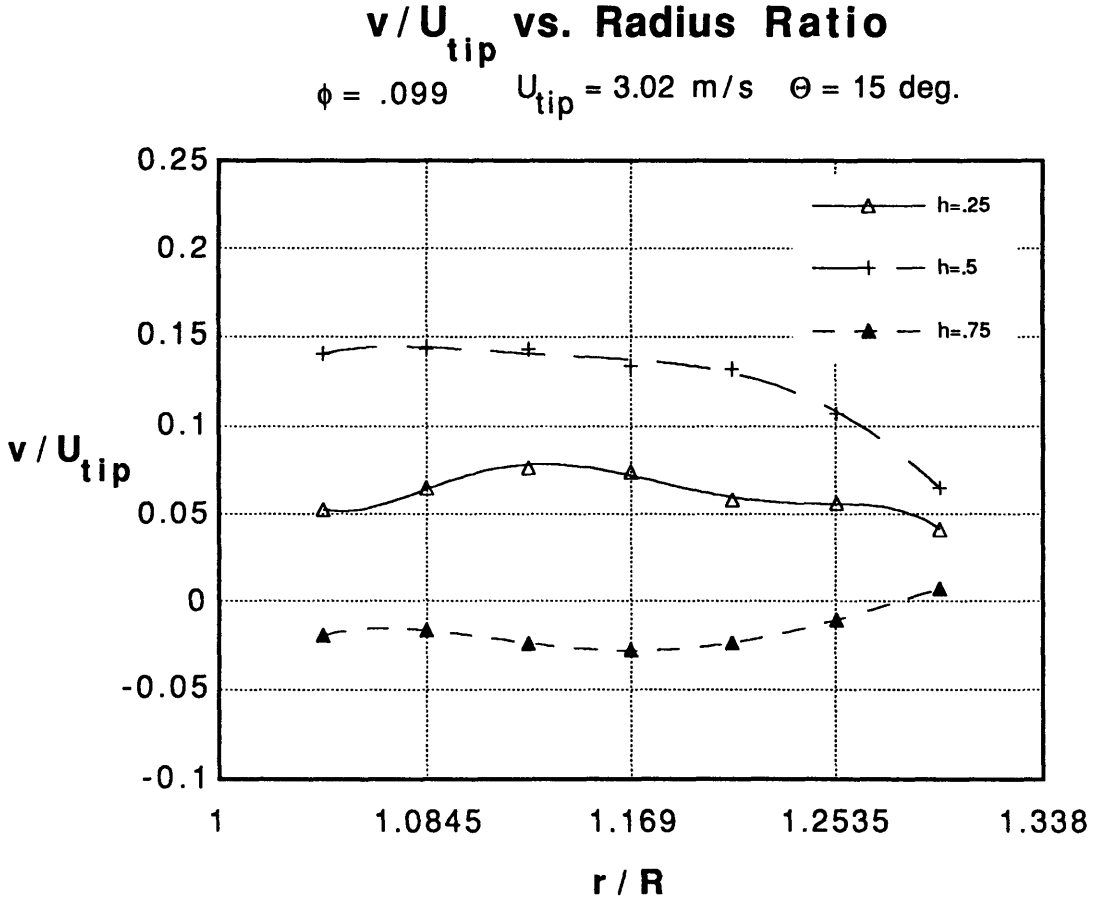
v / U tip vs. Radius Ratio
ϕ = .099 U tip = 3.02 m/s Θ = 15 deg.
0.25
0.2
0.15
0.1
0.05
0
-0.05
-0.1
v / U tip
h=.25
h=.5
h=.75
1
1.0845
1.169
1.2535
1.338
r / R

Figure 3.26

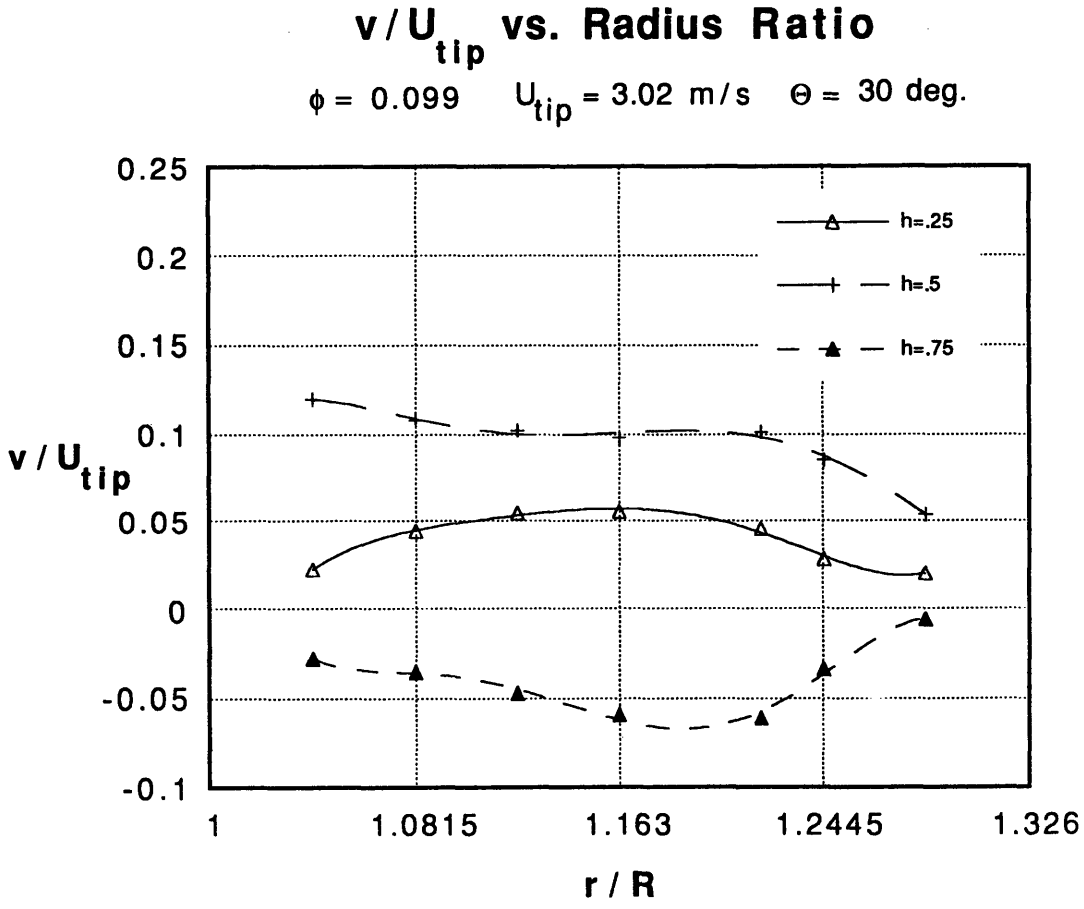
v / U tip vs. Radius Ratio
ϕ = 0.099 U tip = 3.02 m/s Θ = 30 deg.
0.25
0.2
0.15
0.1
0.05
0
-0.05
-0.1
v / U tip
h=.25
h=.5
h=.75
1
1.0815
1.163
1.2445
1.326
r / R

Figure 3.27

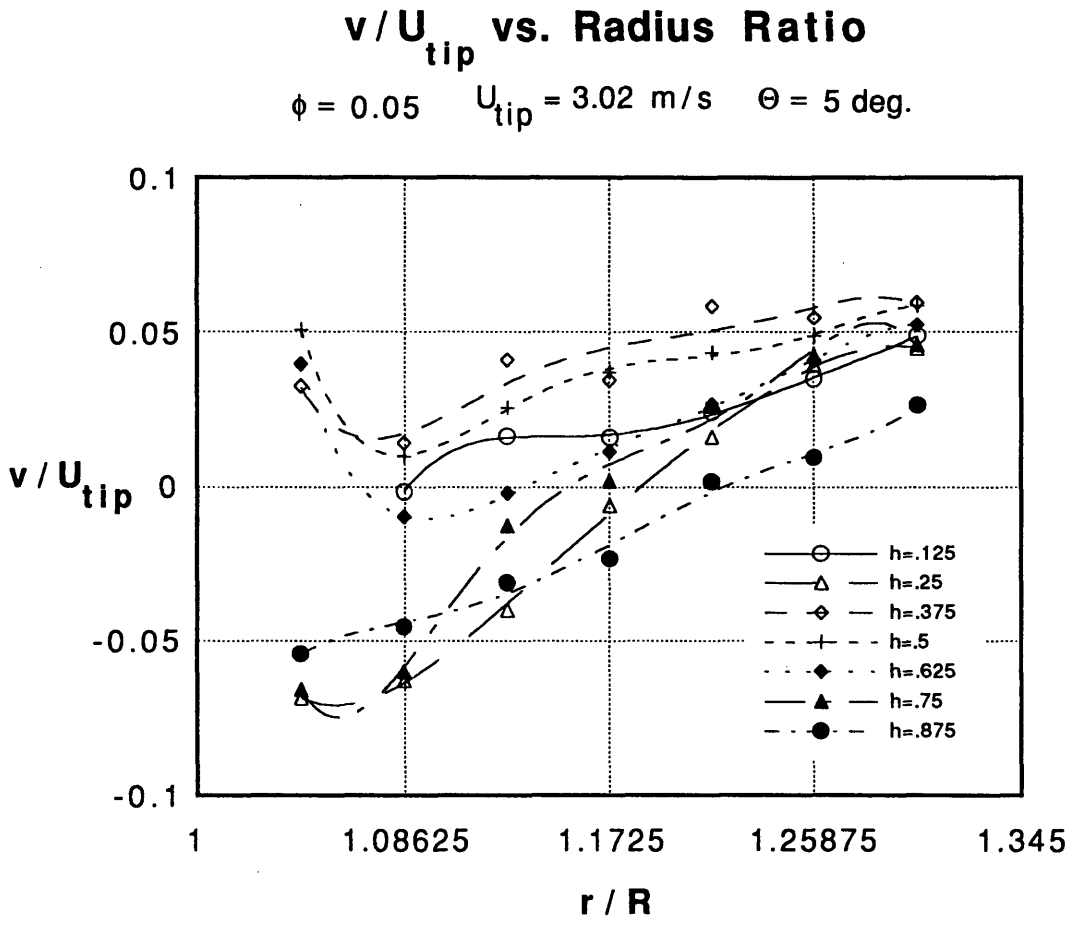
v / U tip vs. Radius Ratio
ϕ = 0.05 U tip = 3.02 m/s Θ = 5 deg.
0.1
0.05
0
-0.05
-0.1
v / U tip
1
1.08625
1.1725
1.25875
1.345
r / R
h=.125
h=.25
h=.375
h=.5
h=.625
h=.75
h=.875

Figure 3.28

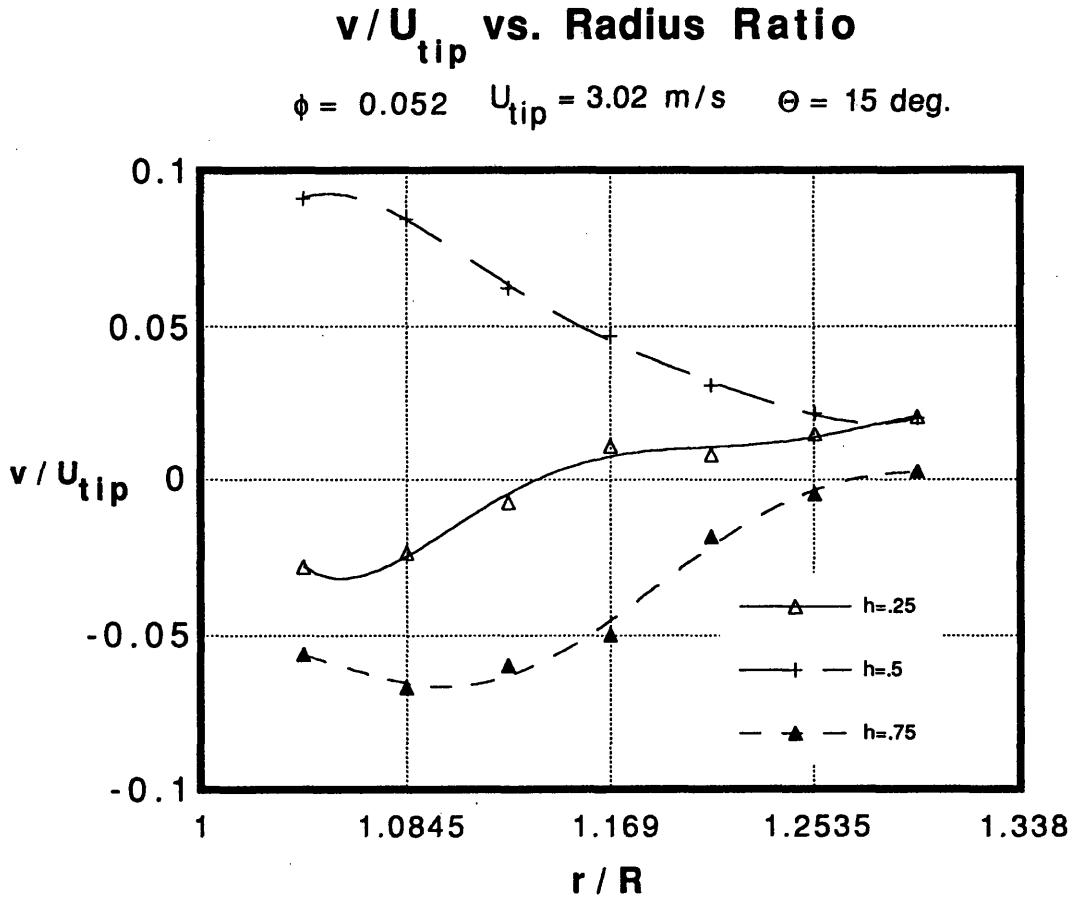
v / U tip vs. Radius Ratio
ϕ = 0.052 U tip = 3.02 m/s Θ = 15 deg.
0.1
0.05
0
-0.05
-0.1
v / U tip
1
1.0845
1.169
1.2535
1.338
r / R
h=.25
h=.5
h=.75

Figure 3.29

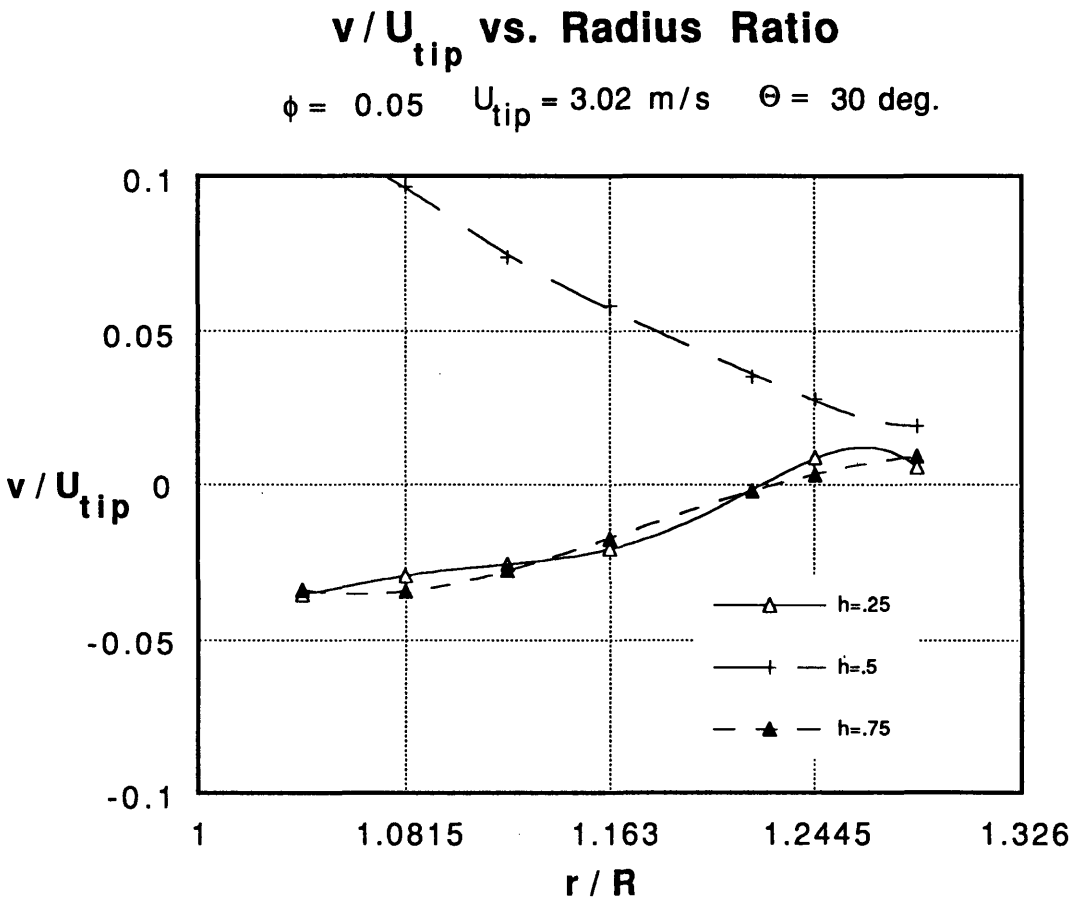
v / U tip vs. Radius Ratio
ϕ = 0.05 U tip = 3.02 m/s Θ = 30 deg.
0.1
0.05
0
-0.05
-0.1
v / U tip
1
1.0815
1.163
1.2445
1.326
r / R
h=.25
h=.5
h=.75

Figure 3.30

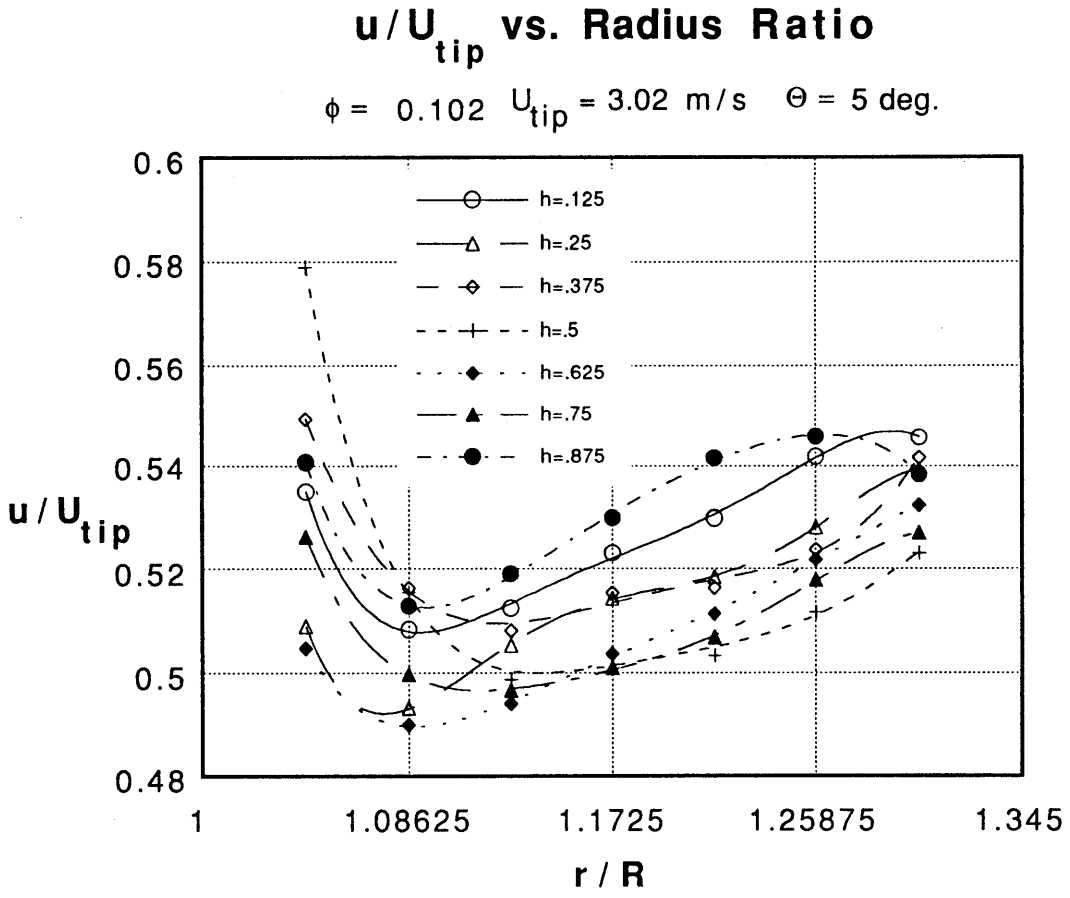
u/U tip vs. Radius Ratio
ϕ = 0.102 U tip = 3.02 m/s Θ = 5 deg.
h=.125
h=.25
h=.375
h=.5
h=.625
h=.75
h=.875
u/U tip
0.6
0.58
0.56
0.54
0.52
0.5
0.48
1
1.08625
1.1725
1.25875
1.345
r / R

Figure 3.31

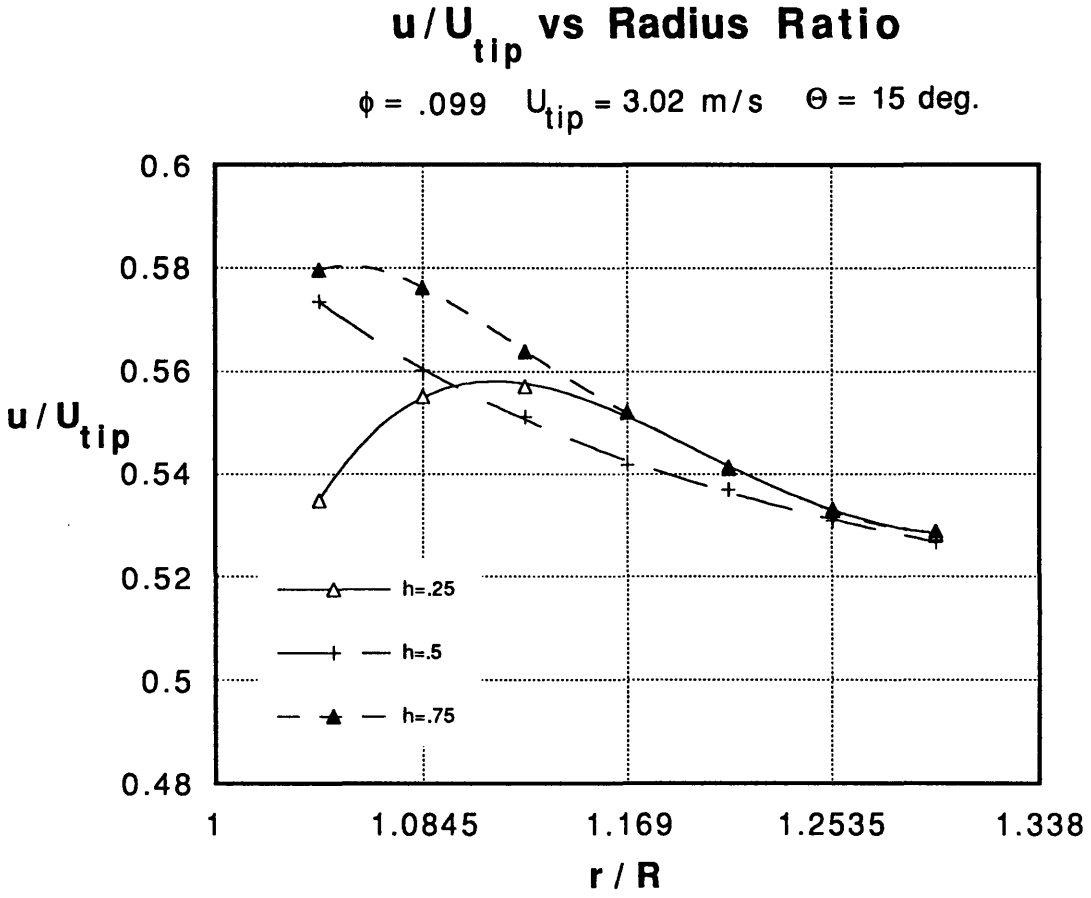
u/U tip vs Radius Ratio
ϕ = .099 U tip = 3.02 m/s Θ = 15 deg.
0.6
0.58
0.56
0.54
0.52
0.5
0.48
u/U tip
h=.25
h=.5
h=.75
1
1.0845
1.169
1.2535
1.338
r / R

Figure 3.32

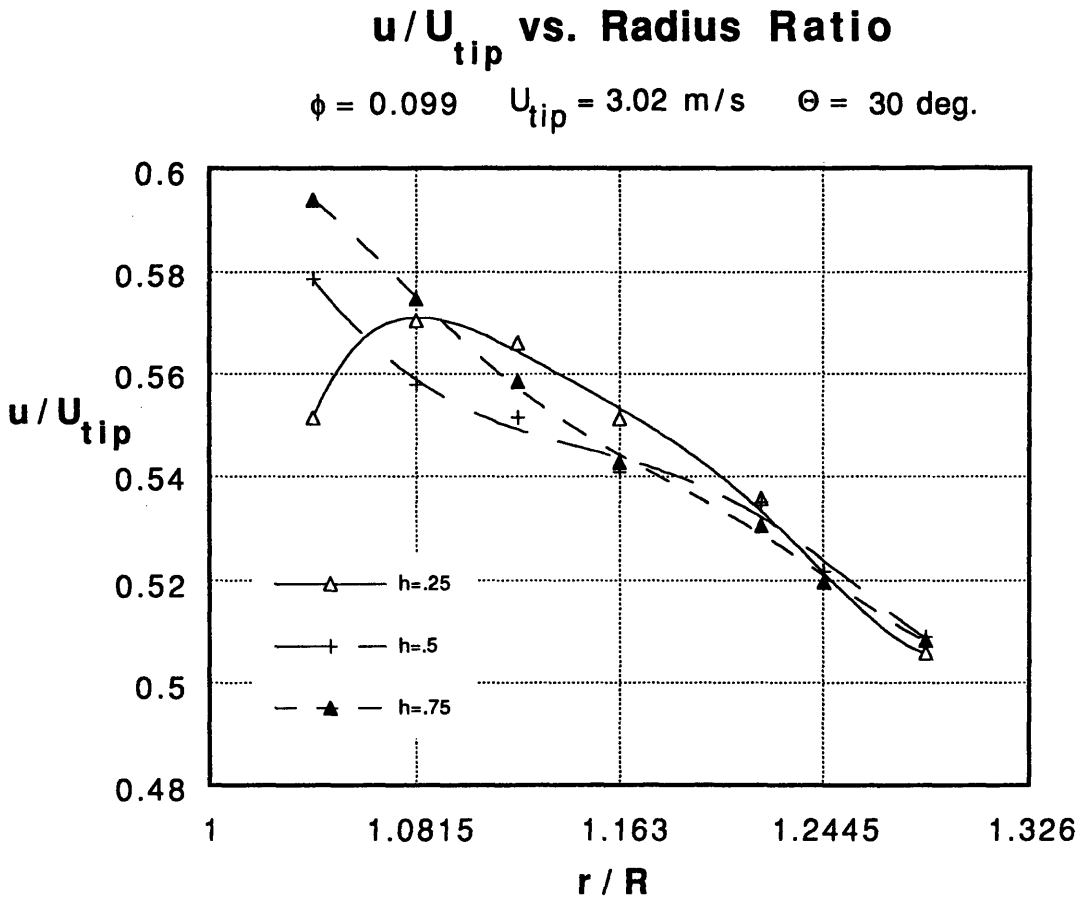
u/U tip vs. Radius Ratio
ϕ = 0.099 U tip = 3.02 m/s Θ = 30 deg.
0.6
0.58
0.56
0.54
0.52
0.5
0.48
u / U tip
h=.25
h=.5
h=.75
1
1.0815
1.163
1.2445
1.326
r / R

Figure 3.33

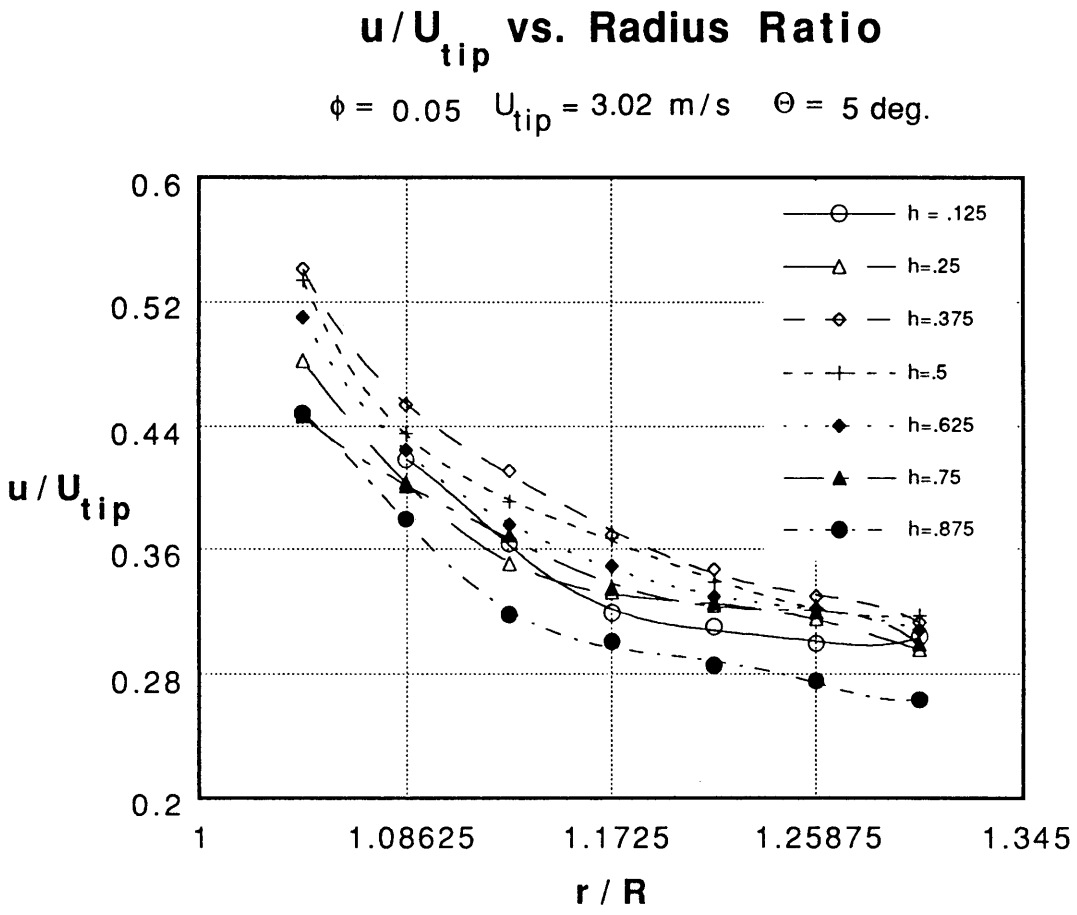
u/U tip vs. Radius Ratio
ϕ = 0.05 U tip = 3.02 m/s Θ = 5 deg.
0.6
0.52
0.44
0.36
0.28
0.2
u / U tip
1
1.08625
1.1725
1.25875
1.345
r / R
h = .125
h=.25
h=.375
h=.5
h=.625
h=.75
h=.875

Figure 3.34

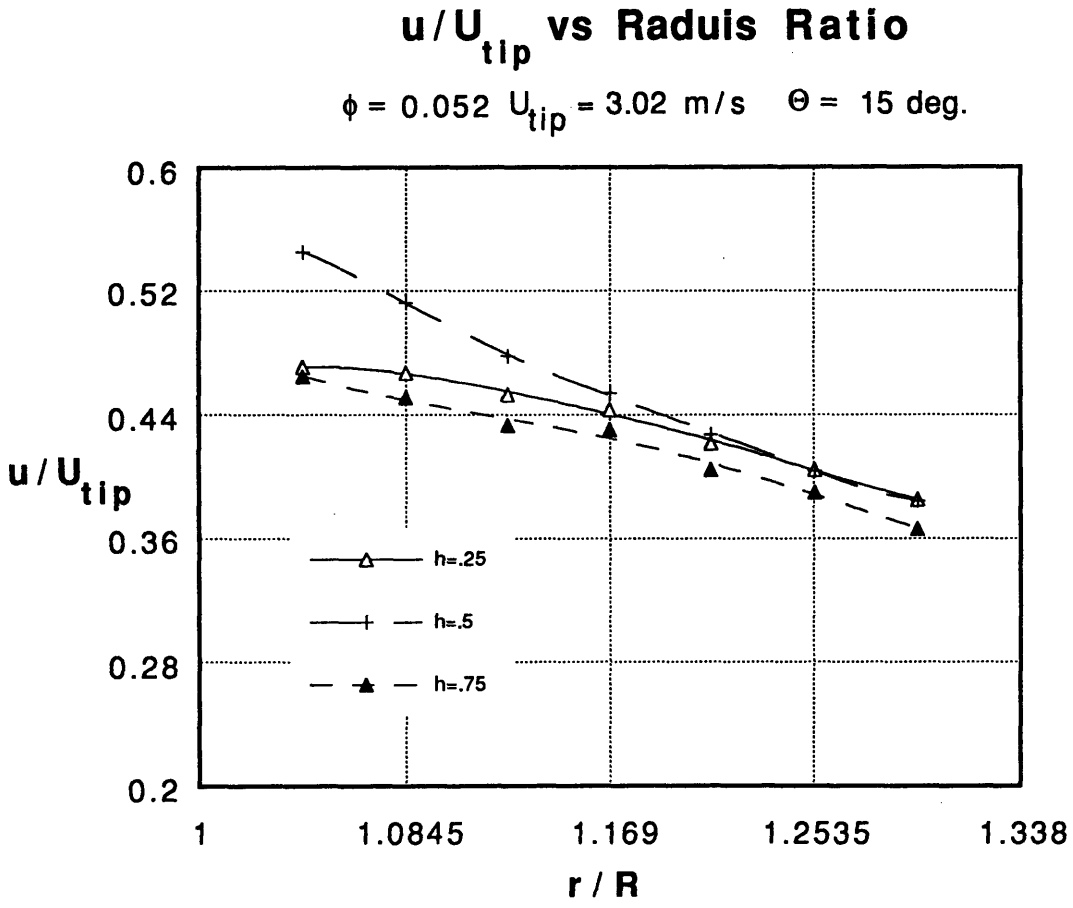
u/U tip vs Raduis Ratio
ϕ = 0.052 U tip = 3.02 m/s Θ = 15 deg.
0.6
0.52
0.44
0.36
0.28
0.2
u/U tip
h=.25
h=.5
h=.75
1
1.0845
1.169
1.2535
1.338
r / R

Figure 3.35

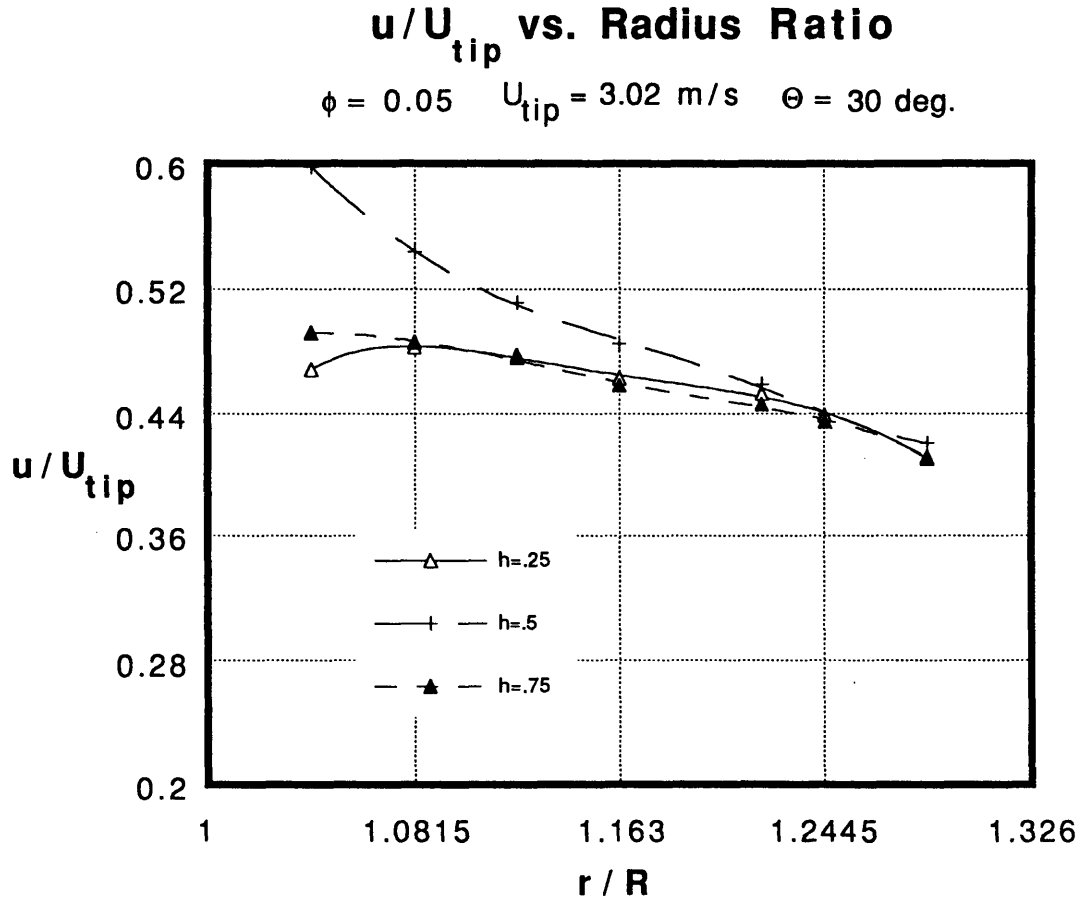
u/U tip vs. Radius Ratio
ϕ = 0.05 U tip = 3.02 m/s Θ = 30 deg.
0.6
0.52
0.44
0.36
0.28
0.2
u/U tip
h=.25
h=.5
h=.75
1
1.0815
1.163
1.2445
1.326
r / R

Figure 3.36

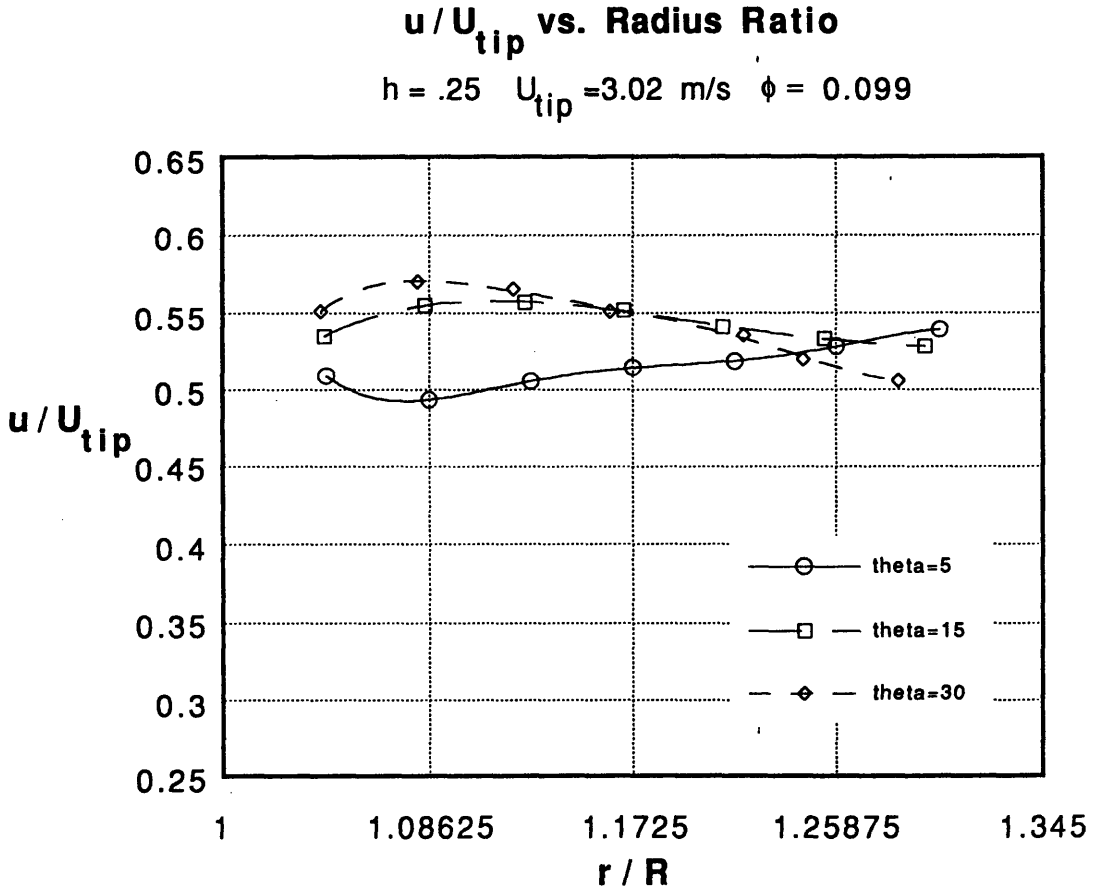
u / U tip vs. Radius Ratio
h = .25 U tip =3.02 m/s ϕ = 0.099
u / U tip
0.65
0.6
0.55
0.5
0.45
0.4
0.35
0.3
0.25
1
1.08625
1.1725
1.25875
1.345
r / R
theta=5
theta=15
theta=30

Figure 3.37

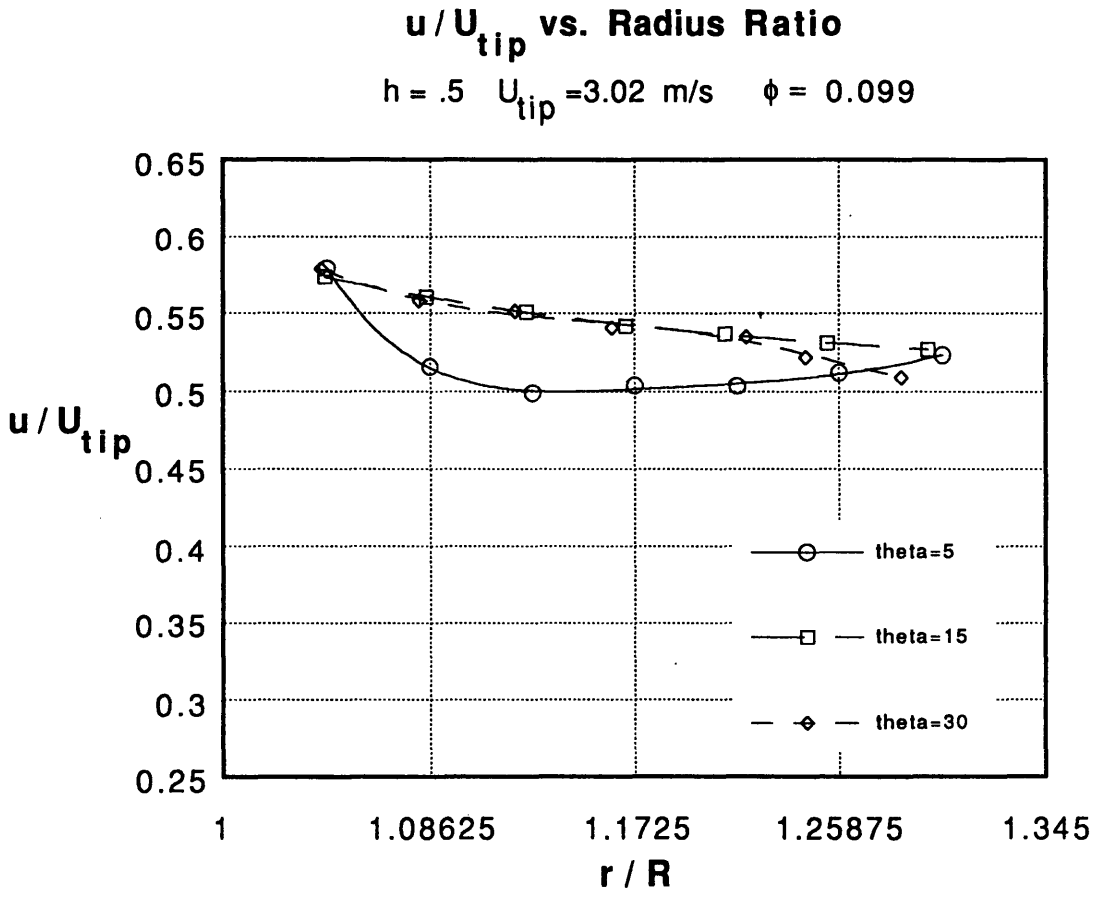
u / U tip vs. Radius Ratio
h = .5 U tip =3.02 m/s ϕ = 0.099
u / U tip
0.65
0.6
0.55
0.5
0.45
0.4
0.35
0.3
0.25
1
1.08625
1.1725
1.25875
1.345
r / R
theta=5
theta=15
theta=30

Figure 3.38

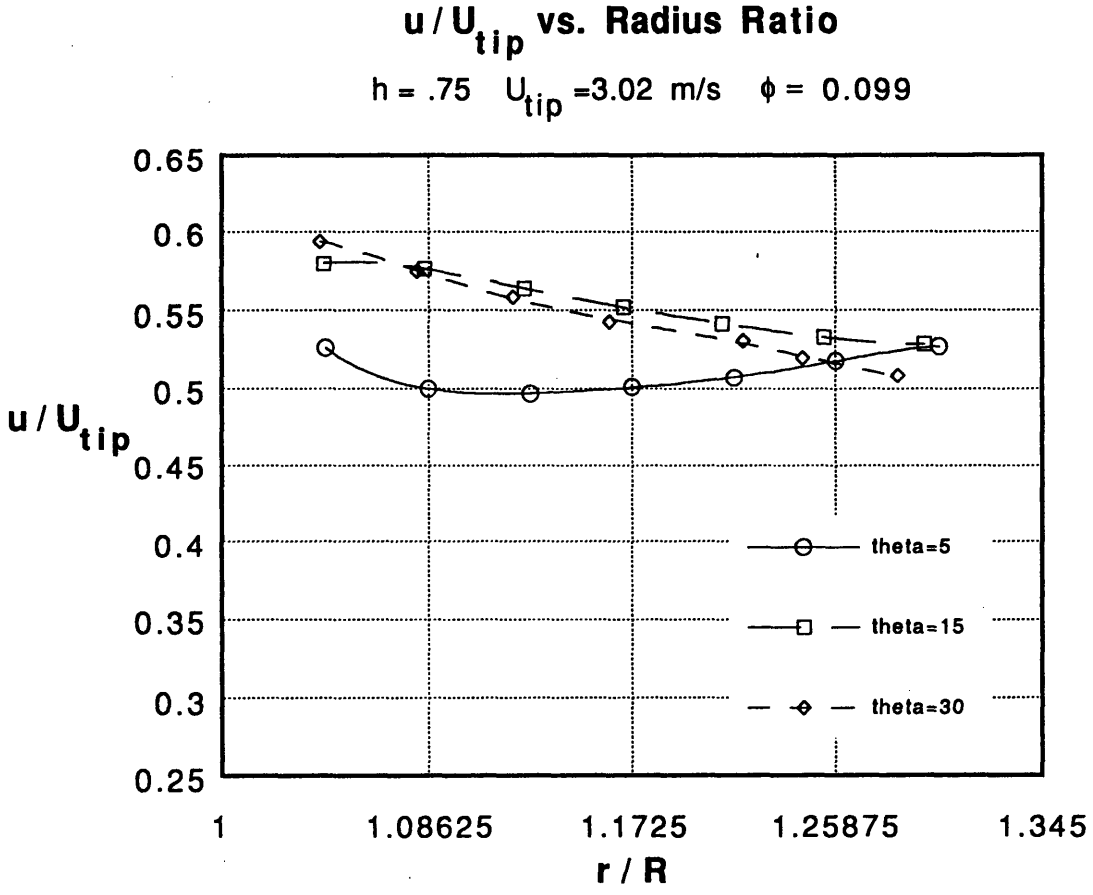
u / U tip vs. Radius Ratio
h = .75 U tip =3.02 m/s ϕ = 0.099
u / U tip
0.65
0.6
0.55
0.5
0.45
0.4
0.35
0.3
0.25
1
1.08625
1.1725
1.25875
1.345
r / R
theta=5
theta=15
theta=30

Figure 3.39

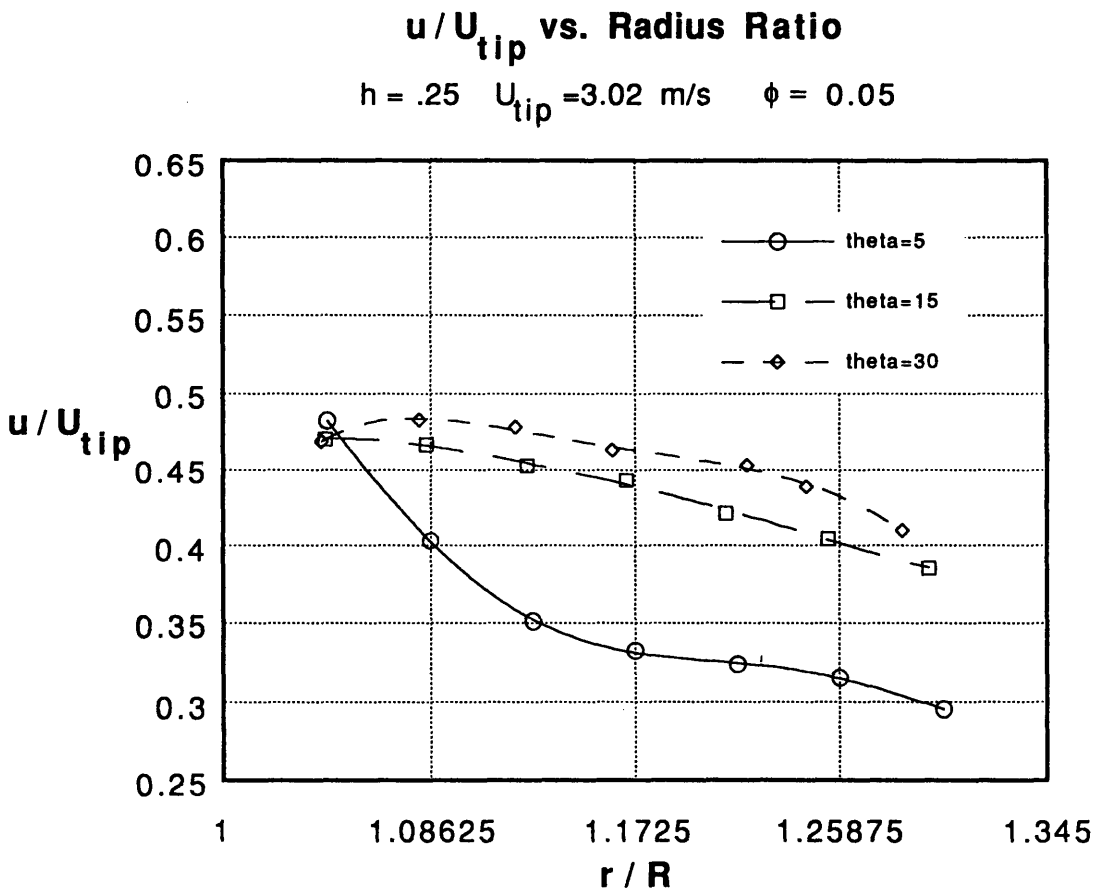
u / U tip vs. Radius Ratio
h = .25 U tip =3.02 m/s ϕ = 0.05
u / U tip
0.65
0.6
0.55
0.5
0.45
0.4
0.35
0.3
0.25
1
1.08625
1.1725
1.25875
1.345
r / R
theta=5
theta=15
theta=30

Figure 3.40

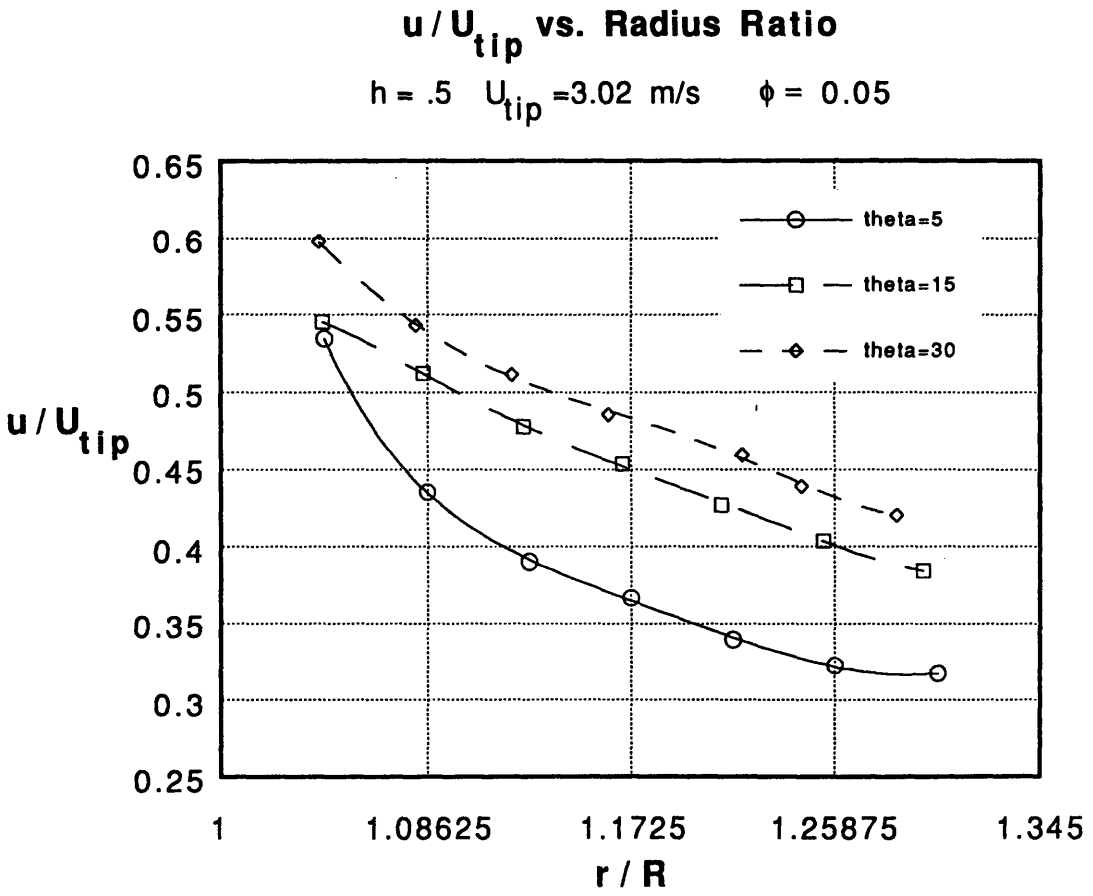
u / U tip vs. Radius Ratio
h = .5 U tip =3.02 m/s ϕ = 0.05
0.65
0.6
0.55
0.5
0.45
0.4
0.35
0.3
0.25
u / U tip
theta=5
theta=15
theta=30
1
1.08625
1.1725
1.25875
1.345
r / R

Figure 3.41

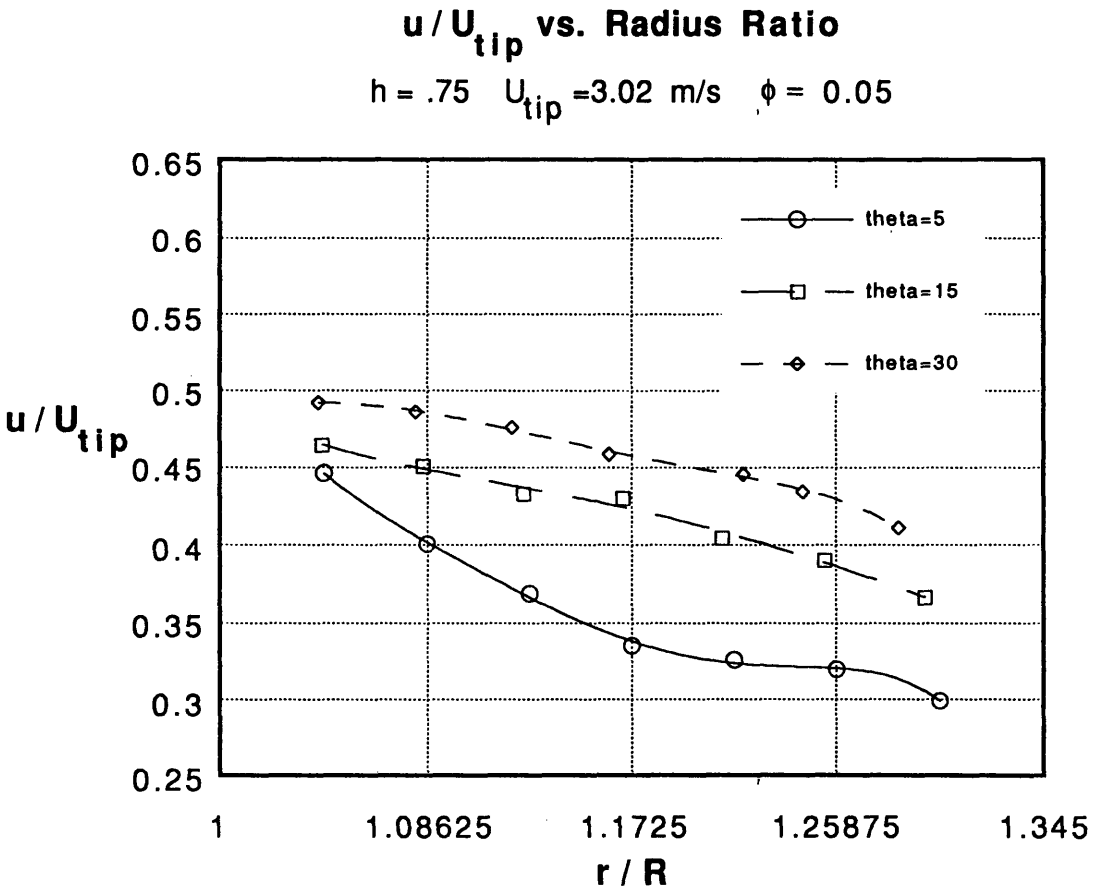
u / U tip vs. Radius Ratio
h = .75 U tip =3.02 m/s ϕ = 0.05
u / U tip
0.65
0.6
0.55
0.5
0.45
0.4
0.35
0.3
0.25
theta=5
theta=15
theta=30
1
1.08625
1.1725
1.25875
1.345
r / R

Figure 3.42

Outlet Velocity Triangle

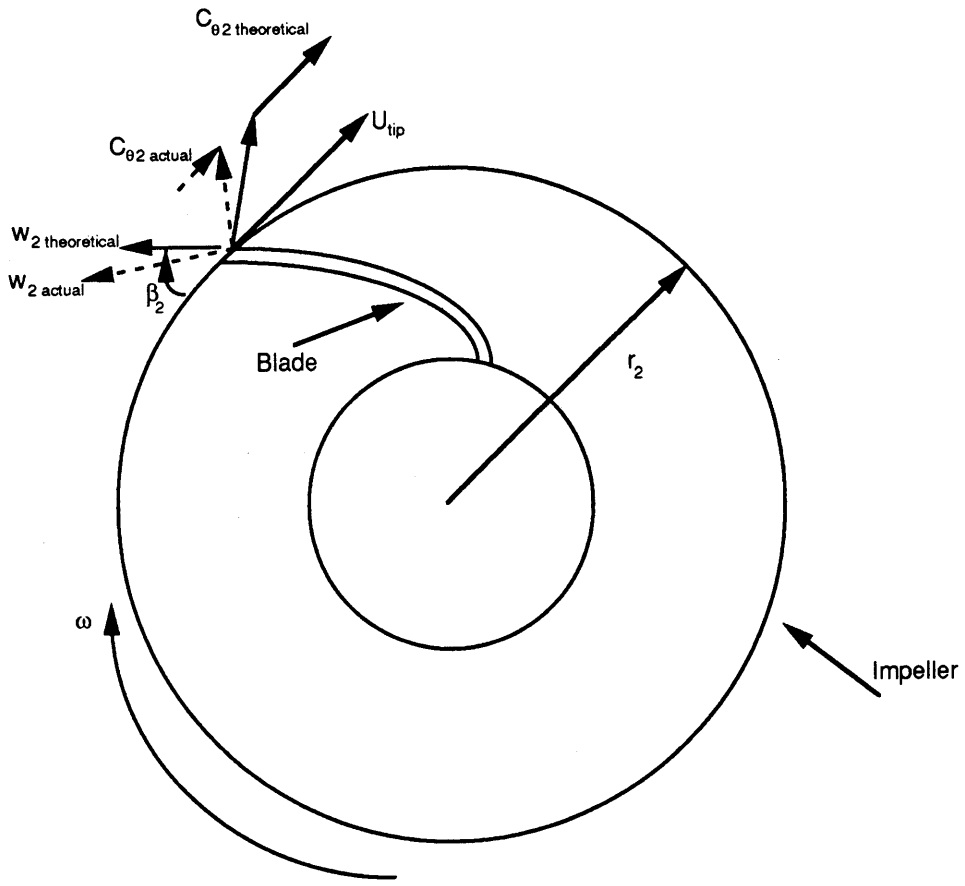

Figure 3.43

Comparison of Local Values of Slip Factor and Static Pressure

50% Speedline, Original Volute

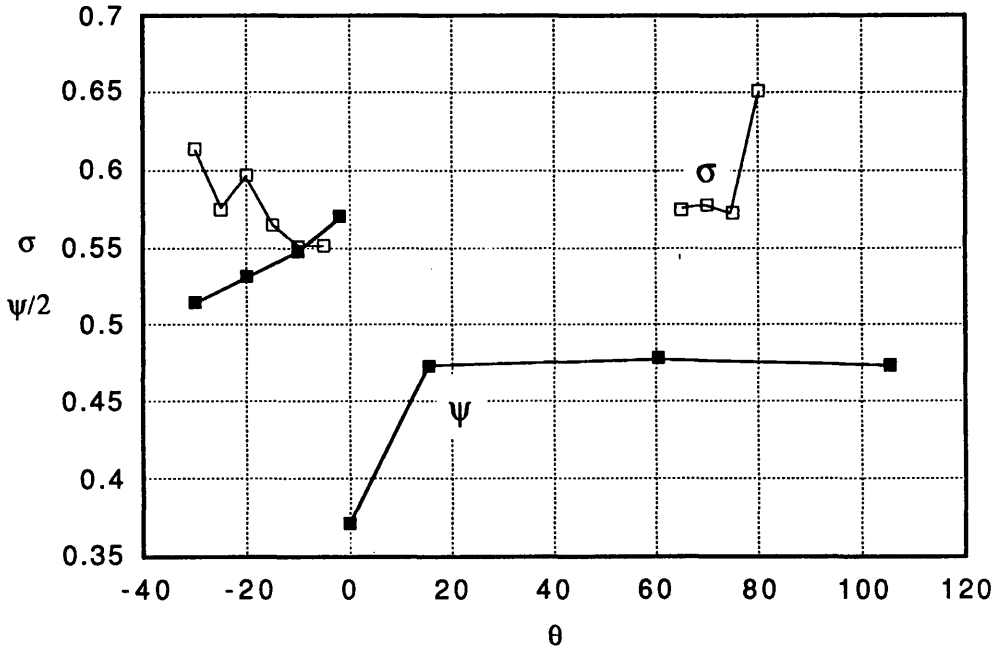

Figure 3.44

Comparison of Local Values of Slip Factor and Static Pressure

80% Speedline, Original Volute

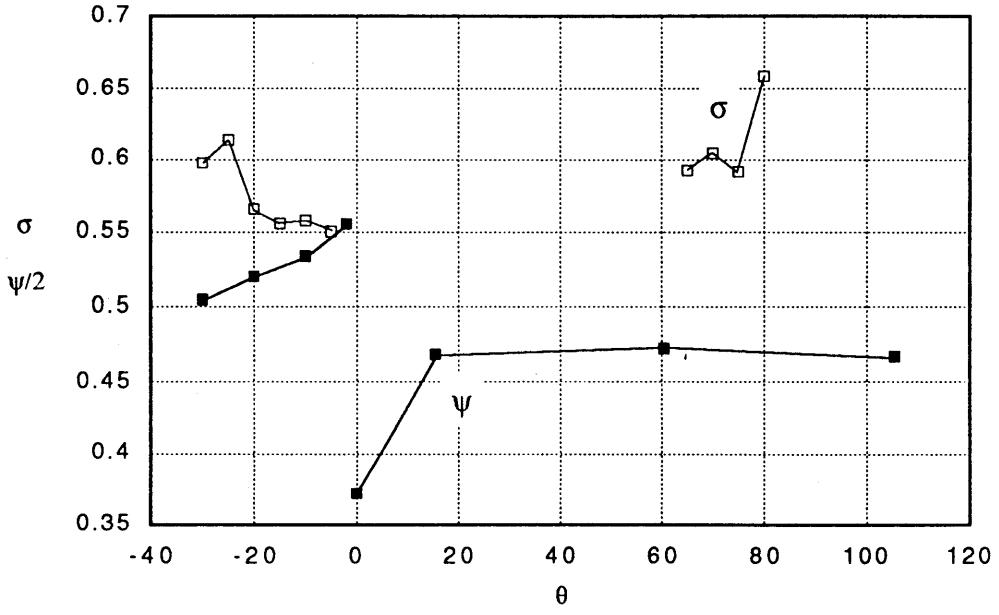

Figure 3.45

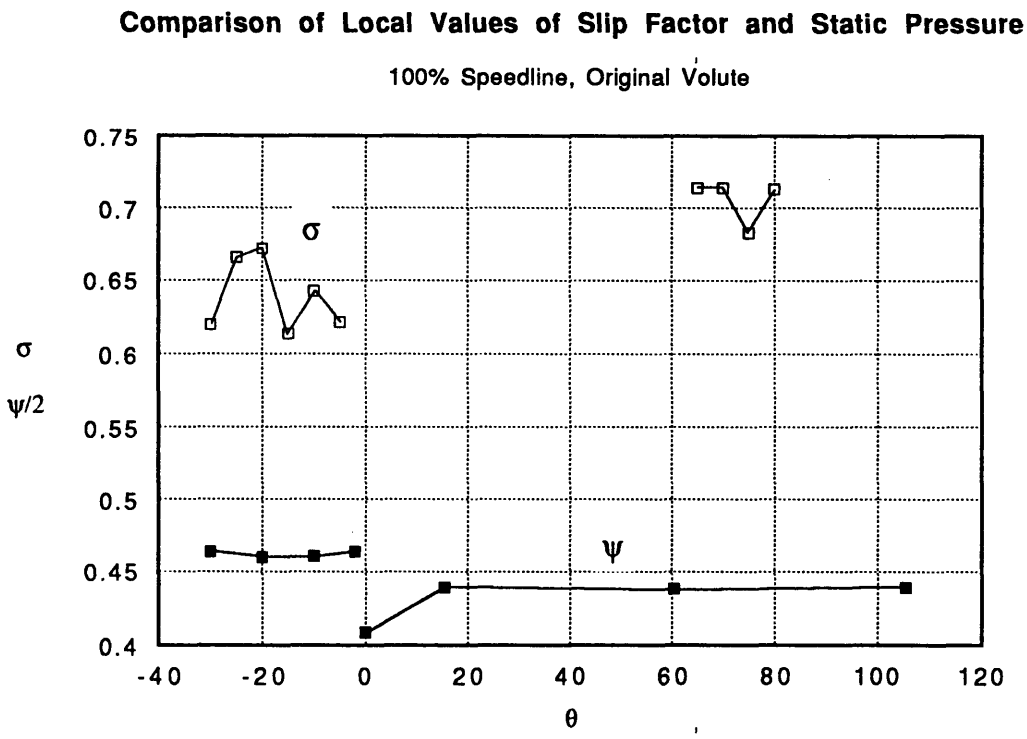
Comparison of Local Values of Slip Factor and Static Pressure
100% Speedline, Original Volute
σ
ψ/2
0.75
0.7
0.65
0.6
0.55
0.5
0.45
0.4
σ
ψ
-40
-20
0
20
40
60
80
100
120
θ

Figure 3.46

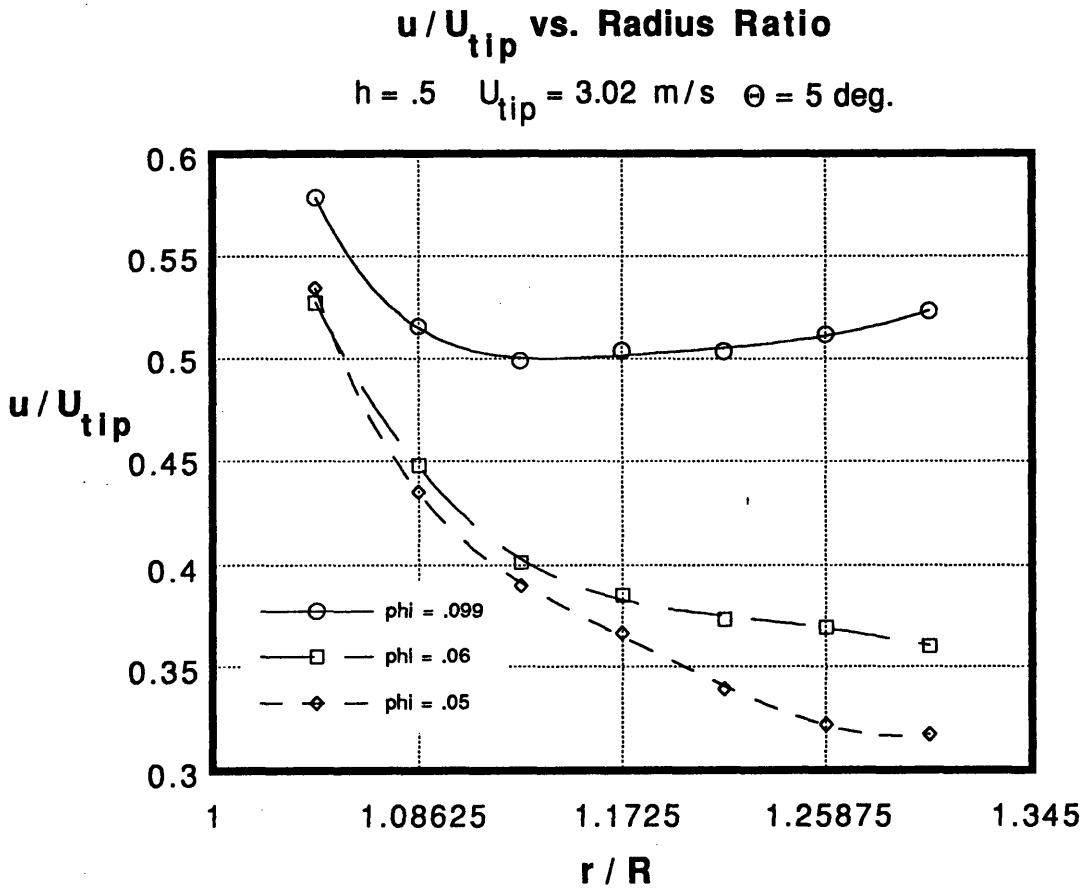
u / U tip vs. Radius Ratio
h = .5 U tip = 3.02 m/s Θ = 5 deg.
0.6
0.55
0.5
0.45
0.4
0.35
0.3
u / U tip
phi = .099
phi = .06
phi = .05
1
1.08625
1.1725
1.25875
1.345
r / R

Figure 3.47

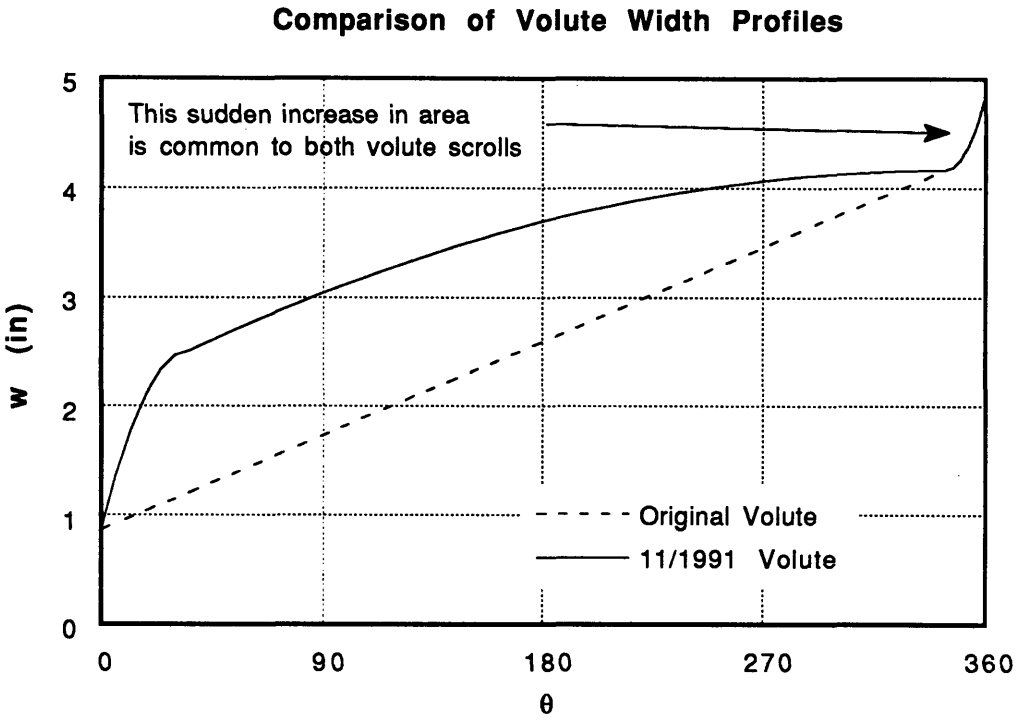
Comparison of Volute Width Profiles
This sudden increase in area
is common to both volute scrolls
Original Volute
11/1991 Volute
w (in)
θ
0
1
2
3
4
5
0
90
180
270
360

Figure 4.1

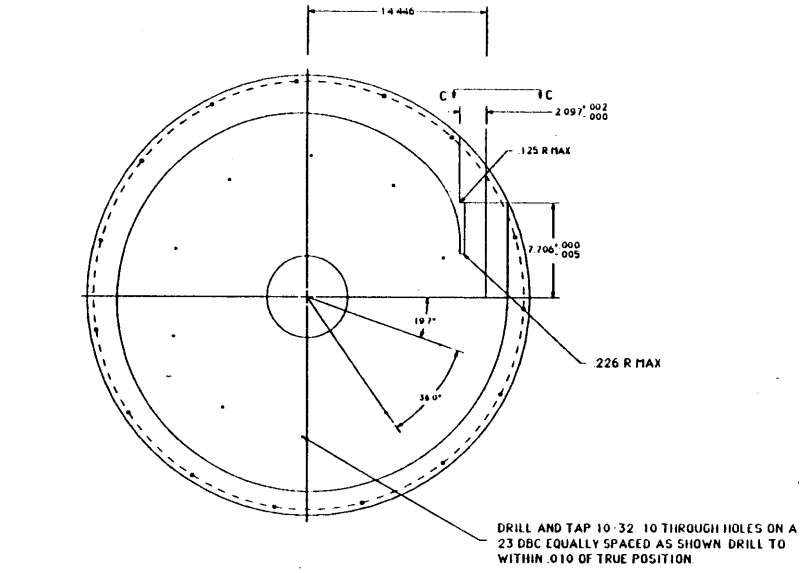

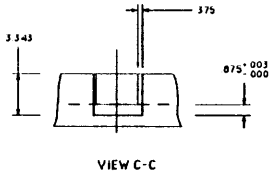

VIEW C-C

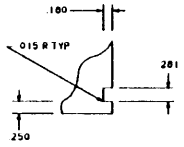

VIEW D

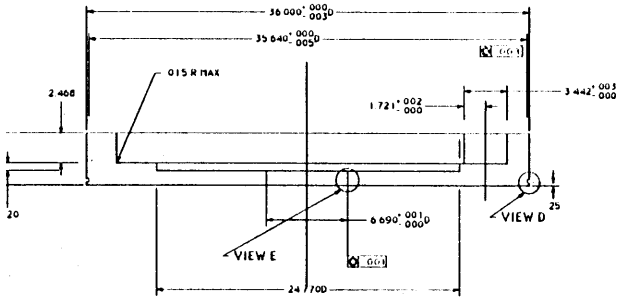

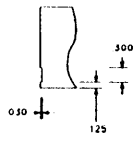

VIEW E

M.I.T GAS TURBINE LABORAT	
VOLUTE #2	
TOLERANCES UNLESS OTHERWISE SPECIFIED	DRAWN BY SCOTT B SANDLER
	SCALE 1/4

Figure 4.2

Modified Volute Pressure Tap Locations

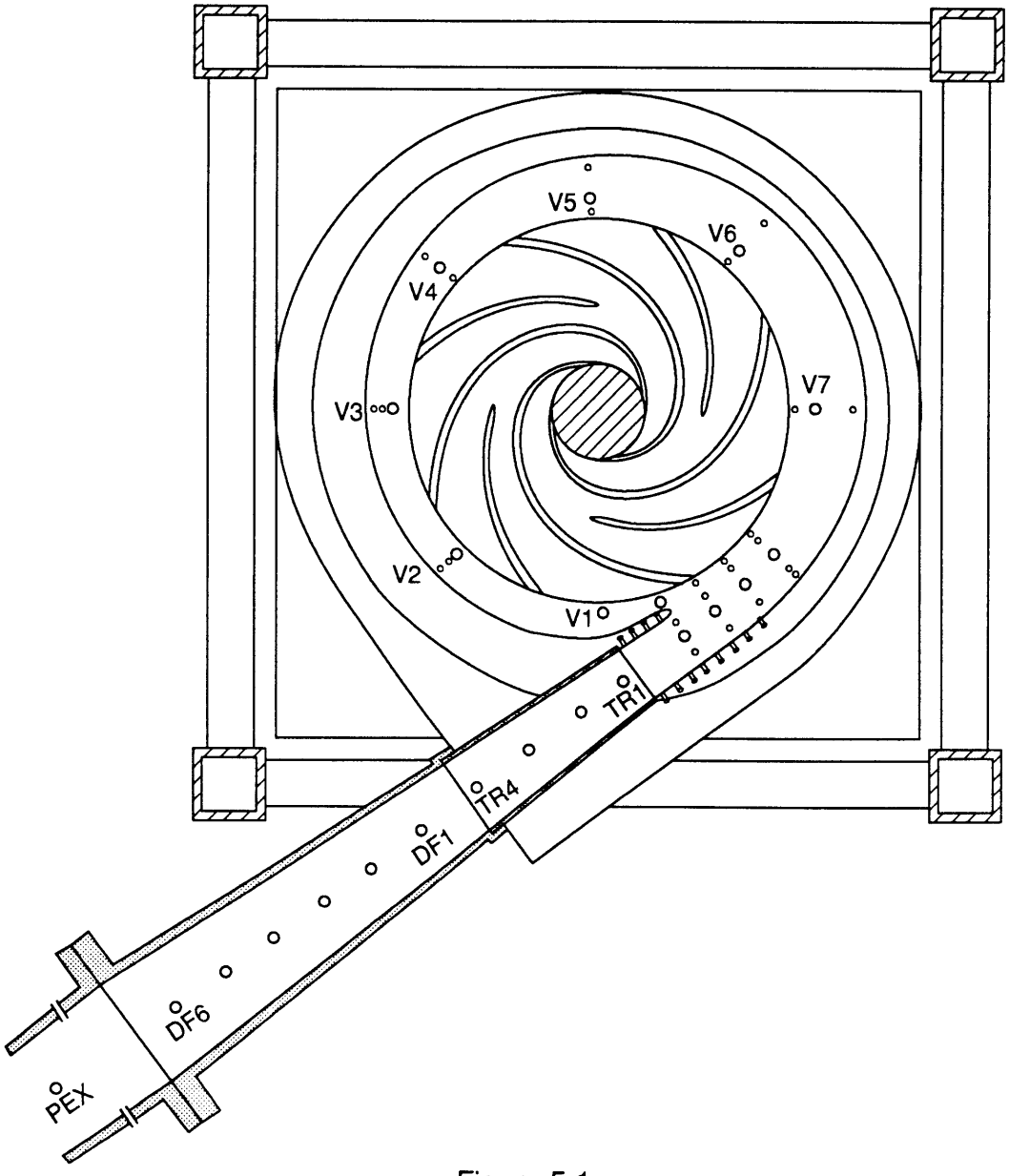

Figure 5.1

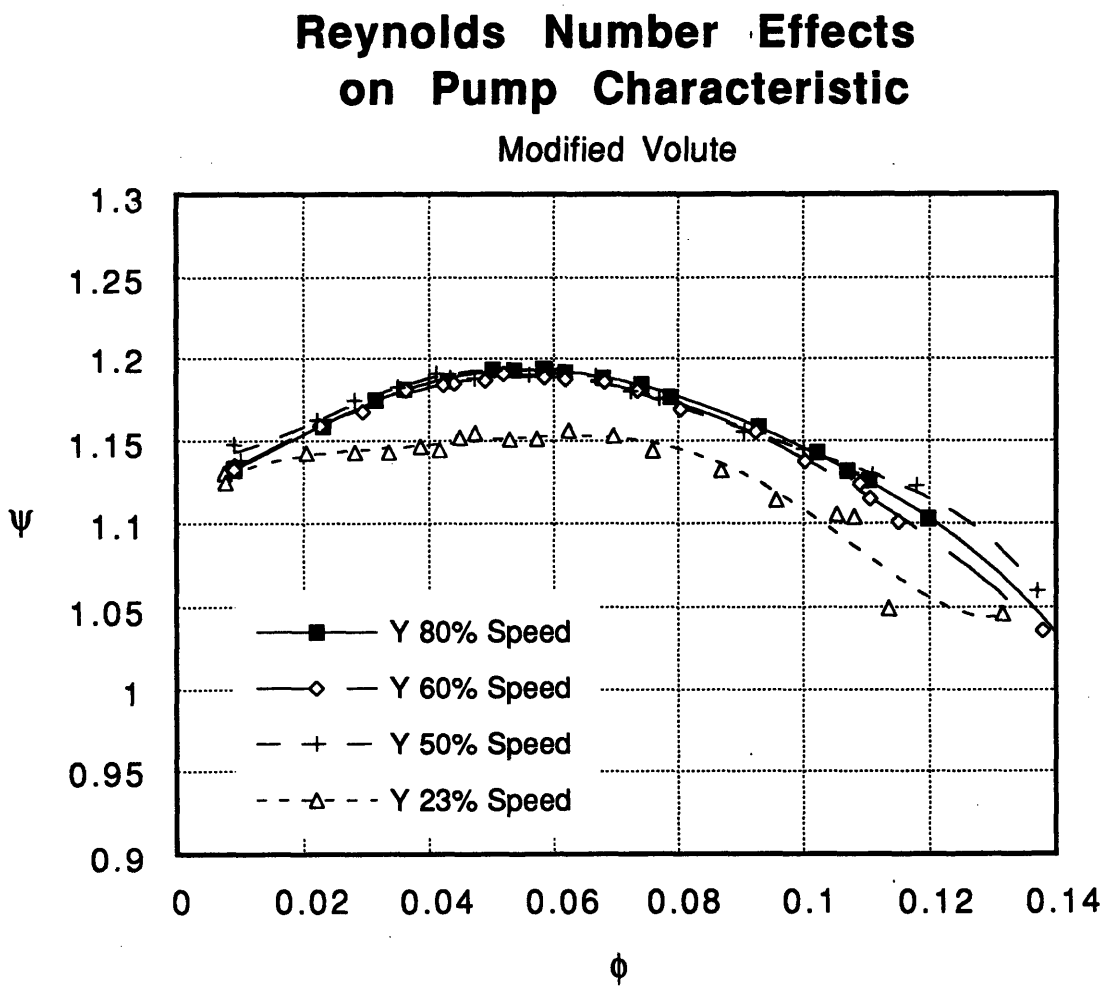
Reynolds Number Effects
on Pump Characteristic
Modified Volute
1.3
1.25
1.2
1.15
1.1
1.05
1
0.95
0.9
Ψ
0
0.02
0.04
0.06
0.08
0.1
0.12
0.14
ϕ
Y 80% Speed
Y 60% Speed
Y 50% Speed
Y 23% Speed

Figure 5.2

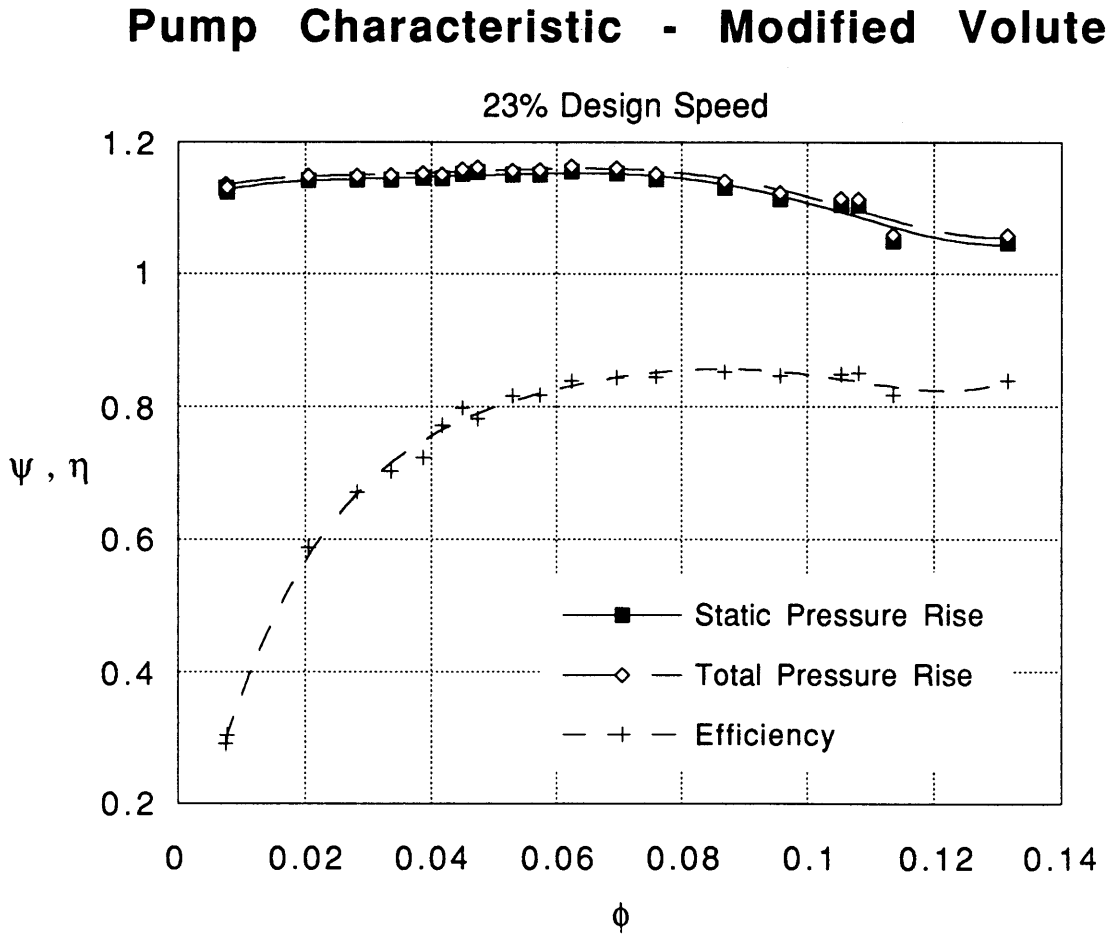
Pump Characteristic - Modified Volute
23% Design Speed
1.2
1
0.8
0.6
0.4
0.2
ψ , η
0
0.02
0.04
0.06
0.08
0.1
0.12
0.14
ϕ
Static Pressure Rise
Total Pressure Rise
Efficiency

Figure 5.3

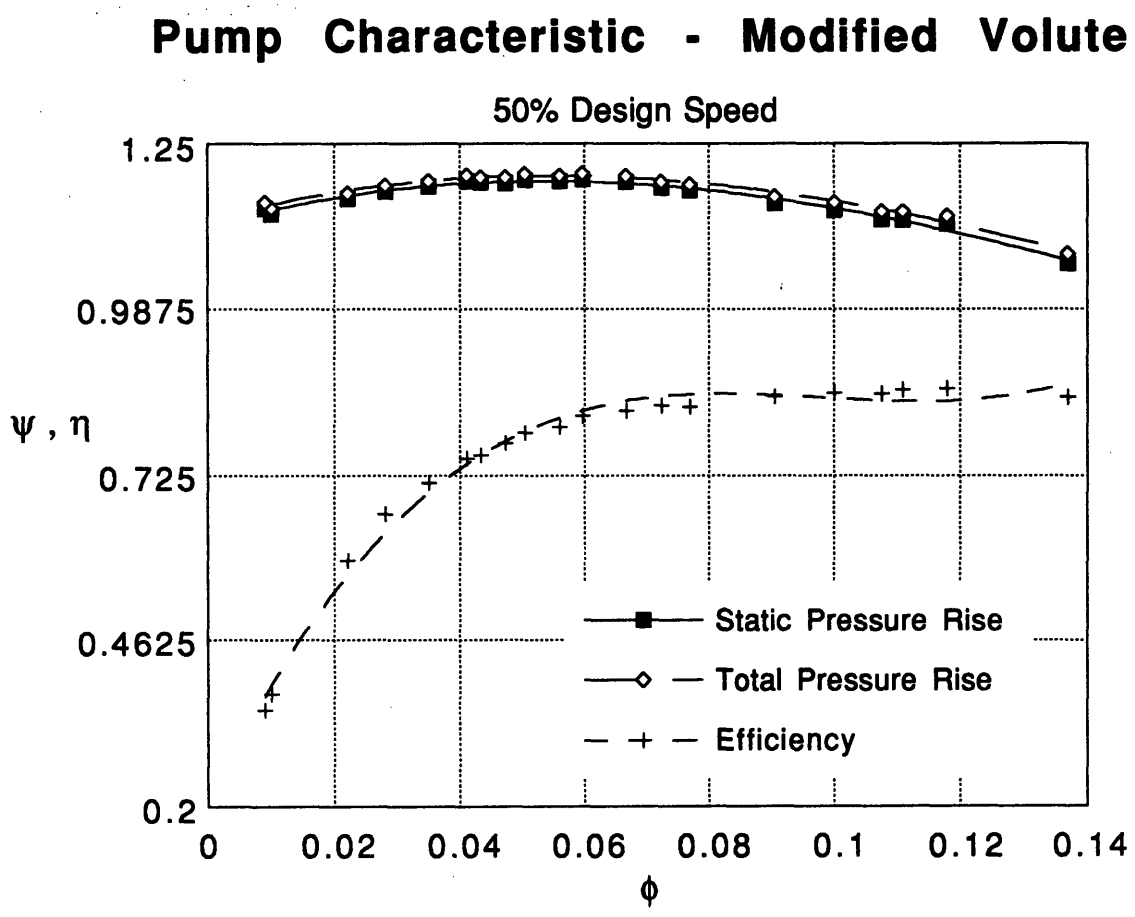
Pump Characteristic - Modified Volute
50% Design Speed
1.25
0.9875
0.725
0.4625
0.2
ψ , η
0
0.02
0.04
0.06
0.08
0.1
0.12
0.14
ϕ
Static Pressure Rise
Total Pressure Rise
Efficiency

Figure 5.4

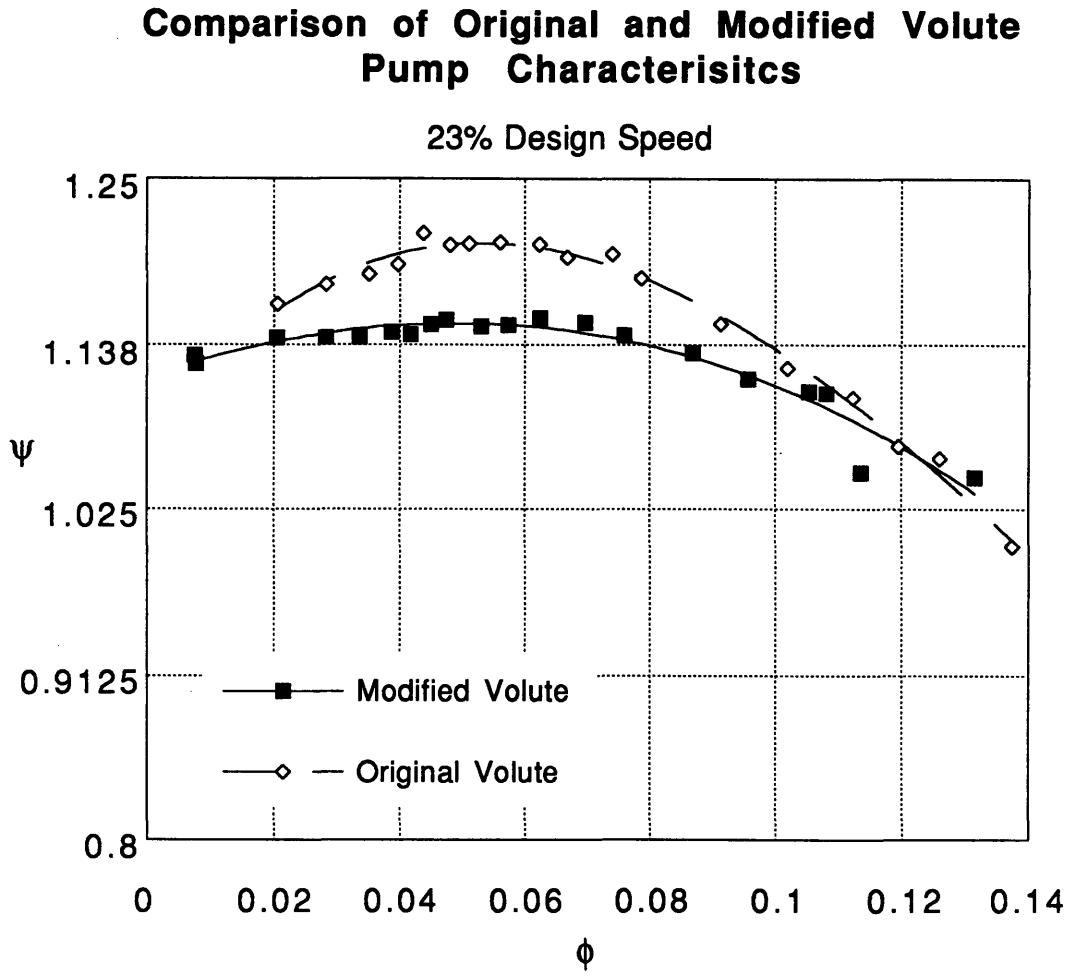
Comparison of Original and Modified Volute Pump Characterisitcs
23% Design Speed
1.25
1.138
1.025
0.9125
0.8
ψ
Modified Volute
Original Volute
0
0.02
0.04
0.06
0.08
0.1
0.12
0.14
ϕ

Figure 5.5

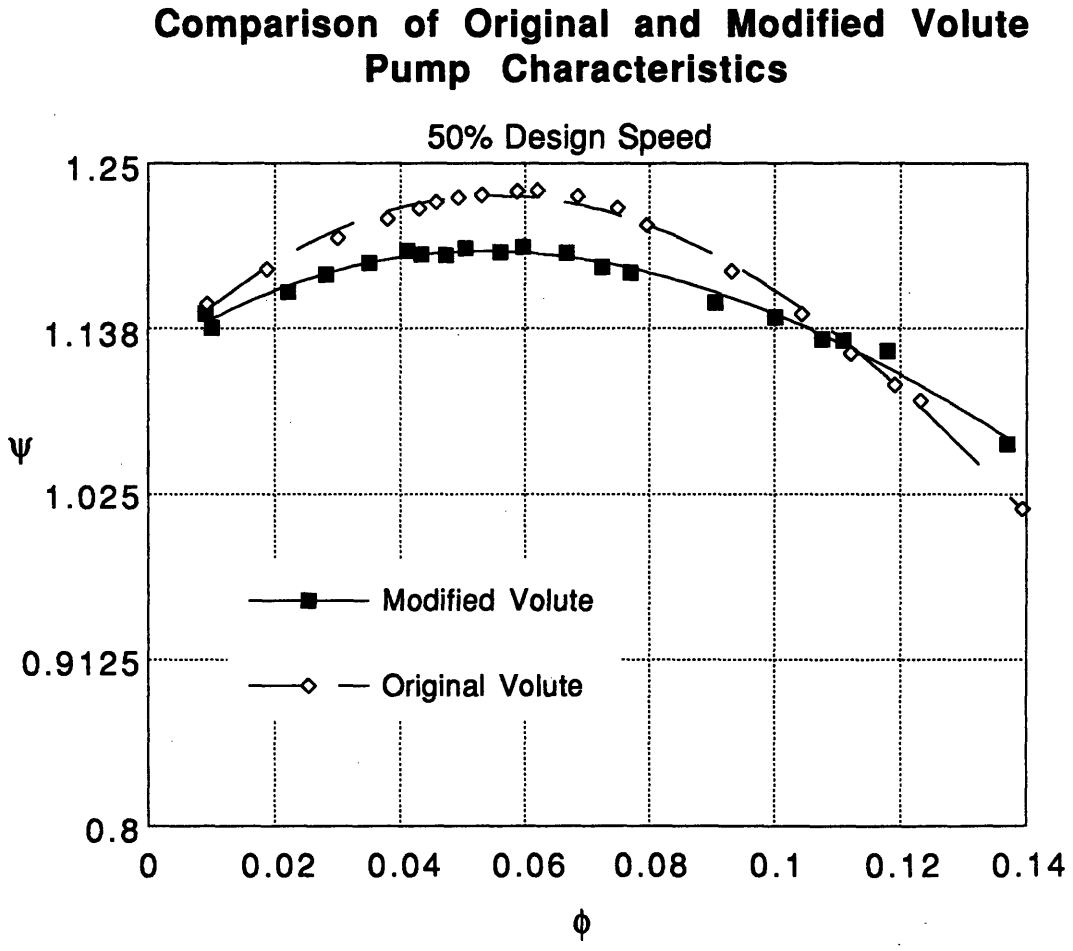
Comparison of Original and Modified Volute Pump Characteristics
50% Design Speed
1.25
1.138
1.025
0.9125
0.8
ψ
0
0.02
0.04
0.06
0.08
0.1
0.12
0.14
ϕ
Modified Volute
Original Volute

Figure 5.6

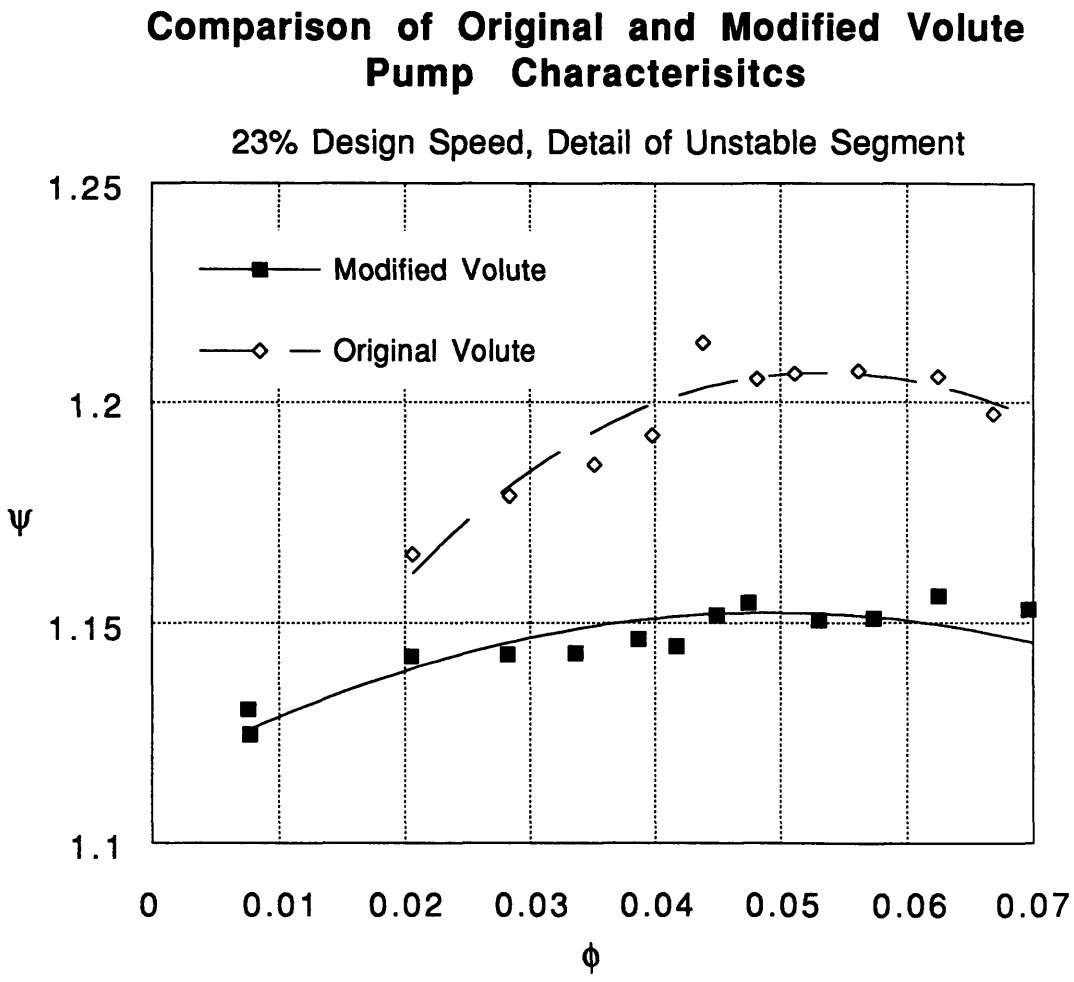
Comparison of Original and Modified Volute Pump Characterisitcs
23% Design Speed, Detail of Unstable Segment
1.25
1.2
1.15
1.1
ψ
Modified Volute
Original Volute
0
0.01
0.02
0.03
0.04
0.05
0.06
0.07
ϕ

Figure 5.7

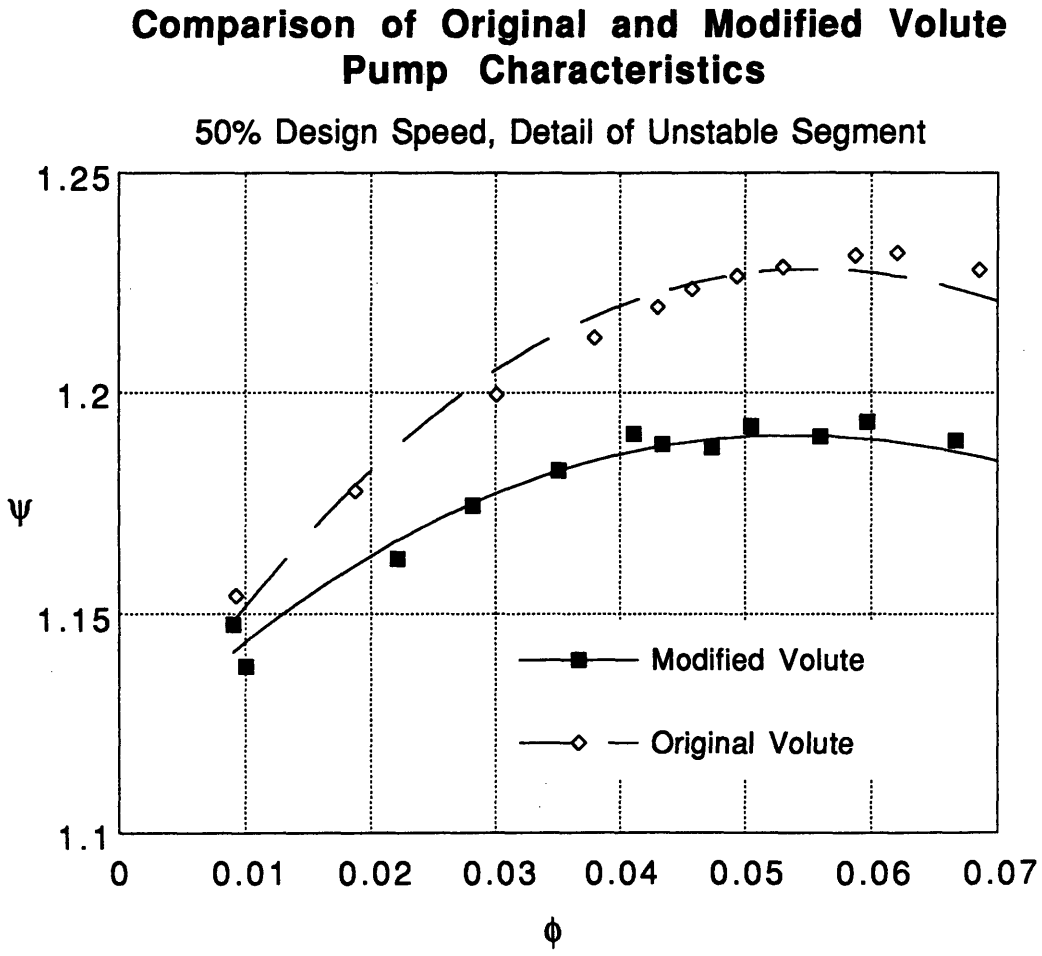
Comparison of Original and Modified Volute Pump Characteristics
50% Design Speed, Detail of Unstable Segment
1.25
1.2
1.15
1.1
ψ
0
0.01
0.02
0.03
0.04
0.05
0.06
0.07
ϕ
Modified Volute
Original Volute

Figure 5.8

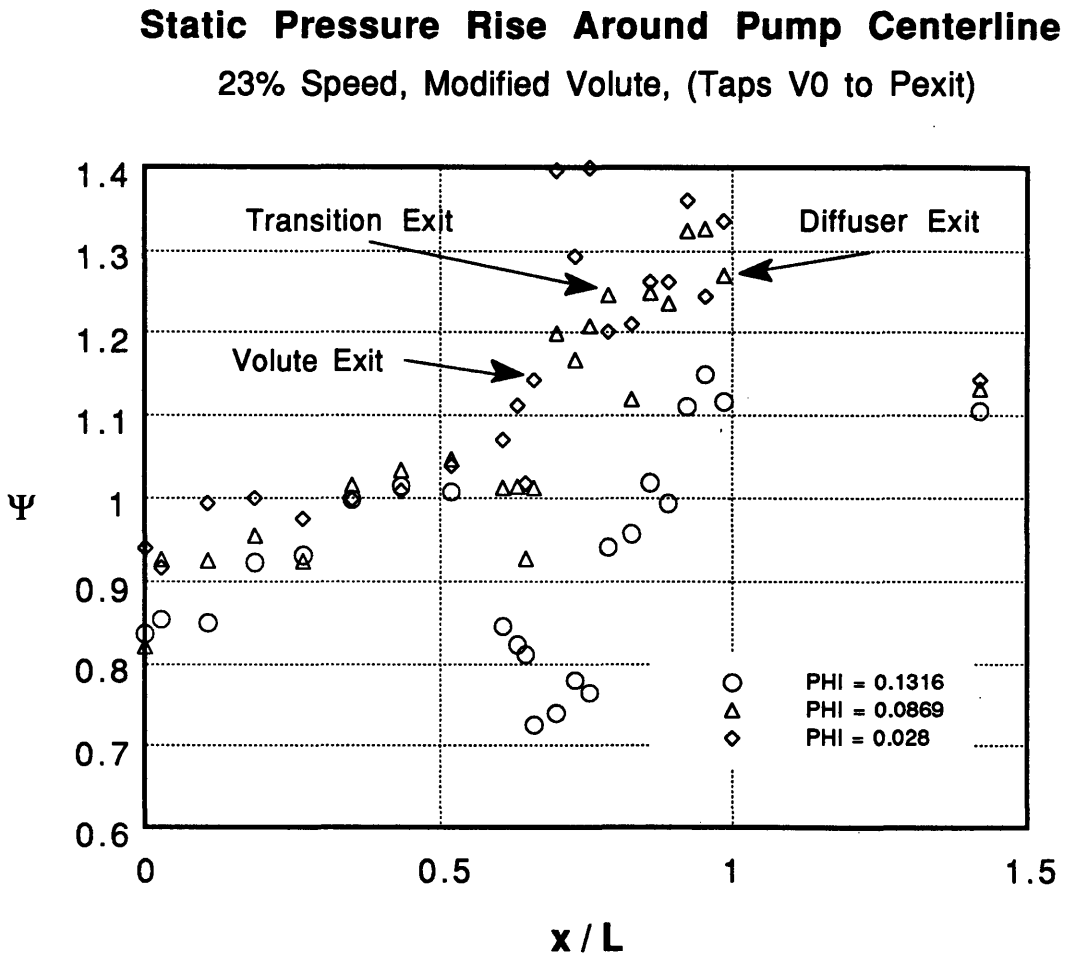
Static Pressure Rise Around Pump Centerline
23% Speed, Modified Volute, (Taps V0 to Pexit)
Transition Exit
Diffuser Exit
Volute Exit
PHI = 0.1316
PHI = 0.0869
PHI = 0.028
Ψ
1.4
1.3
1.2
1.1
1
0.9
0.8
0.7
0.6
0
0.5
1
1.5
x / L

Figure 5.9

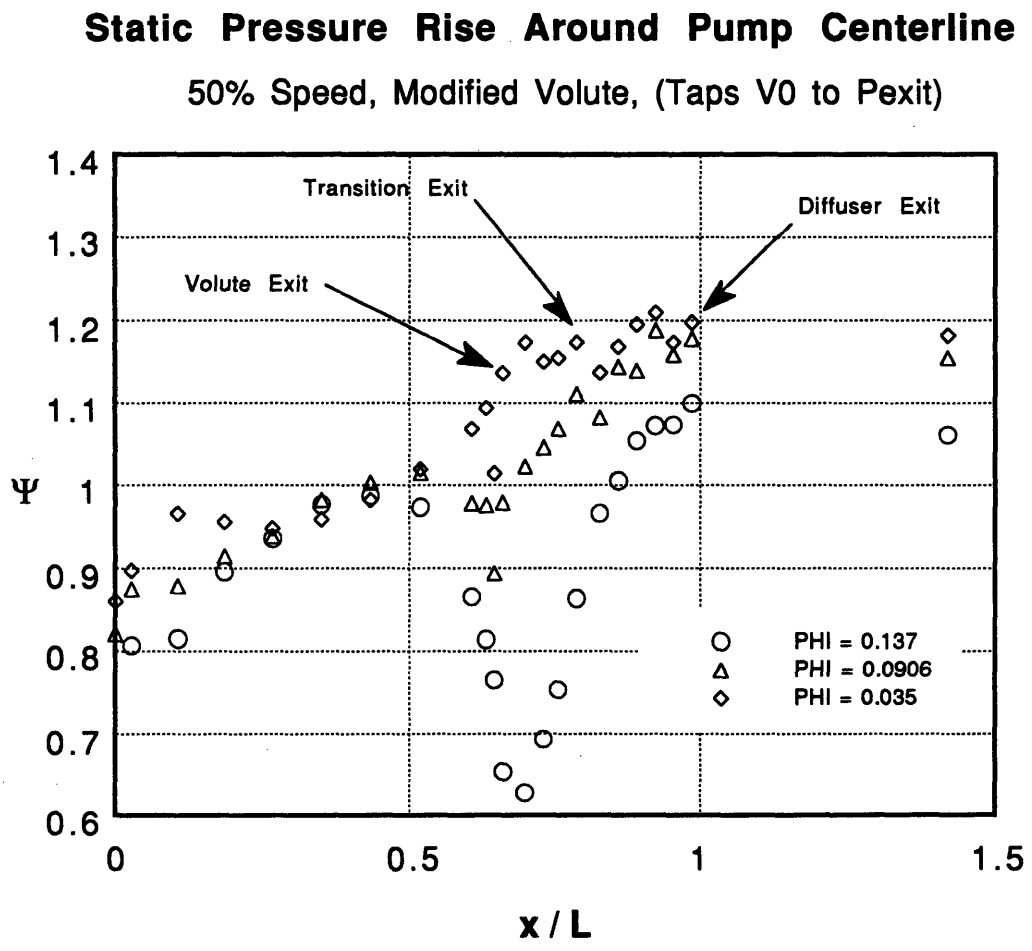
Static Pressure Rise Around Pump Centerline
50% Speed, Modified Volute, (Taps V0 to Pexit)
Transition Exit
Diffuser Exit
Volute Exit
PHI = 0.137
PHI = 0.0906
PHI = 0.035
Ψ
1.4
1.3
1.2
1.1
1
0.9
0.8
0.7
0.6
0
0.5
1
1.5
x / L

Figure 5.10

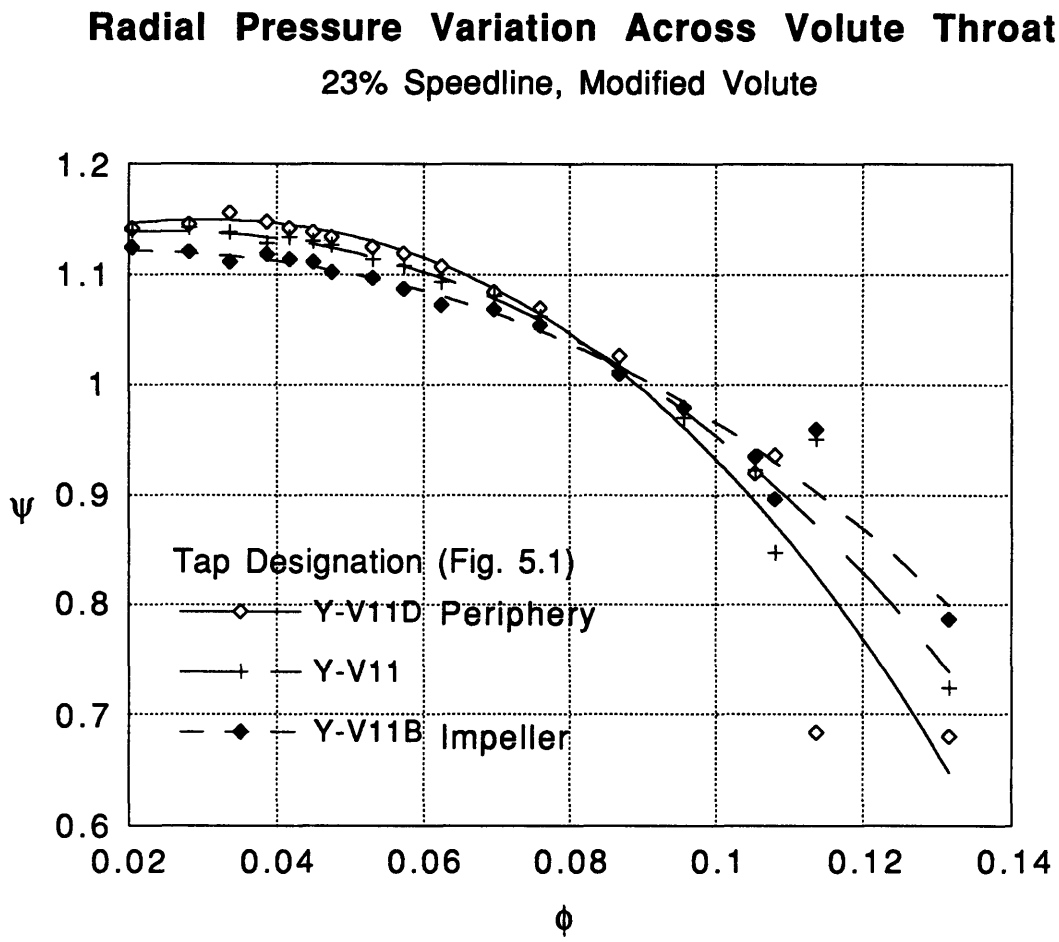
Radial Pressure Variation Across Volute Throat
23% Speedline, Modified Volute
1.2
1.1
1
0.9
0.8
0.7
0.6
ψ
0.02
0.04
0.06
0.08
0.1
0.12
0.14
ϕ
Tap Designation (Fig. 5.1)
Y-V11D Periphery
Y-V11
Y-V11B Impeller

Figure 5.11

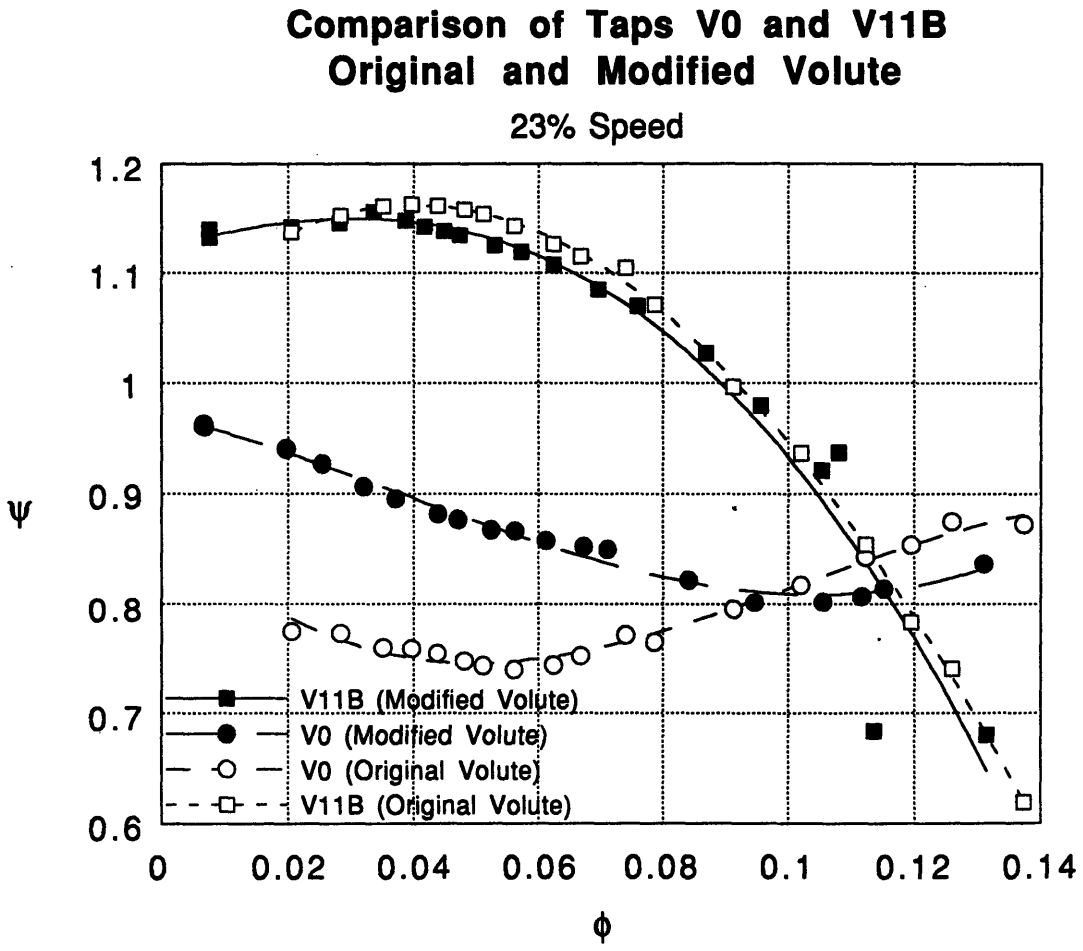
Comparison of Taps V0 and V11B
Original and Modified Volute
23% Speed
1.2
1.1
1
0.9
0.8
0.7
0.6
ψ
0
0.02
0.04
0.06
0.08
0.1
0.12
0.14
ϕ
V11B (Modified Volute)
V0 (Modified Volute)
V0 (Original Volute)
V11B (Original Volute)

Figure 5.12

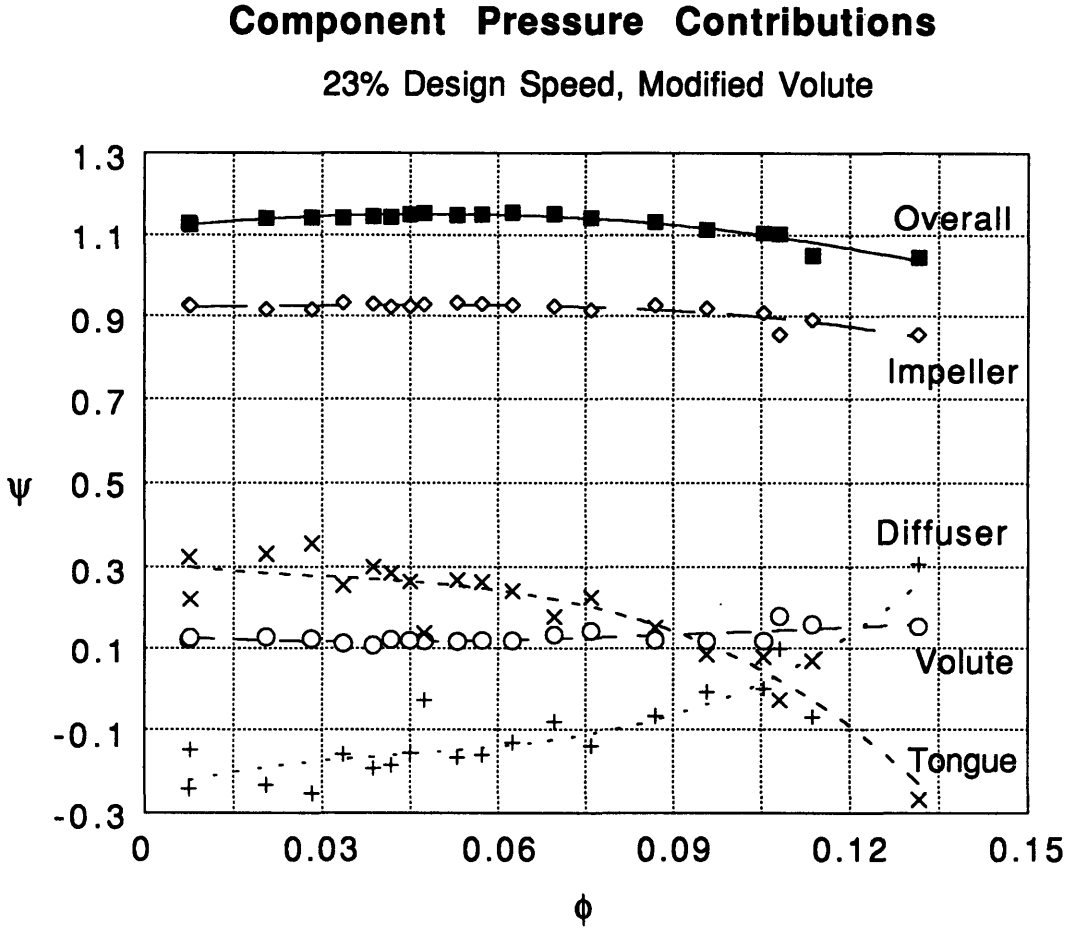
Component Pressure Contributions
23% Design Speed, Modified Volute
1.3
1.1
0.9
0.7
0.5
0.3
0.1
-0.1
-0.3
ψ
0
0.03
0.06
0.09
0.12
0.15
ϕ
Overall
Impeller
Diffuser
Volute
Tongue

Figure 5.13

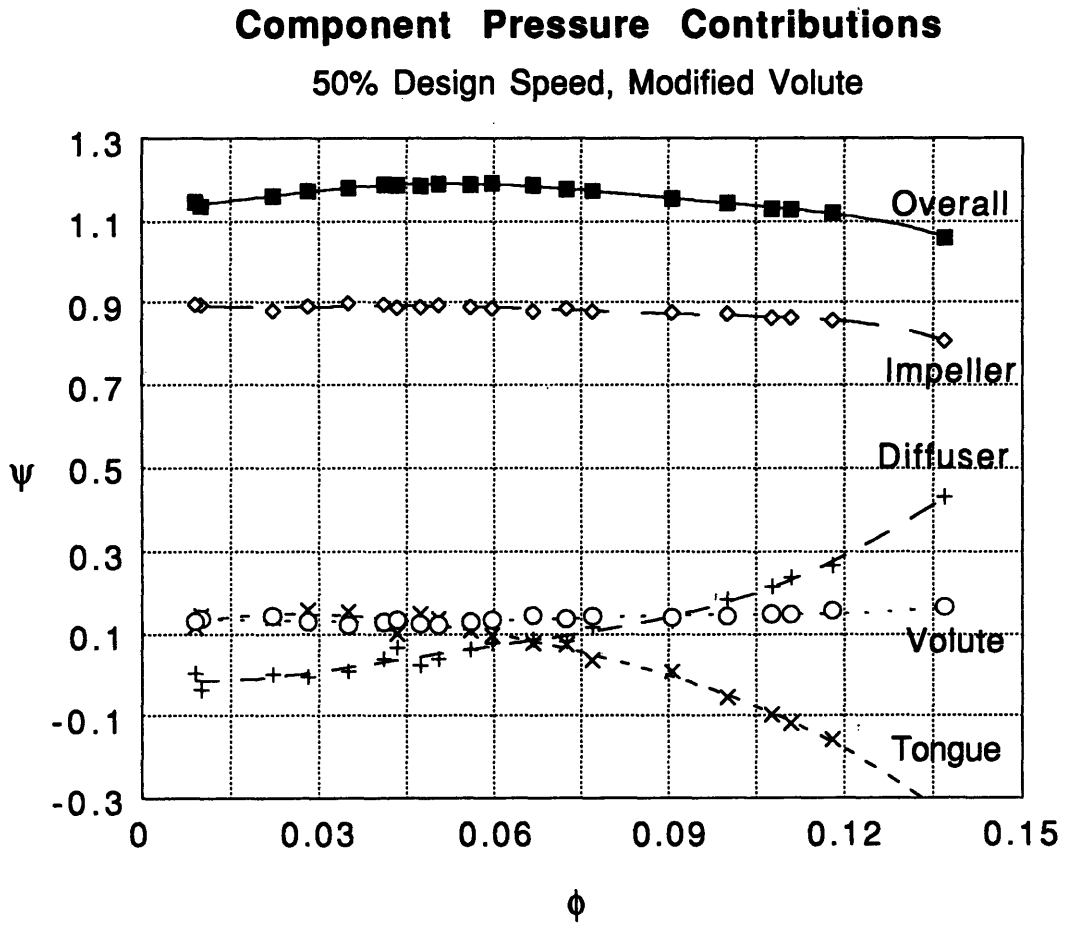
Component Pressure Contributions
50% Design Speed, Modified Volute
1.3
1.1
0.9
0.7
0.5
0.3
0.1
-0.1
-0.3
ψ
0
0.03
0.06
0.09
0.12
0.15
ϕ
Overall
Impeller
Diffuser
Volute
Tongue

Figure 5.14

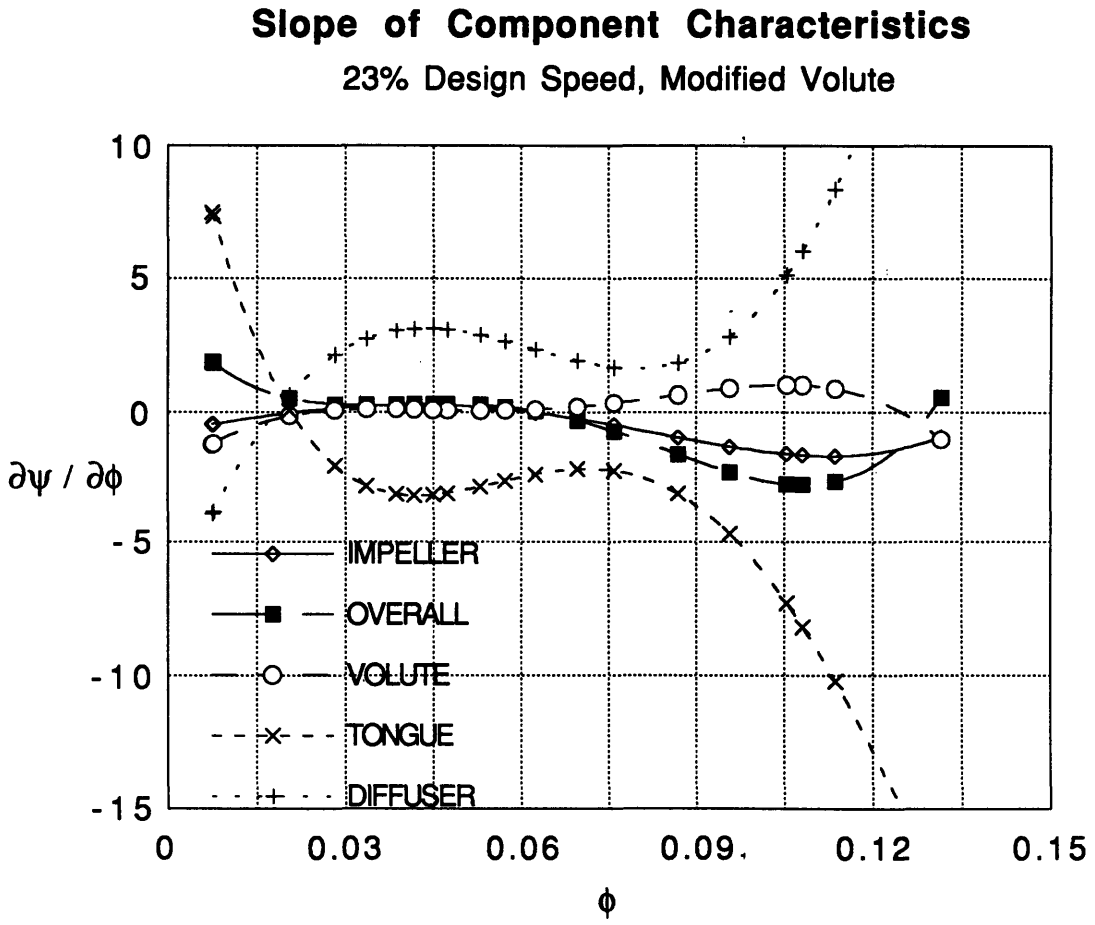
Slope of Component Characteristics
23% Design Speed, Modified Volute
10
5
0
-5
-10
-15
∂ψ / ∂ϕ
0
0.03
0.06
0.09
0.12
0.15
ϕ
IMPELLER
OVERALL
VOLUTE
TONGUE
DIFFUSER

Figure 5.15

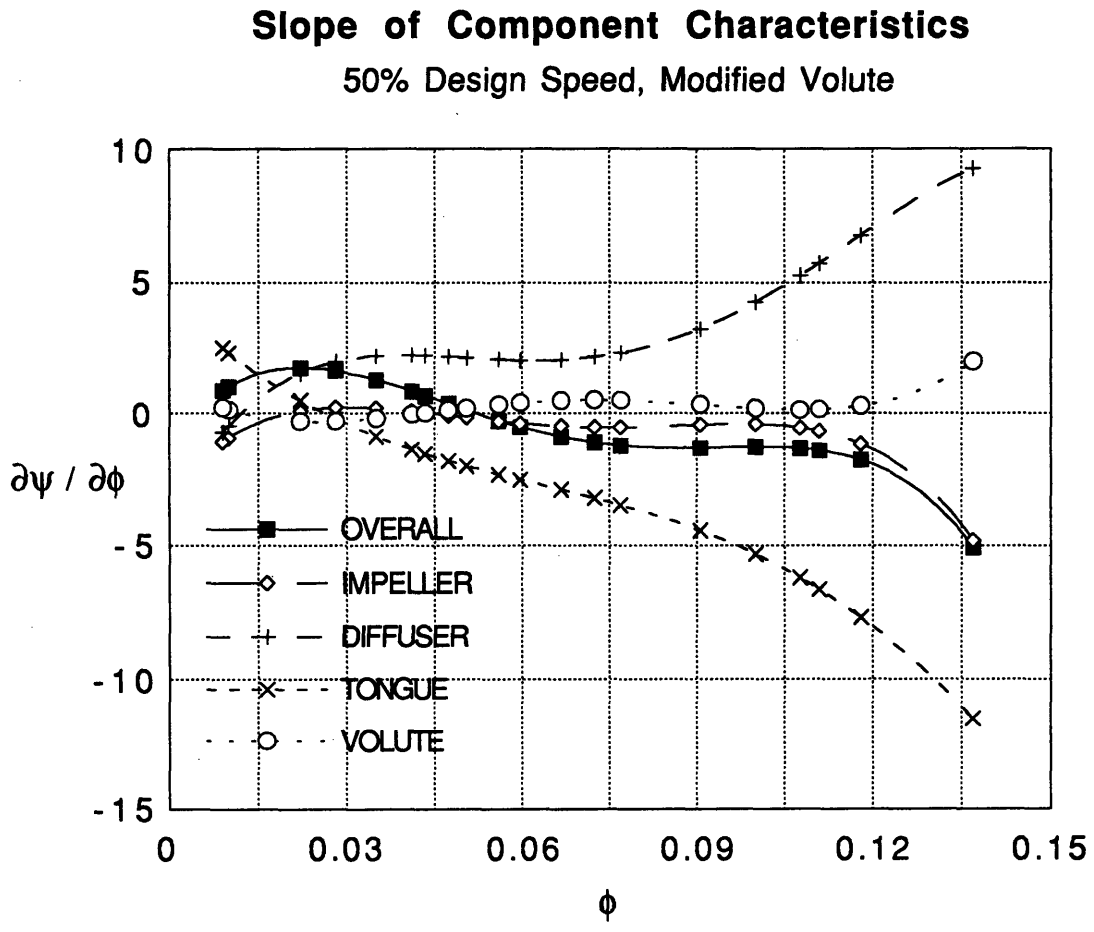
Slope of Component Characteristics
50% Design Speed, Modified Volute
10
5
0
-5
-10
-15
∂ψ / ∂ϕ
0
0.03
0.06
0.09
0.12
0.15
ϕ
OVERALL
IMPELLER
DIFFUSER
TONGUE
VOLUTE

Figure 5.16

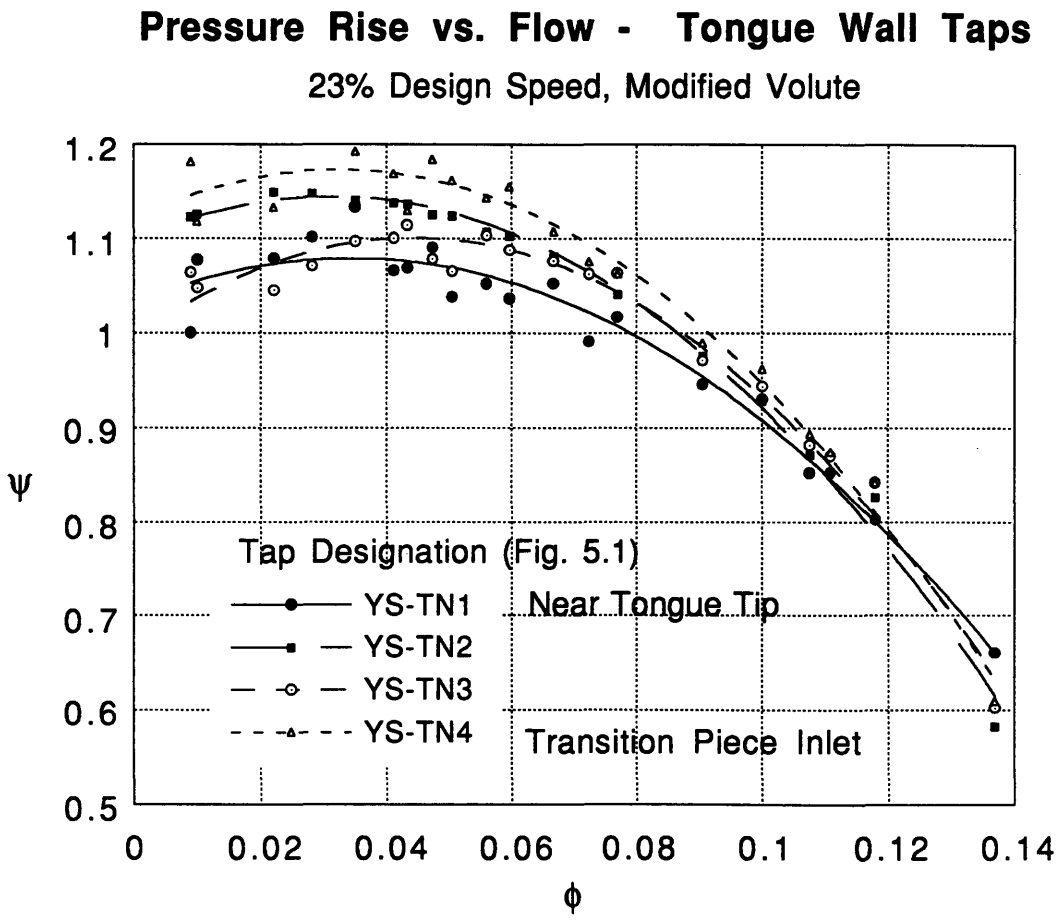
Pressure Rise vs. Flow - Tongue Wall Taps
23% Design Speed, Modified Volute
1.2
1.1
1
0.9
0.8
0.7
0.6
0.5
ψ
0
0.02
0.04
0.06
0.08
0.1
0.12
0.14
ϕ
Tap Designation (Fig. 5.1)
YS-TN1
YS-TN2
YS-TN3
YS-TN4
Near Tongue Tip
Transition Piece Inlet

Figure 5.17

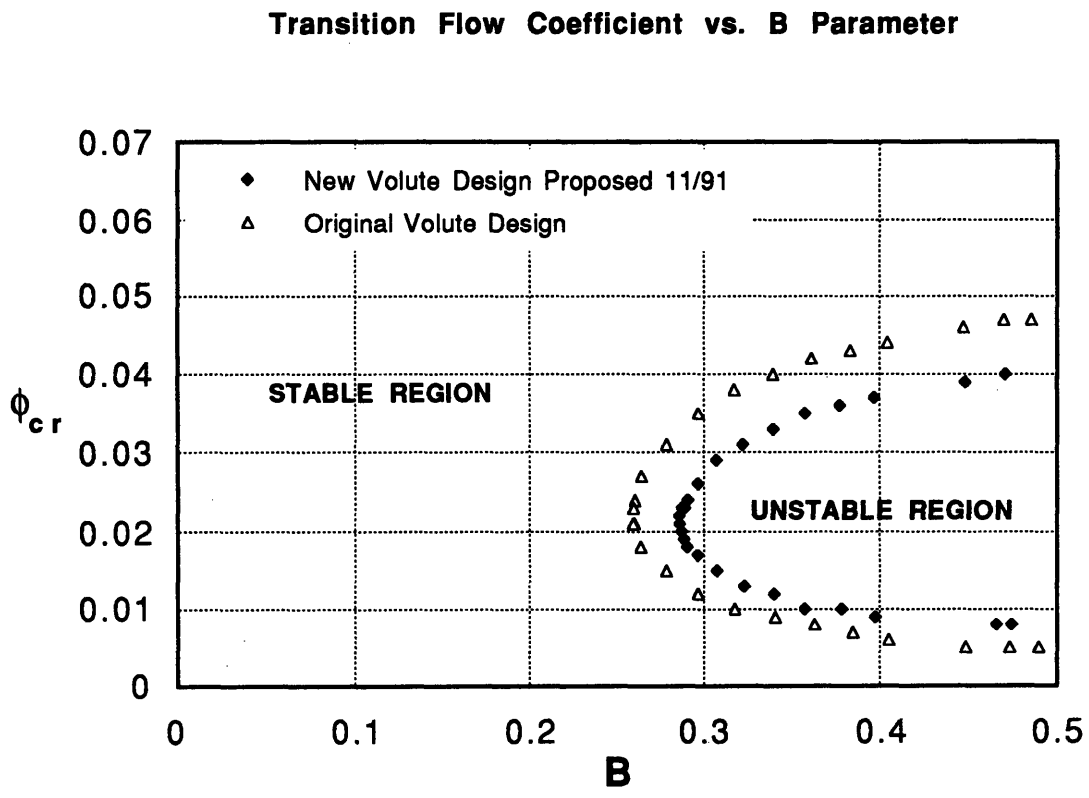

Figure 5.18
from Reference [6]

Reduced Frequency vs. Air Volume in Small Plenum

80% Speedline, Modified Volute

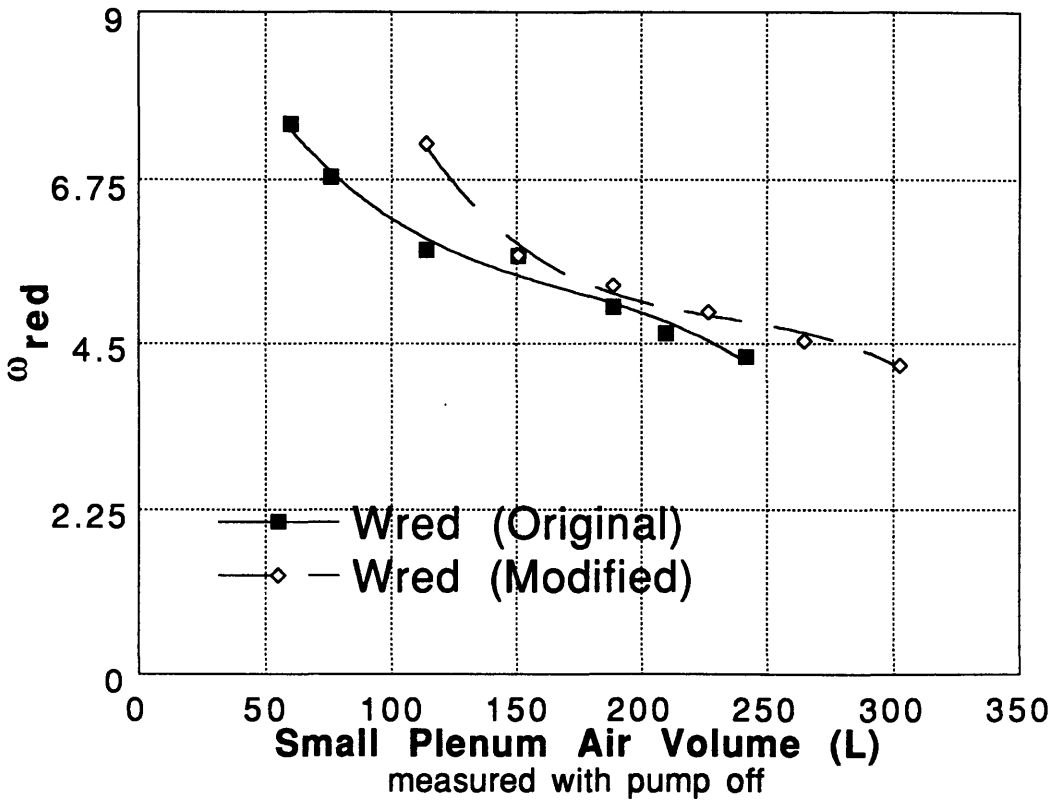

Figure 5.19

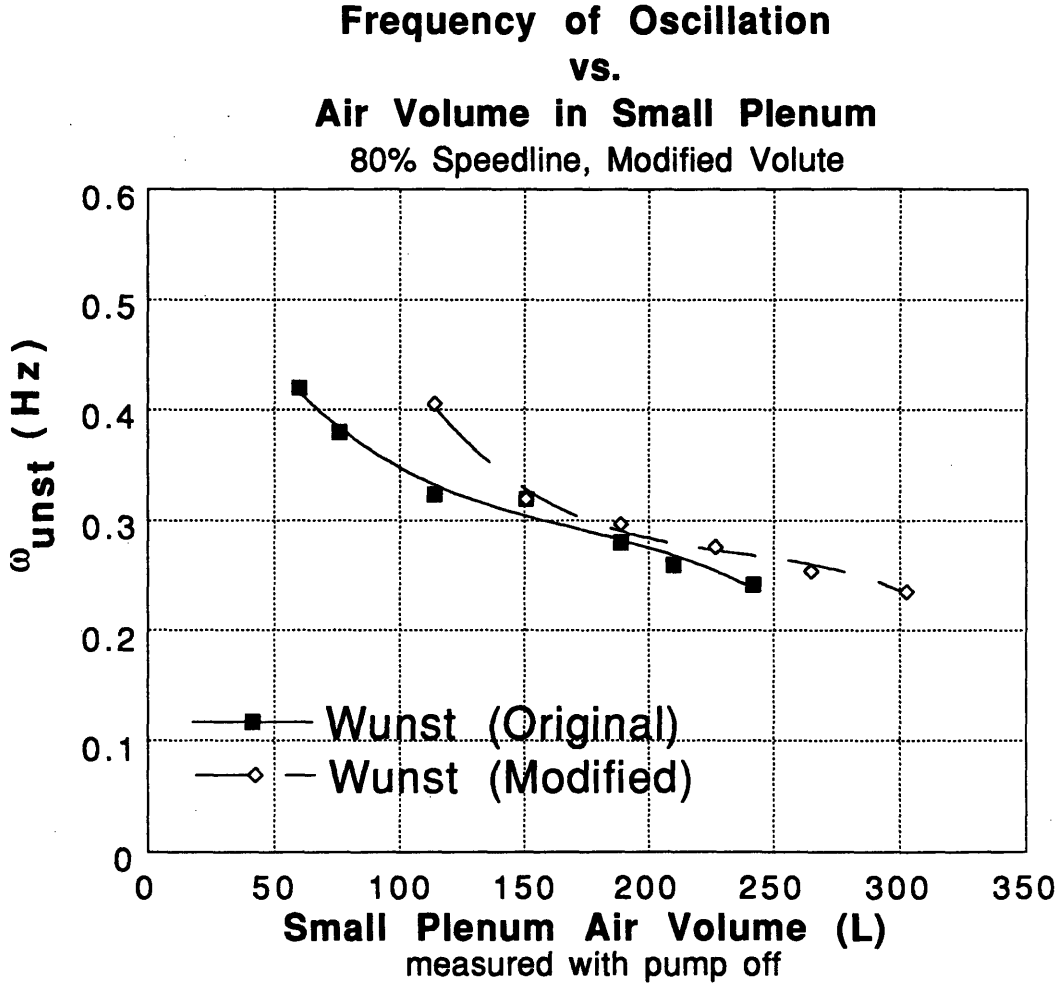
Frequency of Oscillation
vs.
Air Volume in Small Plenum
80% Speedline, Modified Volute
0.6
0.5
0.4
0.3
0.2
0.1
0
ω unst (Hz)
Wunst (Original)
Wunst (Modified)
0
50
100
150
200
250
300
350
Small Plenum Air Volume (L)
measured with pump off

Figure 5.20

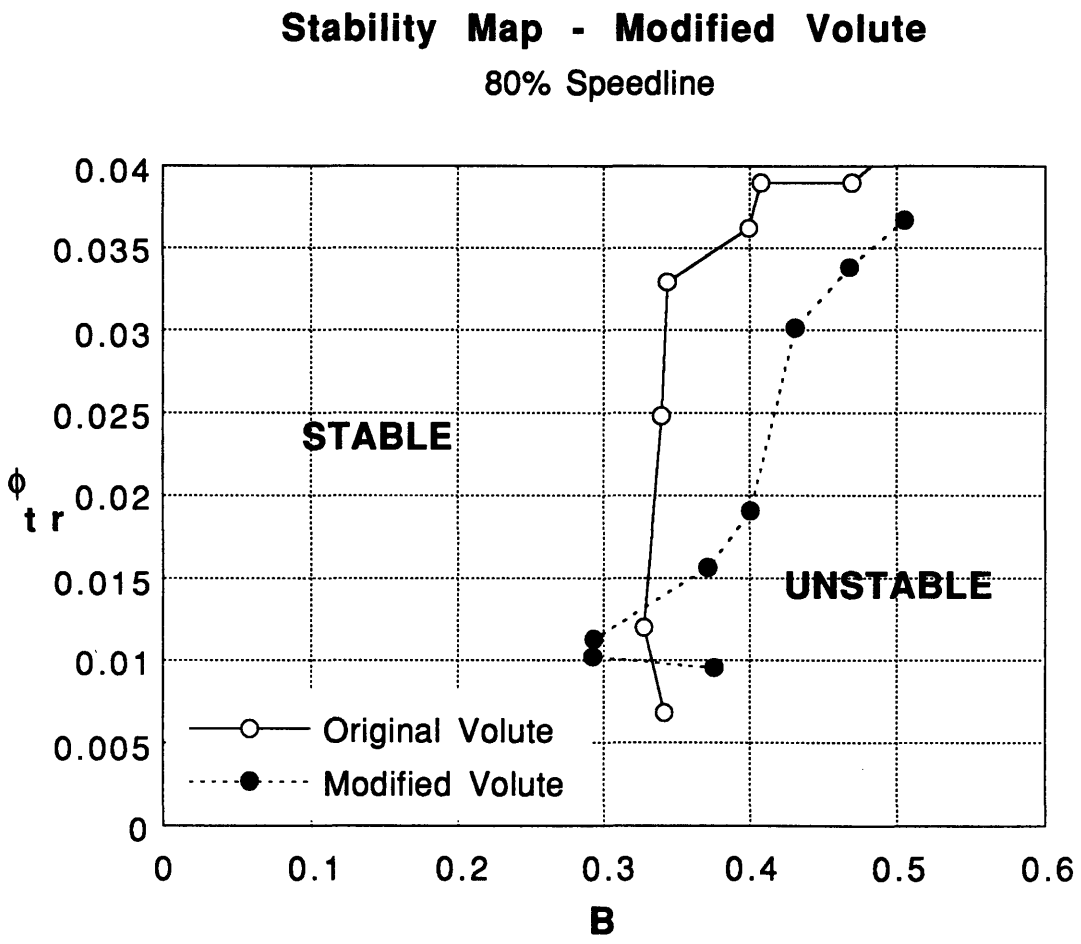
Stability Map - Modified Volute
80% Speedline
0.04
0.035
0.03
0.025
0.02
0.015
0.01
0.005
0
ϕ_{tr}
STABLE
UNSTABLE
Original Volute
Modified Volute
0
0.1
0.2
0.3
0.4
0.5
0.6
B

Figure 5.21

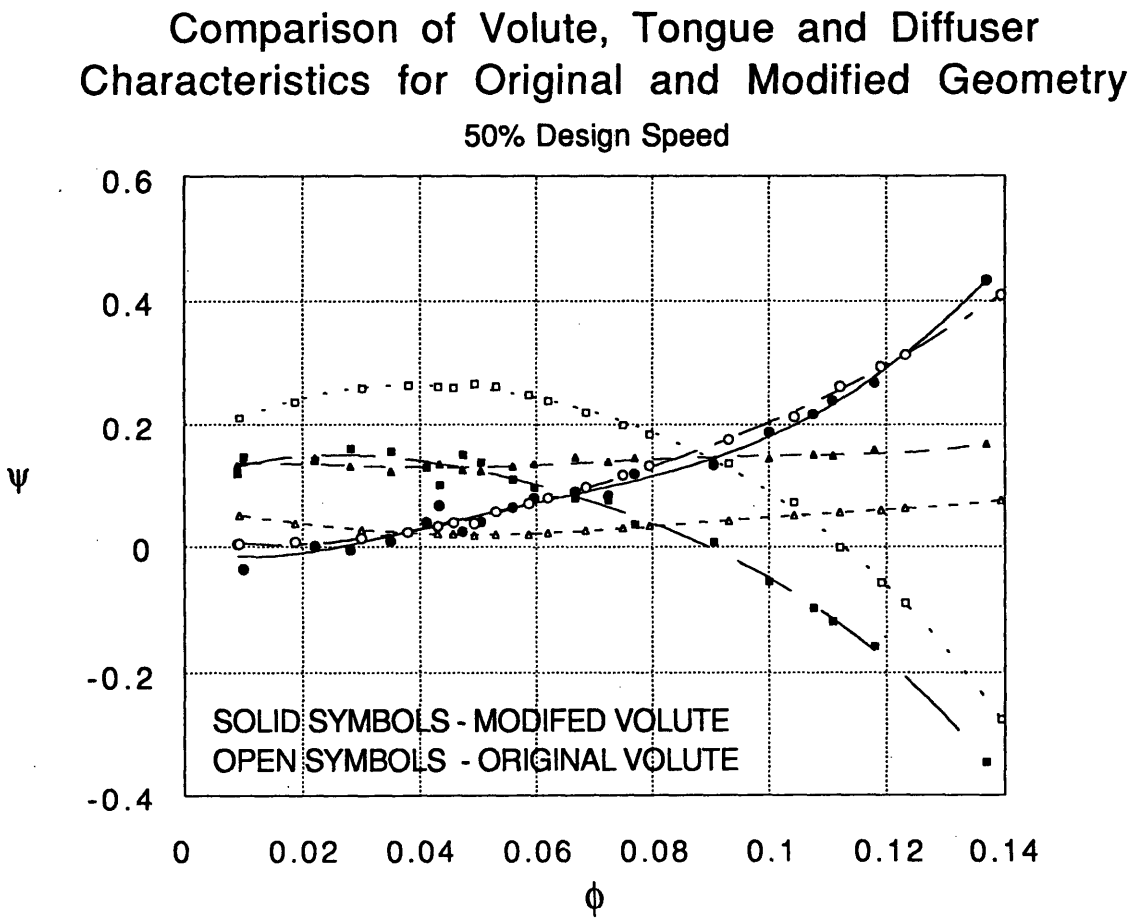
Comparison of Volute, Tongue and Diffuser Characteristics for Original and Modified Geometry
50% Design Speed
0.6
0.4
0.2
0
-0.2
-0.4
ψ
SOLID SYMBOLS - MODIFED VOLUTE
OPEN SYMBOLS - ORIGINAL VOLUTE
0
0.02
0.04
0.06
0.08
0.1
0.12
0.14
ϕ

Figure 5.22

FRINGE PATTERN DIAGRAM

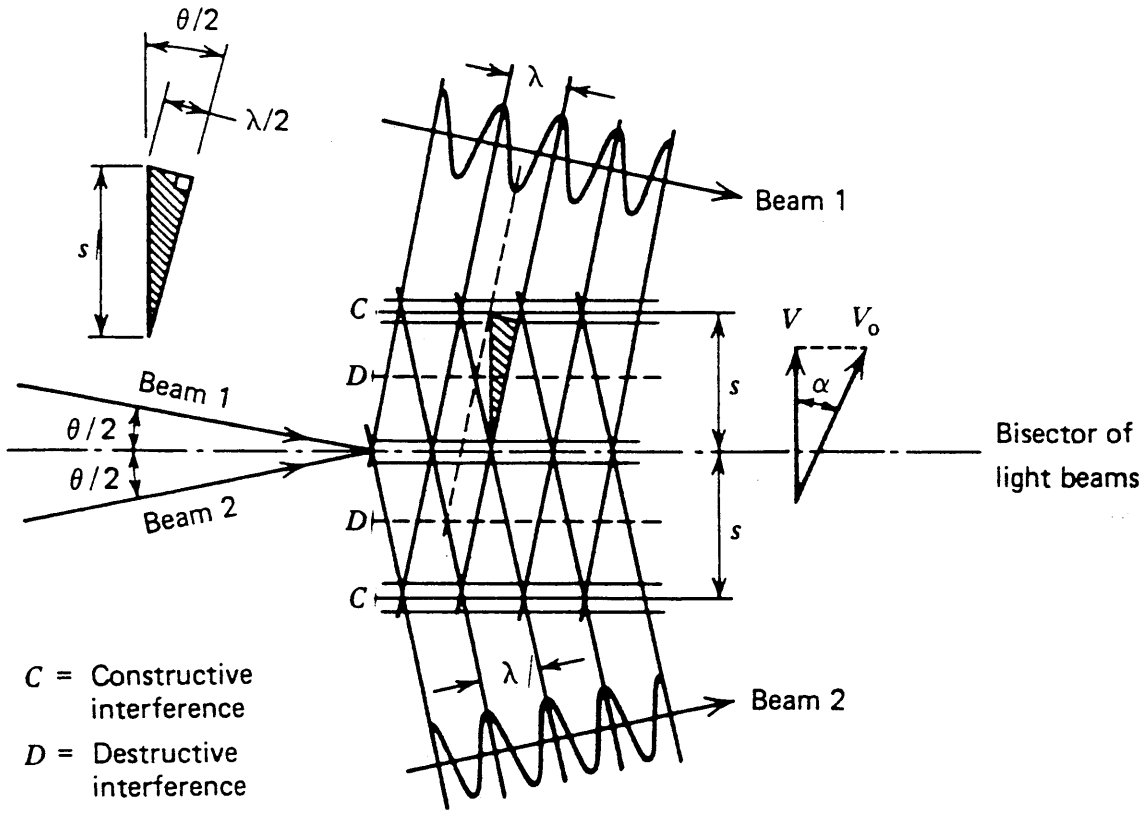

Figure A.1
from Reference [7]

PROBE VOLUME DIAGRAM

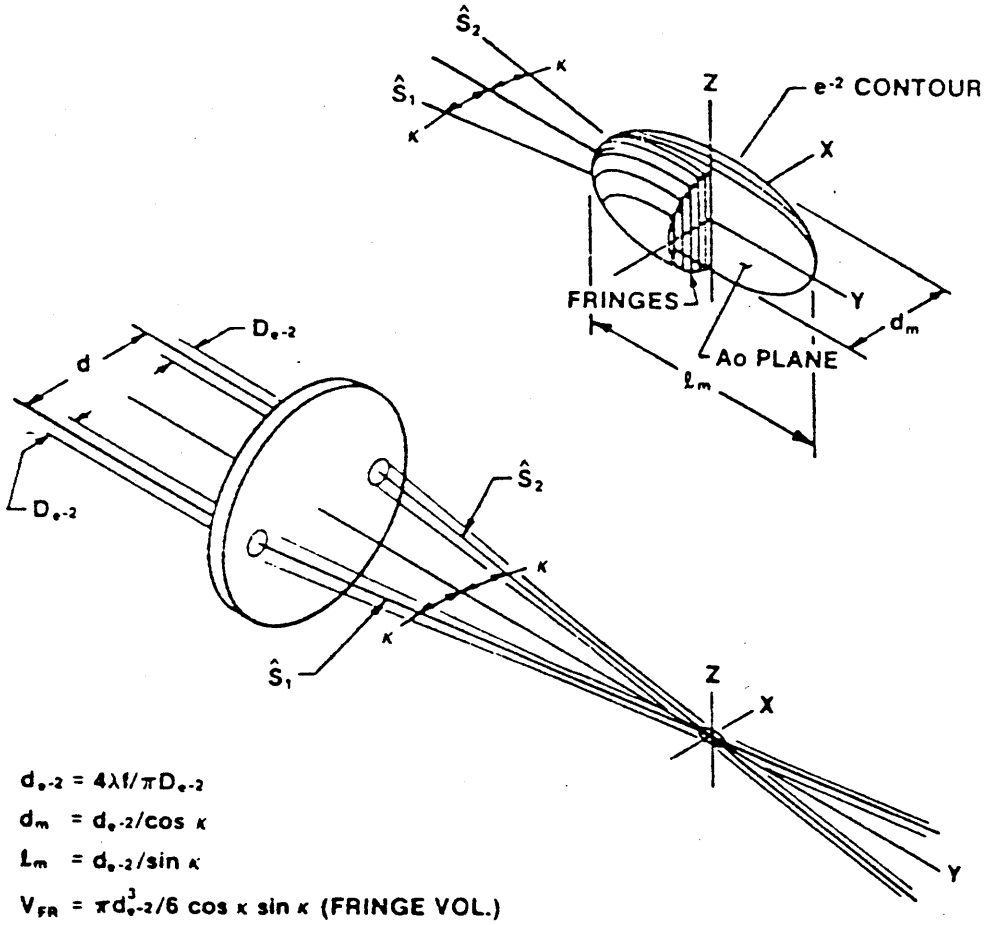

$d_{e^{-2}} = 4\lambda f/\pi D_{e^{-2}}$

$d_m = d_{e^{-2}}/\cos \kappa$

$\ell_m = d_{e^{-2}}/\sin \kappa$

$V_{FR} = \pi d^3_{e^{-2}}/6 \cos \kappa \sin \kappa$ (FRINGE VOL.)

$N_{FR} = \frac{d_m}{d_f} = \frac{1.27d}{D_{e^{-2}}}$ (NO. OF FRINGES)

Figure A.2
from Reference [25]

APPENDIX A
LASER VELOCIMETRY THEORY

Laser velocimetry is a non-intrusive technique used to measure velocity by detecting the Doppler shift of light scattered by a moving object. If V_0 is the particle velocity, one can show that:

$$f_D = \frac{2\, V_0 \cos\alpha}{\lambda} \sin\frac{\theta}{2} \qquad (A.1)$$

The term $V_0 \cos\alpha$ is the velocity component which is perpendicular to the bisector of the two light beams. The measured velocity component, V, is shown in Figure A.1. The velocity is in terms of the geometry and Doppler frequency by rearranging Equation (A.1) as:

$$V = \frac{f_D \lambda}{2 \sin\frac{\theta}{2}} \qquad (A.2)$$

In fluid flow measurements the object in the flow is generally a particle moving with the fluid whether naturally occurring or through a seeding process. The technique most commonly used for measurement of fluid flow is called heterodyne detection. Light from two sources is mixed to obtain a constructive and destructive interference pattern. When the light waves from the two sources are superimposed on the photodetector surface, the mixing process in the photodetector yields the difference frequency. There are three commonly used methods to accomplish the heterodyne technique. In a *dual-scatter system*, scattered light collected from two directions is heterodyned. In the *reference beam system*, the light scattered from a particle in the flow is heterodyned with the direct light coming from the laser. The direct light is called the reference beam. This experiment utilizes a *dual-beam system* or *differential Doppler system*. With this method, light scattered from two

sources of equal intensity are combined. The dual beam system has several advantages over the other two methods:

1.) It is the easiest system to align
2.) It is a better Signal-to-Noise Ratio
3.) It has flexibility since the Doppler frequency is independent of the location of the collection optics.
4.) Since only one particle is in the measuring volume at a time, large apertures can be used.
5.) Can be used when particle concentrations are low

The operation of the dual-beam anemometer can also be explained in terms of the optical interference pattern called a fringe pattern which occurs at the measuring location or probe volume. The measurement volume is an ellipsoid. Its boundaries are defined as the points where the amplitude of the Doppler signal is $1/e^2$ of its centerline value. The size of the probe volume is determined by the diameter of the beams exiting the focusing lens and the half angle between the two beams. These two parameter are a direct function of the focusing lens used. It is desirable to have a small probe volume for greater spatial resolution especially when boundary layer measurements are being made.

An exploded view of the probe volume is shown in Figure A.2. Remember, the component of the velocity which is measured is that which crosses the fringes perpendicularly. The spacing of the fringes is given by:

$$s = \frac{\lambda}{2 \sin(\frac{\theta}{2})} \qquad \text{(A.3)}$$

As a particle moving with a velocity, V_0 at and angle, α to the fringes crosses the interference pattern, it will experience a modulation of light intensity as it moves across the fringe pattern.

The LDV system is has several advantages over other methods of velocity measurements. LDV is a non-intrusive method. This flow field is not disturbed by a probe while the measurements are being made. Laser techniques can be used to make measurements of a wide range of velocities. Measurements can be made is flows that are highly turbulent with the use of frequency shifting. Finally, the velocity is measured in a direct manner and calibration is not required.

APPENDIX B
SCANIVALVE PRESSURE SAMPLING CODE

B.1 PRESCAN5 Instructions

Control and data acquisition procedures are contained in the computer code PRESCAN5. This code is written in BASIC for IBM compatible computers. The source code is then compiled and linked with the data acquisition callable routines provided in the PCLAB software. These callable routines for the BASIC language are in the file PCCBALIB. The compiled code is now in executable form and can be run by typing PRESCAN5 at the C:> prompt. All calculations are carried out in SI units and appropriate conversion factor are used when data is requested from the user in U.S. units.

Upon executing the program, the user is asked if the SDIU should be initialized. A "Y" response performs a power up on the interface unit and the SDIU will return to its preset status. A description of the SDIU configuration commands can be found in the SDIU User's Manual from Scanivalve Inc. All communication with the SDIU is through the General Purpose Interface Bus. By reading and writing to the GPIB input/output files, the SDIU can be commanded to acquire data and send the data to the host computer. Documentation of the GPIB procedures are contained in the Omega MBC-488 Users Manual.

The PRESCAN5 program gives the user two options for data acquisition:

1.) Steady-State Component Pressure Evaluation
2.) Unsteady Pump Performance

The first option allows the user to scan the entire set of pressure taps and calculate a time averaged performance characteristic for each. This option is used for determining the overall steady-state pump characteristic and component pressure contributions. The required user inputs for this subroutine are:

1.) Number of complete scans. This variable set how many times the entire set of pressure taps will be scanned before the an average is taken. The value is stored in the variable NSCAN and is referenced in arrays by the index, S.

2.) Scan rate. This parameter sets the number of ports per seconds that will be scanned. The valid range for this parameter is 1-8 ports/second. It is stored as a string variable named SRATE$.

3.) Number of throttle settings. This variable set the number of times the user will be able to adjust the throttle. The value is stored as the numeric variable, TSET. A value of TSET determines the resolution of the performance characteristics.

4.) Output datafile name. The prompt allow the user to specify the name used for saving data. The filename can be up 8 characters in length and no extension is need. The user must specify the device number, the path and a filename. The file extensions are added by the code and specify a grouping of pressure taps.

After entering this data the code will ask for a confirmation that these values are correct. If there is an error, answering "N" will allow the user to redefine these inputs. The data files are then opened and the appropriate extension is added to the user supplied filename to identify the data contained in the file. The extensions are:

Designation	Description
.SS	Contains overall pump performance
.DF	Diffuser
.TR	Transition region
.TN	Tongue wall
.TS	Tongue outside wall
.TP	Impeller top
.V	Middle volute
.VOT	Volute outside

.VB	Volute "B" taps
.IBP	Impeller discharge
.IN	Impeller inlet
.PLN	Plenums

The data acquisition loop is now repeated for each of the throttle settings specified in the variable TSET. A subroutine is called to sample the flowmeter, torque meter and RPM of the pump. The user will be prompted to enter in the percentage of the design speed being run and the leakage flow in gallons per minute. This subroutine collects only the digital output from the A/D system and a separate subroutine is used to convert this data into the relevant pump variables.

The Scanivalve ports are scanned the requested number of complete cycles as specified by the NSCAN variable. After each scan the SDIU requests service and the data is read from the SDIU's memory into the array D1$(S,M,C). The array holds all the data for each throttle setting. The "S" index is the scan number, the "M" index is the module and the "C" index is the port number. After each scan the data is sent to the host computer. A short routine is run to convert the string data sent by the SDIU into numeric data upon which calculations can be performed. The numeric data is stored in the array DTA(S,M,C). While this process is being performed, a units conversion is are done from psi to Pa. The final reduction is done by referencing the module 1 data, which was originally measured referenced to the V0 pressure tap, to the inlet pressure tap.

After the data acquisition and initial processing are complete, a subroutine is called that calculates the relevant time averaged pump parameters. This routine calculates, the flow coefficient, impeller tip speed (m/s), shaft angular frequency (rev/s and rad/s), volumetric flowrate (gpm and m^3/s) and torque (N - m). The user is also required to input the backplate leakage flow in gallons per minute. After returning from the subroutine, the pressure data is averaged for the samples taken and then non-dimensionalized. The non-dimensionalized head rise is stored in the array PSI(M,C). The total head rise and pump efficiency are determined and the data is output to disk.

NOTE: The pressure tap port assignments are completely arbitrary. Taps can easily be relocated and additional taps added. The code scans all 96 taps, however, only the relevant data is output. The addition of new taps or tap relocation only requires making note of the correct index in the arrays are modifying the data output.

The second option in the main menu is the unsteady pump performance routine. This subroutine only scans port number 29 of module 1, which is the head rise from inlet to exit of the entire pump. An unsteady analysis of individual pump components can be made by changing the NPORT$ variable to another tap number. For example, if an unsteady analysis of the diffuser is desired, the NPORT$ variable can be set to correspond to the DF6 pressure tap. The transducer's reference side should then be connected to the DF1 tap. Thus an unsteady analysis of the pressure rise in the diffuser can be performed. The time resolved pump measurement routine requires the user to input the following parameters:

1.) Data acquisition rate. This value is the frequency the data will be acquired at. Due to the nature of the Scanivalve system, the valid range is limited to 1-8 Hz. Since the frequency of the unsteadiness in the pump loop is around .4 Hz, this range is sufficient to accurately resolve the time response of the system. The value is stored in the string variable, SRATE$.

2.) Time interval. This is the time period over which data will be taken. The SDIU's memory limits this to a value of 25 seconds. However, if the data is sent to the host computer as it is being read, this sample interval is only limited by the PC's memory. The value is stored in the variable, DELT.

3.) Number of throttle settings. This variable set the number of times the user will be able to adjust the throttle. The value is stored as the numeric variable, TSET. A value of TSET determines the resolution of the performance characteristics.

4.) The percentage of design speed being run. The percentage of design speed allows the data flow, rpm and torque reading to be synchronized to the shaft rotation frequency. This value is stored in the SPD variable.

A Fast-Fourier Transform (FFT) routine is used to determine the frequency of the system unsteadiness. The original subroutine was written in FORTRAN

(Reference [2]), but was translated into BASIC for the PRESCAN5 code. This routine requires that the number of data points must be an integer power of 2, i.e, 2^N. For a given set of user inputs the total number of data points is given by DELT * STRATE$. If there are more points than given by 2^N the extras are discarded from the end of the data string. Data acquisition of the pressure and other parameters is carried out simultaneously, unlike the steady-state option in which the pump parameters are evaluated prior to the pressure measurements.

The conversion of the string data to numeric data is done using the same procedure as for the steady-state option. The string data is read into the array D2$(C) and is converted to numeric data in the array DTA2(C). The average values for the pressure and flow are calculated and are subtracted off the time resolved readings to prepare for taking a FFT. The conditional requirement for determining if the system is surging is the same as that used in reference [4]. If the system exhibits a sustained oscillatory pressure with a peak-to-peak amplitude greater than 3% of the BEP pressure rise, then the system is surging. If this condition is not met, the code asks the user to throttle the pump and take data again.

Under surge conditions a FFT of the pressure and flow data is computed. The B parameter and the reduced frequency are calculated. The data is stored in two files. The .AVE file contains the average head and capacity values as well as the percent amplitude of the fluctuations, the B parameter and the reduced frequency. The .INS file contains the instantaneous data for the pressure, flow, RPM, torque and impeller tip speed. If the system is surging, a .SRG extension is substituted for the .INS.

B.2 PRESCAN5 Source Code

```
10      '      ***********************************************
20 ' *
30 ' *                PRESCAN.BAS   Version 3.2
40 ' *                   By: Scott B. Sandler
50 ' *                         3/11/92
60 ' *    Program to read Scanivalve and reduce data for analysis.
70 ' *
80      '      ***********************************************
90 CLS
100     '********************
110 '* DEFINE CONSTANTS *
120     '********************
130 PI = 3.141592654# : D2 = .6096 : B2 = .015 : ' D2 and b2 are in meters
140 RHO = 998 : ' (kg/m3)
150 NBOARD% = 1 : NTIME% = 2000 : NSORCE% = 0 : NOFFSET% = 1 : NCHAN%
= 3
160 ICHL% = 0 : INIT% = 1 : IGAIN% = 1 : IPHI% = 0 : ISIGN = 1
170 CONV = 214.71 : LP = 45.197 : PSIBEP = 1.1625 : PHIBEP = .092
180 AIN = .072966 : AEX = .032429 : ALEAK = .0005067 : ATR4 = .0048436
185 SURGE = 0
190  DIM  IDATA%(6000),PHIXL(20),RVAL(10),AVAL(11),VALU(10),OFFS(10)
200  DIM  CALIB(1000,3)
210 PRINT TAB(35);"PRESSCAN.BAS"
220 PRINT TAB(27);"Written By: SCOTT B. SANDLER"
230  PRINT  TAB(27);"Version 3.2  -  Mar. 11,1992" : PRINT
240  '
250 ' open files for GPIB I/O
260  '
270 OPEN "$DV488" FOR OUTPUT AS #1
280 PRINT#1,"BUFFERCLEAR"                : ' clear computer input buffer
290 OPEN "$DV488" FOR INPUT AS #2
300 PRINT#1,"SYSCON MAD1=3 CIC1=1 BA1=&H200 CLK=12"
310 PRINT#1,"REMOTE 1"                   : ' put SDIU in remote mode
320 INPUT "Do you want to initialize the SDIU (Y/N)";ANS$
330 IF ANS$="Y" OR ANS$="y" THEN PRINT#1,"OUTPUT 1 $ @ RS"
340 FOR X = 1 TO 8000 : NEXT X
350 PRINT#1,"OUTPUT 1 $ @ QS 0 1 47 0 0" : ' set queue configuration
parameters
360 PRINT#1,"OUTPUT 1 $ @ FF 1 1 0 13 10 13 10" : ' set data output format
370 PRINT#1,"OUTPUT 1 $ @ TS 2"          : ' enable SRQ (service requests)
380 PRINT : PRINT "Menu:
390 PRINT "    1.)  Steady State Component Pressure Evaluation"
400 PRINT "    2.)  Time Resolved Overall Pump Evaluation"
410 PRINT : INPUT "Option:";ANS$
420 IF ANS$="1" THEN 440  ELSE IF ANS$="2" THEN 1660
430 PRINT " Option invalid. Please select again" : GOTO 410
440 PRINT : INPUT "How many complete scans";NSCAN
450 PRINT : INPUT "Data scan rate 1-8 ports per second";SRATE$
460 PRINT : INPUT"Number of throttle settings";TSET
470 PRINT:INPUT"Output data file name [device][path][name] (8 characters no
extention)";NM$
```

```
480 PRINT : PRINT "Data Acquisition Parameter Summary:"
490 PRINT "2.) Data Scan Rate: ";SRATE$
500 PRINT "3.) Number of Full Scans: ";NSCAN
510 PRINT "4.) Number of throttle settings: ";TSET
520 PRINT : INPUT "Is this correct (Y/N)";ANS$
530 IF ANS$ ="N" OR ANS$="n" THEN 440
540  DIM  DTA(NSCAN,1,48),D1$(NSCAN,1,48),PSI(1,47)
550     '     **************************
560 ' * OPEN OUTPUT DATA FILES *
570     '     **************************
580 OPEN NM$+".ss" FOR OUTPUT AS #3
590 OPEN NM$+".df" FOR OUTPUT AS #4
600 OPEN NM$+".tr" FOR OUTPUT AS #5
610 OPEN NM$+".ts" FOR OUTPUT AS #6
620 OPEN NM$+".tn" FOR OUTPUT AS #7
630 OPEN NM$+".tp" FOR OUTPUT AS #8
640 OPEN NM$+".in" FOR OUTPUT AS #9
650 OPEN NM$+".ibp" FOR OUTPUT AS #10
660 OPEN NM$+".vot" FOR OUTPUT AS #11
670 OPEN NM$+".vb" FOR OUTPUT AS #12
680 OPEN NM$+".v" FOR OUTPUT AS #13
690 OPEN NM$+".pln" FOR OUTPUT AS #14
700
PRINT#3,"PHI","YSEX","STD","YTEX","EFFIC","TRQ","UTIP(m/s)","GPM","LEAKA
GE"
710  PRINT#4,"PHI","YS-DF1","YS-DF2","YS-DF3","YS-DF4","YS-DF5","YS-
DF6"
720  PRINT#5,"PHI","YS-TR1","YS-TR2","YS-TR3","YS-TR4","YT-TR4"
730  PRINT#6,"PHI","YS-TS1","YS-TS2","YS-TS3","YS-TS4","YS-TS5","YS-
TS6","YS-TS7","YS-TS8"
740  PRINT#7,"PHI","YS-TN1","YS-TN2","YS-TN3","YS-TN4"
750  PRINT#8,"PHI","YS-TP1","YS-TP2","YS-TP3","YS-TP4","YS-TP5","YS-
TP6","YS-TP7","YS-TP8","YS-TP9","YS-TP10"
760  PRINT#9,"PHI","YS-IN8","YS-IN1","YS-IN2","YS-IN3","YS-IN4","YS-
IN5","YS-IN6","YS-IN7"
770  PRINT#10,"PHI","YS-V0","YS-V1","YS-V2","YS-V3","YS-V4A","YS-
V5A","YS-V6A","YS-V7A","YS-V8A","YS-V9A"
780  PRINT#11,"PHI","YS-V1E","YS-V2E","YS-V3E","YS-V4E","YS-V5E","YS-
V6E","YS-V7E","YS-V8E","YS-V9D","YS-V10D","YS-V11D"
790  PRINT#12,"PHI","YS-V8B","YS-V9B","YS-V10B","YS-V11B"
800  PRINT#13,"PHI","YS-V3","YS-V4","YS-V5","YS-V6","YS-V7","YS-
V8","YS-V9","YS-V10","YS-V11"
810  PRINT#14,"PHI","Y-LG","Y-SM","Y-ATM"
820 CLS
830     '     ************************
840 ' * DATA ACQUISITION LOOP *
850     '     ************************
860 FOR T = 1 TO TSET
870 PRINT :INPUT"Set throttle, then hit return to begin.";ANS$
880 GOSUB 3250
890 FOR S = 1 TO NSCAN
900  PRINT#1,"OUTPUT 1 $ @ QF -1"
910   PRINT : PRINT "Taking Data Set ";S;" of throttle setting";T
```

```
920   PRINT#1,"OUTPUT 1 $ @ AD "+SRATE$+" -1 48"
930   PRINT#1,"STATUS 1"
940   INPUT#2,SPOLL%
950   IF ((SPOLL% AND 64) <> 64) THEN 930
960  PRINT : PRINT "Processing Data Set  ";S
970  FOR M = 0 TO 1 STEP 1
980    IF M=0 THEN PRINT#1,"OUTPUT 1 $ @ OM 0"ELSE PRINT#1,"OUTPUT 1 $
@ OM 1"
990   FOR C = 0 TO 48 STEP 1
1000      PRINT#1,"TRIGGER 1":PRINT #1,"ENTER 1 $ @"
1010       INPUT #2,D1$(S,M,C)
1020      IF C = 48 THEN 1100
1030       LN = LEN(D1$(S,M,C)):CH$="":PRES$=""
1040      WHILE CH$ <> " "
1050          CH$ = MID$(D1$(S,M,C),LN,1)
1060       PRES$ = CH$+PRES$
1070        LN = LN - 1
1080      WEND
1090      DTA(S,M,C) = VAL(PRES$) * 6894.733      : ' psi to Pa
1100   NEXT C
1110  NEXT M
1120 NEXT S
1130 FOR S = 1 TO NSCAN STEP 1                      :' This routine references all
1140  FOR C = 0 TO 47                               :' Module 1 ports to the inlet
1150     DTA(S,1,C)=DTA(S,1,C)+DTA(S,0,39)          :' pressure tap
1160  NEXT C                                        :' DTA(s,0,39) = Pvo -
Pinlet
1170 NEXT S
1180 GOSUB 3780
1190     '    ******************************
1200 ' * AVERAGE THE NSCAN SAMPLES *
1210     '    ******************************
1220 FOR M = 0 TO 1 : FOR C = 0 TO 47
1230 PSI(M,C) = 0 : NEXT C,M
1240 FOR M = 0 TO 1
1250 FOR C = 0 TO 47
1260 FOR S = 1 TO NSCAN
1270  PSI(M,C) = PSI(M,C) + DTA(S,M,C)
1280  PEXBAR = PSI(0,29)/NSCAN
1290 NEXT S
1300  PSI(M,C)  =  PSI(M,C)/(NSCAN*.5*RHO*(UTIP)^2)
1310 NEXT C,M
1320     '    ************************************************
1330 ' * DETERMINE TOTAL PRESSURE AT TRANSITION EXIT *
1340 ' * AND TOTAL PRESSURE, EFFICIENCY AT PUMP EXIT *
1350     '    ************************************************
1360  YSEX  =  PSI(0,29)
1370  YTEX  =  YSEX  +  .5*((VEX^2+VLEAK^2-VIN^2)/UTIP^2)
1380 DPTOT = .5 * YTEX * RHO * UTIP^2
1390 ETA = Q * DPTOT / (TRQ * OMEGA)
1400  YTTR4  =  PSI(1,13)  +  .5*((VTR4^2+VLEAK^2-VIN^2)/UTIP^2)
1410     '    ************************
1420 ' * COMPUTE STD DEVIATION *
```

```
1430    '    ************************
1440 SUM = 0
1450 FOR S = 1 TO NSCAN
1460 SUM = SUM + (DTA(S,0,29) - PEXBAR)^2
1470 NEXT S : STD = (SUM/NSCAN)^.5
1480    '    ***********************
1490 ' * WRITE DATA TO FILES *
1500    '    ***********************
1510 PRINT#3,PHI,YSEX,STD,YTEX,ETA,TRQ,UTIP,GPMFLO,LKFLO
1520 PRINT#4,PHI,;:FOR C = 24 TO 29 : PRINT#4,PSI(1,C),;:NEXT C :
PRINT#4,
1530 PRINT#5,PHI,;:FOR C = 10 TO 13 : PRINT#5,PSI(1,C),;:NEXT C :
PRINT#5,YTTR4
1540 PRINT#6,PHI,;:FOR C = 2 TO 9 : PRINT#6,PSI(1,C),;:NEXT C : PRINT#6,
1550   PRINT#7,PHI,PSI(1,33),PSI(0,47),PSI(1,0),PSI(1,1)
1560 PRINT#8,PHI,PSI(1,14),PSI(1,15),PSI(1,31),;:FOR C = 17 TO 23 :
PRINT#8,PSI(1,C),;:NEXT C : PRINT#8,
1570 PRINT#9,PHI,;:FOR C = 0 TO 7 : PRINT#9,PSI(0,C),;:NEXT C : PRINT#9,
1580
PRINT#10,PHI,PSI(0,9),PSI(0,11),PSI(0,14),PSI(0,17),PSI(0,20),PSI(0,23
),PSI(0,42),PSI(0,29),PSI(0,34),PSI(0,38)
1590
PRINT#11,PHI,PSI(0,10),PSI(0,12),PSI(0,15),PSI(0,18),PSI(0,21),PSI(0,2
4),PSI(0,27),PSI(0,30),PSI(0,35),PSI(0,46),PSI(0,43)
1600   PRINT#12,PHI,PSI(0,33),PSI(0,37),PSI(0,41),PSI(0,45)
1610
PRINT#13,PHI,PSI(0,17),PSI(0,19),PSI(0,22),PSI(0,25),PSI(0,28),PSI(0,3
2),PSI(0,36),PSI(0,40),PSI(0,44)
1620   PRINT#14,PHI,PSI(0,9),PSI(0,8),PSI(0,29)
1630 NEXT T
1640   CLOSE   #3,#4,#5,#6,#7,#8,#9,#10,#11,#12,#13,#14
1650 GOTO 4560
1660    '    ****************************************
1670 ' * TIME RESOLVED PRESSURE MEASUREMENTS *
1680    '    ****************************************
1690 OPT = 2 : NPORT$="29"
1700 PRINT : INPUT "Data Scan Rate (1-8 ports/sec)";SRATE$
1710 PRINT : INPUT "Time Interval (sec)";DELT
1720 PRINT : INPUT "Number of Throttle Settings";TSET
1730 PRINT : INPUT "Enter percent of design RPM";SPD
1732 PRINT : INPUT"Volume of Air in Small Plenum (Liters)";VSP
1740 NSCAN$ = STR$(VAL(SRATE$) * DELT)
1750 NSCAN = VAL(NSCAN$)
1760    '    ********************************************
1770 ' * DETERMINE NEAREST POWER OF 2 FOR FFT DATA *
1780    '    ********************************************
1790 NPOW2 = 2
1800 IF NSCAN >= NPOW2 THEN NPOW2=NPOW2*2 ELSE 1820
1810 GOTO 1800
1820 NUSED = NPOW2/2
1830 PRINT : PRINT "Number of useable samples";NUSED
1840 NEXTRA = NSCAN - NUSED
1850 NSTART = NEXTRA/2 : N = 2 * NUSED
```

```
1860 PRINT#1,"OUTPUT 1 $ @ TS 2"
1870 PRINT#1,"OUTPUT 1 $ @ QS 0 0 "+NPORT$+ " 0 "+NPORT$
1880  DIM
D2$(NSCAN),DTA2(NSCAN),TTRQ(NSCAN),TUTIP(NSCAN),TPHI(NSCAN)
1890  DIM
TGPMFLO(NSCAN),TQ(NSCAN),TRPM(NSCAN),RPHI(NSCAN),RPSI(NSCAN)
1900  DIM  RRPM(NSCAN),DAT(N)
1910 PRINT : INPUT"Output Data File Name [device][path][name](5 Characters
Max.)";NM$
1920 OPEN NM$+".ave" FOR OUTPUT AS #3
1925 OPEN
"a:rms"+RIGHT$(STR$(SPD),2)+RIGHT$(STR$(VSP),(LEN(STR$(VSP))-
1))+".dat" FOR OUTPUT AS #5
1930   PRINT#3,"PHI","%AMP(p-p)","YSEX","YTEX","%RMS(p-
p)","psifreq","B","redfreq","phifreq","B","redfreq","effic","Vsp"
1935   PRINT#5,"%RMS-PSI","PHI"
1940 FOR T = 1 TO TSET
1950 PRINT : INPUT "Set throttle, and press <CR> to continue";ANS$
1970 PRINT#1,"OUTPUT 1 $ @ QF -1"
1980 PRINT : PRINT"Taking data....."
1990 GOSUB 3250 : ' begin data acquisition of pressure and flow
2000 PRINT#1,"OUTPUT 1 $ @ QP"
2010 PRINT : PRINT "Processing data....."
2020 PRINT#1,"OUTPUT 1 $ @ OC 0 "+NPORT$+" "+NSCAN$+ " 1"
2030 PSUM = 0
2040 FOR C = 1 TO NSCAN STEP 1
2050     FOR S = 1 TO 3
2060      PRINT#1,"TRIGGER 1" : PRINT#1,"ENTER 1 $ @"
2070        INPUT#2,D2$(C)
2080      IF (S = 1) THEN 2160
2090      IF S = 3 THEN 2170
2100       LN = LEN(D2$(C)) : CH$="":PRES$=""
2110      WHILE CH$<>" "
2120           CH$ = MID$(D2$(C),LN,1)
2130        PRES$ = CH$ + PRES$
2140         LN = LN -1
2150      WEND
2160     NEXT S
2170 DTA2(C) = VAL(PRES$) * 6894.733 : ' Convert PSI to Pa
2180 PSUM = PSUM + DTA2(C)
2190 NEXT C
2200 PBAR = PSUM / NSCAN
2210       '      ******************************************
2220 ' * COMPUTE MEANS OF DATA AND SUBTRACT FROM *
2230 ' * PSI, PHI DATA TO PREPARE FOR FFT       *
2240       '      ******************************************
2250 RPMMAX = 0
2260 FOR I = 1 TO NCHAN% : VALU(I) = 0 : NEXT I          :' set array to zero
2270 FOR J = 1 TO NCHAN%
2280   FOR I = 1 TO NUSED                :' use the first nused # of points
2290       VALU(J) = VALU(J) + CALIB(I,J)
2300   NEXT I
2310 NEXT J
```

```
2320 FOR I = 1 TO NCHAN% : AVAL(I) = VALU(I)/NUSED : RVAL(I)=0 :  NEXT I
2330 GOSUB 3780 : ' calculate time averaged pump parameters
2340 PSIBAR = PBAR / ( .5*RHO*UTIP^2)
2350 GOSUB 3970 : ' calculate time resolved pump parameters
2360 FOR C = 1 TO NUSED
2370  RPHI(C)=0 : RPSI(C)=0 : RRPM(C)=0          :' set reduced variables to zero
2380   DTA2(C) = DTA2(C)/(.5*RHO*TUTIP(C)^2)   :' non-dimensionalize
pressure
2390 NEXT C
2400 SUM = 0 : SUM1=0
2410 FOR C = 1 TO NUSED
2420   RPHI(C) = TPHI(C) - PHI                  :' subtract off mean value
2430   RPSI(C) = DTA2(C) - PSIBAR               :' to prepare for FFT
2440    SUM = SUM + (RPSI(C))^2
2450    SUM1 = SUM1 +(RPHI(C))^2
2460    RRPM(C) = TRPM(C) - RPM
2470  IF TRPM(C) > RPMMAX THEN RPMMAX = TRPM(C)
2480 NEXT C
2490 RMS = (SUM/NUSED)^.5
2500 RMS1 = (SUM1/NUSED)^.5
2510     '     *************************
2520 ' * DETERMINE % AMPLITUDE *
2530     '     *************************
2540 PHIAMP = 100 * (RMS1/PHI)                    :' %rms of phi average
2550 RPMAMP = 100 * (RPMMAX/RPM - 1 )
2560 PSIAMP = 100 * (RMS/PSIBEP)                  :' %rms of psi bep
2565  PRINT#5,PSIAMP,PHI
2570 PRINT : PRINT"% RMS of PSIBEP= ";PSIAMP;"%      PHI ave.= ";PHI
2572  PRINT : PRINT"% RMS of PHIBEP= ";100*(RMS1/PHIBEP);"%"
2580 IF (2^.5) * PSIAMP < 3 THEN 2590 ELSE 2610    :' peak-to-peak amplitude
2590 PRINT : PRINT "Pump is not surging..."
2600 GOTO 3060
2610 PRINT : PRINT "Pump is surging, continuing data processing"
2615 SURGE = 1
2620     '     **********************************
2630 ' * PUT PSI INTO DAT ARRAY FOR FFT *
2640     '     **********************************
2650 FOR C = 1 TO NUSED
2660  DAT(2*C-1) =  RPSI(C)
2670 DAT(2*C) = 0 : NEXT C
2680 GOSUB 4120                    :' do FFT
2690     '     ******************************
2700 ' * FIND LARGEST PSI FREQUENCY *
2710     '     ******************************
2720 PCHECK = 0 : PMAX = 0
2730 FOR I = 1 TO NUSED
2740     PCHECK = (DAT(2*I-1)^2 + DAT(2*I)^2)^.5
2750  IF PCHECK <= PMAX THEN 2780
2760  PSIFREQ = (I-1)/DELT                  :' Hz
2770  PMAX = PCHECK
2780 NEXT I
2790 BPAR1 = UTIP / ( 2 * PSIFREQ * LP)
2800 REDFREQ1 = PSIFREQ / (RPM/60)
```

```
2810     '     ***********************************
2820 ' * PUT PHI INTO DAT ARRAY FOR FFT *
2830     '     ***********************************
2840 FOR C = 1 TO NUSED
2850  DAT(2*C-1)  =  RPHI(C)
2860 DAT(2*C) = 0 : NEXT C
2870 GOSUB 4120                    :' do FFT
2880     '     ******************************
2890 ' * FIND LARGEST PHI FREQUENCY *
2900     '     ******************************
2910 PCHECK = 0 : PMAX = 0
2920 FOR I = 1 TO NUSED
2930     PCHECK  =  (DAT(2*I-1)^2  +  DAT(2*I)^2)^.5
2940  IF PCHECK <= PMAX THEN 2970
2950  PHIFREQ = (I-1)/DELT                    :' Hz
2960  PMAX = PCHECK
2970 NEXT I
2980 BPAR2 = UTIP / ( 2 * PHIFREQ * LP)          :' B parameter based on phi
2990 REDFREQ2 = PHIFREQ / (RPM/60)
3000 YTEX = PSIBAR + .5*((VEX^2 + VLEAK^2 - VIN^2)/UTIP^2)
3010 DPTOT = .5 * PSIBAR  * RHO * UTIP^2          :' Pressure in Pa
3020 ETA = Q * DPTOT / ( TRQ * OMEGA )
3030     '     *********************************************
3040 ' * WRITE RESULTS OF SURGE CYCLE TO DATAFILE *
3050     '     *********************************************
3055
PRINT#3,PHI,(2^.5)*PHIAMP,PSIBAR,YTEX,(2^.5)*PSIAMP,PSIFREQ,BPAR1,RE
DFREQ1,PHIFREQ,BPAR2,REDFREQ2,ETA,VSP
3060 IF SURGE <>1 THEN OPEN NM$+"t"+RIGHT$(STR$(T),(LEN(STR$(T))-
1))+".ins" FOR OUTPUT AS #4
3062 IF SURGE = 1 THEN OPEN NM$+"t"+RIGHT$(STR$(T),(LEN(STR$(T))-
1))+".srg" FOR OUTPUT AS #4
3065 PRINT : INPUT "Throttle Voltage Setting";TV
3070 PRINT#4,"SURGE CYCLE TIME RESOLVED DATA"
3090  PRINT#4,"Design Speed = ";SPD;"%"
3100 PRINT#4,"Average Pressure Rise Coefficient = ";PHIBAR
3110 PRINT#4,"Ave. Flow Coefficient = ";PHI
3112 PRINT#4,"Volume of Air in Small Plenum";VSP
3114  PRINT#4,"Throttle  Voltage",TV
3120  PRINT#4,"TIME","PHI","PSI","UTIP","GPMFLO","TRQ","RPM"
3130 TINT = 0
3140 FOR C = 1 TO NUSED
3150
PRINT#4,TINT,TPHI(C),DTA2(C),TUTIP(C),TGPMFLO(C),TTRQ(C),TRPM(C)
3160  TINT = TINT + (1/VAL(SRATE$))
3170 NEXT C
3175 SURGE = 0
3180 CLOSE #4
3190 NEXT T
3195  CLOSE#3,#5
3200 GOTO 4560
3210 '                          **************
3220 '                        * SUBROUTINES *
```

```
3230 '                          **************
3240 '
3250      '     ******************************************
3260 ' * SUBROUTINE TO READ RPM, TORQUE and ADMAG *
3270      '     ******************************************
3280 '
3290 ' *** SET UP SAMPLING PARAMETERS **
3300 '
3310 IF NOFFSET% = 2 THEN 3390
3320 ICHH% = NCHAN% + ICHL% -1
3330 IF OPT = 2 THEN NSPC% = VAL(NSCAN$) ELSE NSPC%=1000
3340 IF OPT = 2 THEN FREQ = VAL(SRATE$)*NCHAN% ELSE FREQ = (5.6 *
SPD)*NCHAN%
3350 NSAMP% = NSPC% * NCHAN%
3360 ' *** SETUP A/D BOARD FOR DATA TAKING ***
3370 PRINT : INPUT "Turn pump off and hit <CR> to take offsets";ANS$
3380 CALL XINIT
3390 CALL XSB(NBOARD%)
3400  CALL XST(NTIME%)
3410 CALL XFDL(IDATA%,LENDMA%)
3420 IF (LENDMA% < NSAMP%) THEN INIT% = LENDMA% + 2 ELSE INIT% = 1
3430 CALL XSA(NSORCE%,ICHL%,ICHH%,IGAIN%)
3440 CALL XDSC
3450 CALL XSCF(FREQ)
3460 ' *** BEGIN DATA COLLECTION ***
3470 IF (OPT = 2 AND NOFFSET%=2) THEN PRINT#1,"OUTPUT 1 $ @ AD
"+SRATE$+" "+NPORT$+" "+NSCAN$
3480  CALL  XBAD((NSAMP%+1),IDATA%(INIT%))
3490 CALL XTAD(ILEFT%)
3500 IF (ILEFT% > 0) THEN 3490
3510 CALL XSAD
3520 CALL XESC
3530 ' *** MOVE DATA FROM IDATA ARRAY TO CALIB ARRAY AND CONVERT A/D
* * *
3540 FOR I = 1 TO NSPC%
3550   FOR J = 1 TO NCHAN%
3560         INDEX% = (I-1)*NCHAN%+J
3570        ICOUNT% = IDATA%(INIT% + INDEX% -1)
3580      CALL XATV(ICOUNT%,IGAIN%,VALUE)
3590        CALIB(I,J) = VALUE
3600    NEXT J
3610 NEXT I
3620 ' *** COMPUTE MEAN OF SAMPLES TAKEN ***
3630 FOR I = 1 TO NCHAN% : VALU(I) = 0 : NEXT I
3640 FOR J = 1 TO NCHAN%
3650    FOR I = 1 TO NSPC% : VALU(J) = VALU(J) + CALIB(I,J) : NEXT I
3660 NEXT J
3670 FOR I = 1 TO NCHAN%
3680     AVAL(I) = VALU(I) / NSPC% : RVAL(I) = 0
3690 NEXT I
3700 FOR I = NCHAN%+1 TO 11 : AVAL(I) = 0 : NEXT I
3710 ' *** IF 1ST TIME TAKE "OFFSET" DATA ***
3720 IF NOFFSET% <> 1 THEN 3770
```

```
3730 FOR I = 1 TO NCHAN% : OFFS(I) = AVAL(I) : NEXT I
3740 NOFFSET% = 2
3750 PRINT : INPUT "Start the pump and hit <CR> to continue";ANS$
3760 GOTO 3390
3770 RETURN
3780     '     **********************************
3790 ' * CALCULATE RELEVANT PARAMETERS *
3800     '     **********************************
3810 PRINT : INPUT "Enter leakage flow";LKFLO
3820 GPMFLO = LKFLO + (AVAL(3) - OFFS(3))*CONV        :' GAL/MIN
3830 Q = GPMFLO * (.003785/60)                        :' M3/S
3840 VTR4 = Q / ATR4                                  :' M/S
3850 VEX = Q / AEX                                    :' M/S
3860 VLEAK = LKFLO * (.003785/60) / ALEAK             :' M/S
3870 VIN = Q / AIN                                    :' M/S
3880 RPM = (AVAL(1) - OFFS(1)) * 880 / 5.0306         :' REV/MIN
3890 UTIP = RPM * PI * D2 / 60                        :' M/S
3900 OMEGA = RPM * 2 * PI / 60                        :' RAD/S
3910 CHKRPM = AVAL(1) - OFFS(1)
3920  TRQ  =  (AVAL(2)-OFFS(2)-.005-(.005*((AVAL(1)-OFFS(1))-
.4)/.08))*1014.3
3930 IF (CHKRPM < .4) THEN TRQ = (AVAL(2)-OFFS(2)-.005)*1014.3
3940 TRQ = TRQ * (4.448/39.37)                        :' N-M
3950 PHI = Q / (PI * D2 * B2 * UTIP )
3960 RETURN
3970     '     ******************************************
3980 ' * CALCULATE TIME RESOLVED PUMP PARAMETERS *
3990     '     ******************************************
4000 FOR C = 1 TO NUSED
4010 TGPMFLO(C) = LKFLO + (CALIB(C,3) - OFFS(3))*CONV        :' GAL/MIN
4020 TQ(C) = TGPMFLO(C) * (.003785/60)                       :' M3/S
4030 TRPM(C) = (CALIB(C,1) - OFFS(1)) * 880 / 5.0306         :' REV/MIN
4040 TUTIP(C) = TRPM(C) * PI * D2 / 60                       :' M/S
4050 CHKRPM = CALIB(C,1) - OFFS(1)
4060   TTRQ(C)=(CALIB(C,2)-OFFS(2)-.005-(.005*((CALIB(C,1)-OFFS(1))-
.4)/.08))*1014.3
4070 IF (CHKRPM < .4) THEN TTRQ(C) = (CALIB(C,2)-OFFS(2)-.005)*1014.3
4080 TTRQ(C) = TTRQ(C) * (4.448/39.37)                       :' N-M
4090 TPHI(C) = TQ(C) / (PI * D2 * B2 * TUTIP(C))
4100 NEXT C
4110 RETURN
4120     '     ***************
4130 ' * FFT ROUTINE *
4140     '     ***************
4150 PRINT "Starting FFT, please wait....."
4160 J = 1
4170 FOR I = 1 TO N STEP 2
4180   IF J > I THEN 4190 ELSE 4250
4190      TEMPR=DAT(J)
4200       TEMPI=DAT(J+1)
4210      DAT(J) = DAT (I)
4220        DAT(J+1)=DAT(I+1)
4230      DAT(I) = TEMPR
```

```
4240      DAT(I+1) = TEMPI
4250    M = N / 2
4260    IF ((M >= 2) AND (J > M )) THEN 4270 ELSE 4290
4270       J=J-M : M=M/2
4280    GOTO 4260
4290    J = J + M
4300 NEXT I
4310 MMAX = 2
4320 IF N > MMAX THEN 4330 ELSE 4540
4330 ISTEP = 2*MMAX
4340  THETA#= 2! * PI / (ISIGN*MMAX)
4350   WPR#  =  -2#*(SIN(.5#*THETA#))^2
4360   WPI#=SIN(THETA#)
4370  WR#=1# : WI# = 0#
4380 FOR M = 1 TO MMAX STEP 2
4390 FOR I = M TO N STEP ISTEP
4400     J = I + MMAX
4410        TEMPR = WR#*DAT(J)-WI#*DAT(J+1)
4420        TEMPI = WR#*DAT(J+1)+WI#*DAT(J)
4430      DAT(J) = DAT(I) - TEMPR
4440       DAT(J+1) = DAT(I+1) - TEMPI
4450      DAT(I) = DAT(I) + TEMPR
4460       DAT(I+1) = DAT(I+1) + TEMPI
4470    NEXT I
4480     WTEMP# = WR#
4490         WR#=(WR#*WPR#)-(WI#*WPI#)+WR#
4500        WI#  =(WI#*WPR#)+(WTEMP#*WPI#)+WI#
4510 NEXT M
4520 MMAX = ISTEP
4530 GOTO 4320
4540 PRINT "FFT complete ..... "
4550 RETURN
4560 END
```

APPENDIX C
SLIP FACTOR CALCULATIONS

In order to calculate the slip factor, the theoretical value of the impeller discharge tangential velocity must be determined in terms of the experimentally acquired pump parameters and the impeller geometry. The impeller exit velocity in the rotating reference frame of the impeller is expressed as:

$$w_2 = \frac{Q_{imp}}{\pi D_2 b_2 \sin \beta_2} \tag{C.1}$$

The tangential component of this velocity is:

$$w_{\theta,2} = \frac{Q_{imp} \cot \beta_2}{\pi D_2 b_2} \tag{C.2}$$

Substituting into (C.2) the definition of the flow coefficient gives:

$$w_{\theta,2} = \phi U_{tip} \cot \beta_2 \tag{C.3}$$

Transforming coordinates into a stationary reference frame yields:

$$C_{\theta,2} = U_{tip} - w_{\theta,2} \tag{C.4}$$

Substituting Equation (C.3) into Equation (C.4) yields the final result for the theoretical impeller exit tangential velocity in terms of the measured parameters.

$$C_{\theta 2,\,theoretical} = U_{tip} (1 - \phi \cot \beta_2) \tag{C.5}$$

The actual value of the impeller discharge tangential velocity was measured with the Laser Doppler Velocimeter System. The flow coefficient, ϕ, and the

impeller tip speed were measured with the instrumentation discussed in Chapter 2. The angular position in the volute, theta, is defined as zero degrees at the tongue and is positive in the upstream direction of flow. The following table lists the experimentally determined slip factor values.

Angle	ϕ	$C_{\theta,2\ actual}$	$C_{\theta,2\ theoretical}$	σ
Theta=5	0.102	1.748422	2.8122244	0.62172208
	0.06	1.592558	2.88818376	0.55140467
	0.049	1.612888	2.92018623	0.55232368
Theta=10	0.099	1.817594	2.82766768	0.64278911
	0.0599	1.621852	2.90757873	0.55780158
	0.0489	1.613283	2.9300601	0.55059724
Theta=15	0.099	1.731646	2.81833544	0.61442154
	0.0616	1.608759	2.89451983	0.55579478
	0.05226	1.645867	2.91354556	0.56490176
Theta=20	0.098	1.915627	2.8483894	0.67252989
	0.06	1.65755	2.92656494	0.56638073
	0.049	1.76797	2.95886419	0.59751644
Theta=25	0.098	1.891333	2.83905042	0.66618507
	0.06	1.795683	2.92656494	0.61358044
	0.049	1.695418	2.9491947	0.5748749
Theta=30	0.099	1.747087	2.81833544	0.6199003
	0.058	1.736873	2.90185309	0.59853926
	0.05	1.805597	2.93747471	0.61467661

		$C_{\theta,2\ act}/\ U_{tip}$	$C_{\theta,2\ th}/\ U_{tip}$	
Theta=-80	0.1	0.66529	0.93254915	0.71341012
	0.059	0.63259	0.960204	0.65880792
	0.05	0.62926	0.96627457	0.65122277
Theta=-75	0.1	0.63678	0.93254915	0.682838
	0.059	0.56875	0.960204	0.59232205
	0.05	0.5537	0.96627457	0.57302553
Theta=-70	0.1	0.66598	0.93254915	0.71415003
	0.06	0.58049	0.95952949	0.60497359
	0.049	0.55911	0.96694908	0.57822073
Theta=-65	0.1	0.66631	0.93254915	0.7145039
	0.059	0.56946	0.960204	0.59306148
	0.05	0.55598	0.96627457	0.57538511